frontiers | Research Topics

Mechanisms of neurodegeneration in amyotrophic lateral sclerosis and related disorders

Edited by
Danyllo Oliveira and Agnes Lumi Nishimura

Published in
Frontiers in Cellular Neuroscience
Frontiers in Aging Neuroscience
Frontiers in Neuroscience
Frontiers in Neurology

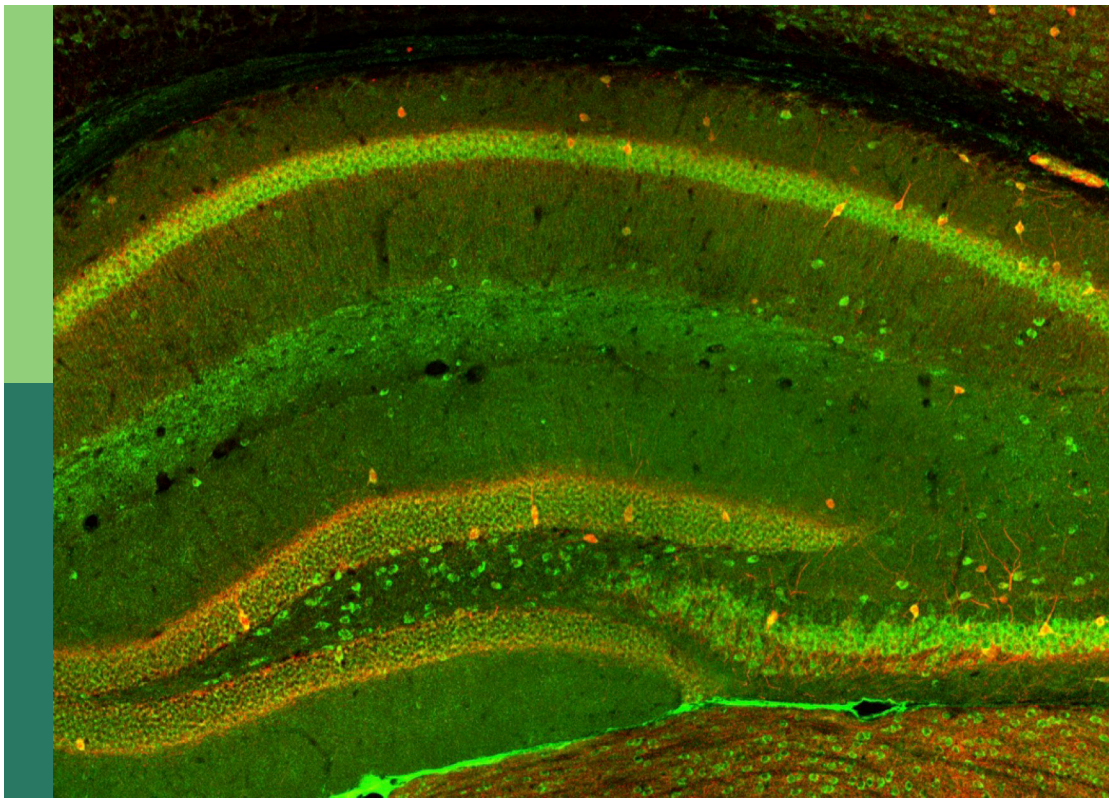

ISSN 1664-8714
ISBN 978-2-8325-5805-8
DOI 10.3389/978-2-8325-5805-8

About Frontiers

Frontiers is more than just an open access publisher of scholarly articles: it is a pioneering approach to the world of academia, radically improving the way scholarly research is managed. The grand vision of Frontiers is a world where all people have an equal opportunity to seek, share and generate knowledge. Frontiers provides immediate and permanent online open access to all its publications, but this alone is not enough to realize our grand goals.

Frontiers journal series

The Frontiers journal series is a multi-tier and interdisciplinary set of open-access, online journals, promising a paradigm shift from the current review, selection and dissemination processes in academic publishing. All Frontiers journals are driven by researchers for researchers; therefore, they constitute a service to the scholarly community. At the same time, the *Frontiers journal series* operates on a revolutionary invention, the tiered publishing system, initially addressing specific communities of scholars, and gradually climbing up to broader public understanding, thus serving the interests of the lay society, too.

Dedication to quality

Each Frontiers article is a landmark of the highest quality, thanks to genuinely collaborative interactions between authors and review editors, who include some of the world's best academicians. Research must be certified by peers before entering a stream of knowledge that may eventually reach the public - and shape society; therefore, Frontiers only applies the most rigorous and unbiased reviews. Frontiers revolutionizes research publishing by freely delivering the most outstanding research, evaluated with no bias from both the academic and social point of view. By applying the most advanced information technologies, Frontiers is catapulting scholarly publishing into a new generation.

What are Frontiers Research Topics?

Frontiers Research Topics are very popular trademarks of the *Frontiers journals series*: they are collections of at least ten articles, all centered on a particular subject. With their unique mix of varied contributions from Original Research to Review Articles, Frontiers Research Topics unify the most influential researchers, the latest key findings and historical advances in a hot research area.

Find out more on how to host your own Frontiers Research Topic or contribute to one as an author by contacting the Frontiers editorial office: frontiersin.org/about/contact

Mechanisms of neurodegeneration in amyotrophic lateral sclerosis and related disorders

Topic editors

Danyllo Oliveira — University of São Paulo, Brazil

Agnes Lumi Nishimura — Queen Mary University of London, United Kingdom

Citation

Oliveira, D., Nishimura, A. L., eds. (2024). *Mechanisms of neurodegeneration in amyotrophic lateral sclerosis and related disorders*. Lausanne: Frontiers Media SA. doi: 10.3389/978-2-8325-5805-8

Table of contents

04 Editorial: Mechanisms of neurodegeneration in amyotrophic lateral sclerosis and related disorders
Danyllo Oliveira and Agnes Lumi Nishimura

07 Immunology of amyotrophic lateral sclerosis – role of the innate and adaptive immunity
Stefan Mimic, Başak Aru, Cemil Pehlivanoğlu, Hadi Sleiman, Pavle R. Andjus and Gülderen Yanıkkaya Demirel

24 Mendelian randomization analysis suggests no associations of human herpes viruses with amyotrophic lateral sclerosis
Qingcong Zheng, Du Wang, Rongjie Lin, Yuchao Chen, Haoen Huang, Zixing Xu, Chunfu Zheng and Weihong Xu

36 Amyotrophic lateral sclerosis and osteoporosis: a two-sample Mendelian randomization study
Junhong Li, Cong Ma, Hui Huang and Hui Liao

46 Autophagy in spinal muscular atrophy: from pathogenic mechanisms to therapeutic approaches
Saman Rashid and Maria Dimitriadi

63 Analyzing the ER stress response in ALS patient derived motor neurons identifies druggable neuroprotective targets
Michelle E. Watts, Richard M. Giadone, Alban Ordureau, Kristina M. Holton, J. Wade Harper and Lee L. Rubin

83 Induced degeneration and regeneration in aged muscle reduce tubular aggregates but not muscle function
Felipe Tadeu Galante Rocha de Vasconcelos, Antonio Fernando Ribeiro Júnior, Brandow Willy Souza, Isabela de Aquino Zogbi, Laura Machado Lara Carvalho, Letícia Nogueira Feitosa, Lucas Santos Souza, Nathália Gagliardi Saldys, Merari de Fátima Ramires Ferrari and Mariz Vainzof

92 TUBA4A downregulation as observed in ALS *post-mortem* motor cortex causes ALS-related abnormalities in zebrafish
Evelien Van Schoor, Dufie Strubbe, Elke Braems, Jochen Weishaupt, Albert C. Ludolph, Philip Van Damme, Dietmar Rudolf Thal, Valérie Bercier and Ludo Van Den Bosch

106 Associations of cerebrospinal fluid profiles with severity and mortality risk of amyotrophic lateral sclerosis
Jiajia Fu, Xiaohui Lai, Qianqian Wei, Xueping Chen and Huifang Shang

115 Causal association between obstructive sleep apnea and amyotrophic lateral sclerosis: a Mendelian randomization study
Rongrong Du, Yahui Zhu, Peng Chen, Mao Li, Ying Zhang and Xusheng Huang

122 Genetic link between *KIF1A* mutations and amyotrophic lateral sclerosis: evidence from whole-exome sequencing
Wei Zheng, Ji He, Lu Chen, Weiyi Yu, Nan Zhang, Xiaoxuan Liu and Dongsheng Fan

frontiers | Frontiers in Cellular Neuroscience

TYPE Editorial
PUBLISHED 05 December 2024
DOI 10.3389/fncel.2024.1531449

OPEN ACCESS

EDITED AND REVIEWED BY
Dirk M. Hermann,
University of Duisburg-Essen, Germany

*CORRESPONDENCE
Agnes Lumi Nishimura
✉ a.nishimura@qmul.ac.uk
Danyllo Oliveira
✉ oliveira.danyllo@gmail.com

RECEIVED 20 November 2024
ACCEPTED 25 November 2024
PUBLISHED 05 December 2024

CITATION
Oliveira D and Nishimura AL (2024) Editorial: Mechanisms of neurodegeneration in amyotrophic lateral sclerosis and related disorders. *Front. Cell. Neurosci.* 18:1531449. doi: 10.3389/fncel.2024.1531449

Editorial: Mechanisms of neurodegeneration in amyotrophic lateral sclerosis and related disorders

Danyllo Oliveira[1,2]* and Agnes Lumi Nishimura[3]*

[1]Department of Genetics and Evolutionary Biology, Human Genome and Stem Cell Research Center, Institute of Biosciences, University of São Paulo, São Paulo, Brazil, [2]School of Medical Sciences Santa Casa and Pathological Sciences Unit, Irmandade Santa Casa de Misericordia de São Paulo, São Paulo, Brazil, [3]Centre for Neuroscience, Surgery and Trauma, Barts and The London School of Medicine and Dentistry, Blizard Institute, Queen Mary University of London, London, United Kingdom

KEYWORDS

amyotrophic lateral sclerosis, neurodegeneration, genetic risk factor, Mendelian randomization, disease mechanisms, spinal muscular atrophy, myopathy

Editorial on the Research Topic
Mechanisms of neurodegeneration in amyotrophic lateral sclerosis and related disorders

This Research Topic, *Mechanisms of Neurodegeneration in Amyotrophic Lateral Sclerosis and Related Disorders*, includes eight original research papers and two reviews on genetic factors and molecular mechanisms associated with Duchenne muscular atrophy, spinal muscular atrophy, and amyotrophic lateral sclerosis. This Research Topic covers how genetic (*KIF1A* and *TUBBA4A*) and environmental factors (e.g., aging, apnea, osteoporosis, and inflammation) can influence these degenerative conditions. It also explores the disease mechanisms of ALS and drug discovery using zebrafish and patient-derived cells.

We open this editorial with a study investigating the effects of aging on the formation of tubular aggregates. These aggregates are formed upon progressive accumulation of sarcoplasmic reticulum protein, which is often associated with myopathies. de Vasconcelos et al. investigated how degeneration and regeneration in skeletal muscle can influence the presence of these tubular aggregates. The authors investigated wild-type animal models and Duchenne muscular dystrophy models to evaluate the effects of muscle regeneration and tubular aggregate formation. To induce regeneration, the animals were subjected to injury using electroporation and left to recover for 5, 15, and 30 days post-electroporation. The findings revealed that tubular aggregates were more prevalent in aged WT animals than those with aged Duchenne muscular dystrophy. Furthermore, the study showed that the number of tubular aggregates decreased progressively from 5 to 30 days post-electroporation, with the WT-aged animals displaying recovery by 5 days after the injury. The authors propose that tubular aggregates accumulate in muscle fibers as a result of aging and that during the regeneration process, new muscle fibers that do not contain these aggregates are produced. These newly produced muscle fibers do not seem to contribute to an extra functional capacity of the muscle.

Moving on to molecular mechanisms of neurodegenerative diseases, Rashid and Dimitriadi review the pathogenic mechanisms of autophagy and potential therapeutic

approaches in spinal muscle atrophy. The authors provide a summary of spinal muscular atrophy, the effect of autophagy on the disease and how alterations in the autophagic flux could be a potential therapeutic route for SMA.

The following studies focused on amyotrophic lateral sclerosis (ALS), a complex condition influenced by genetic and environmental factors. Research has identified various dysregulated proteins in ALS, including those involved in axonal transport. Among these proteins are motor proteins like kinesin, which are essential for transporting cargo, such as vesicles, mRNA, and organelles, from the cell body (soma) to the axon terminals. Mutations in genes associated with axonal transport have been identified in patients with ALS. A recent study discovered mutations in the *KIF1A* gene among ALS patients in southern China, suggesting it may be a genetic risk factor for the disease. To investigate whether *KIF1A* mutations are present in a different cohort of Chinese ALS patients, Zheng W. et al. conducted whole-exome sequencing on 1,068 ALS patients. Of these, 14 patients (1.31%) had mutations in the C-terminal region of the KIF1A gene. Notably, mutations in the motor domain at the N-terminal end of the *KIF1A* gene are linked to hereditary peripheral neuropathy and spastic paraplegia, highlighting that different mutations in this gene can lead to various conditions, thus broadening the spectrum of ALS. This study supports the idea that *KIF1A* mutations are considered a risk factor for ALS within the Chinese population.

The next three studies investigate Mendelian randomization, obstructive sleep apnea, osteoporosis and viral infections. Obstructive sleep apnea (OSA) is a common sleep disorder characterized by reduced hemoglobin oxygen saturation and disrupted sleep due to repeated apneas (pauses in breathing). Previous studies have suggested that patients with amyotrophic lateral sclerosis (ALS) who experience obstructive sleep apnea have worse survival rates compared to those without OSA. OSA can lead to intermittent hypoxia, which negatively affects cells in the central nervous system (CNS), resulting in neuronal injury, increased oxidative stress, and neuroinflammation. This indicates that OSA may contribute to the worsening of ALS symptoms.

Despite the evidence showing that OSA can exacerbate ALS symptoms, it remains unclear whether OSA is a risk factor for ALS. In their study, Du et al. conducted data mining research using Mendelian randomization to explore the relationship between OSA and the risk of developing ALS. The authors analyzed pooled data from genome-wide association studies (GWAS) involving 16,761 OSA patients and 201,194 healthy controls. They also examined meta-analysis data from 22,040 ALS patients and 62,654 healthy controls. By applying the inverse-variance weighted (IVW) method, the authors found that genetic predisposition to OSA was associated with an increased risk of ALS. While the findings should be interpreted with caution, the study highlights how data mining can help identify potential risk factors associated with various conditions.

Next, Li et al. investigated one GWAS dataset with 27,205 ALS cases and 110,881 controls and another GWAS database with 53,236 osteoporosis cases. Bone mineral density in the neck, spine and arm were evaluated. The authors identified 10 qualified SNPs as proxies for ALS. However, no association was observed between osteoporosis and the risk for ALS using IVW. In another study, Zheng Q. et al. conducted a study using Mendelian randomization using the IVW method to investigate a potential association between several viral infections—including herpes simplex virus (HSV), varicella-zoster virus (VZV), Epstein–Barr virus (EBV), cytomegalovirus (CMV), HHV-6, and HHV-7—and ALS. The research analyzed GWAS data from 6,812 subjects affected by these infections and 634,809 controls. The authors concluded that these viruses do not represent a risk factor for ALS.

Deepening on the role of inflammation and innate and adaptive immunity and ALS, Mimic et al. summarize the evidence linking immunity and ALS. In this review, the authors discuss the dual function of astrocytes and microglia as neurotoxic and neuroprotective cells and how other cells play a role in innate and adaptive immunity. The authors also discuss how autoantibodies and cytokines could play a role in the pathogenesis of ALS.

The identification of biomarkers for ALS would have important implications for disease progression, prognosis and treatment effectiveness. Research utilizing ALS biofluids, including serum and cerebrospinal fluid (CSF), has gained popularity in the past decades, although conflicting results have emerged. In this study, Fu et al. investigated the profile of microproteins, albumin, IgG, IgG, index of IgG, albumin quotient, and serum IgG in 870 ALS patients and 96 healthy ALS and healthy controls. The authors observed that approximately one-third of ALS patients in this study showed higher CSF IgG levels. However, CSF IgG index was decreased when compared with healthy controls. Additionally, multiple linear regression analysis indicates that the CSF IgG index is negatively associated with ALS Functional Rating Scale Revised (ALSFRS-R) scores in males with ALS. This suggests that higher levels of CSF IgG are linked to worsening ALS symptoms, leading to an increased risk of mortality in the ALS population. This study suggests that the CSF IgG index could be a potential biomarker for ALS severity.

Closing this Research Topic, two studies delved deeper into ALS disease mechanisms.

Van Schoor et al. evaluated the effects of downregulating the TUBA4A protein in zebrafish. The authors injected an antisense oligonucleotide morpholino into zebrafish and evaluated motor axon morphology and motor behavior (Van Schoor et al.). Downregulation of TUBA4A led to motor axonopathy and motor behavior disturbances, which were rescued by overexpression of wild-type *TUBA4A* mRNA. In addition, the downregulation of TUBA4A altered post-translational modifications of tubulin, acetylation, detyrosination, and polyglutamylation.

Closing this Research Topic, Watts et al. investigated the ER stress response in ALS-patient-derived inducible pluripotent stem cell lines. Three lines were used in this study: one derived from healthy control, one carrying the *TARDBP* G298S mutation, and one carrying the *SOD1* L144F mutation, which differentiated them into motor neurons. These cells were subjected to pharmacologic ER stressors, increasing neuronal death risk. The authors evaluated how thapsigargin and tunicamycin exposure can recapitulate ALS-associated features associated with ER stress, including upregulation of CHOP and BiP and decreased total neurite length. To assess whether pharmacological compounds

could rescue ER-stress-related phenotypes, the authors investigate a selective inhibitor of MAP4K4. This kinase can inhibit kenpaullone, a potential compound tested in ALS patients. The MAP4K4 inhibitor increased viability in thapsigargin- and tunicamycin-treated motor neurons. The authors performed phosphoproteomics on MNs treated with ER stressors and MAP4K4 inhibitors and identified JNK, PKC, and BRAF to be differentially expressed in MAP4K4 inhibitor-treated cells. This study highlights the use of patient-derived cells, compound screening, and evaluation of disease-related pathways altered in ALS.

These studies collectively emphasize the importance of investigating how genetic mutations and environmental factors contribute to neurodegenerative diseases. Using animal models and patient-derived cells can offer valuable insights into the mechanisms of these diseases and help identify novel therapeutic approaches for degenerative conditions.

Author contributions

DO: Writing – review & editing. AN: Writing – original draft, Writing – review & editing.

Funding

The author(s) declare that no financial support was received for the research, authorship, and/or publication of this article.

Conflict of interest

The authors declare that the research was conducted in the absence of any commercial or financial relationships that could be construed as a potential conflict of interest.

The author(s) declared that they were an editorial board member of Frontiers, at the time of submission. This had no impact on the peer review process and the final decision.

Publisher's note

frontiers | Frontiers in Neuroscience

TYPE Review
PUBLISHED 30 November 2023
DOI 10.3389/fnins.2023.1277399

OPEN ACCESS

EDITED BY
Danyllo Oliveira,
University of São Paulo, Brazil

REVIEWED BY
John Andersson,
Karolinska Institutet (KI), Sweden
Chetan Rajpurohit,
Baylor College of Medicine, United States

*CORRESPONDENCE
Pavle R. Andjus
✉ pandjus@bio.bg.ac.rs
Gülderen Yanıkkaya Demirel
✉ gulderen.ydemirel@yeditepe.edu.tr

RECEIVED 14 August 2023
ACCEPTED 07 November 2023
PUBLISHED 30 November 2023

CITATION
Mimic S, Aru B, Pehlivanoğlu C, Sleiman H, Andjus PR and Yanıkkaya Demirel G (2023) Immunology of amyotrophic lateral sclerosis – role of the innate and adaptive immunity. *Front. Neurosci.* 17:1277399. doi: 10.3389/fnins.2023.1277399

Immunology of amyotrophic lateral sclerosis – role of the innate and adaptive immunity

Stefan Mimic[1], Başak Aru[2], Cemil Pehlivanoğlu[2], Hadi Sleiman[3], Pavle R. Andjus[1]* and Gülderen Yanıkkaya Demirel[2]*

[1]Centre for Laser Microscopy, Institute of Physiology and Biochemistry "Jean Giaja", Faculty of Biology, University of Belgrade, Belgrade, Serbia, [2]Immunology Department, Faculty of Medicine, Yeditepe University, Istanbul, Türkiye, [3]Faculty of Medicine, Yeditepe University, Istanbul, Türkiye

This review aims to summarize the latest evidence about the role of innate and adaptive immunity in Amyotrophic Lateral Sclerosis (ALS). ALS is a devastating neurodegenerative disease affecting upper and lower motor neurons, which involves essential cells of the immune system that play a basic role in innate or adaptive immunity, that can be neurotoxic or neuroprotective for neurons. However, distinguishing between the sole neurotoxic or neuroprotective function of certain cells such as astrocytes can be challenging due to intricate nature of these cells, the complexity of the microenvironment and the contextual factors. In this review, in regard to innate immunity we focus on the involvement of monocytes/macrophages, microglia, the complement, NK cells, neutrophils, mast cells, and astrocytes, while regarding adaptive immunity, in addition to humoral immunity the most important features and roles of T and B cells are highlighted, specifically different subsets of $CD4^+$ as well as $CD8^+$ T cells. The role of autoantibodies and cytokines is also discussed in distinct sections of this review.

KEYWORDS

amyotrophic lateral sclerosis, neuroimmunology and neuropathy, innate immune system, adaptive immune system, neurodegeneration

1 Introduction

First described by Jean-Marie Charcot, amyotrophic lateral sclerosis (ALS), also known as Lou Gehrig's disease, is an irreversible neurodegenerative disease affecting both upper and lower motor neurons that progresses over time (Henkel et al., 2014). ALS is an adult-onset disease, most often occurring in men and women under the age of 60 years. The disease leads to very progressive and irreversible neurodegeneration of the upper and lower motor neurons, resulting in muscle weakness, dysarthria, and difficulty to swallow (dysphagia). Patients die within 4–6 years after the onset of the disease. The incidence of the disease is about two per 100,000 people (Logroscino et al., 2010). Although the etiopathogenesis of ALS remains unknown and inadequately studied, it is widely recognized as a complex and multifactorial condition, with immunological mechanisms playing an important role. Namely, there are two forms of ALS: the sporadic form (sALS), which is the most common with an unknown cause, and the familial form (fALS). In fALS, there is a disruption of the genes that code for axonal transport, vesicular traffic, or there occurs a disruption in RNA processing. The hereditary form of ALS is primarily associated with a specific mutation found in the gene responsible for producing superoxide dismutase type 1 (SOD1). It accounts for 20% of all known mutations, and transgenic mouse models of these human SOD1 mutations have provided an opportunity to investigate the disease mechanisms (Motataianu et al., 2020). SOD1 (Cu, Zn SOD)

is a widespread cytosolic enzyme that converts the highly toxic superoxide anion into hydrogen peroxide. However, there are other mutations in focus of recent research, such as mutation in TAR-DNA-binding protein 43 (TDP43), FUS (Fused in Sarcoma), Angiogenin, and hexanucleotide repeats in the gene that codes for C9ORF72. TDP43 is encoded by the TARDP gene and cytoplasmic aggregation of the mutated forms of TDP43 protein are encountered in more 95% than all ALS cases (Neumann et al., 2006). Previously reported to be extensively expressed in peripheral myeloid cells and microglia, C9ORF72 mutations account for the cases of ~40% of fALS and 5–10% of non-fALS (DeJesus-Hernandez et al., 2011; Renton et al., 2011).

Alterations in both innate and adaptive immune cell populations have been shown to influence disease progression in both mouse models and ALS patients (Henkel et al., 2006; Beers et al., 2008; Finkelstein et al., 2011; Butovsky et al., 2012; Lam et al., 2016; Zondler et al., 2016; Jin et al., 2020; Figure 1). In the case of ALS, Wallerian degeneration can occur due to the progressive degeneration of motor neurons and axons in the spinal cord (Beirowski et al., 2005; Coleman and Höke, 2020). This degeneration can lead to the loss of communication between the motor neurons and the muscles they control, ultimately resulting in muscle weakness, atrophy, and paralysis. The exact mechanisms of Wallerian degeneration in ALS are still not fully understood, but it is believed to be related to the accumulation of abnormal proteins within the motor neurons, such as TDP43 and FUS. These abnormal proteins can lead to the formation of aggregates and disrupt normal cellular processes, eventually resulting in the degeneration and death of the motor neurons. Furthermore, Wallerian degeneration can also cause the activation of neuroinflammatory processes, which further contribute to the progression of ALS. The immune system has been shown to play an important role in Wallerian degeneration as immune cells infiltrate the degenerating nerve, clear debris, and support axonal regeneration (Rotshenker, 2011). Herein, we aim to summarize the involvement of immune system in the pathogenesis of ALS.

2 The role of innate immunity in ALS

2.1 Monocytes and macrophages

Monocytes originate from the bone marrow, where they maturate upon colony stimulating factor 1 receptor stimulation (CSF-1R) from

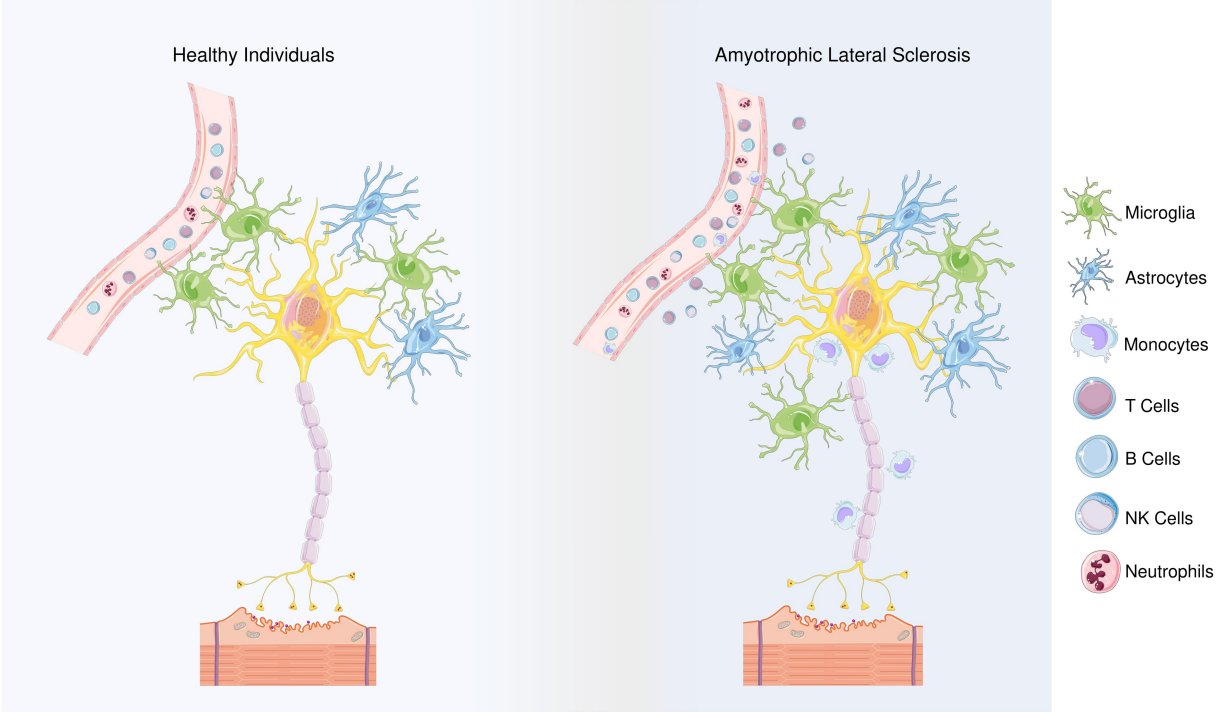

FIGURE 1
Differences between healthy individuals and ALS patients regarding the types of inflammatory cells. Members of the adaptive innate immune system, T and B cells play role in ALS progression, though their involvement may depend on the stage of the disease. Microglia and astrocytes are considered as the main contributors to the non-cell autonomous mechanism in ALS. The neuroprotective M2 microglia provide protection in the beginning of the disease by releasing anti-inflammatory mediators. However, as the disease progresses, a transition from the M2 to the neurotoxic M1 phenotype is observed. Microglial polarization in ALS is regulated with T cells and astrocytes' responses. In terms of the first, anti-inflammatory cytokines IL-4 and IL-10 are released by Th2 cells and T_{regs}, during the early stage of disease, in addition, Th2 cells also secrete various neurotrophic factors while as the disease progresses, Th1 cells release the pro-inflammatory mediators and contribute to the M1 polarization. Similarly, the NF-κB activation in spinal cord astrocytes can promote the neuroprotective phenotype of microglia and inhibit disease progression, but prolonged NF-κB activation in the later stages of the disease promotes pro-inflammatory microglial responses. In addition, impairments in glutamate transporters limits glutamate uptake of astrocytes, ultimately leading to dysfunction of motoneurons. Besides microglia and astrocytes, NK cells and monocytes can infiltrate the region and contribute to the inflammatory response. In the peripheral blood of the ALS patients, neutrophil percentages were reported to be increased, and the increase in their ratio to lymphocytes correlates with the disease progression. By releasing hematopoietic serine proteases, neutrophils also regulate NK cell toxicity.

hematopoietic precursors common to monocytes, certain subsets of macrophages, and dendritic cells (Auffray et al., 2009). Several studies clearly indicate an increased infiltration rate of peripheral monocytes in mouse models of ALS and ALS patients' spinal cords (Butovsky et al., 2012; Zondler et al., 2016) as well as their activation in peripheral blood (Mantovani et al., 2009). Activated monocytes from individuals with ALS show altered secretion of pro-inflammatory cytokines, altered adhesion behavior, and impaired phagocytosis (Zondler et al., 2016, 2017).

A growing number of scientific studies suggest that monocytes can infiltrate the brain and spinal cord during pathological conditions and their role is associated with the disruption of the blood–brain barrier (Cronk et al., 2018). When considering animal models, in mice, peripheral monocyte infiltration is associated with better motor neuron survival (Zondler et al., 2016). In another *in vivo* study, Ly6C^{high} monocytes have been shown to play an important role in disease progression and are associated with motor neuron injury (Butovsky et al., 2012).

Some of the most important pro-inflammatory mediators secreted by monocytes are chemokines C-X-C Motif Chemokine Ligand 1 (CXCL1) and C-X-C Motif Chemokine Ligand 2 (CXCL2), as well as FosB Proto-Oncogene, AP-1 Transcription Factor Subunit, Interleukin (IL)-1β, and Il-8, which unequivocally indicates that monocytes tend to polarize towards a pro-inflammatory phenotype in ALS (Du et al., 2020). Murdock and colleagues suggested that cell surface marker CD16 expression is altered during ALS, however, no correlation was reported between CD16^{+} monocytes and the ALS patient score, ALSFRS-R (Murdock et al., 2016). Figueroa-Romero and colleagues reported increased CCRL2 and CCR3 levels within the CNS (Figueroa-Romero et al., 2012). A comparison between the monocyte subsets indicated that CCRL2 expression is increased in CD16^{+} monocytes, however, no changes were reported in the expression pattern of CCRL2 in CD16 monocytes (Murdock et al., 2016). On the other hand, a significant difference was observed between CD16^{-} and CD16^{+} monocytes in terms of CCR3 expression: CD16^{-} monocytes have been reported to express significantly lower levels of CCR3. Moreover, a lack of correlation was reported between CCRL2 or CCR3 expression and the ALSFRS-R score. These data suggest that CCRL2 and CCR3 expression levels on CD16^{-} monocytes cannot predict the stage of the disease.

In summary, studies involving individuals with ALS revealed that peripheral monocytes are activated and polarized towards the M1 phenotype rather than the M2 phenotype. However, additional studies are still needed in order to clarify the role of peripheral monocytes and macrophages in the pathogenesis of ALS at the molecular-immunological level. Despite the absence of a clear correlation between the ALSFRS-R score and peripheral monocyte markers, it may be beneficial to explore additional markers expressed on monocytes to uncover potential connections between the molecular dynamics of monocyte subsets and ALSFRS-R scoring.

2.2 Microglia

Microglia are a dynamic population of glial cells that can have either neurotoxic or neuroprotective effects. Neuroinflammation is mainly observed at the sites of motor neuron injury, where activated and proliferating microglia, as well as dendritic cells (the most important antigen-presenting cells), are located (Henkel et al., 2009; Philips and Robberecht, 2011). *In vitro*, microglia can be activated by lipopolysaccharide (LPS), which binds to cell surface receptors CD14 and Toll-like receptor (TLR) 2/4, resulting in the release of reactive oxygen species (ROS) and mediating the excitotoxic effects of glutamate and calcium (Zhao et al., 2006).

Microglial cells are resident macrophages of the CNS, and they participate in synaptic remodeling, pruning, and promotion of the formation of blood vessels (angiogenesis) (Du et al., 2017; Jurga et al., 2020). In the adult brain, microglia monitor signals from the environment and initiate inflammatory responses upon danger signals, providing the first line of defense in the brain. Microglia can recognize very subtle changes in the environment due to their surface receptors (Jurga et al., 2020). Although considered today as and oversimplified by analogy to peripheral monocytes, microglia subtypes are traditionally divided in M1 and M2 polarization phenotypes (Lyu et al., 2021). As observed in other diseases, it has been reported that microglia initially play a beneficial role before switching to a negative role in the advanced disease state (Henkel et al., 2009). Various studies have shown that M2 microglia protect motoneurons at the very beginning of ALS, while as the disease progresses, there is a transition from the M2 phenotype to the M1 phenotype (neurotoxic) (Figure 2; Liao et al., 2012; Gravel et al., 2016). This polarization arises from the crosstalk between T cells and microglia and will be discussed in more detail. In an *in vivo* study involving mSOD1 mice, the M2 phenotype of microglia with neuroprotective characteristics was more prevalent compared to their M1 counterparts in the early stages of the disease (Zhao et al., 2006). Activated microglia release inflammatory cytokines IL-1α and TNF-α as well as complement component 1q (C1q) which induce neurotoxic responses of astrocytes (Liddelow et al., 2017). Studies on primary microglia-motoneuron co-cultures have shown the neuroprotective characteristics of M2 microglia (Zhao et al., 2006) by secreting anti-inflammatory cytokines such as IL-10, transforming growth factor beta (TGF-β), fibroblast growth factor (FGF), IGF-1, CSF-1, brain-derived neurotrophic factor (BDNF), nerve growth factor (NGF), GDNF, and various neurotrophins (Colonna and Butovsky, 2017). However, as the disease progresses, polarization towards the neurotoxic M1 phenotype was observed, especially in the terminal stage of ALS (Henkel et al., 2014).

The essential role of microglia in the pathogenesis of motor neuron injury was also demonstrated in PU.1 knockout mice (PU.1−/−) which lack macrophages, neutrophils, T and B cells, and microglia (Beers et al., 2006). Upon bone marrow transplantation from mSOD1 mice, expression of mSOD1 within the CNS microglia was observed in PU.1−/− mice without clear signs of motor neuron injury or damage in ALS while bone marrow transplantation from healthy mice led to a reduction in motoneurons. In this study, the authors point out the extraordinary complexity of microglia by simultaneously expressing both neuroprotective and neurotoxic factors in ALS mice (Chiu et al., 2013).

Microglia exhibit characteristics of immature myeloid cells and undergo specific changes, such as morphological modifications and an activation of their functions, in response to signals from the environment or injury. Thus, they become mature myeloid cells that may present antigens and secrete cytokines and growth factors. Additionally, microglial cells can produce reactive oxygen species (Cardona et al., 2006). The CX3CR1 fractalkine receptor has been

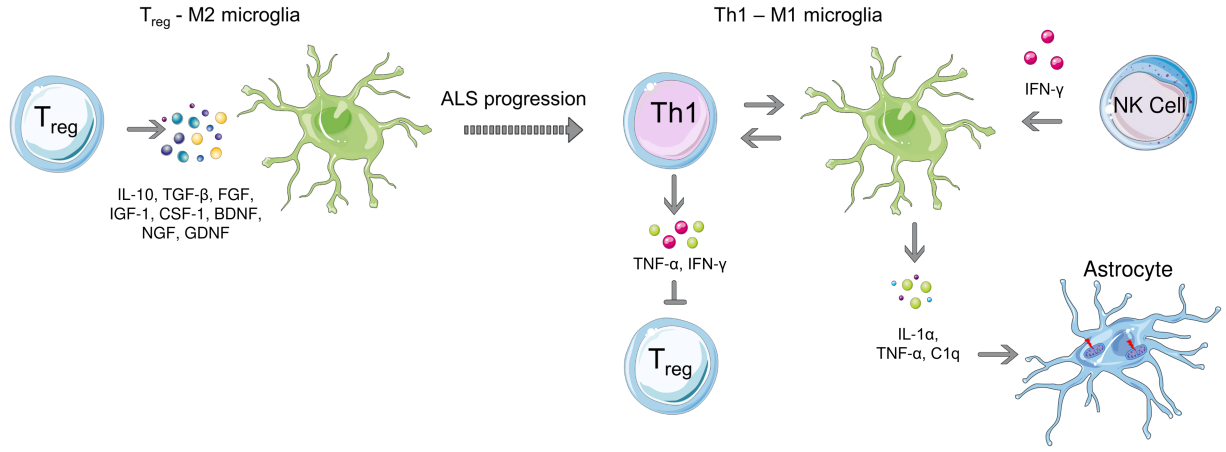

FIGURE 2
Microglial polarization during early **(left)** and late stages **(right)** of ALS. Anti-inflammatory microglia protect motor neurons at the beginning of the disease, while a transition to the neurotoxic M1 phenotype is observed as the disease progresses. T cell-microglia interaction plays role in microglial polarization, NK cells also contribute to the M1 polarization by secreting IFN-γ. Activated microglia release, IL-1α, TNF-α as and C1q which induce neurotoxic responses of astrocytes.

shown to play a role in microglial neurotoxicity in the SOD1G93A model of ALS. As the ligand CX3CL1 is expressed in neurons and the receptor CX3CR1 is expressed in microglia, it is possible to talk about signal transduction from neurons to microglia via the fractalkine receptor (Harrison et al., 1998). Future research should focus on the interactions of CX3CL1 and CX3CR1 to clarify the signal transduction mechanism between neurons and microglia, especially regarding the oxidative stress caused by microglial cells, considering that ALS is also associated with oxidative stress.

In addition to the traditional M1/M2 phenotype, in response to brain injury, a distinctive subset of microglia that expresses CD11c, the dendritic cell marker is observed (Sato-Hashimoto et al., 2019). The first study classifying CD11c + cells in the CNS as microglia dates back to 2006, where the authors have observed CD11c + cell populations in an Alzheimer's Disease (AD) mouse model identified as microglia (Butovsky et al., 2006). Interestingly, in a study performed on a mice ALS model, authors have discovered a distinct signature for these cells in the final stages of the disease in comparison to microglia from healthy brains where the microglia were reported to have CD11c expression (Chiu et al., 2013). In another study, authors have reported the presence of so-called "disease-associated microglia" (DAM) in an *in vivo* AD model which is characterized by the reduced expression of homeostatic genes (Keren-Shaul et al., 2017). DAM have been found in the surrounding of the Aβ plaques, indicating these cells take place in scavenging of extracellular aggregates and cellular debris. DAM were not only observed in AD but also in the spinal cord of the ALS model SOD1G93A mice. In ALS patients, a similar gene expression pattern was detected in the motor cortex, suggesting that DAM may be a general response to the protein accumulation in neurodegeneration. It is still unclear, though, whether these cells are a component of a neuroprotective glial response that is activated late during ALS to mitigate the disease, or if it is instead an excessively reactive response to neuronal death that ultimately contributes to amplifying the damage in the affected CNS regions (Cipollina et al., 2020). Recently, Takahashi revealed the presence of two microglia subgroups of spinal cord lesions in ALS that can be pathologically distinguished according to their TMEM119 expression (Takahashi, 2023). The TMEM119+ microglia group also exhibited expression of the microglial activation marker CD68 and endothelial activation, indicating the presence of inflammatory processes in ALS lesions, and the author have suggested that these cells may represent DAM-independent inflammatory neurodegeneration as DAM suppresses the expression of TMEM119.

2.3 Complement system

The complement system is a complex series of plasma proteins that work together to generate fragments of C3 and C5 proteins through a sequence of cleavage. Recent studies have identified the involvement of the classical pathway of the complement system in the development of amyotrophic lateral sclerosis (ALS), with increased levels of C1q and C4 components observed in the cerebrospinal fluid, CNS, serum, and skeletal muscles of ALS patients (Apostolski et al., 1991; Tsuboi and Yamada, 1994; Yamada et al., 1994; Sta et al., 2011; Bahia El Idrissi et al., 2016). Animal models of ALS have also confirmed the involvement of the upstream pathways of the complement system (Perrin et al., 2005; Ferraiuolo et al., 2007; Lobsiger et al., 2007). However, the role of the terminal component C5 must also be considered, as increased levels of factor C5a and terminal complement complex (C5b-9) have been reported in ALS patients (Mantovani et al., 2014).

Upregulation of C5aR1 signaling has been identified as a potential contributor to motor neuron death in ALS patients, with increased immunostaining for C5aR1 in motor neurons of ALS patients (Bahia El Idrissi et al., 2016). Furthermore, biopsy samples from ALS patients have detected the presence of C59a, a major regulator of the membrane attack complex (Bahia El Idrissi et al., 2016). Despite these findings, further studies are required to fully understand the complex involvement of the complement system in the pathogenesis of ALS, particularly regarding the lack of human studies on the upstream part of the complement system and the C3 component.

2.4 Natural killer cells

Natural killer cells (NK cells) represent the most abundant subset of innate lymphoid cells, and they take part in anti-tumor and anti-viral defense. NK cell function is regulated by a balance between signals from activating and inhibitory receptors. Unlike cytotoxic $CD8^+$ T cells, NK cells do not require prior antigen exposure for an anti-tumor response (Abel et al., 2018). NK cells participate in both innate and adaptive immunity. Thus, NK cells infiltrating the CNS regulate neuroinflammatory processes in neurodegenerative diseases (Infante-Duarte et al., 2005; Poli et al., 2013; Hertwig et al., 2016). NK cells are very important given the fact that motoneurons are sensitive to NK cells during ALS (Song et al., 2016).

NK cells are reported during end-stage disease in the spinal cord of mSOD1 mice (Beers et al., 2008). In addition, an increased number of NK cells was observed in the blood of ALS patients (Beers et al., 2017). Motoneuron degeneration in ALS is associated with dysregulated neuroinflammatory microcirculation (Barbeito et al., 2010; Thonhoff et al., 2018a,b) or microglial activation, which impairs axonal regeneration (Nardo et al., 2016; Spiller et al., 2018). When considering these findings, the degeneration of motor neurons may stem from direct cell-to-cell contacts with NK cells, which release perforin and granzyme B, exerting a direct neurotoxic effect on motor neurons, as well as highlighting the role of innate immunity in neurodegeneration associated with ALS (Garofalo et al., 2020).

The presence of NK cells in the motor cortex and spinal cord of post-mortem samples of ALS patients, as well as the presence of NKG2D ligands expressed on motoneurons, has been previously reported (Garofalo et al., 2020). In this study, it has been demonstrated that NK cells are neurotoxic to motor neurons that express NKG2D ligands in an animal model of ALS. In the mouse model of fALS, it has been shown that NK cells localize in the motor cortex and spinal cord, where the reduction in the number of NK cells leads to attenuation of motoneuron degeneration; the latter was also confirmed on hSOD1G93A and TDP43A315T rodent models (Garofalo et al., 2020). NK cells also secrete the pro-inflammatory IFN-γ, which promotes polarization towards the M1 phenotype of microglia. Increased levels of IFN-γ were detected in hSOD1G93A mice compared to WT (Garofalo et al., 2020). In this study, patients with sALS were investigated in terms of the presence of NK cells as well as the frequency of their subtypes. $NKp46^+$ cells were detected in the motor cortex and spinal cord of ALS individuals, in contrast to control subjects. A reduction of circulating $CD56^+/CD3^-$ cells was also observed in the peripheral blood of sALS patients. The fractalkine receptor CX3CR1 plays an important role in the migration of NK cells in the CNS (Garofalo et al., 2020) as a member of the NKp protein family (Moretta et al., 2000); $CXCR3^+$ expression was shown to be correlated with ALS progression (Murdock et al., 2021a).

Interestingly, NK cells contribute to ALS progression in a sex and age dependent manner. In SOD1G93A mice, NK depletion extended survival in female but not male mice (Murdock et al., 2021a). Moreover, male mice had higher levels of microglia in the CNS which was decreased upon NK depletion. In ALS subjects, a correlation between NKG2D or NKp46 and ALSFRS-R was reported in older patients while a correlation between NKp30 and ALSFRS-R was observed in women, suggesting age and gender specific activation patters of NK cells. Although these data suggest immune responses may be based on sex and age affect the progression of ALS, the underlying mechanisms causing these variations remain unknown. Nevertheless, numerous reports also imply that hormones can directly affect immune responses, including NK cells, and since plasma levels of testosterone and estrogen differ between men and women and change with age or the onset of menopause, sex hormones are the most likely cause of the observed alterations (Murdock et al., 2021a).

2.5 NKT cells

NKT cells are a subset of T cells that can recognize and respond to glycolipid antigens presented by CD1d molecules (Kawano et al., 1997). These cells are primarily found in the liver and are known for their role in regulating immune responses. In neuroinflammation, NKT cells are believed to play a crucial role due to the high lipid content in the CNS (Halder et al., 2007). Research has shown that the numbers of NKT cells are altered in several autoimmune diseases (van der Vliet et al., 2001; Hammond and Kronenberg, 2003; Grajewski et al., 2008). However, the exact role of NKT cells in other neurodegenerative diseases is still not well understood. Rentzos and colleagues have revealed that NKT levels are increased in peripheral blood of ALS patients (Rentzos et al., 2012). In an *in vivo* ALS model, mSOD1 mice, it was shown that the number of NKT cells was increased in the CNS as well as in lymphoid organs (Finkelstein et al., 2011). In this study, administration of α-galactosyl ceramide analogue PBS57 prolonged the survival of mSOD1 mice and alleviated the disease. The lipid antigen PBS57 also decreased the number of NKT cells in addition to hampering their responses. These findings indicate that targeting NKT cells may be a novel aspect in ALS treatment (Finkelstein et al., 2011). However, it should be noted that the therapeutic effect of NKT cell inhibition in ALS is not confirmed with clinical studies yet. Further research is needed to determine the potential of NKT cell-targeted therapies in the treatment of neurodegenerative diseases.

2.6 Neutrophils

Neutrophils are the most abundant population of leukocytes and play a role in inflammation as well as various autoimmune and inflammatory diseases (Németh et al., 2020). The role of neutrophils in ALS pathogenesis is reported to be controversial: some studies suggest that neutrophils have predominantly pro-inflammatory roles in disease pathogenesis and lead to disruption of the blood brain/spinal cord barrier (Weiss, 1989; Garbuzova-Davis and Sanberg, 2014), while other studies suggest that these cells play a role in neuroprotection and in repairing damaged neurons (Butterfield et al., 2006; Kim and Moalem-Taylor, 2011; Kurimoto et al., 2013). However, there are certain studies addressing that neutrophil to monocyte or lymphocyte ratios may serve as potential biomarkers in ALS.

Various studies indicate an increase in neutrophil percentages in ALS (Desport et al., 2001; Banerjee et al., 2008; Keizman et al., 2009; Chiò et al., 2014; Murdock et al., 2016). As the disease progresses, the ratio of neutrophils to monocytes was found to increase significantly, suggesting that this ratio might be considered as a predictor of the disease course (Murdock et al., 2016). In a more recent study, Leone et al. (2022) investigated the relationship between neutrophil-to-lymphocyte ratio (NLR) and ALS progression rate as well as survival

and concluded that NLR may serve as a low cost, fast, and easy biomarker for assessing the disease course. It was suggested that prospective studies are required to elucidate the changes in NLR during the disease progression prior to proposing it as a biomarker in monitoring ALS. Noteworthy, in this study, the patients were not classified according to the genetic background of the disease. Wei et al. (2022) investigated the correlation between NLR and ALS progression in sALS patients by assigning the patients into three groups according to their NLR values and revealed that patients with high NLR had lower ALSFRS-R scores, faster disease progression rates, and older disease onset age. In line with the study published by Leone et al. (2022), these results also confirm that NLR may aid in predicting the disease progression and survival in sALS patients.

In terms of surface proteins expressed on neutrophils, Murdock et al. (2016) reported that the percentage as well as the number of $CD16^{-}$ monocytes along with CCR3 and CCRL2 were decreased in ALS patients, however these findings did not correlate with the ALSFRS-R score. Another cell surface receptor that plays role in neutrophil chemotaxis and neuroinflammatory responses is CXCR2, which was previously found to be overexpressed in a specific subset of ALS patients as well as SOD1G93A mice at symptomatic stages (Aronica et al., 2015; Morello et al., 2017). Neutrophils may also affect other immune cell populations' responses as well: cathepsin G and elastase released by these cells can promote NK cell cytotoxicity (Costantini and Cassatella, 2011). Similar to NK cells, neutrophils also have a sex-specific effect on disease survival, and the crosstalk between these two components of innate immune system can affect disease progression (Murdock et al., 2021b).

2.7 Mast cells

Being a cellular component of the innate immune system, mast cells are differentiated from hematopoietic myeloid precursors, and are found in all vascularized tissues including brain (Kovacs et al., 2021). Precursors of these cells are recruited to the tissues through a trans-endothelial passage and maturate in the local tissue microenvironment. Mast cells are one of the first cells to be activated in response to tissue damage, releasing mediators and enzymes (Abonia et al., 2005; Wernersson and Pejler, 2014). Mast cells can release cytokines, chemokines, leukotrienes, proteases, as well as bioactive polyamines, and play many important roles in pathogen clearance, allergic reactions, and intestinal cancer (Shea-Donohue et al., 2010).

Trias and coworkers revealed significant infiltration of neutrophils and degranulating mast cells in the skeletal muscles of ALS patients (Trias et al., 2018). These cells can interact with each other, muscle fibers, and motor plates, implying coordinated neuroinflammation that is associated with neuromuscular synapse denervation and muscular atrophy. Also, these cells are highly localized around neuromuscular junctions and along degenerating axons of ventral roots and sciatic nerves (Trias et al., 2018). In ALS, mast cells can cross the blood-spinal cord barrier and release various mediators including neuropeptides, proteases, cytokines, and histamine upon degranulation, leading to local neuroinflammation and dysregulated neuronal function (Jones et al., 2019).

In human ALS subjects, the number of mast cells are reported to increase in the quadriceps muscles. Furthermore, the positive correlation between the number of mast cells and neutrophils suggests that these cells act in a very complex and coordinated manner. Mast cells are recruited in response to motor neuron injury, while on the other hand, they can trigger the recruitment of neutrophils (Chen et al., 2001; Wezel et al., 2015). In patients, the density and size of mast cells are reported to be significantly greater compared to controls. Moreover, in ALS, mast cells are reported to localize near muscle fibers while in healthy controls, they are observed around blood vessels (perivascular localization).

Degranulation of mast cells in the muscles of ALS patients indicates multiple responses at the local level mediated by the release of cytokines, proteases, trophic factors, and vasoactive mediators (Krystel-Whittemore et al., 2015). In healthy individuals, mast cells take part in muscle repair. They also initiate damage to muscle fibers and motor plates, causing fibrosis and collagen deposition either directly or indirectly (Levi-Schaffer et al., 2002; Lee and Kalluri, 2010). Mast cells and neutrophils also invade the area of the endoneurium of the sciatic nerve up to the ventral roots (Trias et al., 2017). Chymase released by mast cells is a well-known chemoattractant cytokine for neutrophils that underlies the association between these two cell types (He and Walls, 1998; Tani et al., 2000). In addition to the mentioned factors, mast cells can release very different vasoactive and inflammatory mediators that exert harmful effects during the disease (Zhuang et al., 1996; Sprague and Khalil, 2009; Theoharides et al., 2012). Recently, it is reported that in both ALS patients as well as the murine models of the disease, clusters of mast cells expressing tyrosine kinase receptor c-Kit+ and other characteristic markers which lack the toluidine blue metachromasia are observed between motor neuron somas and nearby microvascular elements in the spinal cord (Jones et al., 2019). Moreover, expression of stem cell factor (SCF) is found to be overexpressed in the reactive astrocytes in ALS, which may act as a chemoattractant and lead to differentiation of mast cells. These findings suggest complex interactions between neurons, mast cells, and reactive microglia in disease pathology in addition to highlighting the potential usage of tyrosine kinase inhibitors in ALS.

The pathological significance of the recruitment of mast cells into the neuromuscular compartment remains unclear in ALS, although certain studies underline that chronic neuroinflammation could be a very important harmful factor (Chiu et al., 2009; Keizman et al., 2009; Martínez-Muriana et al., 2016). Overall, these studies reveal that mast cells and neutrophils are abundant along the peripheral motor pathway in ALS. Mast cells have harmful, cytotoxic effects for motor neurons, where they can be a pharmacological target of tyrosine kinase inhibitors, given that they express the c-Kit as mentioned above (Galli et al., 1993; Wernersson and Pejler, 2014; Jones et al., 2019). Pharmacological inhibition of mast cells with the drug masitinib reduces the level of motor deficit in rats, therefore implying the role of mast cells during disease progression and may be considered as an adjuvant therapy in ALS patients (Trias et al., 2017).

2.8 Astrocytes

Astrocytes are the most abundant type of glial cell in the central nervous system and are involved in many important functions, such as maintaining the blood–brain barrier, regulating neurotransmitter levels, and supporting neuronal function (Sofroniew and Vinters, 2010; Haidet-Phillips et al., 2011). In ALS, astrocytes were reported to

undergo significant changes that contribute to the disease progression by producing excessive amounts of pro-inflammatory cytokines, leading to inflammation and damage to motor neurons (Philips and Robberecht, 2011). In addition to microglia, astrocytes are considered as one of the main contributors to the cell-autonomous mechanism in ALS (Stoklund Dittlau and Van Den Bosch, 2023).

Under normal conditions, astrocytes remove excess glutamate from the synaptic cleft via glutamate transporters. However, in *in vivo* ALS models as well as in ALS patients, the dysfunction of the glutamate transporter-2 (EAAT-2) leads to decreased uptake of glutamate from astrocytes, which in turn affects the function of motoneurons (Howland et al., 2002; Dunlop et al., 2003; Pardo et al., 2006; Papadeas et al., 2011). It has been shown that ALS astrocytes harbor mitochondrial dysfunction (Stoklund Dittlau and Van Den Bosch, 2023), can release inflammatory molecules and mediators such as leukotrienes, prostaglandins, nitric oxide (NO), and NAD(P)H-dependent oxidase NOX2 (Hensley et al., 2006; Marchetto et al., 2008; Haidet-Phillips et al., 2011), and can induce neuronal death by necroptosis (Re et al., 2014; Figure 3). Recent studies also reveal that exosomes released from mSOD1 astrocytes contain mutant SOD1 and have dysregulated miRNA profile that contributes to ALS pathology (Basso et al., 2013; Barbosa et al., 2021). Upregulated miR-155 was reported in ALS mice models in addition to fALS and sALS patients (Cunha et al., 2018). On the contrary, the decreased miR-494-3p release of C9ORF72 astrocytes led to neuronal network damage (Varcianna et al., 2019). Dying neurons also release certain miRNAs including miR-218 that downregulates glutamate transporter-1 that supports reactive astrocytes (Hoye et al., 2018).

Astrocytes have also been shown to support the survival and function of motoneurons as they release neurotrophic factors such as BDNF and ciliary neurotrophic factor (CNTF); in addition, these cells can provide energy substrates which are critical for normal neuronal functions (Moore et al., 2011; Allen and Lyons, 2018). However, Vargas and Johnson (2010) reported that while neurotrophic factors in mice slow the progression of ALS, they fail to provide neuroprotection in humans.

Besides their interactions with neurons, astrocytes can also modulate microglial responses as in the early stages of ALS as in the early stages of the disease, Nuclear factor kappa B (NF-κB) activation in astrocytes reside in the spinal cord can promote anti-inflammatory microglial activity while in later stages of the disease, prolonged activation of this pathway aggravates immune responses that results in pro-inflammatory microglial responses (Ouali Alami et al., 2018). According to our current knowledge, it is clear that astrocytes play important roles in ALS, although the sequence of events that lead to astrocyte dysfunction is still not fully elucidated (Liu and Wang, 2017).

In conclusion, astrocytes play a critical role in the pathogenesis of ALS. Dysfunctional astrocytes can contribute to inflammation, glutamate toxicity, and the formation of protein aggregates, all of which are key features of the disease. Further research on the role of astrocytes in ALS may lead to the development of new therapeutic approaches for this devastating disorder (Peric et al., 2017).

2.9 Microbiome

The microbiome is a collection of microorganisms that live within and on the human body and play an important role in human health. Recent studies suggest that alterations in the gut microbiome may be involved in the pathogenesis of several neurological diseases. A growing body of evidence suggests that dysbiosis, or an imbalance of the gut microbiome, may contribute to the development and progression of ALS.

Recently, Blacher and coworkers reported that ALS-prone Sod1 transgenic mice had alterations in their gut microbiome compared to healthy mice (Blacher et al., 2019). Wu et al. (2015) reported disrupted intestinal intercellular junction in SOD1G93A mouse model in addition to a decrease in butyrate-producing bacteria prior to the symptomatic stage. Zeng et al. (2020) reported alteration in the composition of the gut microbiota in addition to the metabolic products in ALS patients. However, in another study by Brenner and coworkers, it was found that ALS patients do not have a significantly different microbiome in terms of diversity and quantity compared to healthy controls, indicating the requirement of further research in order to reveal the connection between microbiome and ALS (Brenner et al., 2018).

The mechanisms by which the gut microbiome may contribute to ALS pathogenesis are not fully understood, but there is evidence that alterations in the gut microbiome may lead to increased gut permeability and the release of microbial toxins, which can trigger immune responses and inflammation that could contribute to the degeneration of motor neurons (Martin et al., 2022). In summary, there is emerging evidence suggesting that alterations in the gut microbiome may play a role in the pathogenesis of ALS. Further research is needed to fully understand the mechanisms underlying this relationship and to explore the potential for microbiome-targeted therapies for ALS.

3 The role of adaptive immunity in ALS

3.1 CD4$^+$ T cells

CD4 T cells, also known as helper T cells, play a crucial role in orchestrating and regulating the immune response in ALS. These cells show several subsets with distinct functions: Th1, Th2, Th17 cells, and regulatory T cells. Th1 and Th17 subsets show evident pro-inflammatory characteristics releasing IL-6, IL-17, IL-21, IL-22, IL-23, IFN-γ, and TNF-α, while Th2 and regulatory T cells (T_{regs}) show anti-inflammatory characteristics releasing IL-4, IL-10, and TGF-β (Motataianu et al., 2020).

In comparison with the healthy controls, ALS patients were reported to have increased levels of activated CD4$^+$ T cells in CSF, which have an essential role in the early stage of the disease (Henkel et al., 2006; Beers et al., 2008; Chiu et al., 2008) (Rolfes et al., 2021). However, as the disease progresses, Th1 cells begin to exert their harmful effects, and elimination of these cells has been suggested as an effective approach for extending survival (Shao et al., 2013). In addition, the increase in Th1 cells is accompanied by a decrease in Th2 cells (Jin et al., 2020).

CD4$^+$ T cells were observed at the sites of motoneuron injuries in mSOD1 transgenic mouse models and reported to promote neuroprotection and slow down the course of the disease (Motataianu et al., 2020). Role of T cells were also investigated by crossing mSOD1 mice with RAG2−/− mice, which are characterized by a lack of T and B cells, and it was observed that CD4+ T cells contribute to prolonging

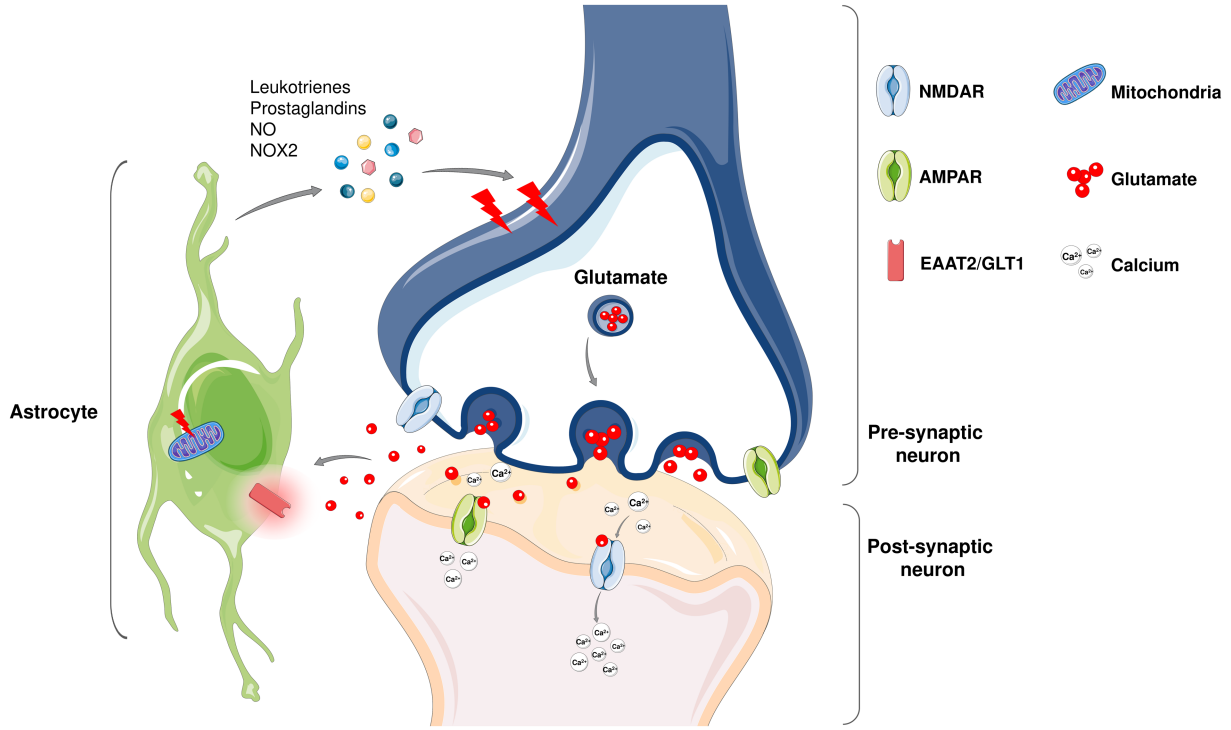

FIGURE 3
Even though ALS is considered as motor neuron disease, not only neurons but glial cells including astrocytes also play a role in the non-cell autonomous disease pathology (Stoklund Dittlau and Van Den Bosch, 2023). Under physiological conditions, astrocytes are involved in the modulation of neuronal synapse plasticity; ion and metabolic homeostasis; cellular communication; supporting blood–brain barrier and providing structural support. In healthy tissues, non-activated astrocytes remain immobile and support neuronal homeostasis while upon damage, they activate and initiate an immune response to fight against the harmful agents together with microglia. In neurodegenerative diseases including ALS, an abnormal astrocyte reactivity that contributes to neuronal death is observed. Being the most abundant excitatory neurotransmitter in the nervous system, glutamate is found at high concentrations in pre-synaptic nerve terminals where it binds to receptors such as α-amino-3-hydroxy-5-methy-4-isoxazolepropionic acid (AMPA) and *N*-methyl-D-aspartate (NMDA) receptors. Since high levels of glutamate may lead to a lethal increase in intracellular calcium astrocytes play a protective role in glutamate clearance from the synaptic cleft via excitatory amino acid transporters (EAATs). Among five EAATs identified, EAAT-1 and EAAT-2 are primarily expressed on astrocytes (Ng and Ng, 2022). Dysregulation of the human counterpart of GLT1, EAAT-2 (Rimmele and Rosenberg, 2016) expression has been shown to be altered in ALS and reported to contribute increased glutamate levels in the cerebrospinal fluid of ALS patients. Moreover, astrocytes produce inflammatory mediators that contribute to neuronal death (Stoklund Dittlau and Van Den Bosch, 2023). Mitochondrial dysfunction in astrocytes also promote neuronal death in ALS (Zhao et al., 2022).

survival (Beers et al., 2008). However, the situation is more complicated, considering that $CD4^+$ T cells with neurotoxic (Th1, Th17) and neuroprotective (Th2, T_{reg}) phenotypes (Tiemessen et al., 2007; Beers et al., 2011) enter direct interaction and communication with microglia cells and macrophages. Accordingly, during the early stage of the disease, the anti-inflammatory cytokines released by Th2 cells in addition to T_{regs}, IL-4 and IL-10 were increased (Tiemessen et al., 2007; Beers et al., 2011). Th2 cells also release neurotrophic factors such as TGF-β, BDNF, and GDNF, which are inversely correlated with the course of the disease (Motataianu et al., 2020). During this phase, regulatory T cells contribute to neuroprotection by interacting with microglia; however, as the disease progresses, the neuroprotective T_{regs}-M2 phenotype changes to the Th1-M1 neurotoxic one, whereby Th1 cells release the pro-inflammatory cytokine IFN-γ (Chiu et al., 2008). Microglia and Th1 cells can secrete TNF-α, inhibiting regulatory T cells' function through their transcription factor FOXP3 (Nie et al., 2013).

Previously, it has been shown that peripheral T cell counts are increased in a time-dependent manner in ALS (Murdock et al., 2017) and pro-inflammatory T cell populations are more prominent (Jin et al., 2020). The decrease in the $CD4^+$ T cell levels, on the other hand, is in correlation with ALS progression and it was suggested that the reduced T cell amount may represent the decreased neuroprotection during ALS progression (Murdock et al., 2017). Previously, Rofles et al. reported elevated levels of $CD4^+$ T cells in CSF (Rolfes et al., 2021). On the other hand, decreased relative numbers $CD3^+$ caused by the net decreased by $CD4^+$ cell number was reported in the peripheral blood of ALS patients compared to healthy controls (Ramachandran et al., 2023). Another study reported that while Th2-differentiated $CD4^+$ central memory T cells were negatively associated with the risk of death in ALS patients, $CD4^+$ effector memory re-expressing CD45RA T cells were positively correlated with risk of death (Cui et al., 2022).

Th17 cells play an important role in autoimmune diseases, and the role of these cells in ALS is becoming increasingly recognized. Investigating immune profiles of ALS patients, Jin and coworkers reported that T cell subtypes in peripheral blood shift towards Th17 in addition to Th1 phenotypes (Jin et al., 2020). Moreover, a moderate negative correlation between Th17 cells and ALSFRS-R was detected. The levels of IL-17 and IL-23 in CSF and serum have been found to be significantly increased in ALS patients compared to patients with non-inflammatory neurodegenerative diseases (Rentzos et al., 2010).

Although the levels of these cytokines did not correlate with the progression of the disease, they are considered markers of inflammation and may be involved in the pathogenesis of ALS in humans. The increase in the cytokine IL-17 may reflect the activation of Th17 cells, suggesting that these cells may play a significant role in ALS pathogenesis. Moreover, in a recent study, it is revealed that motor neurons express IL17 receptors, and IL-17 can directly exert cytotoxicity on these cells which can be rescued by IL17 neutralization or anti-IL17RA treatment (Jin et al., 2021). It should be noted that measuring cytokine levels in the serum may have limitations, and it may not reflect the pathological processes occurring in the brain due to the short half-life of cytokines and their binding to the molecules in the bloodstream. Therefore, further research is needed to fully understand the role of Th17 cells and cytokines in the pathogenesis of ALS.

3.2 CD8$^+$ T cells

CD8$^+$ T cells, also known as cytotoxic or cytolytic T cells, are a crucial component of the adaptive immune system, and their role in the pathogenesis of ALS is an area of active research. In ALS, CD8$^+$ T cells are thought to be involved in the direct killing of motor neurons through the MHC class I complex, as well as by secreting granzymes and perforins. Studies have found that the number of CD8$^+$ T cells increases as ALS progresses, and these cells produce IFN-γ, which affects CD8$^+$ T cells' survival and the killing of motoneurons (Andjus et al., 2009; Bataveljic et al., 2014; Coque et al., 2019). According to Coque et al. (2019) interaction between motor neurons and CD8+ T cells rely on the association between self-antigens and MHC class I molecules, though these autoantigens are still under investigation, and recent data suggest a clonal expansion of CD8+ T cells against an unknown antigen in fALS cases bearing mutation in the SETX gene. Conversely, CD8+ T cells expressing HLA-DR were reported to be increased in the blood and CSF of patients with sALS. Thus, it has been proposed that an ALS-associated antigen may initiate T-cell mediated autoimmune processes (Rodrigues Lima-Junior et al., 2021). In this context, Ramachandran et al. (2023) investigated reactivity of CD8+ T cells of ALS patients and their healthy counterparts against ten TDP43-derived peptides, However, the authors revealed that TFP43 is a weak autoantigen, and the investigations aiming to elucidate the autoantigens continues.

In a study published by Kaur et al. (2022), CD8+ T cells of ALS patients had increased CD28 and CCR7 expression in contrast to decreased IFN-γ receptor, which may be due to the constitutive IFN-γ expression. Promoting not only activation of the immune cells but also regulating the survival and function of NK and CD8+ T cells, absence or decrease in IFN-γ receptors on CD8+ T cells is an important finding which may lead to aforementioned increase in their lifespan and cytotoxic capacity to kill motoneurons.

CD8+ T cells were previously observed in the spinal cord of both ALS patients in addition to ALS SOD1G93A mouse models, and an *in vivo* study revealed that these cells infiltrate CNS at the symptomatic stage where selective ablation of CD8+ T cells in mice decreased spinal motoneuron loss (Ramachandran et al., 2023). Rolfes et al. (2021) reported an increase in CD8+ T cell frequencies expressing HLA-DR in peripheral blood and CSF in comparison with the control group. In this study, authors also underlined that T cell activation observed in the periphery coincided with increased intrathecal T-cell activation, suggesting that CD8+ T cells may contribute to blood/CSF-barrier dysfunction.

Although there is still not enough detailed data on the role and molecular mechanisms of CD8$^+$ T cells in ALS, future studies should aim to elucidate these mechanisms and discover potentially new immunological mechanisms of CD8$^+$ T cells in the etiopathogenesis of ALS, including their interactions with CD4$^+$ T cells and cells of innate immunity. Understanding the role of CD8$^+$ T cells in ALS could provide new therapeutic targets for treating this devastating disease.

3.3 T regulatory cells

T regulatory cells (T_{regs}) are a subpopulation of T cells that play a crucial role in maintaining immune homeostasis and self-tolerance. They regulate the activity of other immune cells, such as T helper cells and cytotoxic T cells, by suppressing their activation and proliferation (Sakaguchi et al., 2010). Clinical studies on the potential neuroprotective function of T cells have revealed evidence of the protective function of CD4+FOXP3+ regulatory T_{regs}, with the quantity of Treg cells in the blood of ALS patients negatively correlated with the rate of disease progression (Henkel et al., 2013; Rolfes et al., 2021). Compared to healthy controls, T_{regs} increase at early, slowly progressing stages of ALS, and then their numbers as well as their immunosuppressive functions decline (Beers et al., 2017). According to Henkel and colleagues, T_{reg} numbers along with their FOXP3 protein expression were reduced in patients with rapidly progressing ALS (Henkel et al., 2006). In addition, authors have reported a reduction of the FoxP3 protein in post-mortem spinal cord of ALS patients with rapid progression, a GATA3 increase in patients with slower progression, suggesting that the decline in FOXP3 levels may be used as a marker for rapid progression. The reduction in T_{reg} cell number and function, along with the pro-inflammatory phenotype, contributes to the aberrant immune response and neuroinflammation observed in ALS. In a recent study, high proportion of activated T_{regs} in the peripheral blood of ALS patients were shown to be linked with better survival (Yazdani et al., 2022).

Even though these data underline the crucial role for T_{reg} cells in ALS pathogenesis, the therapeutic potential of T_{reg} cells in ALS highlights the need for further research in this area as clinical trials targeting these cells in ALS is still rare. In a phase 2 randomized trial, low-dose IL-2 has been reported to increase the percentage of T_{regs} (Camu et al., 2020). In another study, it was discovered that the infusion of expanded autologous T_{regs} revealed enhanced suppressive activity and slowed the disease progression (Thonhoff et al., 2018a,b). Further studies, on the other hand, are still needed in order to develop more effective cellular therapies including administration of T_{regs} in ALS.

3.4 The role of humoral immunity – antibodies in ALS

ALS patients are reported to have increased serum autoantibody levels compared to healthy controls (Provinciali et al., 1988). One study indicated increased levels of IgG and IgM, where the severity of the disease is correlated with higher antibody levels (May et al., 2014).

Additionally, ALS patients with longer survival were reported to have IgM antibodies against modified, oxidized SOD1 protein compared to human control subjects (van Blitterswijk et al., 2011). Bataveljic et al. (2014) reviewed the humoral immunological markers, such as circulating immune complexes (CICs) and immunoglobulins. Saleh et al. (2009) assessed the humoral immune response during disease progression over 6 months, finding increased levels of CICs and IgG in the sera of ALS patients at the initial stage of the disease. After 6 months, in the same group of ALS patients, CICs were reduced to control levels, whereas IgG was increased compared to those in human control subjects. The presence of CICs is emphasized in various studies (Tavolato et al., 1975; Oldstone et al., 1976; Bartfeld et al., 1982).

Interestingly, the literature data differ concerning the levels of IgG in the sera of ALS patients. Some data suggest elevated IgG levels and normal IgM levels (Provinciali et al., 1988; Apostolski et al., 1991; Duarte et al., 1991; Saleh et al., 2009), while others do not detect any alterations in Ig levels (Bartfeld et al., 1982) or even detect a decrease in immunoglobulin levels (Zhang et al., 2005). Discrepant results could be due to different criteria for selecting ALS patients with different stages of the disease. Even in a study by Apostolski et al. (1991), it was shown that there is a significantly higher titer of IgG in the sera and CSF of patients with ALS (this study also showed a significantly increased mean value of the C4 component of the complement, as well as a significantly reduced value of THC – the total hemolytic titer complement). The results regarding the studies investigating the involvement of humoral immunity in ALS are rather inconsistent: in one study, no differences were found between the levels of IgG, IgM, IgA, in addition to the complement component C3 in ALS patients and controls (Bartfeld et al., 1982), whereas in another study, elevated mean serum IgG values were observed in a small group of ALS patients (Tavolato et al., 1975). Yet another study indicated increased levels of IgA and IgE in the sera of ALS subjects (Appel et al., 1986).

Numerous autoantibodies have been observed in ALS patients, such as antibodies against ganglioside GM1 (van Schaik et al., 1995) which localize near the nodes of Ranvier, and it is suggested that they are patient-specific for ALS patients with affected lower motor neurons (Pestronk et al., 1988). One study showed that the most frequently increased levels of anti-AGM1-gangliosides are in the sera of up to 1/3 of patients with ALS, whereas in the cerebrospinal fluid, the frequency of anti-GM1-gangliosides is higher compared to anti-AGM1-gangliosides and anti-sulfatides (Niebroj-Dobosz et al., 1999). This study revealed that ALS and other neurodegenerative diseases, as well as various forms of neuropathies such as non-sensory neuropathy, have a high concentration of anti-sulfatide antibodies. Additionally, in rare cases of ALS patients, elevated levels of antibodies against acetylcholine receptors were found (Mehanna et al., 2012). Autoantibodies targeting calcium channels (La Bella et al., 1997) and the Fas protein were also observed (Yi et al., 2000; Sengun and Appel, 2003), in addition to the antibodies against Low-Density Lipoprotein Receptor-Related Protein 4, which is essential for the development and function of the neuromuscular synapse (Tzartos et al., 2014). The Fas molecule, or CD95, is a membrane receptor that belongs to the TNF family and has a primary role in the transduction of programmed cell death (apoptosis) signals. It is highly represented in tissues and organs such as thymocytes, hepatocytes, kidneys, and the heart (Sengun and Appel, 2003).

Previously, it was reported that 25% of patients with sporadic ALS and 22% of patients with familial ALS had extremely high levels of anti-Fas antibodies. These high levels were observed not only in ALS but also in other neurodegenerative diseases. However, no relationship between anti-Fas antibody levels and disease duration or stage was found in ALS (Sengun and Appel, 2003). Another study has reported elevated levels of autoantibodies against neuronal cytoskeleton proteins (especially neurofilaments) in ALS patients, particularly during the later stages of the disease. Antibodies against light (NF-L) and heavy chain (NF-H) were found to be good surrogate markers of treatment response (Lu et al., 2011, 2012). However, anti-NF-L Abs were also elevated in other neuroinflammatory and neurodegenerative diseases such as multiple sclerosis (Fialová et al., 2009, 2012). The uniform distribution of antibodies to axonal cytoskeletal antigens in various biological fluids was shown to be a promising platform for discovering new biomarkers and developing immunomodulatory therapies not only for ALS but various neurological diseases (Fialová et al., 2009).

Immunoglobulins can induce pathophysiological processes at a nerve-muscle synapse by passive transfer, thus they can induce immune-mediated mechanisms in ALS pathogenesis (Bataveljić et al., 2011). When rodents were treated with IgG from ALS patients, the treatment led to an increase in intracellular calcium concentration, degenerative structural changes, and the induction of plasticity in nerve-muscular synapses (Uchitel et al., 1988; Engelhardt et al., 1995; Fratantoni et al., 2000; Pullen and Humphreys, 2000; Pullen et al., 2004; Pagani et al., 2006). The ALS IgGs have proven to suppress KCl-induced Ca^{2+} transients via selectively action on P/Q-type calcium channels *in vitro* (Andjus et al., 1996) in addition to exerting indirect effects (via phospholipase C) on N-type calcium channels (Pagani et al., 2006). Moreover, ALS IgGs can promote vesicle mobility and alter cytosolic Ca2+ homeostasis in cultured rat astrocytes (Stenovec et al., 2011; Milošević et al., 2013), induce glutamate release from primary rat hippocampal neurons (Andjus et al., 1997) and enhance oxidative stress while inducing antioxidant responses in a rat microglial cell line (Milošević et al., 2017).

Intravenous immunoglobulin G (IVIg) has been investigated as a potential treatment for ALS to its ability to modulate the immune response and its potential for protecting motor neurons from degeneration. Several clinical studies have been conducted to evaluate the safety and efficacy of IVIg in ALS patients. Both Meucci and coworkers and Dalakas and coauthors found that IVIg treatment had no therapeutic role on the symptoms related with ALS and did not slow the disease progression (Dalakas et al., 1994; Meucci et al., 1996). However, some clinicians still use IVIg in certain cases of ALS, particularly in patients with evidence of autoimmune dysregulation (Burrell et al., 2011). Further studies are needed to clarify the potential role of IVIg in the treatment of ALS.

3.5 Cytokines

Cytokines are small proteins, also known as humoral factors, secreted by cells that interact with other cells. Cytokines have three modes of action - autocrine (acting on themselves), paracrine (acting

on nearby cells), and endocrine (acting over long distances) (Zhang and An, 2007). There are studies indicating the increase of both pro-inflammatory and anti-inflammatory cytokines in sera of *in vivo* ALS models as well as in ALS patients (Mitchell et al., 2009). In this context, the involvement of the cytokines IL-1ß, IL-6, IL-12, IL-15, IL-17, and IL-33 in ALS will be discussed.

3.5.1 Interleukin-1β and-18

Members of the IL-1 family, IL-1β, is synthesized in its inactive form and activated by caspase-1 in response to various "danger" signals which are recognized by cytosolic inflammasome complexes (Martinon et al., 2009). Inflammasomes are defined as multimeric protein complexes that orchestrate caspase-1-mediated inflammatory responses including maturation and secretion of inflammatory cytokines IL-1β and IL-18, and eventually inflammatory cell death, pyroptosis (de Zoete et al., 2014).

The presence of active caspase-1 in the spinal cord and cerebral spinal fluid of ALS patients and ALS models of mice have been recognized more than two decades ago, and *in vivo* studies have revealed that caspase-1 or IL-1β depletion or IL-1β inhibition resulted in prolonged survival without affecting disease onset (Izecka et al., 2001). This study also suggested the involvement of caspase-1 activation in ALS pathogenesis. Based on the results of preclinical studies (Meissner et al., 2010; de Zoete et al., 2014), Maier et al. investigated the safety and efficacy of IL-1β antagonist Anakinra (ANA) (Maier et al., 2015). Authors reported that ANA is well tolerated and can be considered safe in ALS patients. However, ANA administration failed to inhibit the disease progression in comparison with the control group as measured by the ALSFRSr, and in addition, 94% of the ANA group developed anti-ANA antibodies. On the other hand, Italiani and coauthors reported that IL-18 is the only cytokine from the IL-1 family that correlates with ALS and indicated that further investigations are required to define if upregulation of IL-18 in ALS is either a consequence, or one of the causes leading to the disease pathology (Italiani et al., 2014). Both IL-1β and IL-18 are the products of NLR Family Pyrin Domain Containing 3 (NLRP3) inflammasome complex activation. In fact, activation of NLRP3 inflammasome complex has been previously reported in both microglia obtained from mouse models of ALS as well as ALS patients' brain tissue samples, and TDP43 has been shown to be activate microglial NLRP3 (Johann et al., 2015; Zhao et al., 2015; Kadhim et al., 2016). In a more recent study performed with monocyte-derived microglia-like cells obtained from ALS patients, the cells were reported to have abnormally aggregated TDP43 in the cytoplasm, which is accompanied by an increase in IL-18 levels along with IL-8, TNF-α and TGF-β (Quek et al., 2022). However, when considering the involvement of NLRP3 inflammasome activation in ALS (Deora et al., 2020), more studies focusing on IL-18 may provide better insights if blocking inflammasomes may be a beneficial strategy in ALS treatment.

3.5.2 Interleukin-6

IL-6 is one of the first cytokines which is found to be elevated in several neurodegenerative diseases including ALS (Sekizawa et al., 1998). Ehrhart et al. reported significant elevation of IL-6 levels in the blood samples in ALS patients; moreover, normalization of IL-6 along with IL-5 at the follow up was found to be associated with decreased IL-2 and increased IL-8 levels (Ehrhart et al., 2015), indicating that different humoral factors are involved in different inflammatory responses during the disease course. Similarly, Lu and coauthors reported an IL-6 increase in certain subgroups of ALS patients including male patients in contrast to females, patients with spinal onset, patients with slow progression, and patients receiving riluzole treatment (Lu et al., 2016). Interestingly, a correlation between IL-6 and the ALSFRS-R was reported in another study (Quek et al., 2022). On the other hand, a more recent study revealed that serum IL-6 levels are negatively correlated with ALSFRS-R in patients carrying IL6R358Ala variant (Wosiski-Kuhn et al., 2021).

Targeting IL-6 signaling has proposed as a therapeutic strategy in ALS: in a clinical trial, IL-6 receptor blocker tocilizumab (Actemra) was reported to decrease C-reactive protein (CRP) levels in plasma and CSF, in addition to being well tolerated and safe in ALS patients (Milligan et al., 2021). However, further studies are needed to conclude its benefits on the disease treatment.

3.5.3 Interleukin-12 and-15

IL-12 and IL-15 are pro-inflammatory cytokines that are increased in the serum and cerebrospinal fluid of ALS patients. However, it has not been demonstrated that these interleukins have a mutual dependence on the duration of the disease (Rentzos et al., 2010). IL-12 is a heterodimer synthesized by monocytes, macrophages, dendritic cells, and microglia in response to various immunological and infectious signals (Ma and Trinchieri, 2001). Its role is to stimulate the proliferation and differentiation of T cells and the production of pro-inflammatory cytokines such as IFN-γ and TNF-α (Li et al., 2003). Monocytes produce IL-15 similarly to IL-12, as do macrophages, dendritic cells, and glial cells (Grabstein et al., 1994; Doherty et al., 1996; Lee et al., 1996; Jonuleit et al., 1997). IL-15 promotes the proliferation of T cells, induces NK cells, cytotoxic cells, as well as cells of humoral immunity by inducing the maturation of B cells and the secretion of antibodies (Carson et al., 1994). These data suggest that IL-12 and IL-15, which act through the Th1 response, may be associated, and involved in the pathophysiological mechanisms of ALS (Rentzos et al., 2010).

3.5.4 Interleukin-17

According to literature, IL-17A regulates the responses of central nervous system resident cells, boosts the neuroinflammatory response, and contributes to the pathogenesis of neurodegenerative diseases. However, there is still debate and ambiguity surrounding the function of TH17/IL-17A in neurodegenerative diseases (Fu et al., 2022). IL-17 is produced by the Th17 cells and is implicated in various autoimmune and inflammatory diseases, and studies have shown that IL-17 may play a role in the pathogenesis of ALS. Along with IL-23, IL-17 levels were significantly increased in the serum and CSF samples of ALS patients, however the levels of the cytokines did correlate with the disease duration, disability scale or the subtype of the disease (Rentzos et al., 2010). Chen and coworkers indicated a significant association between ALS and IL17 levels (Carson et al., 1994). Fiala and coauthors reported IL17A$^+$ cytotoxic T cells and mast cells in the spinal cords of ALS patients (Fiala et al., 2010). Regarding *in vivo* ALS models, IL-17A levels were found to be gradually increasing with age in SOD1G93A mice (Noh et al., 2014). More recently, Jin and coauthors reported the potential therapeutic benefits of anti-IL-17 treatment to alleviate neurodegeneration observed in ALS (Jin et al., 2021). Even

though these findings suggest that IL-17 may be a potential therapeutic target for the treatment of ALS, currently there are no clinical data investigating the effect of targeting Th17 cells or IL17 in ALS.

3.5.5 Interleukin-33

IL-33 is a cytokine that functions as an alarmin, which is released from damaged tissue. This cytokine is one important cytokine responsible for the shift in T cell responses and stimulates innate type 2 immune cells to produce Th2 cytokines (Korhonen et al., 2019). IL-33 receptor, ST2, can exist in the membrane or soluble form. In a study evaluating the levels of IL-33 in addition to its soluble receptor revealed significantly reduced levels of IL-33 and elevated levels of sST2 in ALS patients (Lin et al., 2012). The reason for the reduced levels of IL-33 is that motor neurons in ALS die through programmed cell death of the apoptosis type, and IL-33 is degraded by the action of the executioners of apoptosis, i.e., by the action of caspases (Sathasivam et al., 2001). It is also known that the sST2 receptor can act as a positive or negative feedback regulator, suppressing or stimulating cytokine expression. Furthermore, one study suggested that the sST2 receptor acts as a degradation receptor by inhibiting IL-33-mediated signaling (Miller, 2011). However, the regulation of sST2 receptor levels has not been fully clarified (Lin et al., 2012).

In vitro studies have suggested that instead of directly acting on neurons and astrocytes, IL-33 regulates responses of peripheral T cells (Korhonen et al., 2019). *In vivo*, long-term recombinant IL-33 treatment delayed the disease onset on female mice in a transgenic mouse model of ALS expressing SOD1-G93A while male mice remained unresponsive. These findings indicate that strategies targeting to modulate the peripheral immune system may have therapeutic potential in ALS, and the effect of the gender should be considered when designing therapeutic strategies. It should be noted that further research is required to determine the ideal method for delivering IL-33 to the CNS in order to reduce inflammation without causing adverse effects in other organs since IL-33 is a potent cytokine (Sun et al., 2021).

4 Conclusion remarks and future perspectives

This review highlights the complex interplay between neuroimmunology and neuroinflammation in the pathogenesis of ALS, which is a devastating disease that currently has no effective cure. Several points were highlighted regarding innate immunity, including the limited information available on the monocyte's role in ALS, the diversity of microglia as either neurotoxic or neuroprotective, the complex role of the complement system in ALS, and the contribution of NK cells, NKT cells, mast cells, neutrophils, and astrocytes. From the perspective of adaptive immunity, $CD4^+$T cells were identified as early disease markers possessing a neuroprotective identity, while $CD8^+$T cells were late disease markers with cytotoxic properties. The role of humoral immunity, specifically IgG and IgM, needs further clarification, and the contribution of autoantibodies to ALS neurodegeneration requires better understanding.

Our review suggests that a more comprehensive understanding of the neuroimmunology and neuroinflammatory aspects of ALS will pave the way for the development of new therapeutic strategies for this devastating disease. Moving forward, future research should focus on exploring the potential of NKT cell-targeted therapies, identifying potential biomarkers in ALS, clarifying the role of IVIg in treatment, and further investigating the impact of alterations in the gut microbiome on ALS pathogenesis. Additionally, expanding research to include more context on adaptive immunity, $CD8^+$T cells, and autoantibodies may lead to a more complete understanding of the immune response in ALS and instate the development of new therapeutic approaches. Overall, continued research into neuroimmunology and neuroinflammation in ALS has the potential to improve patient outcomes and provide hope for those suffering from this devastating disease.

Author contributions

SM: Conceptualization, Data curation, Investigation, Visualization, Writing – original draft. BA: Conceptualization, Data curation, Investigation, Visualization, Writing – original draft. CP: Conceptualization, Data curation, Investigation, Visualization, Writing – original draft. HS: Data curation, Investigation, Writing – original draft. PA: Conceptualization, Funding acquisition, Project administration, Resources, Supervision, Writing – review & editing. GYD: Conceptualization, Funding acquisition, Project administration, Resources, Supervision, Writing – review & editing.

Funding

The author(s) declare financial support was received for the research, authorship, and/or publication of this article. The work on this publication was supported by the European Union's Horizon 2020 Research and Innovation Program under the Marie Skłodowska-Curie grant agreement No: 778405.

Acknowledgments

We kindly thank to Pervin Yanıkkaya Aydemir for carefully reading and editing the manuscript.

Conflict of interest

The authors declare that the research was conducted in the absence of any commercial or financial relationships that could be construed as a potential conflict of interest.

Publisher's note

References

Abel, A. M., Yang, C., Thakar, M. S., and Malarkannan, S. (2018). Natural killer cells: development, maturation, and clinical utilization. *Front. Immunol.* 9:1869. doi: 10.3389/fimmu.2018.01869

Abonia, J. P., Friend, D. S., Austen, W. G. Jr., Moore, F. D. Jr., Carroll, M. C., Chan, R., et al. (2005). Mast cell protease 5 mediates ischemia-reperfusion injury of mouse skeletal muscle. *J. Immunol.* 174, 7285–7291. doi: 10.4049/jimmunol.174.11.7285

Allen, N. J., and Lyons, D. A. (2018). Glia as architects of central nervous system formation and function. *Science* 362, 181–185. doi: 10.1126/science.aat0473

Andjus, P. R., Bataveljić, D., Vanhoutte, G., Mitrecic, D., Pizzolante, F., Djogo, N., et al. (2009). In vivo morphological changes in animal models of amyotrophic lateral sclerosis and Alzheimer's-like disease: MRI approach. *Anat. Rec. (Hoboken)* 292, 1882–1892. doi: 10.1002/ar.20995

Andjus, P. R., Khiroug, L., Nistri, A., and Cherubini, E. (1996). ALS IgGs suppress [Ca2+]i rise through P/Q-type calcium channels in central neurones in culture. *Neuroreport* 7, 1914–1916. doi: 10.1097/00001756-199608120-00008

Andjus, P. R., Stevic-Marinkovic, Z., and Cherubini, E. (1997). Immunoglobulins from motoneurone disease patients enhance glutamate release from rat hippocampal neurones in culture. *J. Physiol.* 504, 103–112. doi: 10.1111/j.1469-7793.1997.103bf.x

Apostolski, S., Nikolić, J., Bugarski-Prokopljević, C., Miletić, V., Pavlović, S., and Filipović, S. (1991). Serum and CSF immunological findings in ALS. *Acta Neurol. Scand.* 83, 96–98. doi: 10.1111/j.1600-0404.1991.tb04656.x

Appel, S. H., Stockton-Appel, V., Stewart, S. S., and Kerman, R. H. (1986). Amyotrophic lateral sclerosis. Associated clinical disorders and immunological evaluations. *Arch. Neurol.* 43, 234–238. doi: 10.1001/archneur.1986.00520030026007

Aronica, E., Baas, F., Iyer, A., ten Asbroek, A. L., Morello, G., and Cavallaro, S. (2015). Molecular classification of amyotrophic lateral sclerosis by unsupervised clustering of gene expression in motor cortex. *Neurobiol. Dis.* 74, 359–376. doi: 10.1016/j.nbd.2014.12.002

Auffray, C., Sieweke, M. H., and Geissmann, F. (2009). Blood monocytes: development, heterogeneity, and relationship with dendritic cells. *Annu. Rev. Immunol.* 27, 669–692. doi: 10.1146/annurev.immunol.021908.132557

Bahia El Idrissi, N., Bosch, S., Ramaglia, V., Aronica, E., Baas, F., and Troost, D. (2016). Complement activation at the motor end-plates in amyotrophic lateral sclerosis. *J. Neuroinflammation* 13:72. doi: 10.1186/s12974-016-0538-2

Banerjee, R., Mosley, R. L., Reynolds, A. D., Dhar, A., Jackson-Lewis, V., Gordon, P. H., et al. (2008). Adaptive immune neuroprotection in G93A-SOD1 amyotrophic lateral sclerosis mice. *PLoS One* 3:e2740. doi: 10.1371/journal.pone.0002740

Barbeito, A. G., Mesci, P., and Boillée, S. (2010). Motor neuron-immune interactions: the vicious circle of ALS. *J. Neural Transm. (Vienna)* 117, 981–1000. doi: 10.1007/s00702-010-0429-0

Barbosa, M., Gomes, C., Sequeira, C., Gonçalves-Ribeiro, J., Pina, C. C., Carvalho, L. A., et al. (2021). Recovery of depleted miR-146a in ALS cortical astrocytes reverts cell aberrancies and prevents paracrine pathogenicity on microglia and motor neurons. *Front. Cell Dev. Biol.* 9:634355. doi: 10.3389/fcell.2021.634355

Bartfeld, H., Dham, C., Donnenfeld, H., Jashnani, L., Carp, R., Kascsak, R., et al. (1982). Immunological profile of amyotrophic lateral sclerosis patients and their cell-mediated immune responses to viral and CNS antigens. *Clin. Exp. Immunol.* 48, 137–146.

Basso, M., Pozzi, S., Tortarolo, M., Fiordaliso, F., Bisighini, C., Pasetto, L., et al. (2013). Mutant copper-zinc superoxide dismutase (SOD1) induces protein secretion pathway alterations and exosome release in astrocytes: implications for disease spreading and motor neuron pathology in amyotrophic lateral sclerosis. *J. Biol. Chem.* 288, 15699–15711. doi: 10.1074/jbc.M112.425066

Bataveljic, D., Milosevic, M., Radenovic, L., and Andjus, P. (2014). Novel molecular biomarkers at the blood-brain barrier in ALS. *Biomed. Res. Int.* 2014:907545. doi: 10.1155/2014/907545

Bataveljić, D., Stamenković, S., Bačić, G., and Andjus, P. R. (2011). Imaging cellular markers of neuroinflammation in the brain of the rat model of amyotrophic lateral sclerosis. *Acta Physiol. Hung.* 98, 27–31. doi: 10.1556/APhysiol.98.2011.1.4

Beers, D. R., Henkel, J. S., Xiao, Q., Zhao, W., Wang, J., Yen, A. A., et al. (2006). Wild-type microglia extend survival in PU.1 knockout mice with familial amyotrophic lateral sclerosis. *Proc. Natl. Acad. Sci. U. S. A.* 103, 16021–16026. doi: 10.1073/pnas.0607423103

Beers, D. R., Henkel, J. S., Zhao, W., Wang, J., and Appel, S. H. (2008). CD4+ T cells support glial neuroprotection, slow disease progression, and modify glial morphology in an animal model of inherited ALS. *Proc. Natl. Acad. Sci. U. S. A.* 105, 15558–15563. doi: 10.1073/pnas.0807419105

Beers, D. R., Henkel, J. S., Zhao, W., Wang, J., Huang, A., Wen, S., et al. (2011). Endogenous regulatory T lymphocytes ameliorate amyotrophic lateral sclerosis in mice and correlate with disease progression in patients with amyotrophic lateral sclerosis. *Brain* 134, 1293–1314. doi: 10.1093/brain/awr074

Beers, D. R., Zhao, W., Wang, J., Zhang, X., Wen, S., Neal, D., et al. (2017). ALS patients' regulatory T lymphocytes are dysfunctional, and correlate with disease progression rate and severity. *JCI Insight* 2:e89530. doi: 10.1172/jci.insight.89530

Beirowski, B., Adalbert, R., Wagner, D., Grumme, D. S., Addicks, K., Ribchester, R. R., et al. (2005). The progressive nature of Wallerian degeneration in wild-type and slow Wallerian degeneration (WldS) nerves. *BMC Neurosci.* 6:6. doi: 10.1186/1471-2202-6-6

Blacher, E., Bashiardes, S., Shapiro, H., Rothschild, D., Mor, U., Dori-Bachash, M., et al. (2019). Potential roles of gut microbiome and metabolites in modulating ALS in mice. *Nature* 572, 474–480. doi: 10.1038/s41586-019-1443-5

Brenner, D., Hiergeist, A., Adis, C., Mayer, B., Gessner, A., Ludolph, A. C., et al. (2018). The fecal microbiome of ALS patients. *Neurobiol. Aging* 61, 132–137. doi: 10.1016/j.neurobiolaging.2017.09.023

Burrell, J. R., Yiannikas, C., Rowe, D., and Kiernan, M. C. (2011). Predicting a positive response to intravenous immunoglobulin in isolated lower motor neuron syndromes. *PLoS One* 6:e27041. doi: 10.1371/journal.pone.0027041

Butovsky, O., Koronyo-Hamaoui, M., Kunis, G., Ophir, E., Landa, G., Cohen, H., et al. (2006). Glatiramer acetate fights against Alzheimer's disease by inducing dendritic-like microglia expressing insulin-like growth factor 1. *Proc. Natl. Acad. Sci. U. S. A.* 103, 11784–11789. doi: 10.1073/pnas.0604681103

Butovsky, O., Siddiqui, S., Gabriely, G., Lanser, A. J., Dake, B., Murugaiyan, G., et al. (2012). Modulating inflammatory monocytes with a unique microRNA gene signature ameliorates murine ALS. *J. Clin. Invest.* 122, 3063–3087. doi: 10.1172/jci62636

Butterfield, T. A., Best, T. M., and Merrick, M. A. (2006). The dual roles of neutrophils and macrophages in inflammation: a critical balance between tissue damage and repair. *J. Athl. Train.* 41, 457–465.

Camu, W., Mickunas, M., Veyrune, J. L., Payan, C., Garlanda, C., Locati, M., et al. (2020). Repeated 5-day cycles of low dose aldesleukin in amyotrophic lateral sclerosis (IMODALS): a phase 2a randomised, double-blind, placebo-controlled trial. *EBioMedicine* 59:102844. doi: 10.1016/j.ebiom.2020.102844

Cardona, A. E., Pioro, E. P., Sasse, M. E., Kostenko, V., Cardona, S. M., Dijkstra, I. M., et al. (2006). Control of microglial neurotoxicity by the fractalkine receptor. *Nat. Neurosci.* 9, 917–924. doi: 10.1038/nn1715

Carson, W. E., Giri, J. G., Lindemann, M. J., Linett, M. L., Ahdieh, M., Paxton, R., et al. (1994). Interleukin (IL) 15 is a novel cytokine that activates human natural killer cells via components of the IL-2 receptor. *J. Exp. Med.* 180, 1395–1403. doi: 10.1084/jem.180.4.1395

Chen, R., Ning, G., Zhao, M. L., Fleming, M. G., Diaz, L. A., Werb, Z., et al. (2001). Mast cells play a key role in neutrophil recruitment in experimental bullous pemphigoid. *J. Clin. Invest.* 108, 1151–1158. doi: 10.1172/jci11494

Chiò, A., Calvo, A., Bovio, G., Canosa, A., Bertuzzo, D., Galmozzi, F., et al. (2014). Amyotrophic lateral sclerosis outcome measures and the role of albumin and creatinine: a population-based study. *JAMA Neurol.* 71, 1134–1142. doi: 10.1001/jamaneurol.2014.1129

Chiu, I. M., Chen, A., Zheng, Y., Kosaras, B., Tsiftsoglou, S. A., Vartanian, T. K., et al. (2008). T lymphocytes potentiate endogenous neuroprotective inflammation in a mouse model of ALS. *Proc. Natl. Acad. Sci. U. S. A.* 105, 17913–17918. doi: 10.1073/pnas.0804610105

Chiu, I. M., Morimoto, E. T., Goodarzi, H., Liao, J. T., O'keeffe, S., Phatnani, H. P., et al. (2013). A neurodegeneration-specific gene-expression signature of acutely isolated microglia from an amyotrophic lateral sclerosis mouse model. *Cell Rep.* 4, 385–401. doi: 10.1016/j.celrep.2013.06.018

Chiu, I. M., Phatnani, H., Kuligowski, M., Tapia, J. C., Carrasco, M. A., Zhang, M., et al. (2009). Activation of innate and humoral immunity in the peripheral nervous system of ALS transgenic mice. *Proc. Natl. Acad. Sci. U. S. A.* 106, 20960–20965. doi: 10.1073/pnas.0911405106

Cipollina, G., Davari Serej, A., Di Nolfi, G., Gazzano, A., Marsala, A., Spatafora, M. G., et al. (2020). Heterogeneity of Neuroinflammatory responses in amyotrophic lateral sclerosis: a challenge or an opportunity? *Int. J. Mol. Sci.* 21, 1–21. doi: 10.3390/ijms21217923

Coleman, M. P., and Höke, A. (2020). Programmed axon degeneration: from mouse to mechanism to medicine. *Nat. Rev. Neurosci.* 21, 183–196. doi: 10.1038/s41583-020-0269-3

Colonna, M., and Butovsky, O. (2017). Microglia function in the central nervous system during health and neurodegeneration. *Annu. Rev. Immunol.* 35, 441–468. doi: 10.1146/annurev-immunol-051116-052358

Coque, E., Salsac, C., Espinosa-Carrasco, G., Varga, B., Degauque, N., Cadoux, M., et al. (2019). Cytotoxic CD8(+) T lymphocytes expressing ALS-causing SOD1 mutant selectively trigger death of spinal motoneurons. *Proc. Natl. Acad. Sci. U. S. A.* 116, 2312–2317. doi: 10.1073/pnas.1815961116

Costantini, C., and Cassatella, M. A. (2011). The defensive alliance between neutrophils and NK cells as a novel arm of innate immunity. *J. Leukoc. Biol.* 89, 221–233. doi: 10.1189/jlb.0510250

Cronk, J. C., Filiano, A. J., Louveau, A., Marin, I., Marsh, R., Ji, E., et al. (2018). Peripherally derived macrophages can engraft the brain independent of irradiation and maintain an identity distinct from microglia. *J. Exp. Med.* 215, 1627–1647. doi: 10.1084/jem.20180247

Cui, C., Ingre, C., Yin, L., Li, X., Andersson, J., Seitz, C., et al. (2022). Correlation between leukocyte phenotypes and prognosis of amyotrophic lateral sclerosis. *eLife* 11, 1–16. doi: 10.7554/eLife.74065

Cunha, C., Santos, C., Gomes, C., Fernandes, A., Correia, A. M., Sebastião, A. M., et al. (2018). Downregulated glia interplay and increased miRNA-155 as promising markers to track ALS at an early stage. *Mol. Neurobiol.* 55, 4207–4224. doi: 10.1007/s12035-017-0631-2

Dalakas, M. C., Stein, D. P., Otero, C., Sekul, E., Cupler, E. J., and McCrosky, S. (1994). Effect of high-dose intravenous immunoglobulin on amyotrophic lateral sclerosis and multifocal motor neuropathy. *Arch. Neurol.* 51, 861–864. doi: 10.1001/archneur.1994.00540210031010

Dejesus-Hernandez, M., Mackenzie, I. R., Boeve, B. F., Boxer, A. L., Baker, M., Rutherford, N. J., et al. (2011). Expanded GGGGCC hexanucleotide repeat in noncoding region of C9ORF72 causes chromosome 9p-linked FTD and ALS. *Neuron* 72, 245–256. doi: 10.1016/j.neuron.2011.09.011

Deora, V., Lee, J. D., Albornoz, E. A., McAlary, L., Jagaraj, C. J., Robertson, A. A. B., et al. (2020). The microglial NLRP3 inflammasome is activated by amyotrophic lateral sclerosis proteins. *Glia* 68, 407–421. doi: 10.1002/glia.23728

Desport, J. C., Preux, P. M., Magy, L., Boirie, Y., Vallat, J. M., Beaufrère, B., et al. (2001). Factors correlated with hypermetabolism in patients with amyotrophic lateral sclerosis. *Am. J. Clin. Nutr.* 74, 328–334. doi: 10.1093/ajcn/74.3.328

de Zoete, M. R., Palm, N. W., Zhu, S., and Flavell, R. A. (2014). Inflammasomes. *Cold Spring Harb. Perspect. Biol.* 6:a016287. doi: 10.1101/cshperspect.a016287

Doherty, T. M., Seder, R. A., and Sher, A. (1996). Induction and regulation of IL-15 expression in murine macrophages. *J. Immunol.* 156, 735–741. doi: 10.4049/jimmunol.156.2.735

Duarte, F., Binet, S., Lacomblez, L., Bouche, P., Preud'homme, J.-L., and Meininger, V. (1991). Quantitative analysis of monoclonal immunoglobulins in serum of patients with amyotrophic lateral sclerosis. *J. Neurol. Sci.* 104, 88–91. doi: 10.1016/0022-510X(91)90220-2

Du, L., Zhang, Y., Chen, Y., Zhu, J., Yang, Y., and Zhang, H. L. (2017). Role of microglia in neurological disorders and their potentials as a therapeutic target. *Mol. Neurobiol.* 54, 7567–7584. doi: 10.1007/s12035-016-0245-0

Du, Y., Zhao, W., Thonhoff, J. R., Wang, J., Wen, S., and Appel, S. H. (2020). Increased activation ability of monocytes from ALS patients. *Exp. Neurol.* 328:113259. doi: 10.1016/j.expneurol.2020.113259

Dunlop, J., Beal McIlvain, H., She, Y., and Howland, D. S. (2003). Impaired spinal cord glutamate transport capacity and reduced sensitivity to riluzole in a transgenic superoxide dismutase mutant rat model of amyotrophic lateral sclerosis. *J. Neurosci.* 23, 1688–1696. doi: 10.1523/jneurosci.23-05-01688.2003

Ehrhart, J., Smith, A. J., Kuzmin-Nichols, N., Zesiewicz, T. A., Jahan, I., Shytle, R. D., et al. (2015). Humoral factors in ALS patients during disease progression. *J. Neuroinflammation* 12:127. doi: 10.1186/s12974-015-0350-4

Engelhardt, J. I., Siklós, L., Kömüves, L., Smith, R. G., and Appel, S. H. (1995). Antibodies to calcium channels from ALS patients passively transferred to mice selectively increase intracellular calcium and induce ultrastructural changes in motoneurons. *Synapse* 20, 185–199. doi: 10.1002/syn.890200302

Ferraiuolo, L., Heath, P. R., Holden, H., Kasher, P., Kirby, J., and Shaw, P. J. (2007). Microarray analysis of the cellular pathways involved in the adaptation to and progression of motor neuron injury in the SOD1 G93A mouse model of familial ALS. *J. Neurosci.* 27, 9201–9219. doi: 10.1523/jneurosci.1470-07.2007

Fiala, M., Chattopadhay, M., La Cava, A., Tse, E., Liu, G., Lourenco, E., et al. (2010). IL-17A is increased in the serum and in spinal cord CD8 and mast cells of ALS patients. *J. Neuroinflammation* 7:76. doi: 10.1186/1742-2094-7-76

Fialová, L., Bartos, A., Soukupová, J., Svarcová, J., Ridzon, P., and Malbohan, I. (2009). Synergy of serum and cerebrospinal fluid antibodies against axonal cytoskeletal proteins in patients with different neurological diseases. *Folia Biol. (Praha)* 55, 23–26.

Fialová, L., Švarcová, J., Bartos, A., and Malbohan, I. (2012). Avidity of anti-neurocytoskeletal antibodies in cerebrospinal fluid and serum. *Folia Microbiol. (Praha)* 57, 415–419. doi: 10.1007/s12223-012-0105-x

Figueroa-Romero, C., Hur, J., Bender, D. E., Delaney, C. E., Cataldo, M. D., Smith, A. L., et al. (2012). Identification of epigenetically altered genes in sporadic amyotrophic lateral sclerosis. *PLoS One* 7:e52672. doi: 10.1371/journal.pone.0052672

Finkelstein, A., Kunis, G., Seksenyan, A., Ronen, A., Berkutzki, T., Azoulay, D., et al. (2011). Abnormal changes in NKT cells, the IGF-1 axis, and liver pathology in an animal model of ALS. *PLoS One* 6:e22374. doi: 10.1371/journal.pone.0022374

Fratantoni, S. A., Weisz, G., Pardal, A. M., Reisin, R. C., and Uchitel, O. D. (2000). Amyotrophic lateral sclerosis IgG-treated neuromuscular junctions develop sensitivity to L-type calcium channel blocker. *Muscle Nerve* 23, 543–550. doi: 10.1002/(sici)1097-4598(200004)23:4<543::aid-mus13>3.0.co;2-s

Fu, J., Huang, Y., Bao, T., Liu, C., Liu, X., and Chen, X. (2022). The role of Th17 cells/IL-17A in AD, PD, ALS and the strategic therapy targeting on IL-17A. *J. Neuroinflammation* 19:98. doi: 10.1186/s12974-022-02446-6

Galli, S. J., Tsai, M., and Wershil, B. K. (1993). The c-kit receptor, stem cell factor, and mast cells. What each is teaching us about the others. *Am. J. Pathol.* 142, 965–974.

Garbuzova-Davis, S., and Sanberg, P. R. (2014). Blood-CNS barrier impairment in ALS patients versus an animal model. *Front. Cell. Neurosci.* 8:21. doi: 10.3389/fncel.2014.00021

Garofalo, S., Cocozza, G., Porzia, A., Inghilleri, M., Raspa, M., Scavizzi, F., et al. (2020). Natural killer cells modulate motor neuron-immune cell cross talk in models of amyotrophic lateral sclerosis. *Nat. Commun.* 11:1773. doi: 10.1038/s41467-020-15644-8

Grabstein, K. H., Eisenman, J., Shanebeck, K., Rauch, C., Srinivasan, S., Fung, V., et al. (1994). Cloning of a T cell growth factor that interacts with the beta chain of the interleukin-2 receptor. *Science* 264, 965–968. doi: 10.1126/science.8178155

Grajewski, R. S., Hansen, A. M., Agarwal, R. K., Kronenberg, M., Sidobre, S., Su, S. B., et al. (2008). Activation of invariant NKT cells ameliorates experimental ocular autoimmunity by a mechanism involving innate IFN-gamma production and dampening of the adaptive Th1 and Th17 responses. *J. Immunol.* 181, 4791–4797. doi: 10.4049/jimmunol.181.7.4791

Gravel, M., Béland, L. C., Soucy, G., Abdelhamid, E., Rahimian, R., Gravel, C., et al. (2016). IL-10 controls early microglial phenotypes and disease onset in ALS caused by misfolded superoxide dismutase 1. *J. Neurosci.* 36, 1031–1048. doi: 10.1523/jneurosci.0854-15.2016

Haidet-Phillips, A. M., Hester, M. E., Miranda, C. J., Meyer, K., Braun, L., Frakes, A., et al. (2011). Astrocytes from familial and sporadic ALS patients are toxic to motor neurons. *Nat. Biotechnol.* 29, 824–828. doi: 10.1038/nbt.1957

Halder, R. C., Jahng, A., Maricic, I., and Kumar, V. (2007). Mini review: immune response to myelin-derived sulfatide and CNS-demyelination. *Neurochem. Res.* 32, 257–262. doi: 10.1007/s11064-006-9145-4

Hammond, K. J., and Kronenberg, M. (2003). Natural killer T cells: natural or unnatural regulators of autoimmunity? *Curr. Opin. Immunol.* 15, 683–689. doi: 10.1016/j.coi.2003.09.014

Harrison, J. K., Jiang, Y., Chen, S., Xia, Y., Maciejewski, D., McNamara, R. K., et al. (1998). Role for neuronally derived fractalkine in mediating interactions between neurons and CX3CR1-expressing microglia. *Proc. Natl. Acad. Sci. U. S. A.* 95, 10896–10901. doi: 10.1073/pnas.95.18.10896

Henkel, J. S., Beers, D. R., Siklós, L., and Appel, S. H. (2006). The chemokine MCP-1 and the dendritic and myeloid cells it attracts are increased in the mSOD1 mouse model of ALS. *Mol. Cell. Neurosci.* 31, 427–437. doi: 10.1016/j.mcn.2005.10.016

Henkel, J. S., Beers, D. R., Wen, S., Rivera, A. L., Toennis, K. M., Appel, J. E., et al. (2013). Regulatory T-lymphocytes mediate amyotrophic lateral sclerosis progression and survival. *EMBO Mol. Med.* 5, 64–79. doi: 10.1002/emmm.201201544

Henkel, J. S., Beers, D. R., Zhao, W., and Appel, S. H. (2009). Microglia in ALS: the good, the bad, and the resting. *J. Neuroimmune Pharmacol.* 4, 389–398. doi: 10.1007/s11481-009-9171-5

Henkel, J. S., Beers, D. R., Zhao, W., and Appel, S. H. (2014). "Neuroimmunology of amyotrophic lateral sclerosis" in *Neuroinflammation and CNS disorders*, 185–209. doi: 10.1002/9781118406557.ch8

Hensley, K., Abdel-Moaty, H., Hunter, J., Mhatre, M., Mou, S., Nguyen, K., et al. (2006). Primary glia expressing the G93A-SOD1 mutation present a neuroinflammatory phenotype and provide a cellular system for studies of glial inflammation. *J. Neuroinflammation* 3:2. doi: 10.1186/1742-2094-3-2

Hertwig, L., Hamann, I., Romero-Suarez, S., Millward, J. M., Pietrek, R., Chanvillard, C., et al. (2016). CX3CR1-dependent recruitment of mature NK cells into the central nervous system contributes to control autoimmune neuroinflammation. *Eur. J. Immunol.* 46, 1984–1996. doi: 10.1002/eji.201546194

He, S., and Walls, A. F. (1998). Human mast cell chymase induces the accumulation of neutrophils, eosinophils and other inflammatory cells in vivo. *Br. J. Pharmacol.* 125, 1491–1500. doi: 10.1038/sj.bjp.0702223

Howland, D. S., Liu, J., She, Y., Goad, B., Maragakis, N. J., Kim, B., et al. (2002). Focal loss of the glutamate transporter EAAT2 in a transgenic rat model of SOD1 mutant-mediated amyotrophic lateral sclerosis (ALS). *Proc. Natl. Acad. Sci. U. S. A.* 99, 1604–1609. doi: 10.1073/pnas.032539299

Hoye, M. L., Regan, M. R., Jensen, L. A., Lake, A. M., Reddy, L. V., Vidensky, S., et al. (2018). Motor neuron-derived microRNAs cause astrocyte dysfunction in amyotrophic lateral sclerosis. *Brain* 141, 2561–2575. doi: 10.1093/brain/awy182

Iłzecka, J., Stelmasiak, Z., and Dobosz, B. (2001). Interleukin-1beta converting enzyme/Caspase-1 (ICE/Caspase-1) and soluble APO-1/Fas/CD 95 receptor in amyotrophic lateral sclerosis patients. *Acta Neurol. Scand.* 103, 255–258. doi: 10.1034/j.1600-0404.2001.103004255.x

Infante-Duarte, C., Weber, A., Krätzschmar, J., Prozorovski, T., Pikol, S., Hamann, I., et al. (2005). Frequency of blood CX3CR1-positive natural killer cells correlates with disease activity in multiple sclerosis patients. *FASEB J.* 19, 1902–1904. doi: 10.1096/fj.05-3832fje

Italiani, P., Carlesi, C., Giungato, P., Puxeddu, I., Borroni, B., Bossù, P., et al. (2014). Evaluating the levels of interleukin-1 family cytokines in sporadic amyotrophic lateral sclerosis. *J. Neuroinflammation* 11:94. doi: 10.1186/1742-2094-11-94

Jin, M., Akgün, K., Ziemssen, T., Kipp, M., Günther, R., and Hermann, A. (2021). Interleukin-17 and Th17 lymphocytes directly impair Motoneuron survival of wildtype and FUS-ALS mutant human iPSCs. *Int. J. Mol. Sci.* 22, 1–15. doi: 10.3390/ijms22158042

Jin, M., Günther, R., Akgün, K., Hermann, A., and Ziemssen, T. (2020). Peripheral proinflammatory Th1/Th17 immune cell shift is linked to disease severity in amyotrophic lateral sclerosis. *Sci. Rep.* 10:5941. doi: 10.1038/s41598-020-62756-8

Johann, S., Heitzer, M., Kanagaratnam, M., Goswami, A., Rizo, T., Weis, J., et al. (2015). NLRP3 inflammasome is expressed by astrocytes in the SOD1 mouse model of ALS and in human sporadic ALS patients. *Glia* 63, 2260–2273. doi: 10.1002/glia.22891

Jones, M. K., Nair, A., and Gupta, M. (2019). Mast cells in neurodegenerative disease. *Front. Cell. Neurosci.* 13:171. doi: 10.3389/fncel.2019.00171

Jonuleit, H., Wiedemann, K., Müller, G., Degwert, J., Hoppe, U., Knop, J., et al. (1997). Induction of IL-15 messenger RNA and protein in human blood-derived dendritic cells: a role for IL-15 in attraction of T cells. *J. Immunol.* 158, 2610–2615. doi: 10.4049/jimmunol.158.6.2610

Jurga, A. M., Paleczna, M., and Kuter, K. Z. (2020). Overview of general and discriminating markers of differential microglia phenotypes. *Front. Cell. Neurosci.* 14:198. doi: 10.3389/fncel.2020.00198

Kadhim, H., Deltenre, P., Martin, J. J., and Sébire, G. (2016). In-situ expression of Interleukin-18 and associated mediators in the human brain of sALS patients: hypothesis for a role for immune-inflammatory mechanisms. *Med. Hypotheses* 86, 14–17. doi: 10.1016/j.mehy.2015.11.022

Kaur, K., Chen, P. C., Ko, M. W., Mei, A., Chovatiya, N., Huerta-Yepez, S., et al (2022). The potential role of cytotoxic immune effectors in induction, progression and pathogenesis of amyotrophic lateral sclerosis (ALS). *Cells* 11. doi: 10.3390/cells11213431

Kawano, T., Cui, J., Koezuka, Y., Toura, I., Kaneko, Y., Motoki, K., et al. (1997). CD1d-restricted and TCR-mediated activation of valpha14 NKT cells by glycosylceramides. *Science* 278, 1626–1629. doi: 10.1126/science.278.5343.1626

Keizman, D., Rogowski, O., Berliner, S., Ish-Shalom, M., Maimon, N., Nefussy, B., et al. (2009). Low-grade systemic inflammation in patients with amyotrophic lateral sclerosis. *Acta Neurol. Scand.* 119, 383–389. doi: 10.1111/j.1600-0404.2008.01112.x

Keren-Shaul, H., Spinrad, A., Weiner, A., Matcovitch-Natan, O., Dvir-Szternfeld, R., Ulland, T. K., et al. (2017). A unique microglia type associated with restricting development of Alzheimer's disease. *Cells* 169, 1276–1290.e17. doi: 10.1016/j.cell.2017.05.018

Kim, C. F., and Moalem-Taylor, G. (2011). Detailed characterization of neuro-immune responses following neuropathic injury in mice. *Brain Res.* 1405, 95–108. doi: 10.1016/j.brainres.2011.06.022

Korhonen, P., Pollari, E., Kanninen, K. M., Savchenko, E., Lehtonen, Š., Wojciechowski, S., et al. (2019). Long-term interleukin-33 treatment delays disease onset and alleviates astrocytic activation in a transgenic mouse model of amyotrophic lateral sclerosis. *IBRO Rep.* 6, 74–86. doi: 10.1016/j.ibror.2019.01.005

Kovacs, M., Alamón, C., Maciel, C., Varela, V., Ibarburu, S., Tarragó, L., et al. (2021). The pathogenic role of c-kit+ mast cells in the spinal motor neuron-vascular niche in ALS. *Acta Neuropathol. Commun.* 9:136. doi: 10.1186/s40478-021-01241-3

Krystel-Whittemore, M., Dileepan, K. N., and Wood, J. G. (2015). Mast cell: a multi-functional master cell. *Front. Immunol.* 6:620. doi: 10.3389/fimmu.2015.00620

Kurimoto, T., Yin, Y., Habboub, G., Gilbert, H. Y., Li, Y., Nakao, S., et al. (2013). Neutrophils express oncomodulin and promote optic nerve regeneration. *J. Neurosci.* 33, 14816–14824. doi: 10.1523/jneurosci.5511-12.2013

La Bella, V., Goodman, J. C., and Appel, S. H. (1997). Increased CSF glutamate following injection of ALS immunoglobulins. *Neurology* 48, 1270–1272. doi: 10.1212/wnl.48.5.1270

Lam, L., Chin, L., Halder, R. C., Sagong, B., Famenini, S., Sayre, J., et al. (2016). Epigenetic changes in T-cell and monocyte signatures and production of neurotoxic cytokines in ALS patients. *FASEB J.* 30, 3461–3473. doi: 10.1096/fj.201600259RR

Lee, S. B., and Kalluri, R. (2010). Mechanistic connection between inflammation and fibrosis. *Kidney Int. Suppl.* 78, S22–S26. doi: 10.1038/ki.2010.418

Lee, Y. B., Satoh, J., Walker, D. G., and Kim, S. U. (1996). Interleukin-15 gene expression in human astrocytes and microglia in culture. *Neuroreport* 7, 1062–1066. doi: 10.1097/00001756-199604100-00022

Leone, M. A., Mandrioli, J., Russo, S., Cucovici, A., Gianferrari, G., Lisnic, V., et al. (2022). Neutrophils-to-lymphocyte ratio is associated with progression and overall survival in amyotrophic lateral sclerosis. *Biomedicine* 10, 1–13. doi: 10.3390/biomedicines10020354

Levi-Schaffer, F., Micera, A., Zamir, E., Mechoulam, H., Puxeddu, I., Piliponsky, A. M., et al. (2002). Nerve growth factor and eosinophils in inflamed juvenile conjunctival nevus. *Invest. Ophthalmol. Vis. Sci.* 43, 1850–1856.

Liao, B., Zhao, W., Beers, D. R., Henkel, J. S., and Appel, S. H. (2012). Transformation from a neuroprotective to a neurotoxic microglial phenotype in a mouse model of ALS. *Exp. Neurol.* 237, 147–152. doi: 10.1016/j.expneurol.2012.06.011

Liddelow, S. A., Guttenplan, K. A., Clarke, L. E., Bennett, F. C., Bohlen, C. J., Schirmer, L., et al. (2017). Neurotoxic reactive astrocytes are induced by activated microglia. *Nature* 541, 481–487. doi: 10.1038/nature21029

Li, J., Gran, B., Zhang, G. X., Ventura, E. S., Siglienti, I., Rostami, A., et al. (2003). Differential expression and regulation of IL-23 and IL-12 subunits and receptors in adult mouse microglia. *J. Neurol. Sci.* 215, 95–103. doi: 10.1016/s0022-510x(03)00203-x

Lin, C. Y., Pfluger, C. M., Henderson, R. D., and McCombe, P. A. (2012). Reduced levels of interleukin 33 and increased levels of soluble ST2 in subjects with amyotrophic lateral sclerosis. *J. Neuroimmunol.* 249, 93–95. doi: 10.1016/j.jneuroim.2012.05.001

Liu, J., and Wang, F. (2017). Role of neuroinflammation in amyotrophic lateral sclerosis: Cellular mechanisms and therapeutic implications. *Front. Immunol.* 8, 1–12. doi: 10.3389/fimmu.2017.01005

Lobsiger, C. S., Boillée, S., and Cleveland, D. W. (2007). Toxicity from different SOD1 mutants dysregulates the complement system and the neuronal regenerative response in ALS motor neurons. *Proc. Natl. Acad. Sci. U. S. A.* 104, 7319–7326. doi: 10.1073/pnas.0702230104

Logroscino, G., Traynor, B. J., Hardiman, O., Chiò, A., Mitchell, D., Swingler, R. J., et al. (2010). Incidence of amyotrophic lateral sclerosis in Europe. *J. Neurol. Neurosurg. Psychiatry* 81, 385–390. doi: 10.1136/jnnp.2009.183525

Lu, C. H., Allen, K., Oei, F., Leoni, E., Kuhle, J., Tree, T., et al. (2016). Systemic inflammatory response and neuromuscular involvement in amyotrophic lateral sclerosis. *Neurol. Neuroimmunol. Neuroinflamm.* 3:e244. doi: 10.1212/nxi.0000000000000244

Lu, C. H., Kalmar, B., Malaspina, A., Greensmith, L., and Petzold, A. (2011). A method to solubilise protein aggregates for immunoassay quantification which overcomes the neurofilament "hook" effect. *J. Neurosci. Methods* 195, 143–150. doi: 10.1016/j.jneumeth.2010.11.026

Lu, C. H., Petzold, A., Kalmar, B., Dick, J., Malaspina, A., and Greensmith, L. (2012). Plasma neurofilament heavy chain levels correlate to markers of late stage disease progression and treatment response in SOD1 (G93A) mice that model ALS. *PLoS One* 7:e40998. doi: 10.1371/journal.pone.0040998

Lyu, J., Jiang, X., Leak, R. K., Shi, Y., Hu, X., and Chen, J. (2021). Microglial responses to brain injury and disease: functional diversity and new opportunities. *Transl. Stroke Res.* 12, 474–495. doi: 10.1007/s12975-020-00857-2

Maier, A., Deigendesch, N., Müller, K., Weishaupt, J. H., Krannich, A., Röhle, R., et al. (2015). Interleukin-1 antagonist Anakinra in amyotrophic lateral sclerosis--a pilot study. *PLoS One* 10:e0139684. doi: 10.1371/journal.pone.0139684

Mantovani, S., Garbelli, S., Pasini, A., Alimonti, D., Perotti, C., Melazzini, M., et al. (2009). Immune system alterations in sporadic amyotrophic lateral sclerosis patients suggest an ongoing neuroinflammatory process. *J. Neuroimmunol.* 210, 73–79. doi: 10.1016/j.jneuroim.2009.02.012

Mantovani, S., Gordon, R., Macmaw, J. K., Pfluger, C. M., Henderson, R. D., Noakes, P. G., et al. (2014). Elevation of the terminal complement activation products C5a and C5b-9 in ALS patient blood. *J. Neuroimmunol.* 276, 213–218. doi: 10.1016/j.jneuroim.2014.09.005

Marchetto, M. C., Muotri, A. R., Mu, Y., Smith, A. M., Cezar, G. G., and Gage, F. H. (2008). Non-cell-autonomous effect of human SOD1 G37R astrocytes on motor neurons derived from human embryonic stem cells. *Cell Stem Cell* 3, 649–657. doi: 10.1016/j.stem.2008.10.001

Martínez-Muriana, A., Mancuso, R., Francos-Quijorna, I., Olmos-Alonso, A., Osta, R., Perry, V. H., et al. (2016). CSF1R blockade slows the progression of amyotrophic lateral sclerosis by reducing microgliosis and invasion of macrophages into peripheral nerves. *Sci. Rep.* 6:25663. doi: 10.1038/srep25663

Martinon, F., Mayor, A., and Tschopp, J. (2009). The inflammasomes: guardians of the body. *Annu. Rev. Immunol.* 27, 229–265. doi: 10.1146/annurev.immunol.021908.132715

Martin, S., Battistini, C., and Sun, J. (2022). A gut feeling in amyotrophic lateral sclerosis: microbiome of mice and men. *Front. Cell. Infect. Microbiol.* 12:839526. doi: 10.3389/fcimb.2022.839526

Ma, X., and Trinchieri, G. (2001). Regulation of interleukin-12 production in antigen-presenting cells. *Adv. Immunol.* 79, 55–92. doi: 10.1016/s0065-2776(01)79002-5

May, C., Nordhoff, E., Casjens, S., Turewicz, M., Eisenacher, M., Gold, R., et al. (2014). Highly immunoreactive IgG antibodies directed against a set of twenty human proteins in the sera of patients with amyotrophic lateral sclerosis identified by protein array. *PLoS One* 9:e89596. doi: 10.1371/journal.pone.0089596

Mehanna, R., Patton, E. L. Jr., Phan, C. L., and Harati, Y. (2012). Amyotrophic lateral sclerosis with positive anti-acetylcholine receptor antibodies. Case report and review of the literature. *J. Clin. Neuromuscul. Dis.* 14, 82–85. doi: 10.1097/CND.0b013e31824db163

Meissner, F., Molawi, K., and Zychlinsky, A. (2010). Mutant superoxide dismutase 1-induced IL-1beta accelerates ALS pathogenesis. *Proc. Natl. Acad. Sci. U. S. A.* 107, 13046–13050. doi: 10.1073/pnas.1002396107

Meucci, N., Nobile-Orazio, E., and Scarlato, G. (1996). Intravenous immunoglobulin therapy in amyotrophic lateral sclerosis. *J. Neurol.* 243, 117–120. doi: 10.1007/bf02444000

Miller, A. M. (2011). Role of IL-33 in inflammation and disease. *J Inflamm (Lond)* 8:22. doi: 10.1186/1476-9255-8-22

Milligan, C., Atassi, N., Babu, S., Barohn, R. J., Caress, J. B., Cudkowicz, M. E., et al. (2021). Tocilizumab is safe and tolerable and reduces C-reactive protein concentrations in the plasma and cerebrospinal fluid of ALS patients. *Muscle Nerve* 64, 309–320. doi: 10.1002/mus.27339

Milošević, M., Milićević, K., Božić, I., Lavrnja, I., Stevanović, I., Bijelić, D., et al. (2017). Immunoglobulins G from sera of amyotrophic lateral sclerosis patients induce oxidative stress and upregulation of antioxidative system in BV-2 microglial cell line. *Front. Immunol.* 8:1619. doi: 10.3389/fimmu.2017.01619

Milošević, M., Stenovec, M., Kreft, M., Petrušić, V., Stević, Z., Trkov, S., et al. (2013). Immunoglobulins G from patients with sporadic amyotrophic lateral sclerosis affects cytosolic Ca2+ homeostasis in cultured rat astrocytes. *Cell Calcium* 54, 17–25. doi: 10.1016/j.ceca.2013.03.005

Mitchell, R. M., Freeman, W. M., Randazzo, W. T., Stephens, H. E., Beard, J. L., Simmons, Z., et al. (2009). A CSF biomarker panel for identification of patients with amyotrophic lateral sclerosis. *Neurology* 72, 14–19. doi: 10.1212/01.wnl.0000333251.36681.a5

Moore, C. S., Abdullah, S. L., Brown, A., Arulpragasam, A., and Crocker, S. J. (2011). How factors secreted from astrocytes impact myelin repair. *J. Neurosci. Res.* 89, 13–21. doi: 10.1002/jnr.22482

Morello, G., Spampinato, A. G., and Cavallaro, S. (2017). Molecular taxonomy of sporadic amyotrophic lateral sclerosis using disease-associated genes. *Front. Neurol.* 8:152. doi: 10.3389/fneur.2017.00152

Moretta, A., Biassoni, R., Bottino, C., Mingari, M. C., and Moretta, L. (2000). Natural cytotoxicity receptors that trigger human NK-cell-mediated cytolysis. *Immunol. Today* 21, 228–234. doi: 10.1016/s0167-5699(00)01596-6

Motataianu, A., Barcutean, L., and Balasa, R. (2020). Neuroimmunity in amyotrophic lateral sclerosis: focus on microglia. *Amyotroph Lateral Scler Frontotemporal Degener* 21, 159–166. doi: 10.1080/21678421.2019.1708949

Murdock, B. J., Bender, D. E., Kashlan, S. R., Figueroa-Romero, C., Backus, C., Callaghan, B. C., et al. (2016). Increased ratio of circulating neutrophils to monocytes in amyotrophic lateral sclerosis. *Neurol. Neuroimmunol. Neuroinflamm.* 3:e242. doi: 10.1212/nxi.0000000000000242

Murdock, B. J., Famie, J. P., Piecuch, C. E., Pawlowski, K. D., Mendelson, F. E., Pieroni, C. H., et al. (2021a). NK cells associate with ALS in a sex-and age-dependent manner. JCI. *Insight* 6, 1–15. doi: 10.1172/jci.insight.147129

Murdock, B. J., Goutman, S. A., Boss, J., Kim, S., and Feldman, E. L. (2021b). Amyotrophic lateral sclerosis survival associates with neutrophils in a sex-specific manner. *Neurol. Neuroimmunol. Neuroinflamm.* 8:e953. doi: 10.1212/nxi.0000000000000953

Murdock, B. J., Zhou, T., Kashlan, S. R., Little, R. J., Goutman, S. A., and Feldman, E. L. (2017). Correlation of peripheral immunity with rapid amyotrophic lateral sclerosis progression. *JAMA Neurol.* 74, 1446–1454. doi: 10.1001/jamaneurol.2017.2255

Nardo, G., Trolese, M. C., de Vito, G., Cecchi, R., Riva, N., Dina, G., et al. (2016). Immune response in peripheral axons delays disease progression in SOD1 (G93A) mice. *J. Neuroinflammation* 13:261. doi: 10.1186/s12974-016-0732-2

Németh, T., Sperandio, M., and Mócsai, A. (2020). Neutrophils as emerging therapeutic targets. *Nat. Rev. Drug Discov.* 19, 253–275. doi: 10.1038/s41573-019-0054-z

Neumann, M., Sampathu, D. M., Kwong, L. K., Truax, A. C., Micsenyi, M. C., Chou, T. T., et al. (2006). Ubiquitinated TDP-43 in frontotemporal lobar degeneration and amyotrophic lateral sclerosis. *Science* 314, 130–133. doi: 10.1126/science.1134108

Ng, W., and Ng, S. Y. (2022). Remodeling of astrocyte secretome in amyotrophic lateral sclerosis: uncovering novel targets to combat astrocyte-mediated toxicity. *Transl. Neurodegener.* 11:54. doi: 10.1186/s40035-022-00332-y

Niebroj-Dobosz, I., Jamrozik, Z., Janik, P., Hausmanowa-Petrusewicz, I., and Kwieciński, H. (1999). Anti-neural antibodies in serum and cerebrospinal fluid of amyotrophic lateral sclerosis (ALS) patients. *Acta Neurol. Scand.* 100, 238–243. doi: 10.1111/j.1600-0404.1999.tb00387.x

Nie, H., Zheng, Y., Li, R., Guo, T. B., He, D., Fang, L., et al. (2013). Phosphorylation of FOXP3 controls regulatory T cell function and is inhibited by TNF-α in rheumatoid arthritis. *Nat. Med.* 19, 322–328. doi: 10.1038/nm.3085

Noh, M. Y., Cho, K. A., Kim, H., Kim, S. M., and Kim, S. H. (2014). Erythropoietin modulates the immune-inflammatory response of a SOD1 (G93A) transgenic mouse model of amyotrophic lateral sclerosis (ALS). *Neurosci. Lett.* 574, 53–58. doi: 10.1016/j.neulet.2014.05.001

Oldstone, M. B., Wilson, C. B., Perrin, L. H., and Norris, F. H. Jr. (1976). Evidence for immune-complex formation in patients with amyotrophic lateral sclerosis. *Lancet* 2, 169–172. doi: 10.1016/s0140-6736(76)92345-x

Ouali Alami, N., Schurr, C., Olde Heuvel, F., Tang, L., Li, Q., Tasdogan, A., et al. (2018). NF-κB activation in astrocytes drives a stage-specific beneficial neuroimmunological response in ALS. *EMBO J.* 37, 1–23. doi: 10.15252/embj.201798697

Pagani, M. R., Reisin, R. C., and Uchitel, O. D. (2006). Calcium signaling pathways mediating synaptic potentiation triggered by amyotrophic lateral sclerosis IgG in motor nerve terminals. *J. Neurosci.* 26, 2661–2672. doi: 10.1523/jneurosci.4394-05.2006

Papadeas, S. T., Kraig, S. E., O'Banion, C., Lepore, A. C., and Maragakis, N. J. (2011). Astrocytes carrying the superoxide dismutase 1 (SOD1G93A) mutation induce wild-type motor neuron degeneration in vivo. *Proc. Natl. Acad. Sci. U. S. A.* 108, 17803–17808. doi: 10.1073/pnas.1103141108

Pardo, A. C., Wong, V., Benson, L. M., Dykes, M., Tanaka, K., Rothstein, J. D., et al. (2006). Loss of the astrocyte glutamate transporter GLT1 modifies disease in SOD1 (G93A) mice. *Exp. Neurol.* 201, 120–130. doi: 10.1016/j.expneurol.2006.03.028

Peric, M., Mitrecic, D., and Andjus, P. R. (2017). Targeting astrocytes for treatment in amyotrophic lateral sclerosis. *Curr. Pharm. Des.* 23, 5037–5044. doi: 10.2174/1381612823666170615110446

Perrin, F. E., Boisset, G., Docquier, M., Schaad, O., Descombes, P., and Kato, A. C. (2005). No widespread induction of cell death genes occurs in pure motoneurons in an amyotrophic lateral sclerosis mouse model. *Hum. Mol. Genet.* 14, 3309–3320. doi: 10.1093/hmg/ddi357

Pestronk, A., Adams, R. N., Clawson, L., Cornblath, D., Kuncl, R. W., Griffin, D., et al. (1988). Serum antibodies to GM1 ganglioside in amyotrophic lateral sclerosis. *Neurology* 38, 1457–1461. doi: 10.1212/wnl.38.9.1457

Philips, T., and Robberecht, W. (2011). Neuroinflammation in amyotrophic lateral sclerosis: role of glial activation in motor neuron disease. *Lancet Neurol.* 10, 253–263. doi: 10.1016/s1474-4422(11)70015-1

Poli, A., Kmiecik, J., Domingues, O., Hentges, F., Bléry, M., Chekenya, M., et al. (2013). NK cells in central nervous system disorders. *J. Immunol.* 190, 5355–5362. doi: 10.4049/jimmunol.1203401

Provinciali, L., Laurenzi, M. A., Vesprini, L., Giovagnoli, A. R., Bartocci, C., Montroni, M., et al. (1988). Immunity assessment in the early stages of amyotrophic lateral sclerosis: a study of virus antibodies and lymphocyte subsets. *Acta Neurol. Scand.* 78, 449–454. doi: 10.1111/j.1600-0404.1988.tb03686.x

Pullen, A. H., Demestre, M., Howard, R. S., and Orrell, R. W. (2004). Passive transfer of purified IgG from patients with amyotrophic lateral sclerosis to mice results in degeneration of motor neurons accompanied by Ca2+ enhancement. *Acta Neuropathol.* 107, 35–46. doi: 10.1007/s00401-003-0777-z

Pullen, A. H., and Humphreys, P. (2000). Ultrastructural analysis of spinal motoneurones from mice treated with IgG from ALS patients, healthy individuals, or disease controls. *J. Neurol. Sci.* 180, 35–45. doi: 10.1016/s0022-510x(00)00427-5

Quek, H., Cuní-López, C., Stewart, R., Colletti, T., Notaro, A., Nguyen, T. H., et al. (2022). ALS monocyte-derived microglia-like cells reveal cytoplasmic TDP-43 accumulation, DNA damage, and cell-specific impairment of phagocytosis associated with disease progression. *J. Neuroinflammation* 19:58. doi: 10.1186/s12974-022-02421-1

Ramachandran, S., Grozdanov, V., Leins, B., Kandler, K., Witzel, S., Mulaw, M., et al. (2023). Low T-cell reactivity to TDP-43 peptides in ALS. *Front. Immunol.* 14, 1–10. doi: 10.3389/fimmu.2023.1193507

Re, D. B., Le Verche, V., Yu, C., Amoroso, M. W., Politi, K. A., Phani, S., et al. (2014). Necroptosis drives motor neuron death in models of both sporadic and familial ALS. *Neuron* 81, 1001–1008. doi: 10.1016/j.neuron.2014.01.011

Renton, A. E., Majounie, E., Waite, A., Simón-Sánchez, J., Rollinson, S., Gibbs, J. R., et al. (2011). A hexanucleotide repeat expansion in C9ORF72 is the cause of chromosome 9p21-linked ALS-FTD. *Neuron* 72, 257–268. doi: 10.1016/j.neuron.2011.09.010

Rentzos, M., Evangelopoulos, E., Sereti, E., Zouvelou, V., Marmara, S., Alexakis, T., et al. (2012). Alterations of T cell subsets in ALS: a systemic immune activation? *Acta Neurol. Scand.* 125, 260–264. doi: 10.1111/j.1600-0404.2011.01528.x

Rentzos, M., Rombos, A., Nikolaou, C., Zoga, M., Zouvelou, V., Dimitrakopoulos, A., et al. (2010). Interleukin-17 and interleukin-23 are elevated in serum and cerebrospinal fluid of patients with ALS: a reflection of Th17 cells activation? *Acta Neurol. Scand.* 122, 425–429. doi: 10.1111/j.1600-0404.2010.01333.x

Rimmele, T. S., and Rosenberg, P. A. (2016). GLT-1: The elusive presynaptic glutamate transporter. *Neurochem. Int.* 98, 19–28. doi: 10.1016/j.neuint.2016.04.010

Rodrigues Lima-Junior, J., Sulzer, D., Lindestam Arlehamn, C. S., and Sette, A. (2021). The role of immune-mediated alterations and disorders in ALS disease. *Hum. Immunol.* 82, 155–161. doi: 10.1016/j.humimm.2021.01.017

Rolfes, L., Schulte-Mecklenbeck, A., Schreiber, S., Vielhaber, S., Herty, M., Marten, A., et al. (2021). Amyotrophic lateral sclerosis patients show increased peripheral and intrathecal T-cell activation. *Brain Commun* 3, 1–11. doi: 10.1093/braincomms/fcab157

Rotshenker, S. (2011). Wallerian degeneration: the innate-immune response to traumatic nerve injury. *J. Neuroinflammation* 8:109. doi: 10.1186/1742-2094-8-109

Sakaguchi, S., Miyara, M., Costantino, C. M., and Hafler, D. A. (2010). FOXP3+ regulatory T cells in the human immune system. *Nat. Rev. Immunol.* 10, 490–500. doi: 10.1038/nri2785

Saleh, I. A., Zesiewicz, T., Xie, Y., Sullivan, K. L., Miller, A. M., Kuzmin-Nichols, N., et al. (2009). Evaluation of humoral immune response in adaptive immunity in ALS patients during disease progression. *J. Neuroimmunol.* 215, 96–101. doi: 10.1016/j.jneuroim.2009.07.011

Sathasivam, S., Ince, P. G., and Shaw, P. J. (2001). Apoptosis in amyotrophic lateral sclerosis: a review of the evidence. *Neuropathol. Appl. Neurobiol.* 27, 257–274. doi: 10.1046/j.0305-1846.2001.00332.x

Sato-Hashimoto, M., Nozu, T., Toriba, R., Horikoshi, A., Akaike, M., Kawamoto, K., et al. (2019). Microglial SIRPα regulates the emergence of CD11c(+) microglia and demyelination damage in white matter. *eLife* 8, 1–29. doi: 10.7554/eLife.42025

Sekizawa, T., Openshaw, H., Ohbo, K., Sugamura, K., Itoyama, Y., and Niland, J. C. (1998). Cerebrospinal fluid interleukin 6 in amyotrophic lateral sclerosis: immunological parameter and comparison with inflammatory and non-inflammatory central nervous system diseases. *J. Neurol. Sci.* 154, 194–199. doi: 10.1016/s0022-510x(97)00228-1

Sengun, I. S., and Appel, S. H. (2003). Serum anti-Fas antibody levels in amyotrophic lateral sclerosis. *J. Neuroimmunol.* 142, 137–140. doi: 10.1016/s0165-5728(03)00263-7

Shao, H., He, Y., Li, K. C., and Zhou, X. (2013). A system mathematical model of a cell-cell communication network in amyotrophic lateral sclerosis. *Mol. BioSyst.* 9, 398–406. doi: 10.1039/c2mb25370d

Shea-Donohue, T., Stiltz, J., Zhao, A., and Notari, L. (2010). Mast cells. *Curr. Gastroenterol. Rep.* 12, 349–357. doi: 10.1007/s11894-010-0132-1

Sofroniew, M. V., and Vinters, H. V. (2010). Astrocytes: biology and pathology. *Acta Neuropathol.* 119, 7–35. doi: 10.1007/s00401-009-0619-8

Song, S., Miranda, C. J., Braun, L., Meyer, K., Frakes, A. E., Ferraiuolo, L., et al. (2016). Major histocompatibility complex class I molecules protect motor neurons from astrocyte-induced toxicity in amyotrophic lateral sclerosis. *Nat. Med.* 22, 397–403. doi: 10.1038/nm.4052

Spiller, K. J., Restrepo, C. R., Khan, T., Dominique, M. A., Fang, T. C., Canter, R. G., et al. (2018). Microglia-mediated recovery from ALS-relevant motor neuron degeneration in a mouse model of TDP-43 proteinopathy. *Nat. Neurosci.* 21, 329–340. doi: 10.1038/s41593-018-0083-7

Sprague, A. H., and Khalil, R. A. (2009). Inflammatory cytokines in vascular dysfunction and vascular disease. *Biochem. Pharmacol.* 78, 539–552. doi: 10.1016/j.bcp.2009.04.029

Sta, M., Sylva-Steenland, R. M., Casula, M., de Jong, J. M., Troost, D., Aronica, E., et al. (2011). Innate and adaptive immunity in amyotrophic lateral sclerosis: evidence of complement activation. *Neurobiol. Dis.* 42, 211–220. doi: 10.1016/j.nbd.2011.01.002

Stenovec, M., Milošević, M., Petrušić, V., Potokar, M., Stević, Z., Prebil, M., et al. (2011). Amyotrophic lateral sclerosis immunoglobulins G enhance the mobility of Lysotracker-labelled vesicles in cultured rat astrocytes. *Acta Physiol (Oxf.)* 203, 457–471. doi: 10.1111/j.1748-1716.2011.02337.x

Stoklund Dittlau, K., and Van Den Bosch, L. (2023). Why should we care about astrocytes in a motor neuron disease? *Front. Molec. Med.* 3:1047540. doi: 10.3389/fmmed.2023.1047540

Sun, Y., Wen, Y., Wang, L., Wen, L., You, W., Wei, S., et al. (2021). Therapeutic opportunities of Interleukin-33 in the central nervous system. *Front. Immunol.* 12:654626. doi: 10.3389/fimmu.2021.654626

Takahashi, K. (2023). Microglial heterogeneity in amyotrophic lateral sclerosis. *J. Neuropathol. Exp. Neurol.* 82, 140–149. doi: 10.1093/jnen/nlac110

Tani, K., Ogushi, F., Kido, H., Kawano, T., Kunori, Y., Kamimura, T., et al. (2000). Chymase is a potent chemoattractant for human monocytes and neutrophils. *J. Leukoc. Biol.* 67, 585–589. doi: 10.1002/jlb.67.4.585

Tavolato, B. F., Licandro, A. C., and Saia, A. (1975). Motor neurone disease: an immunological study. *Eur. Neurol.* 13, 433–440. doi: 10.1159/000114699

Theoharides, T. C., Alysandratos, K. D., Angelidou, A., Delivanis, D. A., Sismanopoulos, N., Zhang, B., et al. (2012). Mast cells and inflammation. *Biochim. Biophys. Acta* 1822, 21–33. doi: 10.1016/j.bbadis.2010.12.014

Thonhoff, J. R., Beers, D. R., Zhao, W., Pleitez, M., Simpson, E. P., Berry, J. D., et al. (2018a). Expanded autologous regulatory T-lymphocyte infusions in ALS: a phase I, first-in-human study. *Neurol. Neuroimmunol. Neuroinflamm.* 5:e465. doi: 10.1212/nxi.0000000000000465

Thonhoff, J. R., Simpson, E. P., and Appel, S. H. (2018b). Neuroinflammatory mechanisms in amyotrophic lateral sclerosis pathogenesis. *Curr. Opin. Neurol.* 31, 635–639. doi: 10.1097/wco.0000000000000599

Tiemessen, M. M., Jagger, A. L., Evans, H. G., van Herwijnen, M. J., John, S., and Taams, L. S. (2007). CD4+CD25+Foxp3+ regulatory T cells induce alternative activation of human monocytes/macrophages. *Proc. Natl. Acad. Sci. U. S. A.* 104, 19446–19451. doi: 10.1073/pnas.0706832104

Trias, E., Ibarburu, S., Barreto-Núñez, R., Varela, V., Moura, I. C., Dubreuil, P., et al. (2017). Evidence for mast cells contributing to neuromuscular pathology in an inherited model of ALS. *JCI Insight* 2, 1–14. doi: 10.1172/jci.insight.95934

Trias, E., King, P. H., Si, Y., Kwon, Y., Varela, V., Ibarburu, S., et al. (2018). Mast cells and neutrophils mediate peripheral motor pathway degeneration in ALS. *JCI Insight* 3, 1–16. doi: 10.1172/jci.insight.123249

Tsuboi, Y., and Yamada, T. (1994). Increased concentration of C4d complement protein in CSF in amyotrophic lateral sclerosis. *J. Neurol. Neurosurg. Psychiatry* 57, 859–861. doi: 10.1136/jnnp.57.7.859

Tzartos, J. S., Zisimopoulou, P., Rentzos, M., Karandreas, N., Zouvelou, V., Evangelakou, P., et al. (2014). LRP4 antibodies in serum and CSF from amyotrophic lateral sclerosis patients. *Ann. Clin. Transl. Neurol.* 1, 80–87. doi: 10.1002/acn3.26

Uchitel, O. D., Appel, S. H., Crawford, F., and Sczcupak, L. (1988). Immunoglobulins from amyotrophic lateral sclerosis patients enhance spontaneous transmitter release from motor-nerve terminals. *Proc. Natl. Acad. Sci. U. S. A.* 85, 7371–7374. doi: 10.1073/pnas.85.19.7371

van Blitterswijk, M., Gulati, S., Smoot, E., Jaffa, M., Maher, N., Hyman, B. T., et al. (2011). Anti-superoxide dismutase antibodies are associated with survival in patients with sporadic amyotrophic lateral sclerosis. *Amyotroph. Lateral Scler.* 12, 430–438. doi: 10.3109/17482968.2011.585163

van der Vliet, H. J., von Blomberg, B. M., Nishi, N., Reijm, M., Voskuyl, A. E., van Bodegraven, A. A., et al. (2001). Circulating V (alpha24+) Vbeta11+ NKT cell numbers are decreased in a wide variety of diseases that are characterized by autoreactive tissue damage. *Clin. Immunol.* 100, 144–148. doi: 10.1006/clim.2001.5060

van Schaik, I. N., Bossuyt, P. M., Brand, A., and Vermeulen, M. (1995). Diagnostic value of GM1 antibodies in motor neuron disorders and neuropathies: a meta-analysis. *Neurology* 45, 1570–1577. doi: 10.1212/wnl.45.8.1570

Varcianna, A., Myszczynska, M. A., Castelli, L. M., O'Neill, B., Kim, Y., Talbot, J., et al. (2019). Micro-RNAs secreted through astrocyte-derived extracellular vesicles cause neuronal network degeneration in C9orf72 ALS. *EBioMedicine* 40, 626–635. doi: 10.1016/j.ebiom.2018.11.067

Vargas, M. R., and Johnson, J. A. (2010). Astrogliosis in amyotrophic lateral sclerosis: role and therapeutic potential of astrocytes. *Neurotherapeutics* 7, 471–481. doi: 10.1016/j.nurt.2010.05.012

Wei, Q. Q., Hou, Y. B., Zhang, L. Y., Ou, R. W., Cao, B., Chen, Y. P., et al. (2022). Neutrophil-to-lymphocyte ratio in sporadic amyotrophic lateral sclerosis. *Neural Regen. Res.* 17, 875–880. doi: 10.4103/1673-5374.322476

Weiss, S. J. (1989). Tissue destruction by neutrophils. *N. Engl. J. Med.* 320, 365–376. doi: 10.1056/nejm198902093200606

Wernersson, S., and Pejler, G. (2014). Mast cell secretory granules: armed for battle. *Nat. Rev. Immunol.* 14, 478–494. doi: 10.1038/nri3690

Wezel, A., Lagraauw, H. M., van der Velden, D., de Jager, S. C., Quax, P. H., Kuiper, J., et al. (2015). Mast cells mediate neutrophil recruitment during atherosclerotic plaque progression. *Atherosclerosis* 241, 289–296. doi: 10.1016/j.atherosclerosis.2015.05.028

Wosiski-Kuhn, M., Caress, J. B., Cartwright, M. S., Hawkins, G. A., and Milligan, C. (2021). Interleukin 6 (IL6) level is a biomarker for functional disease progression within IL6R(358) ala variant groups in amyotrophic lateral sclerosis patients. *Amyotroph Lateral Scler Frontotemporal Degener* 22, 248–259. doi: 10.1080/21678421.2020.1813310

Wu, S., Yi, J., Zhang, Y. G., Zhou, J., and Sun, J. (2015). Leaky intestine and impaired microbiome in an amyotrophic lateral sclerosis mouse model. *Physiol. Rep.* 3, 1–10. doi: 10.14814/phy2.12356

Yamada, T., Moroo, I., Koguchi, Y., Asahina, M., and Hirayama, K. (1994). Increased concentration of C4d complement protein in the cerebrospinal fluids in progressive supranuclear palsy. *Acta Neurol. Scand.* 89, 42–46. doi: 10.1111/j.1600-0404.1994.tb01631.x

Yazdani, S., Seitz, C., Cui, C., Lovik, A., Pan, L., Piehl, F., et al. (2022). T cell responses at diagnosis of amyotrophic lateral sclerosis predict disease progression. *Nat. Commun.* 13:6733. doi: 10.1038/s41467-022-34526-9

Yi, F. H., Lautrette, C., Vermot-Desroches, C., Bordessoule, D., Couratier, P., Wijdenes, J., et al. (2000). In vitro induction of neuronal apoptosis by anti-Fas antibody-containing sera from amyotrophic lateral sclerosis patients. *J. Neuroimmunol.* 109, 211–220. doi: 10.1016/s0165-5728(00)00288-5

Zeng, Q., Shen, J., Chen, K., Zhou, J., Liao, Q., Lu, K., et al. (2020). The alteration of gut microbiome and metabolism in amyotrophic lateral sclerosis patients. *Sci. Rep.* 10:12998. doi: 10.1038/s41598-020-69845-8

Zhang, J. M., and An, J. (2007). Cytokines, inflammation, and pain. *Int. Anesthesiol. Clin.* 45, 27–37. doi: 10.1097/AIA.0b013e318034194e

Zhang, R., Gascon, R., Miller, R. G., Gelinas, D. F., Mass, J., Hadlock, K., et al (2005). Evidence for systemic immune system alterations in sporadic amyotrophic lateral sclerosis (sALS). *J. Neuroimmunol.* 159, 215–224. doi: 10.1016/j.jneuroim.2004.10.009

Zhao, J., Wang, X., Huo, Z., Chen, Y., Liu, J., Zhao, Z., et al. (2022). The impact of mitochondrial dysfunction in amyotrophic lateral sclerosis. *Cells* 11, 1–21. doi: 10.3390/cells11132049

Zhao, W., Beers, D. R., Bell, S., Wang, J., Wen, S., Baloh, R. H., et al. (2015). TDP-43 activates microglia through NF-κB and NLRP3 inflammasome. *Exp. Neurol.* 273, 24–35. doi: 10.1016/j.expneurol.2015.07.019

Zhao, W., Xie, W., Xiao, Q., Beers, D. R., and Appel, S. H. (2006). Protective effects of an anti-inflammatory cytokine, interleukin-4, on motoneuron toxicity induced by activated microglia. *J. Neurochem.* 99, 1176–1187. doi: 10.1111/j.1471-4159.2006.04172.x

Zhuang, X., Silverman, A. J., and Silver, R. (1996). Brain mast cell degranulation regulates blood-brain barrier. *J. Neurobiol.* 31, 393–403. doi: 10.1002/(sici)1097-4695(199612)31:4<393::Aid-neu1>3.0.Co;2-4

Zondler, L., Feiler, M. S., Freischmidt, A., Ruf, W. P., Ludolph, A. C., Danzer, K. M., et al. (2017). Impaired activation of ALS monocytes by exosomes. *Immunol. Cell Biol.* 95, 207–214. doi: 10.1038/icb.2016.89

Zondler, L., Müller, K., Khalaji, S., Bliederhäuser, C., Ruf, W. P., Grozdanov, V., et al. (2016). Peripheral monocytes are functionally altered and invade the CNS in ALS patients. *Acta Neuropathol.* 132, 391–411. doi: 10.1007/s00401-016-1548-y

frontiers | Frontiers in Neuroscience

TYPE Original Research
PUBLISHED 12 December 2023
DOI 10.3389/fnins.2023.1299122

OPEN ACCESS

EDITED BY
Danyllo Oliveira,
University of São Paulo, Brazil

REVIEWED BY
Mateus Castro,
University of São Paulo, Brazil
João Locke De Araújo,
Federal University of Minas Gerais, Brazil

*CORRESPONDENCE
Zixing Xu
✉ xuzixing@fjmu.edu.cn
Chunfu Zheng
✉ zheng.alan@hotmail.com
Weihong Xu
✉ xuweihong815@126.com

†These authors have contributed equally to this work

RECEIVED 22 September 2023
ACCEPTED 23 November 2023
PUBLISHED 12 December 2023

CITATION
Zheng Q, Wang D, Lin R, Chen Y, Huang H, Xu Z, Zheng C and Xu W (2023) Mendelian randomization analysis suggests no associations of human herpes viruses with amyotrophic lateral sclerosis.
Front. Neurosci. 17:1299122.
doi: 10.3389/fnins.2023.1299122

Mendelian randomization analysis suggests no associations of human herpes viruses with amyotrophic lateral sclerosis

Qingcong Zheng[1,2†], Du Wang[3†], Rongjie Lin[4†], Yuchao Chen[5], Haoen Huang[1], Zixing Xu[1,2*], Chunfu Zheng[6*] and Weihong Xu[1,2*]

[1]Department of Spinal Surgery, the First Affiliated Hospital of Fujian Medical University, Fuzhou, China, [2]Department of Orthopedics, National Regional Medical Center, Binhai Campus of the First Affiliated Hospital, Fujian Medical University, Fuzhou, China, [3]Arthritis Clinical and Research Center, Peking University People's Hospital, Beijing, China, [4]Department of Orthopedic Surgery, Fujian Medical University Union Hospital, Fuzhou, China, [5]Department of Paediatrics, Fujian Provincial Hospital South Branch, Fuzhou, China, [6]Department of Microbiology, Immunology and Infectious Diseases, University of Calgary, Calgary, AB, Canada

Background: The causal associations between infections with human herpes viruses (HHVs) and amyotrophic lateral sclerosis (ALS) has been disputed. This study investigated the causal associations between herpes simplex virus (HSV), varicella-zoster virus (VZV), Epstein–Barr virus (EBV), cytomegalovirus (CMV), HHV-6, and HHV-7 infections and ALS through a bidirectional Mendelian randomization (MR) method.

Methods: The genome-wide association studies (GWAS) database were analyzed by inverse variance weighted (IVW), MR-Egger, weighted median, simple mode, and weighted mode methods. MR-Egger intercept test, MR-PRESSO test, Cochran's Q test, funnel plots, and leaveone-out analysis were used to verify the validity and robustness of the MR results.

Results: In the forward MR analysis of the IVW, genetically predicted HSV infections [odds ratio (OR)=0.9917; 95% confidence interval (CI): 0.9685–1.0154; p=0.4886], HSV keratitis and keratoconjunctivitis (OR=0.9897; 95% CI: 0.9739–1.0059; p=0.2107), anogenital HSV infection (OR=1.0062; 95% CI: 0.9826–1.0304; p=0.6081), VZV IgG (OR=1.0003; 95% CI: 0.9849–1.0160; p=0.9659), EBV IgG (OR=0.9509; 95% CI: 0.8879–1.0183; p=0.1497), CMV (OR=0.9481; 95% CI: 0.8680–1.0357; p=0.2374), HHV-6 IgG (OR=0.9884; 95% CI: 0.9486–1.0298; p=0.5765) and HHV-7 IgG (OR=0.9991; 95% CI: 0.9693–1.0299; p=0.9557) were not causally associated with ALS. The reverse MR analysis of the IVW revealed comparable findings, indicating no link between HHVs infections and ALS. The reliability and validity of the findings were verified by the sensitivity analysis.

Conclusion: According to the MR study, there is no evidence of causal associations between genetically predicted HHVs (HSV, VZV, EBV, CMV, HHV-6, and HHV-7) and ALS.

KEYWORDS

amyotrophic lateral sclerosis, human herpes virus, Mendelian randomization, causal association, neurodegenerative diseases

1 Introduction

Amyotrophic lateral sclerosis is a rapidly progressive and fatal neuronal disease characterized by progressive degeneration of motor neurons in the brain and spinal cord, ultimately leading to almost total skeletal muscle paralysis (van Es et al., 2017). Patients with ALS often present

with progressive weakness and atrophy of the extremities, gradually leading to an inability to walk, talk, swallow, and breathe (Taylor et al., 2016). ALS is a rare disease with an incidence of 3.1 per 100,000 person-years (Vasta et al., 2022), with familial ALS (fALS) accounting for 10% of cases and sporadic ALS (sALS) accounting for 90% of cases (Pham et al., 2020) and the average survival after diagnosis is in the range of 3–5 years (Brown and Al-Chalabi, 2017). The number of ALS cases is expected to increase by 69% from 2015 to 2040 due to global aging (Arthur et al., 2016). However, little is known despite the time and money spent investigating ALS's pathogenic mechanisms. ALS is believed to be caused by genetic and environmental interactions (Celeste and Miller, 2018; Schram et al., 2020; Julian et al., 2021; Motataianu et al., 2022; Goutman et al., 2023), with some investigators suggesting that viruses are an important environmental factor in ALS (Celeste and Miller, 2018; Castanedo-Vazquez et al., 2019).

Human herpes viruses are one of the largest families of double-stranded DNA viruses, comprising three main subfamilies: α, β, and γ-herpesviruses. α-herpesviruses include HSV-1, HSV-2, and VZV (HSV-3), β-herpesviruses include CMV (HHV-5), HHV-6, and HHV-7, and γ-herpesviruses include EBV (HHV-4) and HHV-8 (Sehrawat et al., 2018). Epidemiological data showed that billions of people were infected with HSV-1, and 500 million had HSV-1/HSV-2 genital infections in 2016 (James et al., 2020). A global disease burden on VZV reported that new cases surpassed 80 million in 2019 alone and continue to rise (Huang et al., 2022). More than 90% of adults worldwide are chronically infected with EBV (Huang et al., 2021). Moreover, the general population has a seropositivity rate of 83% for CMV IgG antibodies (Zuhair et al., 2019). Approximately 80–90% of adults worldwide have herpesviruses (Khalesi et al., 2023).

Studies have shown that enteroviruses and herpesviruses are the two most common viruses infecting hospitalized patients' central nervous system (CNS) (Roshdy et al., 2023). The α/β/γ-herpesviruses are neurotoxic and neurotropic viruses and are often considered important risk factors for neurodegenerative disease (NDD) (Osorio et al., 2022). However, the relationship between HHVs and ALS is unknown. A study reported that herpesvirus infection and ALS can flare up simultaneously. Nevertheless, there is no way to determine if it is accidental or intentional (Ferri-de-Barros and Moreira, 2010). Some investigators have suggested that HSV-1 can latently infect the trigeminal ganglion and may be a causative factor in ALS (Feng et al., 2022). In addition, the pathogenic risk of ALS was slightly associated with HHV-6 seropositivity in a case–control study (Cermelli et al., 2003). In contrast, no significant correlation was found between ALS and IgG antibodies to HSV and CMV in an immunological evaluation of early ALS (Provinciali et al., 1988). These studies with conflicting conclusions may be due to methodological flaws, including confounders and reverse causality in observational studies. We have no method of determining the association, let alone the causality, between HHVs and ALS.

Random control trials (RCTs) are a type of experimental research methodology that evaluates the effect of a causative factor or a treatment regimen on a disease by randomizing study subjects into groups, implementing different interventions for different groups, and finally comparing the results. RCTs are the gold standard for clinical diagnosis and can determine the causal association between exposure and outcome. There are no reported RCTs on the association between HHVs and ALS, mainly due to the strict constraints of the design process and medical ethics and few reports of observational studies and their mixed conclusions, which makes it important to carry out MR analyses in this context. MR is an epidemiological investigation method based on instrumental variables (IVs) to analyze summary-level data from GWAS, which can greatly reduce confounding bias and consistently and reliably infer causality between exposures and outcomes due to the stochastic nature of the genetic variants and the fact that alleles are not affected by disease (Emdin et al., 2017). Two-sample Mendelian randomization (TSMR) refers to using genetic variants as IVs in both exposure and outcome samples to investigate the effects of modifiable risk factors for disease. Although lower than RCTs, the strength of evidence from MR analyses is stronger than observational studies (Davies et al., 2018). Particularly in rare diseases, MR can achieve more reliable results by analyzing and evaluating much larger sample sizes than in conventional clinical trials. Therefore, our study investigated whether there is a causal association between HHVs and ALS using a bidirectional TSMR method based on GWAS data.

2 Materials and methods

2.1 Study design

This study strengthened epidemiological observational studies using Mendelian randomization (STROBE-MR) (Skrivankova et al., 2021). All data were obtained from the publicly available GWAS database without re-ethical approval. In MR, SNPs as IVs must fulfill the following three assumptions. (1) The relevance assumption: IVs are closely related to exposure; (2) the independence assumption: the IVs are not associated with the potential confounders; (3) the exclusion restriction assumption: IVs affect outcomes only through the exposure pathway (no directional pleiotropy) (Supplementary Figure S1).

2.2 GWAS data sources

The summary-level statistics for all cases and controls in this study are of European ancestry, and the study subjects were residents recruited from multiple research centers in Europe to minimize bias due to race-related confounding factors. GWAS data for HHV-8 of suitable European ancestry could not be found and were therefore not analyzed.

2.2.1 Exposure

The exposure factors and the dataset for this study were as follows. HSV: the finn-b-AB1_HERPES_SIMPLEX (1,595 cases, 211,856 controls and 16,380,457 SNPs), finn-b-H7_HERPESKERATITIS (573 cases, 209,287 controls and 16,380,429 SNPs) and finn-b-AB1_ANOGENITAL_HERPES_SIMPLEX (10,118,743 SNPs) datasets were searched in the latest FinnGen.[1] VZV IgG: The GCST90006928 (25,472,218 SNPs) dataset was searched in GWAS.[2] EBV: the finn-b-AB1_EBV (1,238 cases, 213,666 controls, and 16,380,461 SNPs) dataset was searched for in FinnGen (r9). CMV IgG: The ieu-b-4900 (7,002,835 SNPs) dataset was searched in the Integrative Epidemiology Unit (IEU, https://gwas.mrcieu.ac.uk/). HHV-6 IgG: The GCST90006902 (25,472,218 SNPs) dataset was searched in the GWAS database. HHV-7 IgG: The GCST900069028 (25,472,218 SNPs) dataset was searched in the GWAS database.

1 https://r9.finngen.fi/

2 https://www.ebi.ac.uk/gwas/home

2.2.2 Outcome

The ALS dataset for GCST90027164 (27,205 cases, 110,881 controls, and 10,461,755 SNPs) was searched in the GWAS database. After cleaning and conversion, we saved the data downloaded from the FinnGen database in GWAS database format. After comparing the sources of participants in the eight datasets for HHVs with the one dataset for ALS, we consider the samples for HHVs and ALS to be independent. We list these data in Supplementary Table S1.

2.3 Selection of instrumental variables

A critical step in MR analysis is to obtain valid IVs. We extracted SNPs ($p < 5 \times 10^{-5}$) with significant correlation with HSV, VZV, EBV, CMV, HHV-6, and HHV-7 from the eight exposure datasets. Subsequently, we performed linkage disequilibrium (LD) analysis on the obtained SNPs with "$r^2 < 0.001$, 10,000 = kb" by using the "clump_data" function to exclude the mutual linkage SNPs and to discard non-biallelic SNPs. We used the F-statistic to assess the strength of the association between the selected IVs and exposure. F-statistic is calculated as $F = (\beta/se(\beta))^2$ (Zhang et al., 2023) when $F > 10$ indicates that IVs are strong instrumental variables, which avoids the bias caused by weak IVs. In addition, the summary set may produce errors if the effect alleles for the SNP effects are different in the GWAS data for exposure and outcome. Therefore, we used the "harmonise_data" function to test the causal direction of the screened SNPs in exposure and outcome, excluded palindromic alleles, and selected the SNPs with "TRUE" results for MR analysis.

2.4 TSMR analysis

The data in this study were analyzed based on the "TwoSampleMR" package of R version 4.2.3 software. Analyses included Forward MR with HHVs infection or IgG as the exposure and ALS as the outcome and reverse MR with ALS as the exposure and HHVs infection or IgG as the outcome. We chose MR Egger, weighted median, IVW, simple mode, and weighted mode methods to calculate the causal relationship between exposure and outcome, and IVW was the most valid and reliable of these methods. We then perform sensitivity analyses. Cochran's Q-statistic was used to test for heterogeneity ($p < 0.05$) between SNPs in MR-Egger and IVW analyses to assess the robustness of IVs (Bowden et al., 2019). Heterogeneity was additionally visualized by constructing a funnel plot of the IVs. MR-PRESSO can detect outliers that may bias the results and give a causal change in exposure and outcome after removing the outlier (Verbanck et al., 2018). Therefore, when MR-PRESSO detects an outlier, we exclude the SNPs and re-perform the MR analysis and evaluation. Pleiotropy refers to the fact that some IVs affect outcomes through pathways other than exposure, which would seriously affect the reliability of the causal association between exposure and outcome (Davey Smith and Hemani, 2014). We used the MR-Egger intercept for bias detection and effect estimation. When the "MR_pleiotropy_test" function calculates $p < 0.05$, it means that there is directional pleiotropy (Bowden et al., 2015). Leave-one-out analysis estimates the effect of the remaining SNPs on the outcome by sequentially removing individual SNPs and then performing the IVW analysis again, which can determine whether any single SNPs drive causality.

3 Results

3.1 Screening of instrumental variables

In forward MR, we ended up with 69, 55, 56, 65, 6, 7, 5, and 6 SNPs that were closely associated with HSV infections, HSV keratitis and keratoconjunctivitis, anogenital HSV infection, VZV IgG, EBV, CMV IgG, HHV-6 IgG, and HHV-7 IgG, respectively. In reverse MR, 9, 9, 8, 10, 9, 8, 10, and 9 SNPs were obtained when ALS was used as the exposure corresponding to HSV infections, HSV keratitis and keratoconjunctivitis, anogenital HSV infection, VZV IgG, EBV, CMV IgG, HHV-6 IgG, HHV-7 IgG, respectively. These SNPs were all strong instrumental variables (F-statistic >10). A total of sixteen MR analyses were performed in this study, and details of the screened IVs can be found in Supplementary Tables S2–S17.

3.2 Forward MR

We list the TSMR and the sensitivity analysis results of HHVs and ALS in Table 1. Using IVW as the primary method, it can be seen that genetically predicted HSV infections (OR = 0.9917; 95% CI: 0.9685–1.0154; $p = 0.4886$), HSV keratitis and keratoconjunctivitis (OR = 0.9897; 95% CI: 0.9739–1.0059; $p = 0.2107$), anogenital HSV infection (OR = 1.0062; 95% CI: 0.9826–1.0304; $p = 0.6081$), VZV IgG (OR = 1.0003; 95% CI: 0.9849–1.0160; $p = 0.9659$), EBV IgG (OR = 0.9509; 95% CI: 0.8879–1.0183; $p = 0.1497$), CMV (OR = 0.9481; 95% CI: 0.8680–1.0357; $p = 0.2374$), HHV-6 IgG (OR = 0.9884; 95% CI: 0.9486–1.0298; $p = 0.5765$) and HHV-7 IgG (OR = 0.9991; 95% CI: 0.9693–1.0299; $p = 0.9557$) were not causally associated with ALS, which completely agrees with the conclusions reached by the four methods: MR-Egger, weighted median, simple mode, and weighted mode (Figure 1). Notably, 57 SNPs obtained from the dataset associated with anogenital HSV infection were tested by MR-PRESSO for $p = 0.004$. The p-value for MR-PRESSO is 0.0273 after excluding the outlier SNP (rs16832436), suggesting no remaining outlier SNPs. At this point, MR Egger's P (Q-statistic) = 0.0410, and IVW's P (Q-statistic) = 0.0283. However, the MR Egger intercept test ($p = 0.1229$) showed no directional pleiotropy, indicating that heterogeneity is unlikely to affect the main estimates. The remaining MR analyses had P (Q-statistic) > 0.05, and the funnel plots of SNPs in IVW had a symmetrical distribution, indicating no significant heterogeneity (Supplementary Figure S2). The p-value of all MR Egger intercept tests was greater than 0.05, suggesting no directional pleiotropy of SNPs, indicating the high validity and robustness of the results of the MR analyses in this study. In addition, no significant individual SNPs were found to influence the association from leave-one-out analyses (Supplementary Figure S3). In conclusion, the forest plot shows that HSV, VZV, EBV, CMV, HHV-6, and HHV-7 were not causally associated with ALS (Figure 2).

3.3 Reverse MR

We further explored the causal association of ALS with HHVs and enumerated the results in Table 2. There was also no causal effect of ALS with HSV infections (OR = 1.4497; 95% CI: 0.8429–2.4933; $p = 0.1796$), HSV keratitis and keratoconjunctivitis (OR = 0.7593; 95% CI: 0.4193–1.3750; $p = 0.3634$), anogenital HSV infection (OR = 1.1641; 95% CI: 0.6906–1.9623; $p = 0.5683$), VZV IgG (OR = 0.8480; 95% CI:

10.3389/fnins.2023.1299122

TABLE 1 The causal effect of human herpes viruses (HHVs) and amyotrophic lateral sclerosis (ALS) by two-sample Mendelian Randomization (TSMR) and the sensitivity analysis results.

Forward MR								
Exposure	SNP	F	Mendelian randomization				Heterogeneity	
			Method	OR	95% confidence interval	*p*	Q	Q_P
HSV infections	69	>10	MR Egger	0.9761	0.9320–1.0221	0.3069	60.0225	0.7146
			Weighted median	0.9971	0.9620–1.0335	0.8739		
			IVW	0.9917	0.9685–1.0154	0.4886	60.6399	0.7250
			Simple mode	1.0402	0.9636–1.1228	0.3161		
			Weighted mode	0.9979	0.9401–1.0592	0.9443		
			MR-PRESSO			0.7357		
			Pleiotropy			0.4348		
HSV keratitis and keratoconjunctivitis	55	>10	MR Egger	0.9820	0.9539–1.0109	0.2248	61.9019	0.1882
			Weighted median	0.9847	0.9623–1.0077	0.1901		
			IVW	0.9897	0.9739–1.0059	0.2107	62.3818	0.2028
			Simple mode	1.0099	0.9578–1.0649	0.7167		
			Weighted mode	0.9836	0.9453–1.02340	0.4180		
			MR-PRESSO			0.2157		
			Pleiotropy			0.5243		
Anogenital HSV infection	56	>10	MR Egger	1.0419	0.9916–1.0947	0.1097	73.3438	0.0410
			Weighted median	1.0080	0.9767–1.0403	0.6206		
			IVW	1.0062	0.9826–1.0304	0.6081	76.6802	0.0283
			Simple mode	0.9611	0.8859–1.0427	0.3443		
			Weighted mode	0.9684	0.9071–1.0339	0.3402		
			MR-PRESSO			0.0273(Outlier: rs16832436)		
			Pleiotropy			0.1229		
VZV lgG	65	>10	MR Egger	1.0110	0.9809–1.0420	0.4820	71.9553	0.2056
			Weighted median	0.9994	0.9776–1.0217	0.9603		
			IVW	1.0003	0.9849–1.0160	0.9659	72.6867	0.2136
			Simple mode	0.9988	0.9475–1.0530	0.9657		
			Weighted mode	1.0024	0.9552–1.0519	0.9230		
			MR-PRESSO			0.2187		
			Pleiotropy			0.4266		
EBV	6	>10	MR Egger	0.8207	0.6170–1.0917	0.2463	3.0553	0.5486
			Weighted median	0.9753	0.8930–1.0653	0.5788		
			IVW	0.9509	0.8879–1.0183	0.1497	4.1400	0.5294
			Simple mode	0.8870	0.7663–1.0268	0.1692		
			Weighted mode	1.0097	0.8865–1.1499	0.8906		
			MR-PRESSO			0.5577		
			Pleiotropy			0.3565		
CMV lgG	7	>10	MR Egger	0.8688	0.7344–1.0279	0.1621	3.6783	0.5966
			Weighted median	0.9603	0.8553–1.0784	0.4938		
			IVW	0.9481	0.8680–1.0357	0.2374	5.1108	0.5297
			Simple mode	0.9595	0.8133–1.1321	0.6419		
			Weighted mode	0.9618	0.8194–1.1289	0.6505		
			MR-PRESSO			0.5770		
			Pleiotropy			0.2850		

(Continued)

TABLE 1 (Continued)

Forward MR								
Exposure	SNP	F	Mendelian randomization				Heterogeneity	
			Method	OR	95% confidence interval	*p*	Q	Q_P
HHV-6 lgG	5	>10	MR Egger	0.9718	0.8714–1.0838	0.6424	1.8228	0.6100
			Weighted median	0.9737	0.9262–1.0237	0.2976		
			IVW	0.9884	0.9486–1.0298	0.5765	1.9307	0.7485
			Simple mode	0.9688	0.9038–1.0385	0.4214		
			Weighted mode	0.9647	0.9003–1.0338	0.3663		
			MR-PRESSO			0.7317		
			Pleiotropy			0.7641		
HHV-7 lgG	6	>10	MR Egger	0.9906	0.8696–1.1284	0.8938	5.2634	0.2613
			Weighted median	1.0156	0.9777–1.0550	0.4242		
			IVW	0.9991	0.9693–1.0299	0.9557	5.2870	0.3819
			Simple mode	1.0232	0.9609–1.0897	0.5059		
			Weighted mode	1.0232	0.9644–1.0857	0.4810		
			MR-PRESSO			0.4127		
			Pleiotropy			0.8999		

0.5017–1.4332; $p=0.5380$), EBV (OR = 0.9153; 95% CI: 0.6104–1.3727; $p=0.6688$), CMV (OR = 0.8332; 95% CI: 0.5996–1.1578; $p=0.2770$), HHV-6 IgG (OR = 1.0292; 95% CI: 0.5298–1.9994; $p=0.9323$) and HHV-7 IgG (OR = 0.5408; 95% CI: 0.2023–1.4457; $p=0.2205$) in the IVW analysis, which generally agreed with the results obtained from the remaining four MR analyses (Figure 3). Notably, the MR-PRESSO of the HSV infections dataset was tested for a *p*-value of 0.0130, but no outlier SNPs. At this point, MR Egger's *P* (Q-statistic) = 0.0404, and IVW's *P* (Q-statistic) = 0.0076. However, the MR Egger intercept test with a *p*-value of 0.1229 did not show directional pleiotropy, suggesting that heterogeneity is unlikely to affect the main estimates. MR-PRESSO test on the anogenital HSV infection dataset found a *p*-value of 0.0270, suggesting heterogeneity, and a *p*-value of 0.3623 for MR-PRESSO after excluding outlier SNPs (rs17524886), and did not identify other outlier SNPs. At this point, MR Egger's *P* (Q-statistic) = 0.2497, and IVW's *P* (Q-statistic) = 0.3346, indicating no heterogeneity. The MR-PRESSO test of the HHV-7 IgG dataset found a *p*-value of 0.0467, a *p*-value of 0.3500 after excluding outlier SNPs (rs4669231) and suggesting no other outlier SNPs, and a *P* (Q-statistic) = 0.2704 for MR Egger and *P* (Q-statistic) = 0.3289, indicating no heterogeneity. The *p*-value of the Q-statistic for the rest of the dataset was greater than 0.05, and the SNPs in the funnel plot of IVW were symmetrically distributed, indicating no significant heterogeneity (Supplementary Figure S4). All MR Egger intercept tests had *p*-values greater than 0.05, suggesting that the SNPs were free of directional pleiotropy, which suggests good validity and robustness of the MR analysis. In addition, no individual SNPs capable of driving causality between exposure and outcome were identified from leave-one-out analyses (Supplementary Figure S5). In conclusion, the forest plot shows that ALS was not causally associated with HSV, VZV, EBV, CMV, HHV-6, and HHV-7 (Figure 4).

4 Discussion

Neurodegenerative diseases can damage and degenerate neurons in the CNS and peripheral nervous system, resulting in severe loss of memory, behavior, and sensory and motor functions due to the inability of the neurons to renew and regenerate. Classic NDDs include Parkinson's disease, Alzheimer's disease, and ALS, which impose an enormous global burden (Wilson et al., 2023). Although the pathogenic mechanism of ALS is unclear, it is believed that it may be due to oxidative stress, apoptosis, mitochondrial dysfunction, axonal degeneration, neuroinflammation, and viruses (Sever et al., 2022).

Among HHVs, the most well-known HSV can infect neurons and reach the CNS through retrograde axonal transport, ultimately leading to diseases such as encephalomyelitis, and several studies have shown that HSV is closely related to NDDs (Carneiro et al., 2022). Primary infection with VZV causes varicella and can latently infect neurons. When the body is immunocompromised or aged, VZV is reactivated and causes a zoster. In addition, VZV can cause neurological syndromes such as myelitis and segmental motor paralysis (Gershon et al., 2015). EBV is most commonly associated with infectious mononucleosis, while primary or latent infections are mostly associated with neurological disorders, such as encephalomyelitis (Andersen et al., 2023). CMV can exhibit tropism for neural stem cells and cause multiple spinal cord radiculitis (Kleinschmidt-DeMasters and Gilden, 2001; Kamte et al., 2021). The viral load of HHV-6 is associated with increased central nervous system demyelination (Lucas et al., 2023). The damage to the CNS system by HHV-7 has also been reported (Li et al., 2022).

However, do these HHVs increase the risk of ALS? Earlier studies reported that chronic viral infections play an important role in the pathogenesis of ALS, and antibody titers to HSV-1 were significantly increased in the sera of ALS patients (Irkeç et al., 1989). In contrast, studies have reported that significant elevations of HSV-1, HSV-2, and VZV antibodies were not detected in the sera of ALS patients (Catalano, 1972). In a mouse model of latent HSV-2 infection, it was found that HSV-2-induced spinal cord inflammation, although similar to that of ALS patients, was insufficient to induce the characteristic changes in the pathology of ALS (Cabrera et al., 2020). In addition, it has been reported that HSV-1, EBV, CMV, and HHV-6 can cause

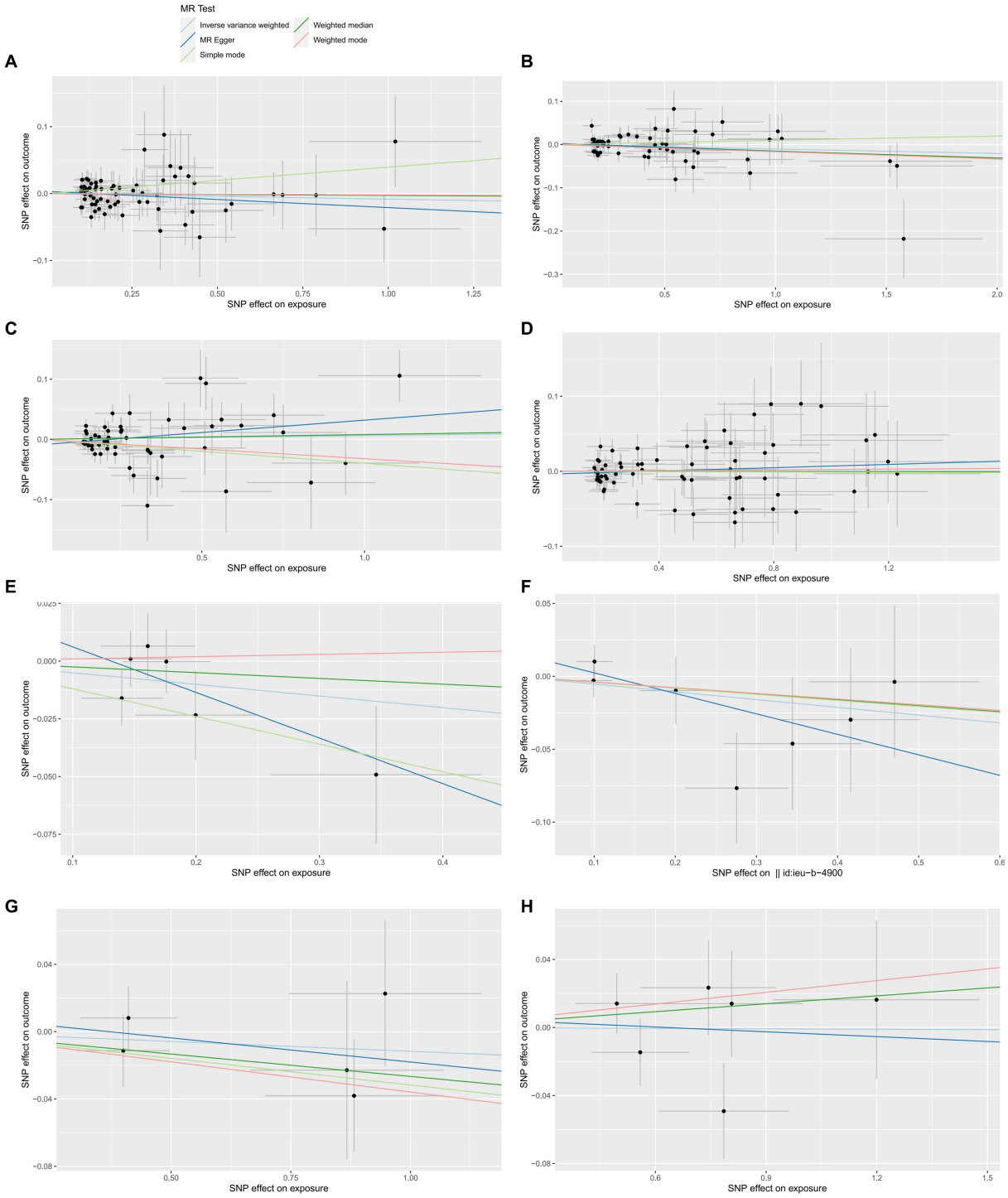

FIGURE 1
The forward MR effect of HHVs and ALS. Scatter plots for MR-Egger, weighted median, IVW, simple mode and weighted mode methods highlighting the effect of HSV infections **(A)**, HSV keratitis and keratoconjunctivitis **(B)**, anogenital HSV infection **(C)**, VZV IgG **(D)**, EBV **(E)**, CMV IgG **(F)**, HHV-6 IgG **(G)**, HHV-7 IgG **(H)**, on ALS.

motor neuron degeneration by activating endogenous retroviruses, thereby inducing the expression of the envelope glycoprotein HERV-K in ALS (Medina et al., 2017; Mayer et al., 2018). However, a subsequent study questioned this view due to their failure to detect highly expressed HERV-K RNA in ALS (Garson et al., 2019). Therefore, a causal association between HHVs and ALS cannot be stated based on the available evidence, and our systematic MR analyses can contribute to related studies.

Thus, studies on the relationship between human herpesviruses and ALS are conflicting, and there are few reports of a causal association between them. We concluded that there is no evidence to support a causal association between HHVs (HSV, VZV, EBV, CMV,

10.3389/fnins.2023.1299122

Methods	nsnp	pval	OR (95% CI)
HSV infections − ALS			
MR Egger	69	0.3069	0.9761 (0.9320 − 1.0221)
Weighted median	69	0.8739	0.9971 (0.9620 − 1.0335)
IVW	69	0.4886	0.9917 (0.9685 − 1.0154)
Simple mode	69	0.3161	1.0402 (0.9636 − 1.1228)
Weighted mode	69	0.9443	0.9979 (0.9401 − 1.0592)
HSV keratitis and keratoconjunctivitis − ALS			
MR Egger	55	0.2248	0.9820 (0.9539 − 1.0109)
Weighted median	55	0.1901	0.9847 (0.9623 − 1.0077)
IVW	55	0.2107	0.9897 (0.9739 − 1.0059)
Simple mode	55	0.7167	1.0099 (0.9578 − 1.0649)
Weighted mode	55	0.4180	0.9836 (0.9453 − 1.0234)
Anogenital HSV infection − ALS			
MR Egger	56	0.1097	1.0419 (0.9916 − 1.0947)
Weighted median	56	0.6206	1.0080 (0.9767 − 1.0403)
IVW	56	0.6081	1.0062 (0.9826 − 1.0304)
Simple mode	56	0.3443	0.9611 (0.8859 − 1.0427)
Weighted mode	56	0.3402	0.9684 (0.9071 − 1.0339)
VZV − ALS			
MR Egger	65	0.4820	1.0110 (0.9809 − 1.0420)
Weighted median	65	0.9603	0.9994 (0.9776 − 1.0217)
IVW	65	0.9659	1.0003 (0.9849 − 1.0160)
Simple mode	65	0.9657	0.9988 (0.9475 − 1.0530)
Weighted mode	65	0.9230	1.0024 (0.9552 − 1.0519)
EBV − ALS			
MR Egger	6	0.2463	0.8207 (0.6170 − 1.0917)
Weighted median	6	0.5788	0.9753 (0.8930 − 1.0653)
IVW	6	0.1497	0.9509 (0.8879 − 1.0183)
Simple mode	6	0.1692	0.8870 (0.7663 − 1.0268)
Weighted mode	6	0.8906	1.0097 (0.8865 − 1.1499)
CMV − ALS			
MR Egger	7	0.1621	0.8688 (0.7344 − 1.0279)
Weighted median	7	0.4938	0.9603 (0.8553 − 1.0784)
IVW	7	0.2374	0.9481 (0.8680 − 1.0357)
Simple mode	7	0.6419	0.9595 (0.8133 − 1.1321)
Weighted mode	7	0.6505	0.9618 (0.8194 − 1.1289)
HHV6 − ALS			
MR Egger	5	0.6424	0.9718 (0.8714 − 1.0838)
Weighted median	5	0.2976	0.9737 (0.9262 − 1.0237)
IVW	5	0.5765	0.9884 (0.9486 − 1.0298)
Simple mode	5	0.4214	0.9688 (0.9038 − 1.0385)
Weighted mode	5	0.3663	0.9647 (0.9003 − 1.0338)
HHV7 − ALS			
MR Egger	6	0.8938	0.9906 (0.8696 − 1.1284)
Weighted median	6	0.4242	1.0156 (0.9777 − 1.0550)
IVW	6	0.9557	0.9991 (0.9693 − 1.0299)
Simple mode	6	0.5059	1.0232 (0.9609 − 1.0897)
Weighted mode	6	0.4810	1.0232 (0.9644 − 1.0857)

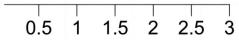

FIGURE 2
Forest plots of causal effect estimates in the forward MR analysis. SNP, single-nucleotide polymorphism; ALS, amyotrophic lateral sclerosis; IVW, inverse variance weighted; OR, odds ratio; 95% CI, 95% confidence interval.

HHV-6, and HHV-7) and ALS using bidirectional TSMR based on a sizable sample of GWAS data, implying that observational studies in which HHVs and ALS are associated may be due to confounding factors such as environment or shared genetic structure.

Our bidirectional TSMR study focused on the causal relationship between HHVs and ALS for the first time. This study has several strengths. Firstly, we are not limited to studying HSV and ALS but have expanded to study the causal relationship between multiple HHVs and ALS. Secondly, a bidirectional TSMR analysis reduces bias from confounding factors and excludes the effects caused by reverse causality. Of course, this study has some limitations. First, the significance threshold was relaxed from 5×10^{-8} to 5×10^{-5} because the number of IVs was so small. Distortion caused by weak instruments is possible, even though the resulting IVs were all defined as strong instrumental variables after calculating the F statistic ($F>10$). Second, although sensitivity analyses of MR indicate robustness among SNPs, there is still the possibility of residual heterogeneity. Finally, we only analyzed GWAS data using European ancestry, and results should be interpreted with caution when applied to other populations.

10.3389/fnins.2023.1299122

TABLE 2 The causal effect of amyotrophic lateral sclerosis (ALS) and human herpes viruses (HHVs) by two-sample Mendelian Randomization (TSMR) and the sensitivity analysis results.

Reverse MR								
Outcome	SNP	F	Mendelian randomization				Heterogeneity	
			Method	OR	95% confidence interval	P	Q	Q_P
HSV infections	9	>10	MR Egger	0.5250	0.1491–1.8485	0.3491	14.6775	0.0404
			Weighted median	1.2276	0.7147–2.1087	0.4574		
			IVW	1.4497	0.8429–2.4933	0.1796	20.8434	0.0076
			Simple mode	0.6305	0.1781–2.2314	0.4947		
			Weighted mode	0.7290	0.2189–2.4282	0.6206		
			MR-PRESSO			0.0130 (No outlier)		
			pleiotropy			0.1301		
HSV keratitis and keratoconjunctivitis	9	>10	MR Egger	0.5082	0.1019–2.5350	0.4363	8.1388	0.3205
			Weighted median	0.7295	0.3192–1.6669	0.4544		
			IVW	0.7593	0.4193–1.3750	0.3634	8.4668	0.3893
			Simple mode	0.3840	0.0887–1.6618	0.2363		
			Weighted mode	0.3613	0.0732–1.7820	0.2465		
			MR-PRESSO			0.3510		
			pleiotropy			0.6118		
Anogenital HSV infection	8	>10	MR Egger	1.4447	0.3428–6.0888	0.6340	7.8441	0.2497
			Weighted median	1.2291	0.6313–2.3927	0.5440		
			IVW	1.1641	0.6906–1.9623	0.5683	7.9774	0.3346
			Simple mode	0.6670	0.2166–2.0540	0.5032		
			Weighted mode	1.8232	0.7162–4.6413	0.2481		
			MR-PRESSO			0.3623 (Outlier: rs17524886)		
			pleiotropy			0.7603		
VZV lgG	10	>10	MR Egger	1.2778	0.3419–4.7762	0.7249	7.0744	0.5286
			Weighted median	0.9059	0.4514–1.8181	0.7811		
			IVW	0.8480	0.5017–1.4332	0.5380	7.5159	0.5836
			Simple mode	0.9145	0.3016–2.7723	0.8779		
			Weighted mode	0.9060	0.3246–2.5289	0.8547		
			MR-PRESSO			0.5907		
			pleiotropy			0.5251		
EBV	9	>10	MR Egger	1.0159	0.3567–2.8939	0.9772	5.1470	0.6420
			Weighted median	0.8890	0.5164–1.5303	0.6711		
			IVW	0.9153	0.6104–1.3727	0.6688	5.1919	0.7369
			Simple mode	0.7376	0.3254–1.6721	0.4869		
			Weighted mode	0.7529	0.3255–1.7413	0.5257		
			MR-PRESSO			0.7260		
			pleiotropy			0.8383		
CMV lgG	8	>10	MR Egger	0.4826	0.2376–0.9802	0.0905	5.0916	0.5321
			Weighted median	0.8155	0.5416–1.2280	0.3288		
			IVW	0.8332	0.5996–1.1578	0.2770	7.9111	0.3405
			Simple mode	0.7831	0.3949–1.5528	0.5065		
			Weighted mode	0.7740	0.3978–1.5061	0.4753		
			MR-PRESSO			0.3553		
			pleiotropy			0.1441		

(Continued)

TABLE 2 (Continued)

Reverse MR								
Outcome	SNP	F	Mendelian randomization				Heterogeneity	
			Method	OR	95% confidence interval	P	Q	Q_P
HHV-6 lgG	10	>10	MR Egger	1.0570	0.1994–5.6030	0.9497	4.3357	0.8256
			Weighted median	1.1747	0.4958–2.7834	0.7144		
			IVW	1.0292	0.5298–1.9994	0.9323	4.3369	0.8879
			Simple mode	1.3468	0.3474–5.2215	0.6769		
			Weighted mode	1.4103	0.3754–5.2987	0.6229		
			MR-PRESSO			0.8853		
			pleiotropy			0.9736		
HHV-7 lgG	9	>10	MR Egger	0.2620	0.0174–3.9373	0.3650	8.7596	0.2704
			Weighted median	0.2803	0.0792–0.9912	0.0484		
			IVW	0.5408	0.2023–1.4457	0.2205	9.1611	0.3289
			Simple mode	0.2053	0.0275–1.5347	0.1615		
			Weighted mode	0.2324	0.0316–1.7070	0.1894		
			MR-PRESSO			0.3500 (Outlier: rs4669231)		
			pleiotropy			0.5888		

5 Conclusion

We have shown no causal association between genetically predicted human herpes viruses (HSV, VZV, EBV, CMV, HHV-6, and HHV-7) and ALS based on Mendelian randomization analysis of currently relevant GWAS data. The associations observed in epidemiological studies may be partly attributable to shared genetic structure or environmental confounders, and we could devote more time and money to studies of other environmental factors associated with ALS and genetic structure.

Data availability statement

The original contributions presented in the study are included in the article/Supplementary material, further inquiries can be directed to the corresponding authors.

Author contributions

QZ: Writing – original draft. DW: Writing – original draft. RL: Writing – original draft. YC: Writing – original draft. HH: Writing – original draft. ZX: Writing – review & editing. CZ: Writing – review & editing. WX: Writing – review & editing.

Funding

The author(s) declare financial support was received for the research, authorship, and/or publication of this article. The Natural Science Foundation of Fujian Province (No. 2020J01947, No. 2021J02035) and Fujian Provincial Health Technology Project (No. 2020CXA039, No. 2021CXA019) supported the study.

Acknowledgments

We want to acknowledge the genome-wide association study consortia, FinnGen study, and the IEU OpenGWAS, who made their summary statistics publicly available.

Conflict of interest

The authors declare that the research was conducted in the absence of any commercial or financial relationships that could be construed as a potential conflict of interest.

Publisher's note

Supplementary material

The Supplementary material for this article can be found online at: https://www.frontiersin.org/articles/10.3389/fnins.2023.1299122/full#supplementary-material

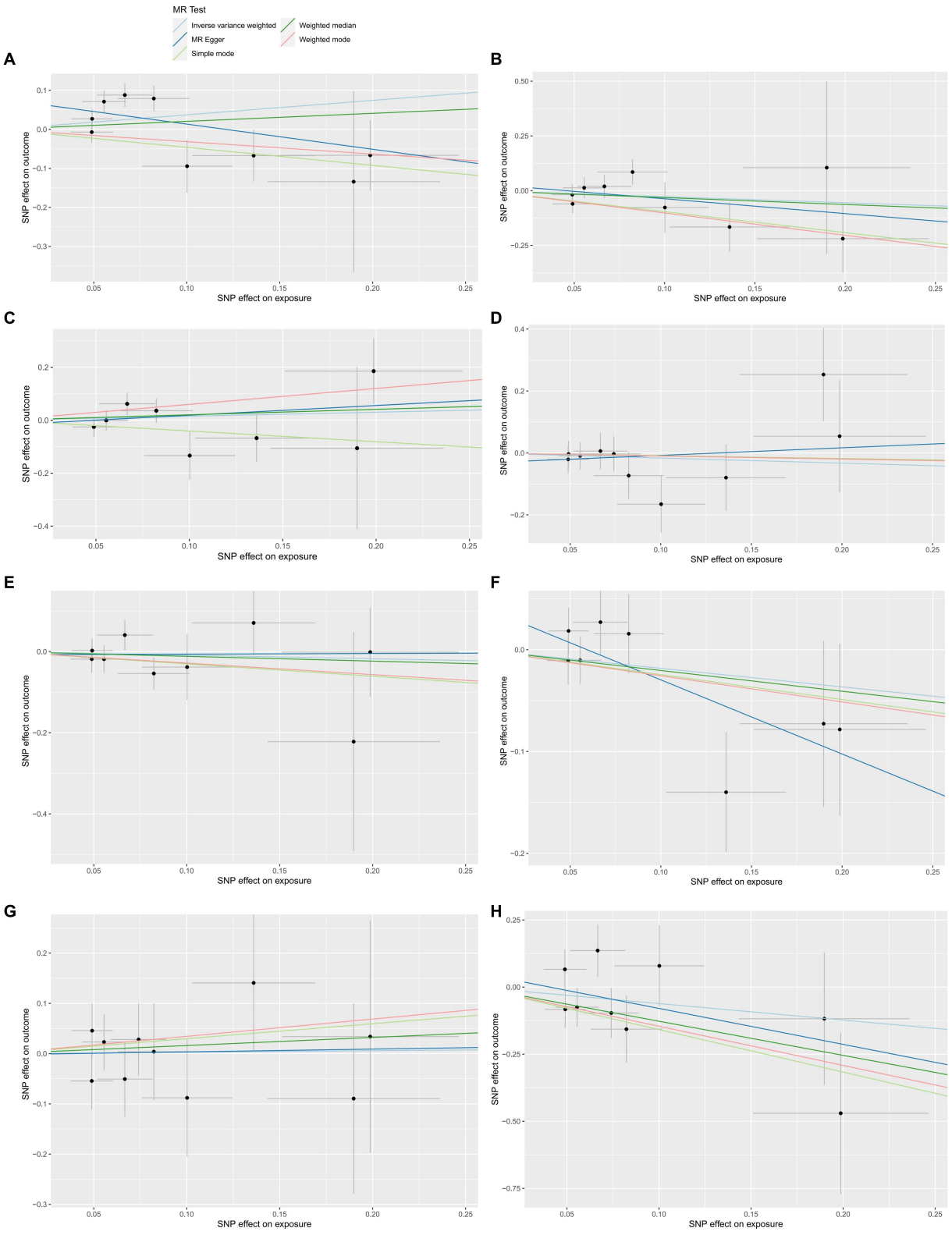

FIGURE 3
The reverse MR effect of ALS and HHVs. Scatter plots for highlighting the effect of ALS on HSV infections**(A)**, HSV keratitis and keratoconjunctivitis **(B)**, anogenital HSV infection **(C)**, VZV IgG **(D)**, EBV **(E)**, CMV IgG **(F)**, HHV-6 IgG **(G)**, HHV-7 IgG **(H)** using the MR-Egger, weighted median, IVW, simple mode and weighted mode methods.

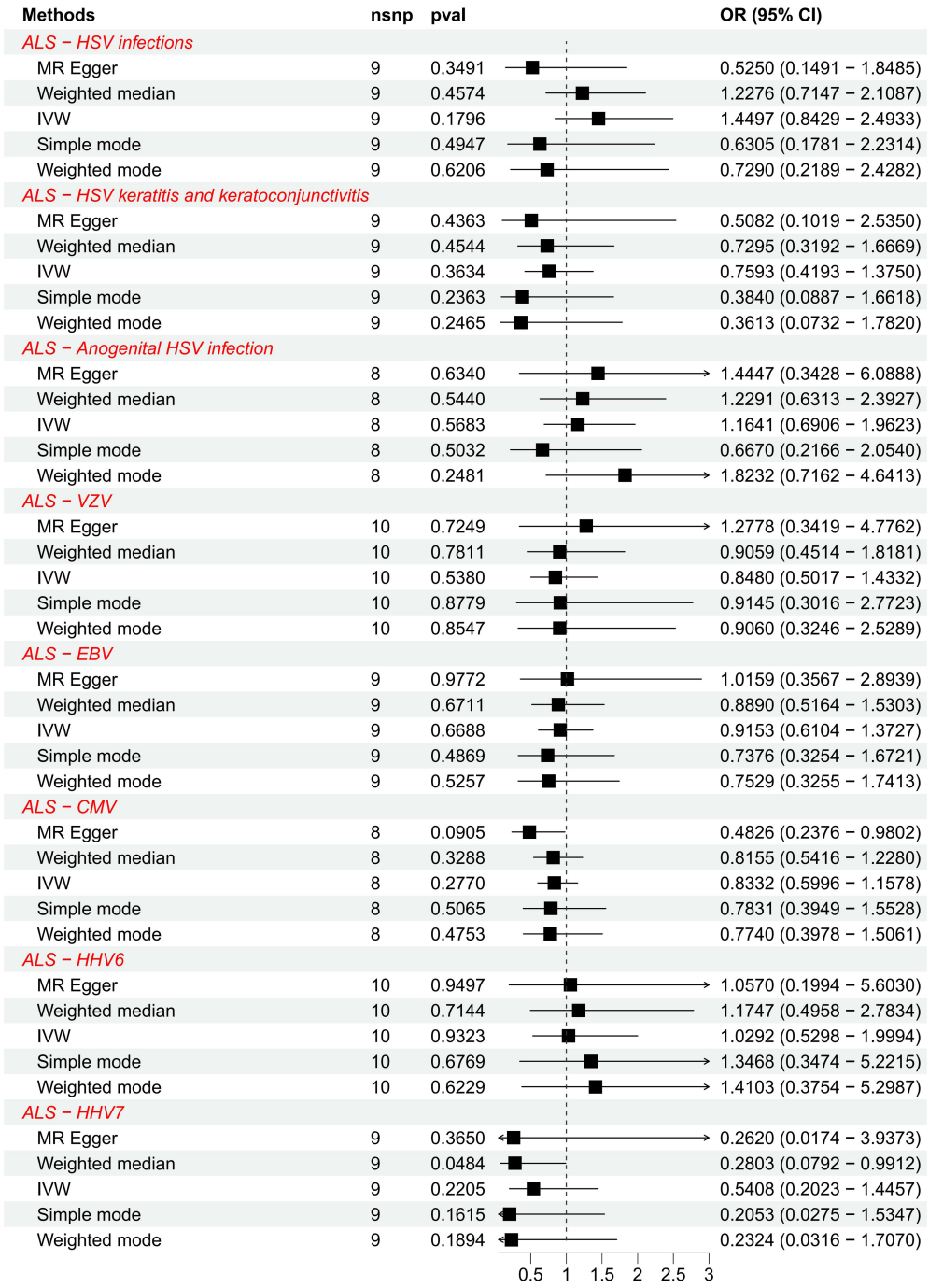

FIGURE 4
Forest plots of causal effect estimates in the reverse MR analysis. SNP, single-nucleotide polymorphism; ALS, amyotrophic lateral sclerosis; IVW, inverse variance weighted; OR, odds ratio; 95% CI, 95% confidence interval.

References

Andersen, O., Ernberg, I., and Hedström, A. K. (2023). Treatment options for Epstein-Barr virus-related disorders of the central nervous system. *Infect. Drug Resist.* 16, 4599–4620. doi: 10.2147/idr.S375624

Arthur, K. C., Calvo, A., Price, T. R., Geiger, J. T., Chiò, A., and Traynor, B. J. (2016). Projected increase in amyotrophic lateral sclerosis from 2015 to 2040. *Nat. Commun.* 7:12408. doi: 10.1038/ncomms12408

Bowden, J., Davey Smith, G., and Burgess, S. (2015). Mendelian randomization with invalid instruments: effect estimation and bias detection through egger regression. *Int. J. Epidemiol.* 44, 512–525. doi: 10.1093/ije/dyv080

Bowden, J., Del Greco, M. F., Minelli, C., Zhao, Q., Lawlor, D. A., Sheehan, N. A., et al. (2019). Improving the accuracy of two-sample summary-data mendelian randomization: moving beyond the NOME assumption. *Int. J. Epidemiol.* 48, 728–742. doi: 10.1093/ije/dyy258

Brown, R. H., and Al-Chalabi, A. (2017). Amyotrophic lateral sclerosis. *N. Engl. J. Med.* 377, 162–172. doi: 10.1056/NEJMra1603471

Cabrera, J. R., Rodríguez-Izquierdo, I., Jiménez, J. L., and Muñoz-Fernández, M. (2020). Analysis of ALS-related proteins during herpes simplex virus-2 latent infection. *J. Neuroinflammation* 17:371. doi: 10.1186/s12974-020-02044-4

Carneiro, V. C. S., Pereira, J. G., and de Paula, V. S. (2022). Family Herpesviridae and neuroinfections: current status and research in progress. *Mem. Inst. Oswaldo Cruz* 117:e220200. doi: 10.1590/0074-02760220200

Castanedo-Vazquez, D., Bosque-Varela, P., Sainz-Pelayo, A., and Riancho, J. (2019). Infectious agents and amyotrophic lateral sclerosis: another piece of the puzzle of motor neuron degeneration. *J. Neurol.* 266, 27–36. doi: 10.1007/s00415-018-8919-3

Catalano, L. W. (1972). Herpesvirus hominis antibody in multiple sclerosis and amyotrophic lateral sclerosis. *Neurology* 22, 473–478. doi: 10.1212/wnl.22.5.473

Celeste, D. B., and Miller, M. S. (2018). Reviewing the evidence for viruses as environmental risk factors for ALS: a new perspective. *Cytokine* 108, 173–178. doi: 10.1016/j.cyto.2018.04.010

Cermelli, C., Vinceti, M., Beretti, F., Pietrini, V., Nacci, G., Pietrosemoli, P., et al. (2003). Risk of sporadic amyotrophic lateral sclerosis associated with seropositivity for herpesviruses and echovirus-7. *Eur. J. Epidemiol.* 18, 123–127. doi: 10.1023/a:1023067728557

Davey Smith, G., and Hemani, G. (2014). Mendelian randomization: genetic anchors for causal inference in epidemiological studies. *Hum. Mol. Genet.* 23, R89–R98. doi: 10.1093/hmg/ddu328

Davies, N. M., Holmes, M. V., and Davey Smith, G. (2018). Reading mendelian randomisation studies: a guide, glossary, and checklist for clinicians. *BMJ* 362:k601. doi: 10.1136/bmj.k601

Emdin, C. A., Khera, A. V., and Kathiresan, S. (2017). Mendelian Randomization. *Jama* 318, 1925–1926. doi: 10.1001/jama.2017.17219

Feng, Z., Zhou, F., Tan, M., Wang, T., Chen, Y., Xu, W., et al. (2022). Targeting m6A modification inhibits herpes virus 1 infection. *Genes Dis.* 9, 1114–1128. doi: 10.1016/j.gendis.2021.02.004

Ferri-de-Barros, J. E., and Moreira, M. (2010). Amyotrophic lateral sclerosis and herpes virus: a casual or causal association? Twelve years after. *Arq. Neuropsiquiatr.* 68:978. doi: 10.1590/s0004-282x2010000600033

Garson, J. A., Usher, L., Al-Chalabi, A., Huggett, J., Day, E. F., and McCormick, A. L. (2019). Quantitative analysis of human endogenous retrovirus-K transcripts in postmortem premotor cortex fails to confirm elevated expression of HERV-K RNA in amyotrophic lateral sclerosis. *Acta Neuropathol. Commun.* 7:45. doi: 10.1186/s40478-019-0698-2

Gershon, A. A., Breuer, J., Cohen, J. I., Cohrs, R. J., Gershon, M. D., Gilden, D., et al. (2015). Varicella zoster virus infection. *Nat. Rev. Dis. Primers.* 1:15016. doi: 10.1038/nrdp.2015.16

Goutman, S. A., Boss, J., Jang, D. G., Mukherjee, B., Richardson, R. J., Batterman, S., et al. (2023). Environmental risk scores of persistent organic pollutants associate with higher ALS risk and shorter survival in a new Michigan case/control cohort. *J. Neurol. Neurosurg. Psychiatry*. jnnp-2023-332121. doi: 10.1136/jnnp-2023-332121

Huang, J., Wu, Y., Wang, M., Jiang, J., Zhu, Y., Kumar, R., et al. (2022). The global disease burden of varicella-zoster virus infection from 1990 to 2019. *J. Med. Virol.* 94, 2736–2746. doi: 10.1002/jmv.27538

Huang, S. Y., Yang, Y. X., Kuo, K., Li, H. Q., Shen, X. N., Chen, S. D., et al. (2021). Herpesvirus infections and Alzheimer's disease: a mendelian randomization study. *Alzheimers Res. Ther.* 13:158. doi: 10.1186/s13195-021-00905-5

Irkeç, C., Ustaçelebi, S., Ozalp, K., Ozdemir, C., and Idrisoğlu, H. A. (1989). The viral etiology of amyotrophic lateral sclerosis. *Mikrobiyol. Bul.* 23, 102–109.

James, C., Harfouche, M., Welton, N. J., Turner, K. M., Abu-Raddad, L. J., Gottlieb, S. L., et al. (2020). Herpes simplex virus: global infection prevalence and incidence estimates, 2016. *Bull. World Health Organ.* 98, 315–329. doi: 10.2471/blt.19.237149

Julian, T. H., Glascow, N., Barry, A. D. F., Moll, T., Harvey, C., Klimentidis, Y. C., et al. (2021). Physical exercise is a risk factor for amyotrophic lateral sclerosis: convergent evidence from mendelian randomisation, transcriptomics and risk genotypes. *EBioMedicine* 68:103397. doi: 10.1016/j.ebiom.2021.103397

Kamte, Y. S., Chandwani, M. N., Michaels, A. C., and O'Donnell, L. A. (2021). Neural stem cells: what happens when they go viral? *Viruses* 13:1468. doi: 10.3390/v13081468

Khalesi, Z., Tamrchi, V., Razizadeh, M. H., Letafati, A., Moradi, P., Habibi, A., et al. (2023). Association between human herpesviruses and multiple sclerosis: a systematic review and meta-analysis. *Microb. Pathog.* 177:106031. doi: 10.1016/j.micpath.2023.106031

Kleinschmidt-DeMasters, B. K., and Gilden, D. H. (2001). The expanding spectrum of herpesvirus infections of the nervous system. *Brain Pathol.* 11, 440–451. doi: 10.1111/j.1750-3639.2001.tb00413.x

Li, S., Wang, M., Li, H., Wang, J., Zhang, Q., Zhou, D., et al. (2022). Case report: overlapping syndrome of anti-NMDAR encephalitis and MOG inflammatory demyelinating disease in a patient with human herpesviruses 7 infection. *Front. Immunol.* 13:799454. doi: 10.3389/fimmu.2022.799454

Lucas, R. M., Lay, M. J., Grant, J., Cherbuin, N., Toi, C. S., Dear, K., et al. (2023). Risk of a first clinical diagnosis of central nervous system demyelination in relation to human herpesviruses in the context of Epstein-Barr virus. *Eur. J. Neurol.* 30, 2752–2760. doi: 10.1111/ene.15919

Mayer, J., Harz, C., Sanchez, L., Pereira, G. C., Maldener, E., Heras, S. R., et al. (2018). Transcriptional profiling of HERV-K(HML-2) in amyotrophic lateral sclerosis and potential implications for expression of HML-2 proteins. *Mol. Neurodegener.* 13:39. doi: 10.1186/s13024-018-0275-3

Medina, J., Charvet, B., Leblanc, P., Germi, R., Horvat, B., Marche, P. N., et al. (2017). Endogenous retroviral sequences in the human genome can play a physiological or pathological role. *Med. Sci. (Paris)* 33, 397–403. doi: 10.1051/medsci/20173304009

Motataianu, A., Serban, G., Barcutean, L., and Balasa, R. (2022). Oxidative stress in amyotrophic lateral sclerosis: synergy of genetic and environmental factors. *Int. J. Mol. Sci.* 23:9339. doi: 10.3390/ijms23169339

Osorio, C., Sfera, A., Anton, J. J., Thomas, K. G., Andronescu, C. V., Li, E., et al. (2022). Virus-Induced Membrane Fusion in Neurodegenerative Disorders. *Front. Cell. Infect. Microbiol.* 12:845580. doi: 10.3389/fcimb.2022.845580

Pham, J., Keon, M., Brennan, S., and Saksena, N. (2020). Connecting RNA-modifying similarities of TDP-43, FUS, and SOD1 with MicroRNA dysregulation amidst a renewed network perspective of amyotrophic lateral sclerosis Proteinopathy. *Int. J. Mol. Sci.* 21:3464. doi: 10.3390/ijms21103464

Provinciali, L., Laurenzi, M. A., Vesprini, L., Giovagnoli, A. R., Bartocci, C., Montroni, M., et al. (1988). Immunity assessment in the early stages of amyotrophic lateral sclerosis: a study of virus antibodies and lymphocyte subsets. *Acta Neurol. Scand.* 78, 449–454. doi: 10.1111/j.1600-0404.1988.tb03686.x

Roshdy, W. H., Kandeil, A., Fahim, M., Naguib, N. Y., Mohsen, G., Shawky, S., et al. (2023). Epidemiological characterization of viral etiological agents of the central nervous system infections among hospitalized patients in Egypt between 2016 and 2019. *Virol. J.* 20:170. doi: 10.1186/s12985-023-02079-y

Schram, S., Loeb, J. A., and Song, F. (2020). Disease propagation in amyotrophic lateral sclerosis (ALS): an interplay between genetics and environment. *J. Neuroinflammation* 17:175. doi: 10.1186/s12974-020-01849-7

Sehrawat, S., Kumar, D., and Rouse, B. T. (2018). Herpesviruses: harmonious pathogens but relevant cofactors in other diseases? *Front. Cell. Infect. Microbiol.* 8:177. doi: 10.3389/fcimb.2018.00177

Sever, B., Ciftci, H., DeMirci, H., Sever, H., Ocak, F., Yulug, B., et al. (2022). Comprehensive research on past and future therapeutic strategies devoted to treatment of amyotrophic lateral sclerosis. *Int. J. Mol. Sci.* 23:2400. doi: 10.3390/ijms23052400

Skrivankova, V. W., Richmond, R. C., Woolf, B. A. R., Yarmolinsky, J., Davies, N. M., Swanson, S. A., et al. (2021). Strengthening the reporting of observational studies in epidemiology using mendelian randomization: the STROBE-MR statement. *JAMA* 326, 1614–1621. doi: 10.1001/jama.2021.18236

Taylor, J. P., Brown, R. H. Jr., and Cleveland, D. W. (2016). Decoding ALS: from genes to mechanism. *Nature* 539, 197–206. doi: 10.1038/nature20413

van Es, M. A., Hardiman, O., Chio, A., Al-Chalabi, A., Pasterkamp, R. J., Veldink, J. H., et al. (2017). Amyotrophic lateral sclerosis. *Lancet* 390, 2084–2098. doi: 10.1016/s0140-6736(17)31287-4

Vasta, R., Chia, R., Traynor, B. J., and Chiò, A. (2022). Unraveling the complex interplay between genes, environment, and climate in ALS. *EBioMedicine* 75:103795. doi: 10.1016/j.ebiom.2021.103795

Verbanck, M., Chen, C. Y., Neale, B., and Do, R. (2018). Detection of widespread horizontal pleiotropy in causal relationships inferred from mendelian randomization between complex traits and diseases. *Nat. Genet.* 50, 693–698. doi: 10.1038/s41588-018-0099-7

Wilson, D. M., Cookson, M. R., Van Den Bosch, L., Zetterberg, H., Holtzman, D. M., and Dewachter, I. (2023). Hallmarks of neurodegenerative diseases. *Cells* 186, 693–714. doi: 10.1016/j.cell.2022.12.032

Zhang, M., Ming, Y., Du, Y., and Xin, Z. (2023). Two-sample mendelian randomization study does not reveal a significant relationship between cytomegalovirus (CMV) infection and autism spectrum disorder. *BMC Psychiatry* 23:559. doi: 10.1186/s12888-023-05035-w

Zuhair, M., Smit, G. S. A., Wallis, G., Jabbar, F., Smith, C., Devleesschauwer, B., et al. (2019). Estimation of the worldwide seroprevalence of cytomegalovirus: a systematic review and meta-analysis. *Rev. Med. Virol.* 29:e2034. doi: 10.1002/rmv.2034

frontiers | Frontiers in Aging Neuroscience

TYPE Original Research
PUBLISHED 14 December 2023
DOI 10.3389/fnagi.2023.1305040

OPEN ACCESS

EDITED BY
Danyllo Oliveira,
University of São Paulo, Brazil

REVIEWED BY
Pierre Duquette,
University of Montreal Hospital Centre (CRCHUM), Canada
Vinicius M. Borges,
Marshall University, United States

*CORRESPONDENCE
Hui Huang
✉ tjgkhh@163.com
Hui Liao
✉ liaohuitjgk@163.com

†These authors have contributed equally to this work

RECEIVED 30 September 2023
ACCEPTED 15 November 2023
PUBLISHED 14 December 2023

CITATION
Li J, Ma C, Huang H and Liao H (2023) Amyotrophic lateral sclerosis and osteoporosis: a two-sample Mendelian randomization study. *Front. Aging Neurosci.* 15:1305040. doi: 10.3389/fnagi.2023.1305040

Amyotrophic lateral sclerosis and osteoporosis: a two-sample Mendelian randomization study

Junhong Li, Cong Ma, Hui Huang*† and Hui Liao*†

Department of Orthopedics, Tongji Hospital, Tongji Medical College, Huazhong University of Science and Technology, Wuhan, China

Background: A few observational studies revealed that amyotrophic lateral sclerosis (ALS) was tightly connected with osteoporosis. However, the results of previous studies were inconsistent, and the causal effect of ALS on osteoporosis has not been investigated. To do so, the two-sample Mendelian randomization (MR) method was employed to estimate the causality.

Methods: The instrumental variables (IVs) for ALS were selected from one GWAS summary dataset (27,205 ALS cases and 110,881 controls), and bone mineral density (BMD) in the femoral neck (FN), lumbar spine (LS), and forearm, extracted from another large-scale GWAS summary database (53,236 cases), were used as phenotypes for osteoporosis. Random-effects inverse variance weighted (IVW), MR Egger, weighted median, simple mode, and weighted mode were conducted to evaluate the causality. Sensitivity analyses were further performed to explore heterogeneity and pleiotropy.

Results: A total of 10 qualified SNPs were finally selected as proxies for ALS. The results of random effects from IVW revealed that ALS has no causal effect on FN-BMD (beta: −0.038, 95% CI: −0.090 to 0.015, SE: 0.027, $p = 0.158$), LS-BMD (beta: −0.015, 95% CI: −0.076 to 0.046, SE: 0.031, $p = 0.629$), and forearm BMD (beta: 0.044, 95% CI: −0.063 to 0.152, SE: 0.055, $p = 0.418$). These results were confirmed using the MR-Egger, weighted median, simple model, and weighted model. No heterogeneity or pleiotropy was detected ($p > 0.05$ for all).

Conclusion: Contrary to previous observational studies, our study figured out that no causal effect existed between ALS and osteoporosis. The disparity in results is probably attributed to secondary effects such as physical inactivity and muscle atrophy caused by ALS.

KEYWORDS

amyotrophic lateral sclerosis, osteoporosis, Mendelian randomization, causality, bone mineral density

1 Introduction

Both amyotrophic lateral sclerosis (ALS) and osteoporosis are age-related diseases that can severely exacerbate the debilitation of the musculoskeletal system (Pandya and Patani, 2020; Ma et al., 2023). ALS is a rare, fatal, and incurable disorder characterized by motor neuron dysfunction leading to progressive skeletal muscle weakness and behavioral deficits, with respiratory failure often the ultimate cause of death (Feldman et al., 2022). Osteoporosis is a generalized systemic skeletal disorder associated with decreased bone mass and disruption of

bone architecture, resulting in a subsequent increase in susceptibility to fractures (including hip, spine, and pelvic fractures) (Genant et al., 1999). Numerous clinical studies have observed that the skeletal health of ALS patients significantly deteriorates due to a lack of muscle contraction and physical activity, manifested as an increased risk of bone loss and osteoporosis (Brown and Al-Chalabi, 2017; Caplliure-Llopis et al., 2020). According to statistics, the annual incidence of osteoporotic fractures caused by osteoporosis exceeds 8.9 million cases worldwide, most of which usually require long-term care, and the mortality rate of patients with a disease duration of more than 1 year is increased by 25%, thereby causing unoptimistic treatment costs and mortality (Ferrari et al., 2016; Ensrud and Crandall, 2017; Johnston and Dagar, 2020). Nonetheless, the problem of comorbid osteoporosis in ALS patients is always underestimated, as ALS patients often have limited mobility and bone loss tends to occur insidiously (usually asymptomatic until the first osteoporotic fracture), which poses a challenge for clinical management and intervention (Johnston and Dagar, 2020; Aibar-Almazán et al., 2022). Non-invasive mechanical ventilation (NIMV) contributes to the prolonged survival of ALS patients, yet growing clinical cases have reported that ALS patients treated with NIMV who are comorbid with severe osteoporosis are more susceptible to respiratory failure due to a low-energy traumatic event that induces osteoporotic vertebral fracture (Hardiman et al., 2017; Portaro et al., 2018). Evaluating the correlation between ALS and osteoporosis, as well as timely identifying and treating ALS patients with the potential risk of osteoporosis and fracture, are bound to be of great clinical importance.

Previous studies have suggested that there is an interacting pathophysiological basis and a close clinical correlation between ALS and osteoporosis (Medinas et al., 2017; Caplliure-Llopis et al., 2020; Ma et al., 2023). Pathophysiological studies have revealed that bone is a key provider of muscle trophic factors (e.g., BMP, VEGF, and IGF-1), whereas muscle is a source of osteoblastic stem cells and certain anabolic stimuli for bone remodeling (Cho et al., 2010; Koh et al., 2012; Zhou et al., 2015). Muscle strength continuously regulates the structure and function of the skeleton, so when ALS causes muscle dysfunction, the skeleton is compromised accordingly; likewise, compromised bone balance can, in turn, contribute to muscle degeneration, which further accelerates ALS progression (Zhou et al., 2015). Clinical studies have found that ALS patients are at increased risk of developing osteoporosis and related fractures because of abnormal energy metabolism, malnutrition, decreased limb flexibility, increased joint stiffness, and frequent falls (Fernando et al., 2019; Morini et al., 2023). According to multiple observational studies, there is a strong statistical correlation between ALS and osteoporosis, whereas it is difficult to state the exact nature of the relationship since these studies are observational (Joyce et al., 2012; Kelly et al., 2020; Sooragonda et al., 2021). Notably Caplliure-Llopis et al. (2020) indicated that deterioration in bone health was not associated with ALS subtype or clinical status but could be related to the levels of metabolic parameters like thyroid-stimulating hormone and vitamin D. Thus, the aforementioned conflicting evidence may weaken the potential causal relationship between these two diseases. It should be recognized that in epidemiological studies (especially observational studies), studies were commonly limited to small sample sizes (due to the rarity of ALS), and the presence of bias introduced by confounders largely interfered with the causal-effect inference of exposure and outcome, thereby rendering the results unreliable (Fewell et al., 2007). Further research focused on the causal relationship between ALS and osteoporosis would be valuable for the prevention and treatment of combined osteoporosis in ALS patients.

Mendelian randomization (MR) is an emerging method in clinical epidemiology that utilizes genetic variants as instrumental variables (IVs) and thus cannot be affected by confounding factors and reverse causation, which exist in cross-sectional studies (Davey Smith and Hemani, 2014). Based on this, the MR method has the ability to identify causal relationships between exposure and outcome and is also regarded as an alternative method for randomized controlled trials, which have been regarded as the gold standard for verifying causality (Davey Smith and Hemani, 2014; Davies et al., 2018). Owing to its strength of causal-effect inference, the two-sample MR method was widely used to find risk factors for a variety of diseases, such as osteoporosis, Parkinson's disease, and prostate cancer (Mitchell et al., 2021; Bottigliengo et al., 2022; Deng and Wong, 2023; Fang et al., 2023). At the same time, a number of close relationships identified by previous cross-sectional studies were further validated and disentangled by recent MR studies (Chen et al., 2022; Zhang et al., 2022). For instance, previous observational studies have found that rheumatoid arthritis is closely related to osteoporosis, while through a two-sample MR analysis, Liu et al. (2021) demonstrated no causal association between rheumatoid arthritis and osteoporosis. Similarly, based on the results of MR analysis, He et al. (2021) did not find a causal relationship between depression and osteoporosis, which is contrary to the results of previous observational research. Unfortunately, to the best of our knowledge, there is still a lack of MR studies exploring the causal relationship between ALS and osteoporosis to validate the results of previously controversial observational studies and to provide guidance for future clinical interventions in ALS patients with comorbid osteoporosis.

The current study, as the first two-sample MR study to explore the causal effect of ALS on osteoporosis, ultimately aims to elucidate the causal relationship between ALS and osteoporosis and to corroborate the findings identified by previous cross-sectional studies.

2 Materials and methods

2.1 Data on ALS and BMD

The largest-scale ALS GWAS summary statistics up to now were extracted from a recent meta-analysis performed by van Rheenen et al. (2021), which involved 27,205 ALS cases and 110,881 controls. All participants were of European ancestry. For the ALS and BMD data sets used in this study (Zheng et al., 2015; van Rheenen et al., 2021), we refer the reader to the primary GWAS manuscripts and their Supplementary material for details on information of cohorts. Cases were diagnosed in accordance with the revised El-Escorial criteria (Brooks et al., 2000), and control subjects were population-based controls matched for sex and age. The summary-level data on ALS among European ancestry is publicly available through the Project MinE website.[1]

1 https://www.projectmine.com/research/download-data/

In the present study, we aimed to explore the causal effect of ALS on osteoporosis. Osteoporosis was diagnosed clinically by measurement of BMD to a large extent (LeBoff et al., 2022). BMD measured at three common bone areas, including femoral neck BMD (FN-BMD), lumbar spine (L1-4) BMD (LS-BMD), and the forearm (distal 1/3 of radius) BMD, were treated as outcome variables in the MR analysis. GWAS summary data for BMD were retrieved from a large meta-analysis involving a total of 53,236 cases of European ancestry, which were selected from the general population (Zheng et al., 2015). Sex, age, age-squared, and weight were covariates in the meta-analysis and adjusted before testing SNPs. BMD was measured by DXA and standardized within each cohort to control systematic differences in BMD measurements. The summary-level data of FN-BMD, LS-BMD, and forearm BMD used in this study were extracted from the GEnetic Factors for OSteoporosis Consortium (GEFOS, http://www.gefos.org/).

Population stratification was regarded as a factor that could contribute to bias in MR analysis caused by different ancestries between exposure and outcome summary statistics. In our study, all the participants were of European ancestry. In addition, the degree of sample overlap was an important factor to consider and could introduce bias or a type 1 error rate if it was substantial in a two-sample MR study (Burgess et al., 2016). We tested the degree through the online tool[2] (Burgess et al., 2016), and no significant sample overlap (<6%) between exposure (ALS) participants and outcome (FN-BMD, LS-BMD, and forearm BMD) participants was found. A large study population, relatively strong IVs, and low sample overlap in this study could minimize the extent of bias caused by overlapped populations to some extent (Burgess et al., 2016). On account of all the GWAS summarized statistics of ALS and BMD used in the present study being publicly available, no ethical consent was needed.

2.2 IVs selection process

To obtain robust results in the MR analysis, MR was required to satisfy the three assumptions as follows: first, the relevance assumption: IVs were strongly associated with ALS in this study; second, the exclusion restriction assumption: IVs could only exert influence on BMD through ALS rather than other pleiotropic pathways; and third, the independence assumption: IVs were independent of confounders (Skrivankova et al., 2021). Accordingly, the SNPs of exposure data that satisfied the strict criteria as follows were employed as IVs. First, SNPs with p-value lower than 5×10^{-8} and F-statistics greater than 10 were regarded as significantly associated with the exposure factor and included in the study. The formula $F=R^2(N-2)/(1-R^2)$ and $R^2=2\times(1-\mathrm{MAF})\times\mathrm{MAF}\times\beta^2$ were used to calculate the strength of every single SNP. N represented the sample size of the ALS GWAS database, and MAF represented minor allele frequency. Second, the clumping process ($r^2<0.001$, kb = 10,000) among all the above-included SNPs was carried out to exclude SNPs that were in linkage disequilibrium (LD) with other SNPs. r^2 was the LD correlation coefficient. Third, if a large portion of SNPs were not found in the GWAS datasets of BMD, variant proxies ($r^2\geq0.8$) were selected by visiting the online website[3] (Li et al., 2022; Seyedsalehi et al., 2023). Fourth, PhenoScanner V2 (available at http://www.phenoscanner.medschl.cam.ac.uk/) is a simple and widely used tool to specify whether a particular SNP is associated with other confounders (Kamat et al., 2019). SNPs related to confounders were excluded by visiting this online website. Previous studies have demonstrated that age at menarche has a causal effect on osteoporosis (Zhang et al., 2018). The SNP rs2077492 was excluded due to its strong association with age at menarche. The SNP rs9275477 was also excluded due to its association with treatment with prednisolone. Finally, SNPs that were significantly (p-value lower than 5×10^{-8}) associated with outcome data were excluded. Incompatible SNPs were also excluded from the harmonization process. Finally, 10 SNPs of ALS were used as the IVs for further MR analysis. The flowchart of this study design was shown in Supplementary Figure S1.

2.3 Mendelian randomization analyses and sensitivity analyses

The causal effects of ALS on osteoporosis risk, including FN-BMD, LS-BMD, and forearm BMD, were estimated using the two-sample MR method. Random effects inverse variance weighted (IVW) was the main analytical method. Other complementary methods, including MR-Egger regression, weighted median, simple model, and weighted model, were also used.

The following sensitivity analyses were applied to explore heterogeneity and pleiotropy. Cochran's Q tests using IVW and MR-Egger were calculated to estimate the heterogeneity. MR-Egger intercept analysis was used to detect the horizontal pleiotropic effects. p-values less than 0.05 indicated pleiotropy. A leave-one-out cross-validation test was applied to detect the effect of potentially influential SNPs and the robustness of the estimates. The MR pleiotropy residual sum and outlier test (MR-PRESSO) was conducted to test pleiotropy and detect and correct the outliers. If there were any outlier SNPs, the MR analysis was performed again after the outlier was corrected. The symmetry of the funnel plot could intuitively reflect potential horizontal pleiotropy, and any asymmetry was a sign of directional pleiotropy (Burgess et al., 2017). Statistical power was tested according to the method proposed by Brion et al. (2013). A p-value less than 0.05 indicated statistical significance in all the sensitivity analysis methods.

2.4 Statistical analysis

Package "TwoSampleMR" (Hemani et al., 2018) in the R software (version 4.1.2) was employed for two-sample MR analysis. Tests were two-tailed. When the number of tests is greater than one, Bonferroni correction should be performed to avoid false-positive estimates (Peng et al., 2022). Bonferroni-corrected statistical significance was 0.05/(1 ALS × 3 BMD) = 0.017 in this study. p-value less than 0.017 was considered significant in the MR analysis. p-value less than 0.05 but more than 0.017 was considered a potential causal relationship.

2 https://sb452.shinyapps.io/overlap/

3 https://snipa.helmholtz-muenchen.de/snipa3/

3 Results

After strict adherence to the criteria of IVs selection, a total of 10 qualified SNPs were finally selected as proxies for ALS in the present study (Supplementary Table S1). No proxy SNPs were employed because all the SNPs identified in the exposure data were found in the outcome data.

3.1 Causal effect of ALS on FN-BMD

Based on the results of the main MR method, ALS had no etiological effect on FN-BMD in IVW [beta: −0.038, 95% confidence interval (CI): −0.090 to 0.015, standard error (SE): 0.027, $p = 0.158$, Figure 1]. The results were validated in other complementary methods, MR-Egger (beta: −0.120, 95% CI: −0.242 to 0.002, SE: 0.062, $p = 0.090$), weighted median (beta: −0.041, 95% CI: −0.112 to 0.029, SE: 0.036, $p = 0.249$), simple model (beta: −0.045, 95% CI: −0.160 to 0.070, SE: 0.059, $p = 0.483$), and weighted model (beta: −0.047, 95% CI: −0.127 to 0.033, SE: 0.041, $p = 0.319$, Figure 1). A scatterplot of the causal associations between ALS and FN-BMD is shown in Figure 2A.

3.2 Causal effect of ALS on LS-BMD

Similarly, no significant causal effect was identified between ALS and LS-BMD, estimated by the following five two-sample MR analysis methods (IVW beta: −0.015, 95% CI: −0.076 to 0.046, SE: 0.031, $p = 0.629$; MR-Egger beta: −0.041, 95% CI: −0.183 to 0.100, SE: 0.072, $p = 0.581$; weighted median beta: −0.025, 95% CI: −0.106 to 0.056, SE:

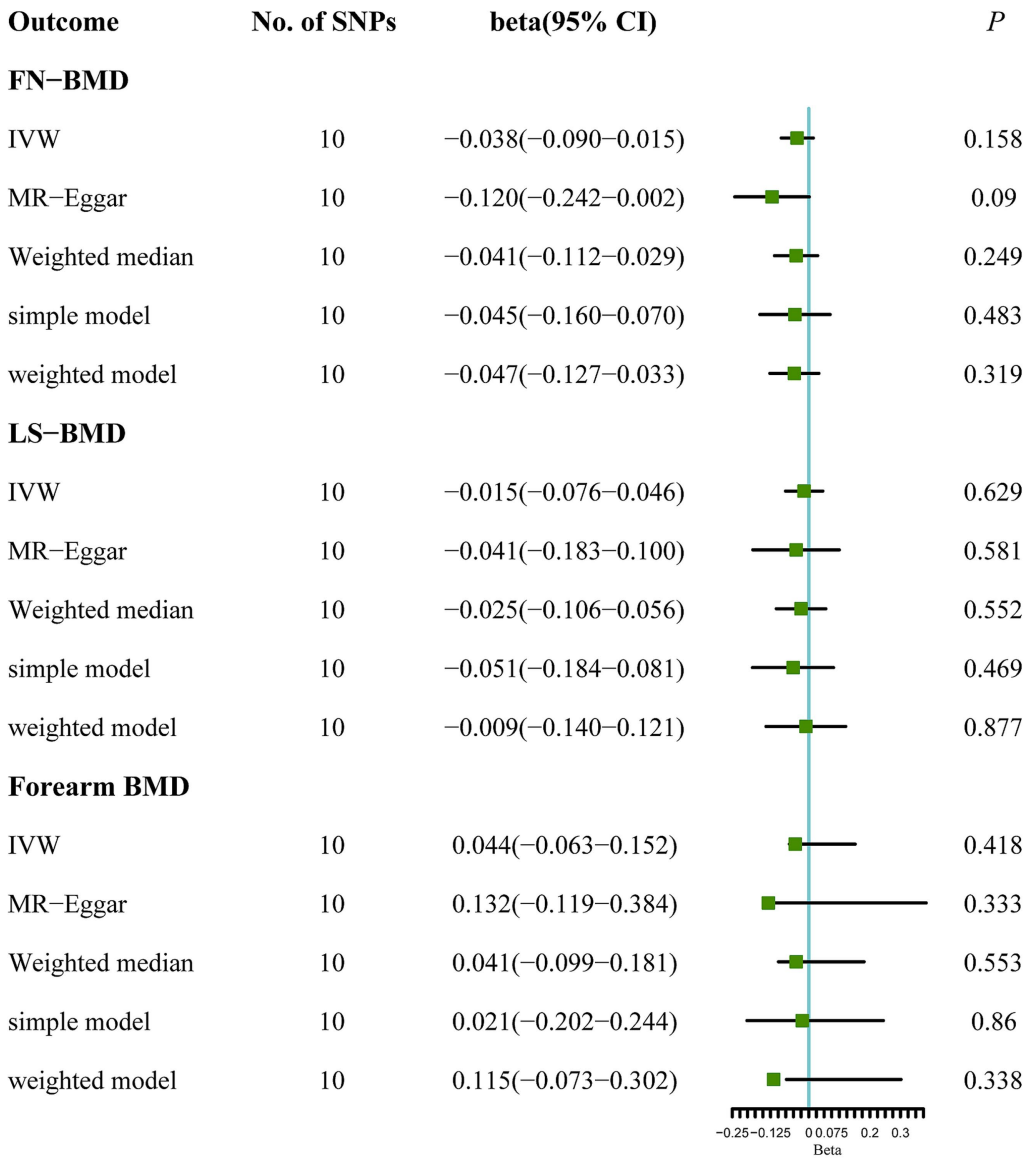

FIGURE 1
MR analysis between ALS and osteoporosis (FN-BMD, LS-BMD, and forearm BMD). Five methods: random-effects IVW, MR Egger, weighted median, simple mode, and weighted mode.

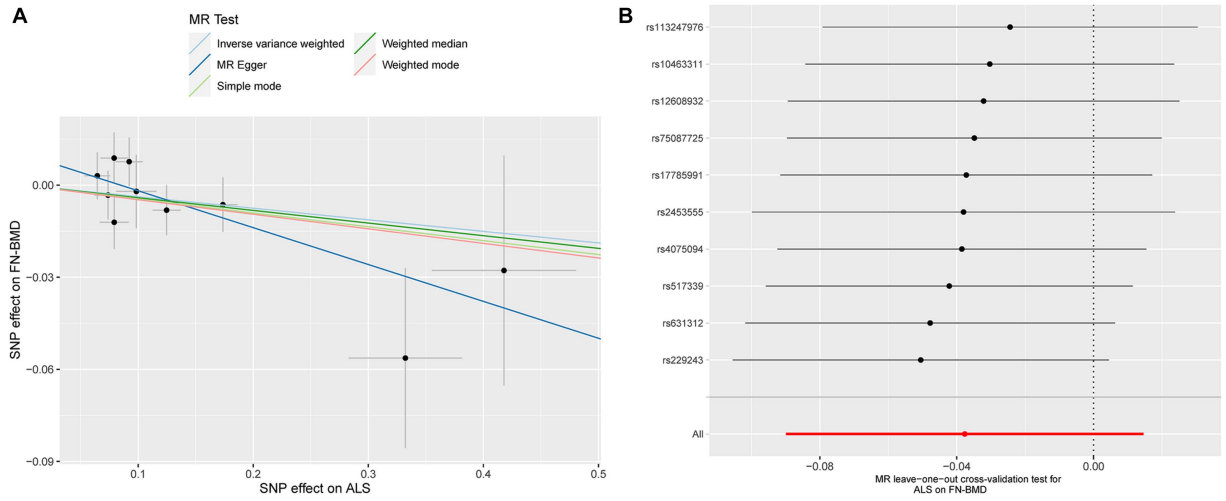

FIGURE 2
Scatterplot of the causal relationships between ALS and FN-BMD **(A)**. MR Leave-one-out cross-validation test for ALS on FN-BMD **(B)**.

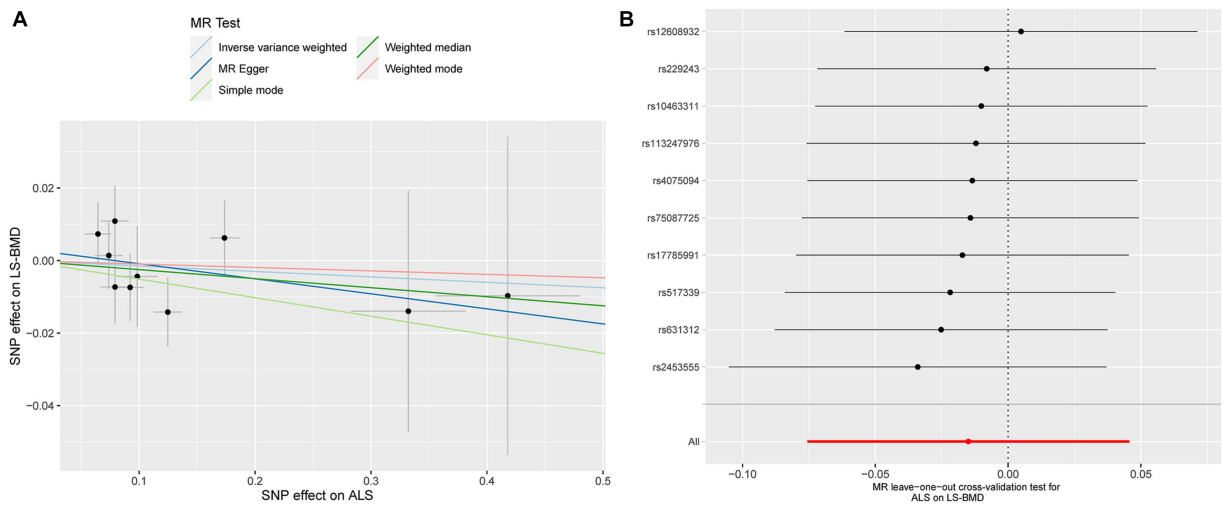

FIGURE 3
Scatterplot of the causal relationships between ALS and LS-BMD **(A)**. MR Leave-one-out cross-validation test for ALS on LS-BMD **(B)**.

0.041, $p = 0.552$; simple model beta: −0.051, 95% CI: −0.184 to 0.081, SE: 0.068, $p = 0.469$; weighted model beta: −0.009, 95% CI: −0.140 to 0.121, SE: 0.067, $p = 0.877$, Figure 1). The forest map of the above five MR methods is shown in Figure 1. A scatterplot of the causal relationships between ALS and LS-BMD is shown in Figure 3A.

3.3 Causal effect of ALS on forearm BMD

ALS also showed a null causal relationship with forearm BMD in IVW (beta: 0.044, 95% CI: −0.063 to 0.152, SE: 0.055, $p = 0.418$), MR-Egger (beta: 0.132, 95% CI: −0.119 to 0.384, SE: 0.128, $p = 0.333$), weighted-median (beta: 0.041, 95% CI: −0.099 to 0.181, SE: 0.072, $p = 0.553$), simple model (beta: 0.021, 95% CI: −0.202 to 0.244, SE: 0.114, $p = 0.860$), and weighted model (beta: 0.115, 95% CI: −0.073 to 0.302, SE: 0.096, $p = 0.338$, Figure 1). The scatterplot of the causal associations between ALS and forearm BMD is shown in Figure 4A.

3.4 Sensitivity analyses

Detailed results of MR-PRESSO, MR-Egger intercept analysis, heterogeneity tests by IVW, and heterogeneity tests by MR-Egger are shown in Table 1. All the p-values were greater than 0.05 in MR-Egger intercept analysis, heterogeneity tests by IVW, and heterogeneity tests by MR-Egger, indicating that no heterogeneity or pleiotropy existed in our study. In addition, no outliers were identified by MR-PRESSO analysis. According to the results of the leave-one-out cross-validation test, we did not detect any potentially influential or problematic SNPs (Figures 2B–4B). As shown in the funnel plots (Supplementary Figure S2), no potential horizontal pleiotropy was

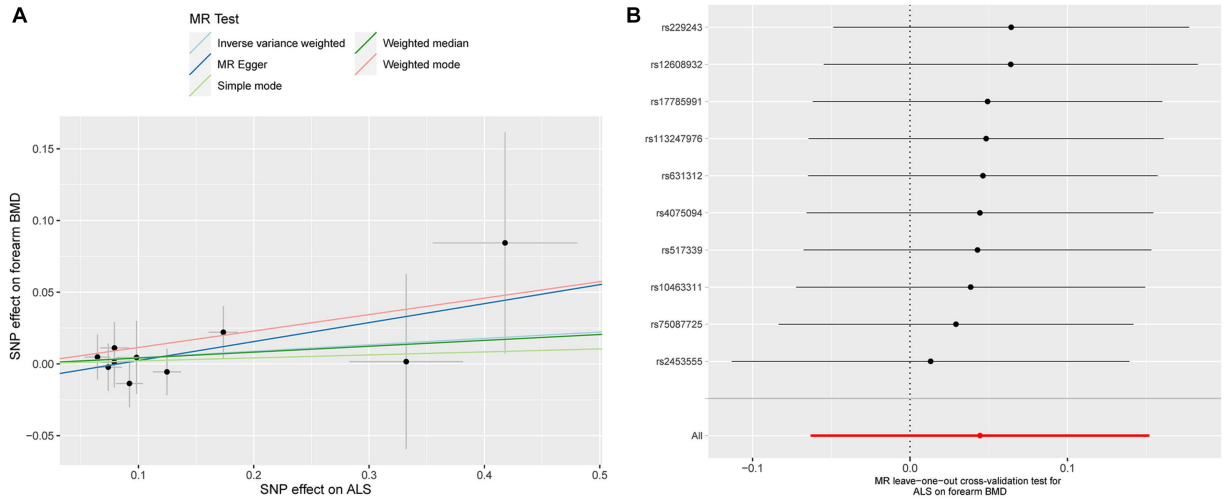

FIGURE 4
Scatterplot of the causal relationships between ALS and forearm BMD **(A)**. MR Leave-one-out cross-validation test for ALS on forearm BMD **(B)**.

TABLE 1 **The results of sensitivity analyses.**

Exposure	Outcome	MR-PRESSO		MR-Egger intercept analysis		Heterogeneity tests by IVW		Heterogeneity tests by MR-Egger	
		Global test *p*-value	Main MR results *p*-value	Intercept	Intercept *p*-value	Cochran's *Q*	*p*-value	Cochran's *Q*	*p*-value
ALS	FN-BMD	0.570	0.171	0.010	0.180	8.120	0.522	5.967	0.651
ALS	LS-BMD	0.725	0.563	0.003	0.694	5.842	0.756	5.676	0.683
ALS	Forearm BMD	0.930	0.217	−0.011	0.470	3.342	0.949	2.768	0.948

$p < 0.05$ was considered significant in sensitivity analyses.

discovered. Based on the consistency of the results estimated by five different MR analytical approaches and the fact that no positive findings existed in the heterogeneity and pleiotropy tests, the results were considered robust.

4 Discussion

As far as we know, this is the first study to estimate the genetic causal effect of ALS on osteoporosis by utilizing the two-sample MR method. Our results demonstrated that ALS was not causally associated with osteoporosis (FN-BMD, LS-BMD, and forearm BMD). In other words, ALS was not an immediate risk factor for osteoporosis. No heterogeneity or pleiotropy existed in the sensitivity analyses, indicating relatively strong robustness of the causal-effect inference in the present study.

Contrary to our findings, several observational epidemiological studies reported robust associations between ALS and osteoporosis, but their findings were contradictory. As far back as 1977, abnormalities in vertebral structure have been observed among ALS patients (Mallette et al., 1977). Subsequently, a significant decrease in cortical bone mass was detected in individuals with ALS (Yanagihara et al., 1984). Likewise, Morini et al. (2023) found that patients with ALS (16 male and 22 female individuals) showed lower BMD. According to a recent cross-sectional study, ALS patients represented statistically significantly worse bone quality parameters (including *T*-score and BMD) compared with the control group matched in sex and age (Caplliure-Llopis et al., 2020). Interestingly, in this series, when analyzing BMD according to different sexes, female patients with ALS (11/12) showed statistically significantly lower BMD than healthy female individuals (4/24); however, differences in the proportion of male individuals with osteoporosis in the ALS group and healthy control group (7/21 vs. 23/42) were not significant. In contrast, one Indian cohort including 30 male ALS subjects and 33 healthy controls suggested a higher level of bone turnover marker in the ALS group; nevertheless, no significant differences in BMD between the two groups were observed (Sooragonda et al., 2021). Yet, all of the above studies were limited by a relatively limited sample size; the associations identified in the observational studies may have been generated by confounders, reverse causality, and a variety of biases, such as selection bias and recall bias. Moreover, inaccurate causal-effect inferences of exposure and outcome still remain, even through rigorous study design and statistical adjustment (Fewell et al., 2007; Davey Smith and Hemani, 2014). Elucidating the causal relationship between ALS and osteoporosis was clinically important.

The mechanism between ALS and osteoporosis has also been widely discussed. Some studies suggest that neurotoxic metals that have been detected in individuals with ALS might have an effect on bone mineralization (Roos et al., 2013). Specifically, evidence from Roos (2014) showed that several neurotoxic metals (e.g., cadmium, lead, and arsenic) accumulate in the bones of ALS patients to disrupt bone remodeling by replacing calcium in hydroxyapatite (one important mineral component of bone). While Ko et al. (2018) revealed that $SOD1^{G93A}$ mice, the mouse model of ALS, exhibited decreased trabecular bone mass, thinner trabeculae, and lower cortical bone thickness when compared with healthy controls. Similarly, by using the G93A mouse model, Zhu et al. (2015) found that mice with serious muscle atrophy showed significantly lower trabecular as well as cortical bone mass. They also found that osteoblast properties, such as osteoblast differentiation capacity, were seriously impaired and that osteoclast formation was markedly improved in the G93A mouse model with serious muscle atrophy. But no striking changes in osteoblast and osteoclast properties were detected in G93A mice without muscle atrophy. Consistently, significant degradation of bone caused by muscle paralysis was found in the murine model (Warner et al., 2006). These animal studies might suggest that muscle atrophy was a direct contributor to osteoporosis, not due to ALS itself.

Accumulative evidence indicated that skeletal muscle load was the major source of mechanical stimulation of bone anabolism; moreover, skeletal muscles were the crucial source of osteogenic growth factors (Hamrick et al., 2010). Clinically, mechanical unloading could lead to bone loss (Lloyd et al., 2014). For instance, one previous study indicated that individuals affected by Duchenne muscular dystrophy showed lower BMD and *Z*-scores (Rufo et al., 2011). Insufficient physical activity was also regarded as a risk factor for osteoporosis (Roos, 2014). Likewise, ALS is a neurodegenerative disease characterized by progressive weakness of skeletal muscles, muscle atrophy, and behavioral deficits. These findings indicated that the presence of osteoporosis in individuals with ALS might be partially intermediated by other elements, including muscle atrophy and physical inactivity. The results of our two-sample MR study revealed no causal relationship between ALS and osteoporosis, which might also suggest an indirect effect, rather than a direct effect, of ALS on osteoporosis.

This study has several strengths. First, our MR study revealed no causal effect of ALS on osteoporosis for the first time at the genetic level, which contributes positively to the genetics of osteoporosis. We further discussed how deteriorated bone health in ALS patients might be due to muscle atrophy or physical inactivity. Based on our results, we recommended that more clinical attention should be paid to the bone health of ALS patients with muscular dystrophy, but osteoporosis should not be dogmatically viewed as a complication of ALS, as our results revealed that ALS may not be causally associated with osteoporosis. The insightful realization that there was no causal association between ALS and osteoporosis helped clinicians place the focus of intervening in osteoporosis in patients with ALS on regular monitoring of bone mineral density and appropriate strategies to nourish the skeletal-muscular system, as well as to enhance muscle contraction and physical activity. Second, the data used in this study were extracted from two large-scale GWAS summary datasets for ALS and osteoporosis separately, which helped to estimate the causality more precisely compared with previous observational studies. Third, there is no significant sample overlap between exposure and outcome datasets in this two-sample MR-designed research. Fourth, BMD in three common bone sites (FN-BMD, LS-BMD, and forearm BMD) was employed as a phenotype for osteoporosis, which might control the statistical bias to some extent. Fifth, no positive findings in the sensitivity analyses excluded the possibility that the MR study was biased by horizontal pleiotropy.

This study has certain limitations. First, considering different bone qualities have been identified between male and female patients with ALS in previous observational studies (Caplliure-Llopis et al., 2020), stratified analysis according to different sexes would have been of clinically great interest. Nevertheless, since we only adopted summary-level databases that are publicly available for MR analyses, it is impossible to perform subgroup analyses. Second, all the participants were of European ancestry; in our study, we did not verify whether a causal effect existed in other populations. Further studies validating the causality among other ethnic groups are needed.

5 Conclusion

Contrary to previous observational studies, our study figured out that no causal effect existed between ALS and osteoporosis. The disparity in results is probably attributed to secondary effects such as physical inactivity and muscle atrophy caused by ALS.

Data availability statement

The original contributions presented in the study are included in the article/Supplementary material, further inquiries can be directed to the corresponding authors.

Ethics statement

This study is secondary data analysis of publicly available datasets. The original studies involving human participants were reviewed and approved by their relevant Ethics Committees and Review Boards. Written informed consent to participate in the original study was provided by the participants.

Author contributions

JL: Data curation, Investigation, Methodology, Software, Validation, Writing – original draft. CM: Investigation, Methodology, Software, Writing – review & editing. HH: Investigation, Methodology, Supervision, Writing – review & editing. HL: Conceptualization, Investigation, Methodology, Supervision, Writing – review & editing.

Funding

The author(s) declare that no financial support was received for the research, authorship, and/or publication of this article.

Conflict of interest

The authors declare that the research was conducted in the absence of any commercial or financial relationships that could be construed as a potential conflict of interest.

Publisher's note

All claims expressed in this article are solely those of the authors and do not necessarily represent those of their affiliated organizations, or those of the publisher, the editors and the reviewers. Any product that may be evaluated in this article, or claim that may be made by its manufacturer, is not guaranteed or endorsed by the publisher.

Supplementary material

The Supplementary material for this article can be found online at: https://www.frontiersin.org/articles/10.3389/fnagi.2023.1305040/full#supplementary-material

References

Aibar-Almazán, A., Voltes-Martínez, A., Castellote-Caballero, Y., Afanador-Restrepo, D. F., Carcelén-Fraile, M. D. C., and López-Ruiz, E. (2022). Current status of the diagnosis and management of osteoporosis. *Int. J. Mol. Sci.* 23:9465. doi: 10.3390/ijms23169465

Bottigliengo, D., Foco, L., Seibler, P., Klein, C., König, I. R., and Del Greco, M. F. (2022). A Mendelian randomization study investigating the causal role of inflammation on Parkinson's disease. *Brain* 145, 3444–3453. doi: 10.1093/brain/awac193

Brion, M. J., Shakhbazov, K., and Visscher, P. M. (2013). Calculating statistical power in Mendelian randomization studies. *Int. J. Epidemiol.* 42, 1497–1501. doi: 10.1093/ije/dyt179

Brooks, B. R., Miller, R. G., Swash, M., and Munsat, T. L. (2000). El Escorial revisited: revised criteria for the diagnosis of amyotrophic lateral sclerosis. *Amyotroph. Lateral Scler. Other Motor Neuron Disord.* 1, 293–299. doi: 10.1080/146608200300079536

Brown, R. H., and Al-Chalabi, A. (2017). Amyotrophic lateral sclerosis. *N. Engl. J. Med.* 377, 162–172. doi: 10.1056/NEJMra1603471

Burgess, S., Bowden, J., Fall, T., Ingelsson, E., and Thompson, S. G. (2017). Sensitivity analyses for robust causal inference from Mendelian randomization analyses with multiple genetic variants. *Epidemiology* 28, 30–42. doi: 10.1097/ede.0000000000000559

Burgess, S., Davies, N. M., and Thompson, S. G. (2016). Bias due to participant overlap in two-sample Mendelian randomization. *Genet. Epidemiol.* 40, 597–608. doi: 10.1002/gepi.21998

Caplliure-Llopis, J., Escrivá, D., Benlloch, M., de la Rubia Ortí, J. E., Estrela, J. M., and Barrios, C. (2020). Poor bone quality in patients with amyotrophic lateral sclerosis. *Front. Neurol.* 11:599216. doi: 10.3389/fneur.2020.599216

Chen, H., Ye, R., and Guo, X. (2022). Lack of causal association between heart failure and osteoporosis: a Mendelian randomization study. *BMC Med. Genet.* 15:232. doi: 10.1186/s12920-022-01385-8

Cho, G. W., Noh, M. Y., Kim, H. Y., Koh, S. H., Kim, K. S., and Kim, S. H. (2010). Bone marrow-derived stromal cells from amyotrophic lateral sclerosis patients have diminished stem cell capacity. *Stem Cells Dev.* 19, 1035–1042. doi: 10.1089/scd.2009.0453

Davey Smith, G., and Hemani, G. (2014). Mendelian randomization: genetic anchors for causal inference in epidemiological studies. *Hum. Mol. Genet.* 23, R89–R98. doi: 10.1093/hmg/ddu328

Davies, N. M., Holmes, M. V., and Davey Smith, G. (2018). Reading Mendelian randomisation studies: a guide, glossary, and checklist for clinicians. *BMJ* 362:k601. doi: 10.1136/bmj.k601

Deng, Y., and Wong, M. C. S. (2023). Association between rheumatoid arthritis and osteoporosis in Japanese populations: a Mendelian randomization study. *Arthritis Rheumatol.* 75, 1334–1343. doi: 10.1002/art.42502

Ensrud, K. E., and Crandall, C. J. (2017). Osteoporosis. *Ann. Intern. Med.* 167:ITC17. doi: 10.7326/aitc201708010

Fang, S., Yarmolinsky, J., Gill, D., Bull, C. J., Perks, C. M., Davey Smith, G., et al. (2023). Association between genetically proxied PCSK9 inhibition and prostate cancer risk: a Mendelian randomisation study. *PLoS Med.* 20:e1003988. doi: 10.1371/journal.pmed.1003988

Feldman, E. L., Goutman, S. A., Petri, S., Mazzini, L., Savelieff, M. G., Shaw, P. J., et al. (2022). Amyotrophic lateral sclerosis. *Lancet* 400, 1363–1380. doi: 10.1016/s0140-6736(22)01272-7

Fernando, R., Drescher, C., Nowotny, K., Grune, T., and Castro, J. P. (2019). Impaired proteostasis during skeletal muscle aging. *Free Radic. Biol. Med.* 132, 58–66. doi: 10.1016/j.freeradbiomed.2018.08.037

Ferrari, S., Reginster, J. Y., Brandi, M. L., Kanis, J. A., Devogelaer, J. P., Kaufman, J. M., et al. (2016). Unmet needs and current and future approaches for osteoporotic patients at high risk of hip fracture. *Arch. Osteoporos.* 11:37. doi: 10.1007/s11657-016-0292-1

Fewell, Z., Davey Smith, G., and Sterne, J. A. (2007). The impact of residual and unmeasured confounding in epidemiologic studies: a simulation study. *Am. J. Epidemiol.* 166, 646–655. doi: 10.1093/aje/kwm165

Genant, H. K., Cooper, C., Poor, G., Reid, I., Ehrlich, G., Kanis, J., et al. (1999). Interim report and recommendations of the World Health Organization task-force for osteoporosis. *Osteoporos. Int.* 10, 259–264. doi: 10.1007/s001980050224

Hamrick, M. W., McNeil, P. L., and Patterson, S. L. (2010). Role of muscle-derived growth factors in bone formation. *J. Musculoskelet. Neuronal Interact.* 10, 64–70.

Hardiman, O., Al-Chalabi, A., Chio, A., Corr, E. M., Logroscino, G., Robberecht, W., et al. (2017). Amyotrophic lateral sclerosis. *Nat. Rev. Dis. Primers.* 3:17071. doi: 10.1038/nrdp.2017.71

He, B., Lyu, Q., Yin, L., Zhang, M., Quan, Z., and Ou, Y. (2021). Depression and osteoporosis: a Mendelian randomization study. *Calcif. Tissue Int.* 109, 675–684. doi: 10.1007/s00223-021-00886-5

Hemani, G., Zheng, J., Elsworth, B., Wade, K. H., Haberland, V., Baird, D., et al. (2018). The MR-base platform supports systematic causal inference across the human phenome. *eLife* 7:e34408. doi: 10.7554/eLife.34408

Johnston, C. B., and Dagar, M. (2020). Osteoporosis in older adults. *Med. Clin. North Am.* 104, 873–884. doi: 10.1016/j.mcna.2020.06.004

Joyce, N. C., Hache, L. P., and Clemens, P. R. (2012). Bone health and associated metabolic complications in neuromuscular diseases. *Phys. Med. Rehabil. Clin. N. Am.* 23, 773–799. doi: 10.1016/j.pmr.2012.08.005

Kamat, M. A., Blackshaw, J. A., Young, R., Surendran, P., Burgess, S., Danesh, J., et al. (2019). PhenoScanner V2: an expanded tool for searching human genotype-phenotype associations. *Bioinformatics* 35, 4851–4853. doi: 10.1093/bioinformatics/btz469

Kelly, R. R., Sidles, S. J., and LaRue, A. C. (2020). Effects of neurological disorders on bone health. *Front. Psychol.* 11:612366. doi: 10.3389/fpsyg.2020.612366

Ko, F. C., Li, J., Brooks, D. J., Rutkove, S. B., and Bouxsein, M. L. (2018). Structural and functional properties of bone are compromised in amyotrophic lateral sclerosis mice. *Amyotroph. Lateral Scler. Frontotemporal. Degener.* 19, 457–462. doi: 10.1080/21678421.2018.1452946

Koh, S. H., Baik, W., Noh, M. Y., Cho, G. W., Kim, H. Y., Kim, K. S., et al. (2012). The functional deficiency of bone marrow mesenchymal stromal cells in ALS patients is proportional to disease progression rate. *Exp. Neurol.* 233, 472–480. doi: 10.1016/j.expneurol.2011.11.021

LeBoff, M. S., Greenspan, S. L., Insogna, K. L., Lewiecki, E. M., Saag, K. G., Singer, A. J., et al. (2022). The clinician's guide to prevention and treatment of osteoporosis. *Osteoporos. Int.* 33, 2049–2102. doi: 10.1007/s00198-021-05900-y

Li, S., Fu, Y., Liu, Y., Zhang, X., Li, H., Tian, L., et al. (2022). Serum uric acid levels and nonalcoholic fatty liver disease: a 2-sample bidirectional Mendelian randomization study. *J. Clin. Endocrinol. Metab.* 107, e3497–e3503. doi: 10.1210/clinem/dgac190

Liu, Y. Q., Liu, Y., Chen, Z. Y., Li, H., and Xiao, T. (2021). Rheumatoid arthritis and osteoporosis: a bi-directional Mendelian randomization study. *Aging* 13, 14109–14130. doi: 10.18632/aging.203029

Lloyd, S. A., Lang, C. H., Zhang, Y., Paul, E. M., Laufenberg, L. J., Lewis, G. S., et al. (2014). Interdependence of muscle atrophy and bone loss induced by mechanical unloading. *J. Bone Miner. Res.* 29, 1118–1130. doi: 10.1002/jbmr.2113

Ma, C., Yu, R., Li, J., Chao, J., and Liu, P. (2023). Targeting proteostasis network in osteoporosis: pathological mechanisms and therapeutic implications. *Ageing Res. Rev.* 90:102024. doi: 10.1016/j.arr.2023.102024

Mallette, L. E., Patten, B., Cook, J. D., and Engel, W. K. (1977). Calcium metabolism in amyotrophic lateral sclerosis. *Dis. Nerv. Syst.* 38, 457–461.

Medinas, D. B., Valenzuela, V., and Hetz, C. (2017). Proteostasis disturbance in amyotrophic lateral sclerosis. *Hum. Mol. Genet.* 26, R91–R104. doi: 10.1093/hmg/ddx274

Mitchell, A., Larsson, S. C., Fall, T., Melhus, H., Michaëlsson, K., and Byberg, L. (2021). Fasting glucose, bone area and bone mineral density: a Mendelian randomisation study. *Diabetologia* 64, 1348–1357. doi: 10.1007/s00125-021-05410-w

Morini, E., Portaro, S., Leonetti, D., De Cola, M. C., De Luca, R., Bonanno, M., et al. (2023). Bone health status in individuals with amyotrophic lateral sclerosis: a cross-sectional study on the role of the trabecular bone score and its implications in neurorehabilitation. *Int. J. Environ. Res. Public Health* 20:2923. doi: 10.3390/ijerph20042923

Pandya, V. A., and Patani, R. (2020). Decoding the relationship between ageing and amyotrophic lateral sclerosis: a cellular perspective. *Brain* 143, 1057–1072. doi: 10.1093/brain/awz360

Peng, H., Wang, S., Wang, M., Ye, Y., Xue, E., Chen, X., et al. (2022). Nonalcoholic fatty liver disease and cardiovascular diseases: a Mendelian randomization study. *Metabolism* 133:155220. doi: 10.1016/j.metabol.2022.155220

Portaro, S., Morini, E., Santoro, M. E., Accorinti, M., Marzullo, P., Naro, A., et al. (2018). Breathlessness in amyotrophic lateral sclerosis: a case report on the role of osteoporosis in the worsening of respiratory failure. *Medicine* 97:e13026. doi: 10.1097/md.0000000000013026

Roos, P. M. (2014). Osteoporosis in neurodegeneration. *J. Trace Elem. Med. Biol.* 28, 418–421. doi: 10.1016/j.jtemb.2014.08.010

Roos, P. M., Vesterberg, O., Syversen, T., Flaten, T. P., and Nordberg, M. (2013). Metal concentrations in cerebrospinal fluid and blood plasma from patients with amyotrophic lateral sclerosis. *Biol. Trace Elem. Res.* 151, 159–170. doi: 10.1007/s12011-012-9547-x

Rufo, A., Del Fattore, A., Capulli, M., Carvello, F., De Pasquale, L., Ferrari, S., et al. (2011). Mechanisms inducing low bone density in Duchenne muscular dystrophy in mice and humans. *J. Bone Miner. Res.* 26, 1891–1903. doi: 10.1002/jbmr.410

Seyedsalehi, A., Warrier, V., Bethlehem, R. A. I., Perry, B. I., Burgess, S., and Murray, G. K. (2023). Educational attainment, structural brain reserve and Alzheimer's disease: a Mendelian randomization analysis. *Brain* 146, 2059–2074. doi: 10.1093/brain/awac392

Skrivankova, V. W., Richmond, R. C., Woolf, B. A. R., Yarmolinsky, J., Davies, N. M., Swanson, S. A., et al. (2021). Strengthening the reporting of observational studies in epidemiology using Mendelian randomization: the STROBE-MR statement. *JAMA* 326, 1614–1621. doi: 10.1001/jama.2021.18236

Sooragonda, B. G., Agarwal, S., Benjamin, R. N., Prabhakar, A. T., Sivadasan, A., Kapoor, N., et al. (2021). Bone mineral density and body composition in males with motor neuron disease: a study from teaching Hospital in Southern Part of India. *Ann. Indian Acad. Neurol.* 24, 211–216. doi: 10.4103/aian.AIAN_293_20

van Rheenen, W., van der Spek, R. A. A., Bakker, M. K., van Vugt, J., Hop, P. J., Zwamborn, R. A. J., et al. (2021). Common and rare variant association analyses in amyotrophic lateral sclerosis identify 15 risk loci with distinct genetic architectures and neuron-specific biology. *Nat. Genet.* 53, 1636–1648. doi: 10.1038/s41588-021-00973-1

Warner, S. E., Sanford, D. A., Becker, B. A., Bain, S. D., Srinivasan, S., and Gross, T. S. (2006). Botox induced muscle paralysis rapidly degrades bone. *Bone* 38, 257–264. doi: 10.1016/j.bone.2005.08.009

Yanagihara, R., Garruto, R. M., Gajdusek, D. C., Tomita, A., Uchikawa, T., Konagaya, Y., et al. (1984). Calcium and vitamin D metabolism in Guamanian Chamorros with amyotrophic lateral sclerosis and parkinsonism-dementia. *Ann. Neurol.* 15, 42–48. doi: 10.1002/ana.410150108

Zhang, Q., Greenbaum, J., Zhang, W. D., Sun, C. Q., and Deng, H. W. (2018). Age at menarche and osteoporosis: a Mendelian randomization study. *Bone* 117, 91–97. doi: 10.1016/j.bone.2018.09.015

Zhang, Y., Mao, X., Yu, X., Huang, X., He, W., and Yang, H. (2022). Bone mineral density and risk of breast cancer: a cohort study and Mendelian randomization analysis. *Cancer* 128, 2768–2776. doi: 10.1002/cncr.34252

Zheng, H. F., Forgetta, V., Hsu, Y. H., Estrada, K., Rosello-Diez, A., Leo, P. J., et al. (2015). Whole-genome sequencing identifies EN1 as a determinant of bone density and fracture. *Nature* 526, 112–117. doi: 10.1038/nature14878

Zhou, J., Yi, J., and Bonewald, L. (2015). Muscle-bone crosstalk in amyotrophic lateral sclerosis. *Curr. Osteoporos. Rep.* 13, 274–279. doi: 10.1007/s11914-015-0281-0

Zhu, K., Yi, J., Xiao, Y., Lai, Y., Song, P., Zheng, W., et al. (2015). Impaired bone homeostasis in amyotrophic lateral sclerosis mice with muscle atrophy. *J. Biol. Chem.* 290, 8081–8094. doi: 10.1074/jbc.M114.603985

Glossary

ALS	Amyotrophic lateral sclerosis
BMD	Bone mineral density
CI	Confidence interval
DXA	Dual energy X-ray absorptiometry
FN	Femoral neck
GEFOS	Genetic factors for osteoporosis consortium
GWAS	Genome-wide association studies
IVs	Instrumental variables
IVW	Inverse variance weighted
LD	Linkage disequilibrium
LS	Lumbar spine
MAF	Minor allele frequency
MR	Mendelian randomization
MR-PRESSO	MR pleiotropy residual sum and outlier test
NIMV	Non-invasive mechanical ventilation
OR	Odds ratio
SE	Standard error
SNP	Single nucleotide polymorphism

frontiers | Frontiers in Cellular Neuroscience

TYPE Review
PUBLISHED 08 January 2024
DOI 10.3389/fncel.2023.1307636

OPEN ACCESS

EDITED BY
Danyllo Oliveira,
University of São Paulo, Brazil

REVIEWED BY
Partha Sarathi Sarkar,
The University of Texas Medical Branch at Galveston, United States
Chih-Wei Zeng,
University of Texas Southwestern Medical Center, United States
Barbara Tedesco,
University of Milan, Italy

*CORRESPONDENCE
Maria Dimitriadi
✉ m.dimitriadi@herts.ac.uk

RECEIVED 04 October 2023
ACCEPTED 14 December 2023
PUBLISHED 08 January 2024

CITATION
Rashid S and Dimitriadi M (2024) Autophagy in spinal muscular atrophy: from pathogenic mechanisms to therapeutic approaches. *Front. Cell. Neurosci.* 17:1307636. doi: 10.3389/fncel.2023.1307636

Autophagy in spinal muscular atrophy: from pathogenic mechanisms to therapeutic approaches

Saman Rashid and Maria Dimitriadi*

School of Life and Medical Science, University of Hertfordshire, Hatfield, United Kingdom

Spinal muscular atrophy (SMA) is a devastating neuromuscular disorder caused by the depletion of the ubiquitously expressed survival motor neuron (SMN) protein. While the genetic cause of SMA has been well documented, the exact mechanism(s) by which SMN depletion results in disease progression remain elusive. A wide body of evidence has highlighted the involvement and dysregulation of autophagy in SMA. Autophagy is a highly conserved lysosomal degradation process which is necessary for cellular homeostasis; defects in the autophagic machinery have been linked with a wide range of neurodegenerative disorders, including amyotrophic lateral sclerosis, Alzheimer's disease and Parkinson's disease. The pathway is particularly known to prevent neurodegeneration and has been suggested to act as a neuroprotective factor, thus presenting an attractive target for novel therapies for SMA patients. In this review, (a) we provide for the first time a comprehensive summary of the perturbations in the autophagic networks that characterize SMA development, (b) highlight the autophagic regulators which may play a key role in SMA pathogenesis and (c) propose decreased autophagic flux as the causative agent underlying the autophagic dysregulation observed in these patients.

KEYWORDS

spinal muscular atrophy, autophagy, macroautophagy, mitophagy, autophagic flux

Spinal muscular atrophy

Spinal muscular atrophy (SMA) is a devastating autosomal recessive neuromuscular disorder, presenting with an overall incidence rate of 1 in 6,000 to 1 in 10,000 live births and a carrier frequency of around 1 in 40 Caucasian adults (Crawford and Pardo, 1996; Verhaart et al., 2017). It is caused by the reduced expression of the ubiquitous survival motor neuron (SMN) protein, resulting in (a) degeneration of the α-motor neurons in the

Abbreviations: AAV9, adeno-associated viral vector serotype 9; ALS, amyotrophic lateral sclerosis; ASO, antisense oligonucleotide; miRNA, microRNA; mTOR, mechanistic target of rapamycin; NMJ, neuromuscular junction; p62/SQSTM1, sequestosome 1; PE, phosphatidylethanolamine; PI3K, phosphatidylinositol 3-kinase; PLS3, plastin 3; ROCK, rho-associated kinase; SMA, spinal muscular atrophy; SMN, survival motor neuron; SMN1, survival motor neuron 1; SMN2, survival motor neuron 2; snRNP, small nuclear ribonucleoproteins; UBA1, ubiquitin-like modifier activating enzyme 1.

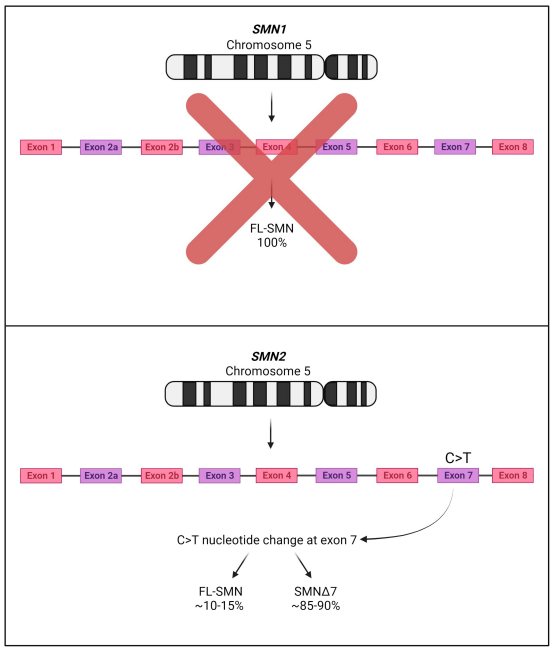

FIGURE 1
SMA associated genes *SMN1* and *SMN2* on human chromosome 5. SMA patients display deletions or mutations in both copies of *SMN1*; although *SMN2* is expressed, most of the *SMN2* mRNA transcripts lack exon 7 due to a C > T nucleotide change. Thus, most of the product deriving from the *SMN2* gene is mostly unstable and rapidly degraded (SMNΔ7).

anterior horn of the spinal cord, (b) neuromuscular junction (NMJ) maturation defects, (c) progressive muscle atrophy and (d) ultimately death (Monani and De Vivo, 2014). It is now well-documented that two genes code for the SMN protein in humans: the telomeric *survival motor neuron 1* (*SMN1*) and the centromeric *survival motor neuron 2* (*SMN2*), both located on chromosome 5q13. Heterozygous carriers of the disease harbor a single copy of *SMN1*, however due to a gene duplication event, multiple copies of *SMN2* can be presented (Lorson et al., 1999; Monani et al., 1999). The *SMN1* gene codes for a fully functional SMN protein, while a single C > T nucleotide change in *SMN2* disrupts an exonic splicing enhancer, a DNA sequence motif which promotes the inclusion of exons into mature transcripts. This genetic change instead creates a new exonic splicing silencer that results in exon 7 skipping and the formation of a truncated variant of the SMN protein - known as SMNΔ7 with diminished function and stability (Lorson et al., 1999; Cartegni and Krainer, 2002; Kashima and Manley, 2003; **Figure 1**). Approximately 85–90% of the *SMN2* gene product accounts for SMNΔ7, while 10–15% codes for a functional SMN protein (Kolb and Kissel, 2015). The latter is not adequate to prevent SMA; although, it is of note that more copies of *SMN2* result in less severe forms of the disease (Wirth, 2021).

Clinical presentations of SMA

Spinal muscular atrophy is typically categorized as proximal and distal SMA. Proximal SMA is the most common form of the disease, accounting for up to 95% of cases and manifests during infancy or early childhood, affecting the proximal regions. Conversely, distal SMA is significantly less common and occurs during childhood but progresses at a slower rate into adulthood (Farrar and Kiernan, 2015). SMA is clinically divided into four types, types I-IV with type 0 referring to prenatal SMA. Diagnosis of disease depends on the severity, age of onset and motor function. Type 0 SMA refers to neonates with one copy of *SMN2*, displaying severe weakness and a history of decreased fetal movements *in utero* (MacLeod et al., 1999). Type I SMA, which is often referred to as Werdnig-Hoffmann disease, manifests within 6 months of age and is characterized by hypotonia, poor head control and an inability to sit unaided. Type I SMA patients have two copies of *SMN2* and apart from poor motor neuron function, they usually develop respiratory complications within 2 years of symptom onset (Thomas and Dubowitz, 1994; Zerres and Rudnik-Schöneborn, 1995; Finkel et al., 2014). In contrast, children with three copies of *SMN2* are categorized under type II SMA (an intermediate form of disease), can sit without aid during their development and display independent head control present with limited hypotonia. SMA type III subjects have three or four *SMN2* copies and are known to walk independently at some point in their lives, although patients present with a progressive weakness in leg muscles. Life expectancy of patients with type III SMA is not affected (Zerres et al., 1997). Patients with more than four copies of *SMN2* are characterized by type IV SMA, which is the mildest form of the disease, making up less than 5% of all cases. Onset of type IV is typically during adulthood and is characterized by mild muscle weakness and reduced fine motor control (Zerres and Rudnik-Schöneborn, 1995).

Molecular mechanisms underlying SMA

Various *in vitro* and *in vivo* models have been used to understand the molecular and cellular mechanisms underlying SMA pathogenesis (Monani et al., 2000; Edens et al., 2015; O'Hern et al., 2017; Nishio et al., 2023). Although a detailed report on SMA pathogenesis is beyond the scope of this review, a few important aspects are discussed below.

Survival motor neuron is expressed in the nucleus and cytoplasm. Its canonical function is the assembly of small nuclear ribonucleoproteins (snRNPs), which are critical for pre-mRNA splicing, through interactions with the Gemin complex (Fischer et al., 1997). Hence, it is of note that splicing defects are described in many aspects of SMA pathology (Burghes and Beattie, 2009; Singh and Singh, 2018). Besides SMN's canonical role, the protein is also involved in RNA transport and local translation in axons, an event particularly important in neuronal cells for proper neuronal development (Fallini et al., 2012). SMN binds RNA via a domain implicated in the localization of β-actin mRNA to the axonal growth cones of motor neurons, a process necessary for correct axonal development (Rossoll et al., 2003). Furthermore, SMN is known to interact with proteins involved in cytoskeletal dynamics and it has been observed that granules containing SMN are associated with cytoskeletal microfilaments essential for cell shape, integrity and transport along the axonal compartment in neurons (Béchade et al., 1999).

Thus, the interaction of SMN with β-actin further highlights the integral role of SMN in cytoskeletal and microtubule dynamics. Interestingly, SMN also binds profilin2a, a neuron specific actin-binding protein (Giesemann et al., 1999). Profilin2a is regulated by Rho-Associated Kinase (ROCK) and ROCK inhibition displayed increased lifespan and amelioration of defects at the NMJ of intermediate SMA mice (Bowerman et al., 2010, 2012). SMN protein has also been implicated in improper proteostasis (Zhang et al., 2013; Lambert-Smith et al., 2020). Proteomic studies revealed SMN depletion resulted in reduced expression of ubiquitin-like modifier activating enzyme 1 (UBA1) – a highly conserved protein ubiquitously expressed throughout all human tissues, canonically tasked with a role in the unfolded protein response and autophagy (Chang et al., 2013; Lambert-Smith et al., 2020). Reduced UBA1 resulted in disrupted proteosome degradation and perturbed axonal morphology (Hosseinibarkooie et al., 2017), whereas restoration of UBA1 mRNA rescued functional and morphological defects in SMA zebrafish (Powis et al., 2016). Furthermore, a growing body of evidence has also highlighted the role of SMN in endocytosis (Dimitriadi et al., 2010; Hosseinibarkooie et al., 2017; Riessland et al., 2017). Given the dependence of endocytosis on cytoskeletal remodeling (Montagnac et al., 2013; Franck et al., 2019), involvement of the SMN protein in endocytosis is not a surprise. Research on mammalian and nematode SMA models demonstrated perturbations in the endocytic pathway. In the nematode *Caenorhabditis elegans*, SMN ortholog depletion impaired synaptic transmission by interfering with the recycling of endocytic synaptic vesicles (Dimitriadi et al., 2010). Furthermore, diminished levels of SMN were noted to cause varying widespread endocytic defects including atypical localization of endosomal proteins, aberrant endosomal trafficking in both neuronal and non-neuronal tissue and impairments in JC polyomavirus infection – a clathrin-mediated endocytosis process (Dimitriadi et al., 2010). It was also documented that endocytic defects arise due to dysregulation of F-actin and calcium dynamics (Hosseinibarkooie et al., 2017). Plastin 3 (PLS3), an actin-bundling protein which interacts with F-actin and calcium, was shown to rescue motor neuron pathology, NMJ structure and function when overexpressed in a variety of SMA animal models (Oprea et al., 2008; Dimitriadi et al., 2010; Hosseinibarkooie et al., 2017). Similar rescue was observed when levels of neurocalcin delta, a negative regulator of endocytosis, were decreased (Riessland et al., 2017; Torres-Benito et al., 2019). Additionally, overexpression of coronin 1C, a calcium dependent F-actin binding protein which binds to PLS3, also rescued SMA defects in zebrafish (Hosseinibarkooie et al., 2017). Alternative roles of the SMN protein have been described in cell proliferation/differentiation (Grice and Liu, 2011), phosphatase and tensin homolog-mediated protein synthesis (Ning et al., 2010), energy homeostasis/mitochondrial function (Acsadi et al., 2009), priming of ribosomes to modulate translation (Lauria et al., 2020) and autophagy (Garcera et al., 2013; Custer and Androphy, 2014; Periyakaruppiah et al., 2016; Piras et al., 2017; Rodriguez-Muela et al., 2018; Sansa et al., 2021). Despite the various documented cellular roles of SMN, the specific interaction most pertinent to the development of SMA remains elusive. Treatment for SMA patients involves gene-targeted therapy in which the defective *SMN1* gene is being replaced or the *SMN2* gene splicing pattern is modulated.

Therapeutic strategies

Three treatments are currently approved by the European Medicines Agency and the US Food and Drugs Administration: Nusinersen (Spinraza; Biogen), Onasemnogene abeparvovec (Zolgensma; Novartis) and Risdiplam (Evrysdi; Roche).

Nusinersen is the first gene therapy for SMA patients to be approved and is administered intrathecally. It costs up to $125,000 per dose and relies on the manipulation of *SMN2* gene splicing to increase the production of full-length, functional SMN protein. Exclusion of exon 7 is regulated by multiple surrounding elements; the most important one for nusinersen treatment is the intronic splicing silencer N1, deletion of which is known to significantly increase exon 7 inclusion in the *SMN2* mRNA transcript (Singh et al., 2006). Fundamentally, targeting this regulatory region via antisense oligonucleotides (ASOs) - modified chains of nucleotides with the ability to target a gene product of interest - forms the basis of nusinersen treatment. Effectiveness of this treatment was tested initially using a mild mouse model of SMA at embryonic, neonatal, and adult stages and it was noted that SMN protein levels were increased resulting in an improvement of the SMA phenotype (Hua et al., 2010). Additionally, the study by Hua et al. (2010) suggested that early treatment, at either the embryonic or neonatal stages resulted in stronger amelioration of the phenotypes observed in mild SMA mice. Furthermore, the ASO displayed an ability to significantly improve lifespan and motor function in severe mouse models of SMA (Passini et al., 2011). Subsequent clinical trials showed nusinersen to be most effective in infants treated before 6 months of life (Finkel et al., 2017) – however, more recent studies have reported improvements in patients of different stages and ages, covering the whole spectrum of SMA (Coratti et al., 2021; Łusakowska et al., 2023).

Onasemnogene abeparvovec is an *SMN1* gene replacement therapy which is administered as a single intravenous injection at a cost of $2,125,000 per dose. Expression of *SMN1* cDNA under the control of a ubiquitous promoter using intravenous delivery of the adeno-associated viral vector serotype 9 (AAV9) was efficient in transducing motor neurons in the spinal cord of mice (Dominguez et al., 2010). Through this technique, *SMN1* gene expression mediated by AAV9 significantly improved lifespan and motor function in SMA mouse models and non-human primates; similarly to nusinersen it was found that earlier intervention resulted in better outcomes (Valori et al., 2010; Meyer et al., 2015). In addition, clinical trials with type I SMA infants treated with onasemnogene abeparvovec displayed significant improvements in motor neuron function, although hepatotoxicity was observed as an adverse side effect (Mendell et al., 2017). Therefore, most patients require the corticosteroid prednisolone to mitigate the negative effects of liver toxicity (Chand et al., 2021). Overall, the aforementioned treatment is targeted at patients below 2 years of age, with bi-allelic mutations in the *SMN1* gene and up to three copies of *SMN2* (Wirth, 2021; Day et al., 2022; Ogbonmide et al., 2023).

Risdiplam, unlike its predecessors, is an orally administered small molecular drug that acts as an *SMN2* splice modulator with a cost of up to $340,000 per year. The molecule binds directly to *SMN2* pre-mRNA at two sites and promotes exon 7 inclusion by facilitating the recruitment of U1-snRNP1 particles to the splice

donor site of intron 7, thus increasing the production of full-length SMN protein (Sivaramakrishnan et al., 2017). In preclinical trials, risdiplam was found to increase full-length functional SMN protein in both mild and severe SMA mice, drastically increasing lifespan and improving motor function defects (Poirier et al., 2018). Risdiplam treatment is offered to type I, II and III SMA patients aged 2 months and older with one to four copies of *SMN2* (Paik, 2022).

Other treatments in development include the myostatin inhibitor apitegromab. Myostatin is primarily expressed in skeletal muscle and serves to inhibit muscle growth (Sharma et al., 2015). Multiple preclinical SMA models have highlighted the effectiveness of myostatin inhibition in maintaining muscle mass and function (Rose et al., 2009; Feng et al., 2016). Apitegromab treatment has shown promise in milder type II and type III forms of disease (Barrett et al., 2021); the inhibitor has passed phase 1 and 2 trials having shown evidence to improve and/or stabilize motor function in SMA patients (Day et al., 2022). The identification of myostatin as a potential target for SMA treatment and the clinical benefit of apitegromab has led to the development of other therapies targeting myostatin as well as phase 3 trials of combination therapy with nusinersen or risdiplam (Day et al., 2022).

Fundamentally, while multiple pipeline treatments are in development and therapies are commercially available, there is no cure for SMA. It remains unclear which of the SMN function(s) result in disease pathogenesis. Firstly, it may be that the canonical role of SMN is the key cause of the disease, stemming from a global decrease in SMN protein function, subsequently interfering with the splicing of essential mRNA transcripts required for correct motor neuron development. There is also the possibility that one of the alternative functions of SMN, which is disrupted by SMN protein depletion results in a gradual deterioration of motor neurons. Our intention is to provide an overview of the role of autophagy in SMA which may in turn identify combinatory approaches that include SMN-dependent and -independent treatments for optimal benefits.

Autophagy

Autophagy is known to play a vital role in cell survival and maintenance of cellular integrity through proteostasis (Das et al., 2012). Autophagy can be upregulated in response to a wide range of stimuli; these include infection, starvation, oxidative stress, temperature, growth and development (Levine and Kroemer, 2008; Mizushima et al., 2008; Mizushima and Levine, 2010; Shang et al., 2011; Summers and Valentine, 2020). It is categorized into three types: macroautophagy, microautophagy and chaperone-mediated autophagy (**Figure 2**). While each type of autophagy ultimately results in lysosomal-mediated degradation of cytoplasmic components, the mode of delivery differs. Macroautophagy involves the formation of an intermediary double membrane vesicle, which engulfs cargo and transports it to the lysosome. Selective macroautophagy, in which specific cellular cargo are targeted for sequestration is dependent on the substrate; for example, the degradation of mitochondria (also known as mitophagy) is controlled by macroautophagy (Shimizu et al., 2014). In contrast, microautophagy involves direct invagination of cytoplasmic material into the lysosome. Chaperone-mediated autophagy is distinct from macro- and microautophagy due to the lack of transporter vesicles. During chaperone-mediated autophagy, cytoplasmic material containing the pentapeptide KFERQ motif are bound and chaperoned by the heat shock cognate 71 kDa protein Hsc70 which is recognized by the lysosomal LAMP2A receptor.

Macroautophagy (henceforth referred to as autophagy) is the main form of autophagy used for the clearance of aggregated proteins and damaged organelles due to its bulk degradation capabilities. As this review focuses on macroautophagy, microautophagy and chaperone-mediated autophagy will not be discussed; they have been extensively described in reviews by Li et al. (2012) and Kaushik and Cuervo (2018), respectively. During autophagy, the cytoplasmic material marked for degradation is sequestered by a nascent membrane known as the phagophore, which is believed to originate from the endoplasmic reticulum (Axe et al., 2008). The phagophore fuses with itself to form the autophagosome; upon completion of this process, the autophagosome fuses with a lysosome to form an autolysosome where lysosomal enzymes facilitate the degradation of cargo (Yorimitsu and Klionsky, 2005). Ultimately, autophagy occurs via five distinct stages: (i) autophagy induction, (ii) vesicle nucleation (iii) vesicle elongation (iv) docking and lysosomal fusion and (v) degradation. The ability of the pathway to progress through these stages is referred to as autophagic flux.

Autophagy is characterized by a multi-step process in which cytoplasmic contents are sequestered within double-membrane vesicles known as autophagosomes (**Figure 3**). In selective autophagy, recognition and delivery of ubiquitinated cargo to the autophagosome is orchestrated by the autophagic receptor Sequestosome 1 (p62/SQSTM1), hereafter referred to as p62 (Kumar et al., 2022). Initiation of the process begins with the dissociation of the mechanistic target of rapamycin (mTOR) from the ULK1/2-ATG13-FIP200 autophagy induction complex (Jung et al., 2009). Subsequent nucleation of the phagophore is orchestrated by a Class III phosphatidylinositol 3-kinase (PI3K) complex composed of Beclin 1, VPS34, VPS15 and ATG14 (Itakura et al., 2008; Burman and Ktistakis, 2010). The nucleated vesicle then expands through maturation of the membrane, guided by an ATG12-ATG5-ATG16L1 complex which catalyzes insertion of LC3 into the vesicle (Fujita et al., 2008). Prior to LC3 insertion into the membrane, LC3 undergoes proteolytic processing by ATG4 into LC3-I, subsequently bound by ATG7 and ATG3 and lastly, conjugated by phosphatidylethanolamine (PE) - the resulting mature form of LC3 is referred to as LC3-II (Kirisako et al., 2000; Ohsumi, 2001; Mizushima et al., 2011). Following LC3-II incorporation, the extending ends of the phagophore fuse with one another, forming the double membraned autophagosome which engulfs a segment of cytoplasm and cargo (Yorimitsu and Klionsky, 2005). The autophagosome is transported along microtubules and fuses with a lysosome to form an autolysosome; the cargo is then degraded by hydrolytic proteases (Pankiv and Johansen, 2010). The docking and fusion of the lysosome to the autophagosome is enabled through the action of small GTPases (such as RAB7), SNAREs and the HOPS complex/EPG5 tethering factors (Lörincz and Juhász, 2020). Ultimately, dismantled cellular components are actively transported for reconstitution into

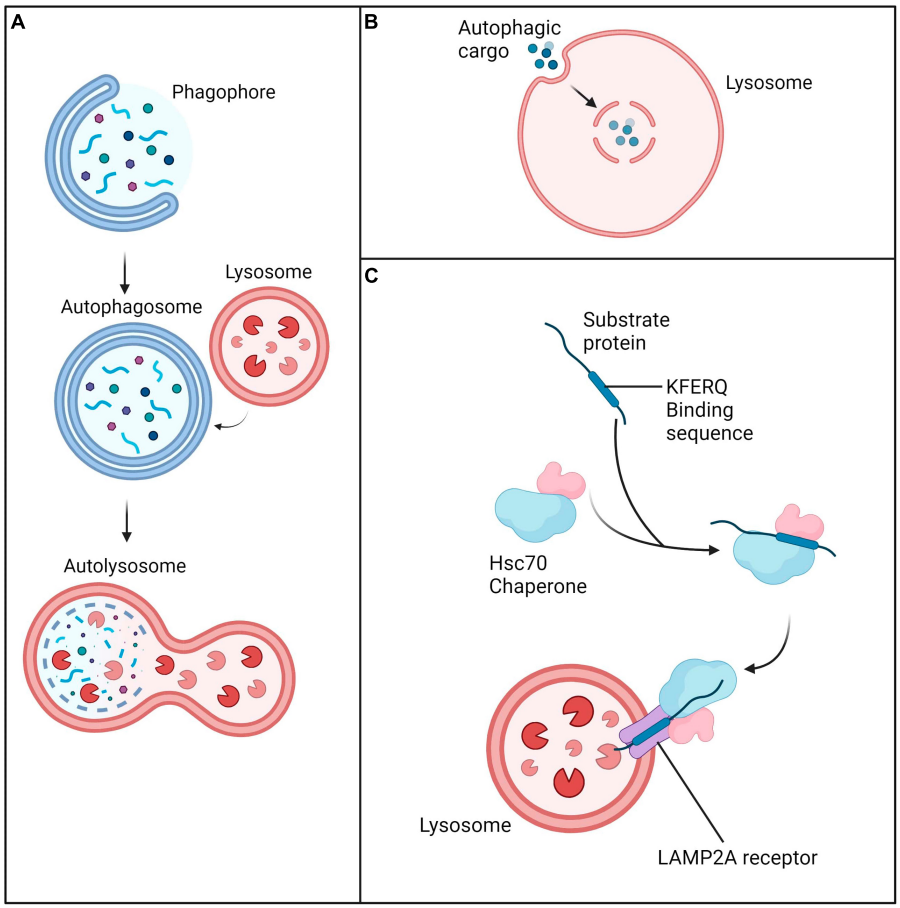

FIGURE 2
Three main forms of autophagy. **(A)** Macroautophagy is characterized by engulfment and transfer of cargo to lysosomes via an intermediary double membrane vesicle. **(B)** Microautophagy is characterized by direct invagination of cytoplasmic material into the lysosome. **(C)** Chaperone-mediated autophagy involves delivery of cargo marked by the Hsc70 chaperone complex to the lysosome via the LAMP2A receptor.

new macromolecules or alternatively, for energy metabolism (Yorimitsu and Klionsky, 2005).

Autophagy is upregulated to act as a protective process to promote survival (Kataura et al., 2022; Yang et al., 2023). However, impaired or excessive autophagy can be detrimental and could result in the accumulation of protein aggregates – a characteristic of many neurodegenerative disorders. The autophagic pathway is particularly known to be perturbed in neurodegenerative disorders such as Alzheimer's disease, Parkinson's disease, amyotrophic lateral sclerosis (ALS) (Ravikumar et al., 2004; Bandyopadhyay and Cuervo, 2007; Hetz et al., 2009; Sarkar et al., 2011; Nilsson and Saido, 2014) and is emerging as a popular topic of investigation in SMA pathogenesis.

Autophagy dysregulation in SMA

Autophagosomes

An increasing body of *in vitro* and *in vivo* evidence suggests dysregulation of autophagy as a key factor in SMA pathogenesis (**Table 1**). LC3-I conversion to LC3-II is considered a general marker of autophagosome formation, while autophagosome abundance is linked with LC3-II protein levels (Mizushima et al., 2004). The presence of autophagosomes and autolysosomes were analyzed in the neurites and cytoplasm of Smn-depleted motor neurons (Garcera et al., 2013). Motor neurons were transduced with lentivirus containing short hairpin RNA sequences targeting specific sites of mouse Smn and it was identified that Smn reduction resulted in an increased autophagosome and autolysosome number compared to controls (Garcera et al., 2013). This increase was observed in both motor neuron soma and neurites. Similar findings were also recapitulated *in vivo*; LC3-II levels were increased in more severe SMA mice [*Smn(-/-); SMN2]* motor neurons, further reinforcing autophagy dysregulation in SMA (Garcera et al., 2013). A study by Custer and Androphy (2014) highlighted similar findings. An NSC-34 cell line – a hybrid line produced by fusing mouse neuroblastoma cells N18TG2 and motor neurons from mouse embryo spinal cords (Cashman et al., 1992), was transfected with GFP-LC3. The latter is known to appear as discrete puncta following lipidation and incorporation to the autophagosome membrane (Custer and Androphy, 2014). It was identified that Smn-depleted cultures displayed increased autophagic puncta, suggesting an increase in autophagosome number. The accumulation of LC3-positive puncta is not unique to the NSC-34 model; SMA-derived human fibroblasts transfected

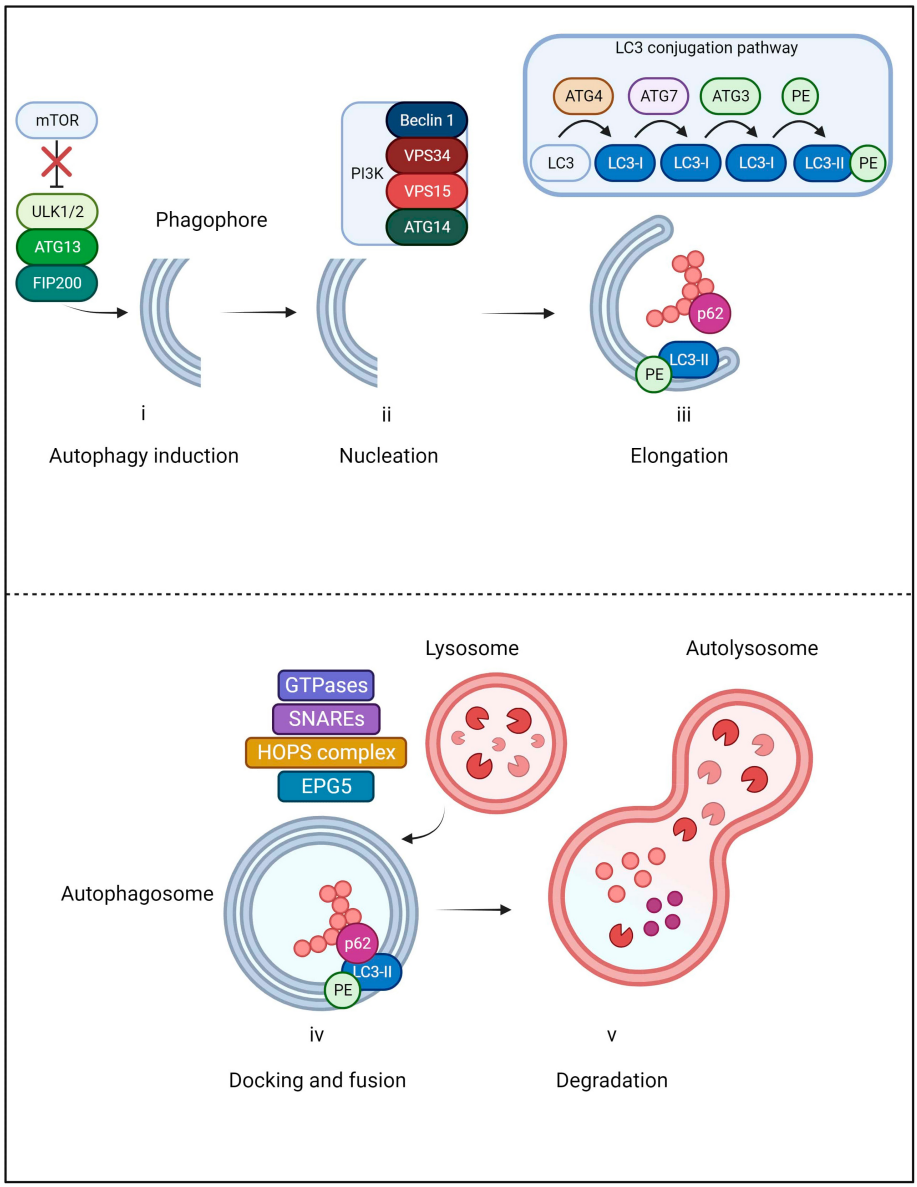

FIGURE 3
Main steps of macroautophagy. The pathway begins with the initiation step in which mTOR dissociates from the ULK1/2-ATG13-FIP200 autophagy induction complex in order for the phagophore to be formed. Subsequently, nucleation of the phagophore is orchestrated by a PI3K complex composed of Beclin 1, VPS34, VPS15 and ATG14. As the vesicle elongates, LC3 undergoes proteolytic cleavage by ATG4 into LC3-I. LC3-I is then bound by ATG7 and ATG3 and finally conjugated by phosphatidylethanolamine (PE); the resultant form is known as LC3-II. Once LC3-II incorporates into the autophagosome membrane, the extending ends join, engulfing cellular cargo. During the process, p62 delivers ubiquitinated cargo to the autophagosome where it binds with LC3-II. The autophagosome is then transported along microtubules to the lysosome which will dock and fuse through the action of small GTPases, SNAREs and the HOPS complex/EPG5 tethering factors. Cellular cargo then undergoes lysosomal degradation and dismantled components are recycled.

with LC3-GFP also displayed an increased number of puncta/cells, further highlighting an increase in autophagosome number in SMA patients. In agreement with these findings, Periyakaruppiah et al. (2016) also demonstrated elevated number of autophagosomes in severe SMA mice [*Smn(-/-); SMN2]* by detecting increased LC3-II levels in their spinal cord motor neurons. These findings were also echoed in the SMNdelta7 mouse model, presenting a severe SMA phenotype; lumbar spinal cord motor neurons obtained from SMNdelta7 mice displayed increased LC3-II and Beclin 1 – a protein component of the vesicle nucleation complex, indicating an increased number of autophagosomes (Piras et al., 2017).

Autophagic flux

Elevated numbers of autophagosomes could be the result of increased synthesis or reduced degradation, the latter being the result of impaired autophagic flux. To determine the cause of increased LC3-II levels, Smn-depleted motor neurons were

TABLE 1 Summary of the autophagic perturbations reported in SMA.

SMA model	Autophagic marker	Autophagosome number	Autophagic flux	Findings	References
Cultured Smn-depleted mice motor neurons More severe SMA mice (*Smn-/-; SMN2)*	LC3-II Beclin 1	Increased	Unaffected	Treatment with the lysosomal proteolysis inhibitor bafilomycin A1 increases LC3-II, suggesting autophagic flux to be unaffected when Smn is reduced. Inhibition of the autophagic regulator Beclin 1 significantly delays neuronal degeneration.	Garcera et al., 2013
NSC-34 cell line Cultured SMA patient fibroblasts (Type I child line 3813T; heterozygous mother line 3814T) Taiwanese severe SMA mouse model (*Smn-/-; SMN2$^{tg/0}$)*	LC3-II p62	Increased	Reduced	Smn depleted cultures transfected with GFP-LC3 display an increase in autophagosome numbers. Treatment with the autophagic inducer rapamycin was followed by assessment of p62 protein levels – accumulation of p62 was indicative of reduced autophagic flux.	Custer and Androphy, 2014
Cultured Smn-depleted mice motor neurons More severe SMA mice (*Smn-/-; SMN2)*	LC3-II p62	Increased	Reduced	p62 levels are significantly increased in spinal cord motor neurons of SMA mice, suggesting reduced autophagic flux. Treatment with the autophagic inhibitor bafilomycin A1 decreases Smn levels in control cells; treatment with the autophagy inducer rapamycin increases Smn levels in control cells.	Periyakaruppiah et al., 2016
Severe SMA mice (*Smn-/-; SMN2; SMNΔ7*)	LC3-II Beclin 1 p62	Increased	Unaffected	p62 levels remain unaltered in severe SMA mice suggesting autophagic flux not to be affected. Treatment with the autophagic inhibitor 3-methyladenine results in reduced autophagosome number, increased Smn levels and prolonged lifespan.	Piras et al., 2017
Severe SMA mice (*Smn-/-; SMN2; SMNΔ7*) SMA patient fibroblasts (Types I, II, III)	LC3-II p62	Increased	Reduced	Exposure to lysosomal inhibitors display a defective flux as evident by an increase in p62 protein levels, implying a reduction in autophagosome clearance. LC3-II levels are increased in the presence of lysosomal inhibitors; LC3 levels remain unchanged in SMA patients further suggesting increased levels of LC3-II are due to reduced autophagic flux rather than increased autophagosome formation. SMN protein is regulated by autophagy; i.e., starvation-induced autophagy causes decreased SMN levels – inhibition of autophagy increases SMN levels in starved cells. SMN protein interacts with p62; increased p62 levels resulted in further SMN protein reduction and elevated mTOR activity.	Rodriguez-Muela et al., 2018
SMA patient fibroblasts SMA patient muscle More severe SMA mice (*Smn-/-; SMN2)*	LC3-II p62 mTOR	Increased in motor neurons Decreased in fibroblasts Decreased in skeletal muscle	Reduced in motor neurons Reduced in fibroblasts Increased in skeletal muscles	LC3-II levels decrease in SMA patient muscle and fibroblasts but increase in motor neurons, suggesting tissue specific outcomes of SMN reduction. p62 decreases in SMA mice muscle suggesting an increase in autophagic flux. Conversely, p62 increases in SMA patient fibroblasts, suggesting a reduced autophagic flux. Similarly, p62 is increased in motor neurons, indicative of a reduced flux. mTOR signaling is found to be increased in motor neurons (autophagy inhibited); decreased in skeletal muscle and fibroblasts (autophagy activated).	Sansa et al., 2021

treated with bafilomycin A1 – a lysosomal degradation inhibitor (Yamamoto et al., 1998; Garcera et al., 2013). LC3-II levels are expected to increase in the presence of bafilomycin A1 demonstrating an efficient autophagic flux (Menzies et al., 2012). Interestingly, bafilomycin-treated Smn motor neurons displayed a further increase in LC3-II compared to non-treated Smn controls (Garcera et al., 2013), an observation which would indicate some degree of functional autophagic flux. While the authors initially stated that autophagic flux was unaffected (Garcera et al., 2013), subsequent studies by the same group identified that flux was in fact reduced in Smn motor neurons by using a more comprehensive analysis (Periyakaruppiah et al., 2016; Sansa et al., 2021). It should be noted that even a partial blockage during the autophagy process could also result in LC3-II increase when bafilomycin A1 treatment is applied; this could be incorrectly interpreted as an unaffected flux (Klionsky et al., 2012). It is therefore important for researchers to assess LC3-II turnover in the presence of bafilomycin A1 with appropriate positive controls such as rapamycin treatment as well as examining the degradation of the autophagy specific substrate p62 (Klionsky et al., 2012).

To further clarify whether the accumulation of autophagosomes is due to an impaired autophagic flux or enhanced generation of autophagosomes, Custer and Androphy (2014) treated NSC-34 cultures with the autophagy activator rapamycin and expressed mRFP-LC3-GFP – a marker which allows for the differentiation between autophagosomes and autolysosomes by initially appearing yellow and subsequently transitioning to red after successful fusion with the lysosome (Custer and Androphy, 2014). An increased ratio of yellow puncta was observed in the Smn-depleted cultured cells treated with rapamycin, highlighting a failure of the autophagosome to fuse with the lysosome and thus, pointing to a reduced autophagic flux. Autophagic flux was further examined by assessing levels of the p62 protein, which is known to be degraded together with bound ubiquitinated substrates by autophagy following fusion with the lysosome. Increased p62 protein levels were observed in the NSC-34 cell line indicative of reduced autophagic flux (Custer and Androphy, 2014). Importantly, these findings were replicated in human SMA patient fibroblasts, as well as in the Taiwanese severe SMA mouse model (*Smn-/-; SMN2*^{tg}/^{0}) – animals carrying the Hung targeted deletion of murine Smn and a human *SMN2* transgene (Hsieh-Li et al., 2000; Custer and Androphy, 2014). However, Piras et al. (2017) found p62 levels to be unchanged in severe SMNdelta7 mice suggesting flux not to be affected. It is noteworthy that Custer and Androphy (2014) employed a more severe SMA mouse model, while Piras et al. (2017) drew conclusions from severe SMA mice which may be the cause of the discrepancies observed. Agreeing with the findings of Custer and Androphy (2014) and contrasting the findings of Garcera et al. (2013) and Piras et al. (2017), it was found that p62 protein levels were also significantly increased in the spinal cord motor neurons of more severe SMA mice, further indicating a reduced autophagic flux (Periyakaruppiah et al., 2016). Moreover, wild-type mouse motor neurons cultured with bafilomycin A1 in the presence of neurotrophic factors displayed increased LC3-II and reduced Smn levels relative to untreated controls, suggesting that inhibitors of autophagic flux resulted in reduced Smn protein levels in healthy controls (Periyakaruppiah et al., 2016). In line with these findings, SMA patient fibroblasts treated with lysosomal inhibitors displayed an accumulation of p62, while LC3-II increase was significantly lower than the increase observed in control fibroblasts, suggesting that autophagosome formation was not impaired (Rodriguez-Muela et al., 2018) A potential mechanism that could underlie the autophagic flux defects observed in SMA may be due to the disrupted SNARE complex assembly, an observation that has recently been described following SMN depletion (Kim et al., 2023). Fundamentally, the SNARE complex is required for autophagosome-lysosome fusion and therefore, when impaired, autophagic flux is expected to be reduced (Mohamud et al., 2018). SNAP25, a core component of the SNARE complex that is capable of mediating autophagosome-lysosome fusion was significantly reduced in more severe SMA mice (Mu et al., 2018; Kim et al., 2023). However, the interaction between SNAP25 and SMN has not been explored in the context of autophagy dysregulation. Overall, these studies point to an increase in autophagosome number, but it remains controversial whether autophagic flux is affected in SMA.

Drug modulators of autophagy

Autophagic drug modulators have also been utilized to study the effect of autophagy in SMA. As mTOR is widely accepted as a major negative regulator of autophagy, rapamycin – an mTOR inhibitor, is commonly used to study autophagy activation (Noda and Ohsumi, 1998; Ravikumar et al., 2004; Berger et al., 2006). Wild-type mouse motor neurons cultured in the presence of neurotrophic factors and treated with rapamycin showed elevated Smn and LC3-II protein levels, while the same type of tissue when treated with bafilomycin A1 displayed reduced Smn protein levels (Periyakaruppiah et al., 2016). Conversely, administration of 3-methyladenine – which inhibits PI3K and subsequently autophagy initiation - reduced Beclin 1 and LC3-II and increased Smn protein levels in SMA cell cultures (Piras et al., 2017). Moreover, it was found that 3-methyladenine significantly increased the lifespan and number of motor neurons in SMA pups, suggesting that autophagy inhibition delayed motor neuron degeneration (Piras et al., 2017). While these studies seem contradictory, it should be noted that the findings of Periyakaruppiah et al. (2016) are based on control animals, whereas those by Piras et al. (2017) derive from severe SMA mice. Therefore, under normal conditions, activating autophagy is able to increase SMN levels. Moreover, it has been shown that rapamycin can increase autophagic flux in primary neurons (Rubinsztein and Nixon, 2010) and 3-methyladenine, surprisingly, presents a dual-role in autophagic regulation being able to inhibit the pathway but also promote autophagic flux due to its transient effects on varying classes of PI3K (Wu et al., 2010). The rescue observed by Piras et al. (2017) when administering 3-methyladenine may be a result of alleviating the defects in autophagic flux and the burden of autophagosome accumulation. Thus, the conclusions driven by the administration of these drugs may not be as straightforward as previously thought, and it is possible that the effect on autophagic flux is responsible for the contradictory findings.

Autophagy-related regulators

Apart from studies on SMA focusing on (i) autophagosome number, (ii), autophagic flux and (iii) SMN endogenous levels following drug treatment, several studies have linked autophagy-related proteins to SMA. Diminished Smn protein levels are known to cause neurite degeneration and non-apoptotic cell death in spinal cord motor neurons of mice (Garcera et al., 2011). This was prevented by overexpression of Bcl-XL - a protein known to inhibit autophagy by binding to Beclin 1 (Pattingre et al., 2005) - without increasing Smn levels in embryonic mouse motor neurons (Garcera et al., 2011). Thus, Smn-depleted motor neurons expressing human Bcl-XL showed significant decreases in LC3-II protein levels (Garcera et al., 2013). This decrease was not observed in controls, suggesting the aforementioned Bcl-XL reduction of LC3-II levels to be specific to the dysregulation caused by Smn knockdown (Garcera et al., 2013).

Furthermore, calpain, a calcium-dependent protease involved in neuronal homeostasis has been suggested to play a role in Smn regulation (Cowan et al., 2008; Fuentes et al., 2010; Yamashima, 2013; de la Fuente et al., 2019). Elevated levels of free cytosolic calcium activate calpains, which in turn inhibit autophagy in an mTOR-independent manner (Kaiser et al., 2006; Williams et al., 2008; Gou-Fabregas et al., 2009). The reduction of endogenous calpain in SMA mice motor neurons resulted in increased autophagy and Smn protein levels (Periyakaruppiah et al., 2016).

Coimmunoprecipitation experiments in SMA mouse motor neurons revealed Smn to interact with p62 (Rodriguez-Muela et al., 2018). Smn protein depletion resulted in increased mTOR signaling activity that was characterized by (i) a reduction in autophagic activity and (ii) a decrease in lysosomal gene expression (Rodriguez-Muela et al., 2018). This was accompanied by increased p62 levels and subsequently a further Smn reduction, which in turn led to elevated mTOR activity (Rodriguez-Muela et al., 2018). In line with this cycle, autophagy induction by starvation in human fibroblasts gave rise to decreased SMN levels, whereas blocking autophagic activity with the lysosomal inhibitors ammonium chloride and leupeptin elevated SMN levels (Rodriguez-Muela et al., 2018). Furthermore, reducing p62 levels promoted motor neuron survival *in vitro* and increased the lifespan in the SMA fly model as well as SMNdelta7 severe SMA mice (Rodriguez-Muela et al., 2018). Ultimately, SMN depletion further exacerbated the observed autophagic dysregulation in SMA and overall, these findings suggest that SMN levels can be altered by targeting autophagy-related regulators.

Tissue-specificity in SMA

It has been well established that SMA is not solely a motor neuron disease and that SMN depletion results in tissue specific aberrations and multi-organ dysfunction (Shababi et al., 2014; Sansa et al., 2021). In relation to autophagy and SMA, while the skeletal muscle of more severe SMA mice showed a decrease in autophagosome formation and an increase in autophagic flux, motor neurons displayed enhanced autophagosome formation and reduced autophagic flux (Sansa et al., 2021). Investigation into patient fibroblasts also revealed decreased LC3-II and increased p62 levels, suggesting decreased autophagosome number and autophagic flux, respectively. Additionally, it was noted that mTOR phosphorylation was reduced in patient fibroblasts and mouse skeletal muscle cells but increased in motor neurons (Sansa et al., 2021). Ultimately, these studies highlight a dysregulation of autophagy and an accumulation of autophagosomes as contributors to SMA pathogenesis. However, the effect of SMN depletion on autophagic flux remains contradictory; it is still poorly explored whether autophagy is in fact a destructive or beneficial factor underlying SMA development. Furthermore, these findings highlight the challenges that would be presented by targeting autophagy in SMA treatment given the observed differences in tissue-dependent autophagic activity.

Autophagy: a key player in SMA onset with therapeutic implications

Autophagosome accumulation: a key feature in SMA

The autophagic pathway is vital for homeostasis; cell functionality and survival are significantly reduced when autophagosome formation is compromised and autophagic bodies accumulate (Garcera et al., 2013; Custer and Androphy, 2014; Periyakaruppiah et al., 2016; Piras et al., 2017; Rodriguez-Muela et al., 2018; Sansa et al., 2021). In normal circumstances, neurons particularly rely on the autophagic pathway to maintain a healthy environment (Nixon, 2013). However, autophagy is considered a 'double-edged sword' which can both contribute to and protect from neuronal damage (Martinet et al., 2009). In neurodegenerative diseases where mutant protein aggregates are observed, it has been suggested that the autophagosome accumulation results in impaired intracellular trafficking and may also become the source of cytotoxic products (Ravikumar et al., 2004; Wong and Cuervo, 2010). While there are no recorded observations of aggregated proteins accumulating in SMA to date, autophagosome accumulation is known to perturb axonal transport which in turn results in neuronal degeneration; a hallmark of SMA pathogenesis observed *in vitro* and *in vivo* models (Rossoll et al., 2003; Burghes and Beattie, 2009; Garcera et al., 2011; Lee et al., 2011).

Autophagy modulators: novel therapeutic targets

Pharmacological inhibition of autophagy using 3-methyladenine reduced autophagosome formation, delayed motor neuron degeneration and significantly improved lifespan in severe SMA mice (Piras et al., 2017). These findings imply that while the underlying cause of axonal deficiencies observed in SMA remains unclear, induction of autophagy and subsequent accumulation of autophagosomes may be a major contributing factor; a hypothesis supported by the finding that inhibition of Beclin 1, a regulator of autophagy required for induction,

significantly delayed neuronal degeneration (Garcera et al., 2013). Moreover, autophagy induction with rapamycin resulted in decreased SMN and SMNΔ7 levels, suggesting both to be directly regulated by autophagy (Rodriguez-Muela et al., 2018). Furthermore, treatment with rapamycin demonstrated a failure in autophagosome-lysosome fusion and reduced lifespan in severe SMA mice (Custer and Androphy, 2014). While these findings demonstrate a possibility of therapy by inhibiting autophagy, the findings of Periyakaruppiah et al. (2016) put this scenario into question as autophagy induction has also been shown to increase full length SMN protein levels. Nevertheless, three studies agree that autophagic flux is reduced (Custer and Androphy, 2014; Periyakaruppiah et al., 2016; Rodriguez-Muela et al., 2018). Custer and Androphy (2014) suggested the use of new rapamycin analogues as these may be beneficial to stimulate autophagy beyond the capabilities of traditional rapamycin and in turn, overcome the altered autophagic flux levels.

ALS and SMA: autophagy markers in two histopathologically similar motor neuron diseases

As previously mentioned, autophagy has been implicated in a range of neurodegenerative disorders. A prime example is ALS, which presents with aggregation of ubiquitinated proteins (such as SOD1, FUS, and TDP-43), while sharing histopathological findings with SMA (Blokhuis et al., 2013; Comley et al., 2016). In ALS, motor neuron survival is directly affected by an impairment in the autophagic pathway. More specifically, axonal transport defects are suggested to be responsible for the autophagosome accumulation observed in ALS mice (Cozzi and Ferrari, 2022). Autophagy is known to be dysregulated in ALS at different steps of the pathway, which results in autophagosome accumulation and a defective autophagic flux (Song et al., 2012; Lee et al., 2015; Nguyen et al., 2019). The aggregation of ALS-associated SOD1 – an antioxidant enzyme highly mutated in more than 20% of familial ALS cases (Corson et al., 1998; Gruzman et al., 2007; Berdyński et al., 2022) and TDP-43–a protein involved in RNA processing regulation (Hergesheimer et al., 2019) occurs in motor neuron axons and results in autophagy dysregulation (Sasaki, 2011; Wei, 2014; Budini et al., 2017). In ALS, autophagy inhibition by 3-methyladenine does not protect from motor neuron degeneration (as seen in SMA) and was suggested to induce TDP-43 aggregation (Caccamo et al., 2009). On the other hand, autophagy induction by rapamycin reduced TDP-43 accumulation, rescued mRNA processing (a key role of the SMN protein), resulted in migration of TDP-43 to its proper nuclear compartment (Caccamo et al., 2009) and significantly improved neuronal survival in ALS models (Barmada et al., 2014). In line with the protective role of autophagy in motor neuron diseases, it has been shown that motor neuron death due to glutamate-induced toxicity could be the result of autophagic pathway impairment (Fulceri et al., 2011). Therefore, the role of autophagy in ALS is especially important in the context of SMA given the similarities of the two diseases. The use of rapamycin showed consistency in its ability to improve disease symptoms in both ALS and SMA, while 3-methyladenine highlighted contrasting views (Caccamo et al., 2009; Periyakaruppiah et al., 2016). However, it must be noted that while SMA is a monogenic disease and primarily affects lower motor neurons, the genetic cause of ALS is complex affecting both upper and lower motor neurons (Burghes and Beattie, 2009; Ragagnin et al., 2019). Therefore, while the two diseases share histopathological similarities, the differences observed in modulating autophagy may be due to the distinct mechanisms of neuromuscular disruption underlying ALS but not SMA pathogenesis (Comley et al., 2016).

Autophagy regulators: understanding the mechanisms behind autophagy dysregulation in SMA

Despite an established body of evidence that autophagosome number increases across a variety of SMA models (Garcera et al., 2013; Custer and Androphy, 2014; Periyakaruppiah et al., 2016; Piras et al., 2017; Rodriguez-Muela et al., 2018; Sansa et al., 2021), it is still debated whether autophagic flux is affected and subsequently whether autophagy itself is increased or decreased. Findings point to autophagy perturbations in SMA and an interaction between SMN and p62 has been suggested (Rodriguez-Muela et al., 2018). While it is documented that the SMN protein levels are regulated by the autophagic pathway, it may be of benefit to further understand the interactions between SMN and autophagy regulators. It was previously established that SMN depletion resulted in decreased levels of UBA1 (Lambert-Smith et al., 2020). Mutations in UBA1 are shown to induce a rare, non-SMN gene associated form of SMA with similar clinical symptoms (Ramser et al., 2008). UBA1 was able to regulate autophagy in an ATG7- and ATG3-independent manner in *Drosophila*, although the exact mechanism remains speculative (Chang et al., 2013). Thus, UBA1 decrease, which inevitably follows SMN depletion, may be contributing to impairments in the autophagic machinery. Moreover, various autophagy marker mRNAs (primarily the autophagy regulator Beclin 1, Atg5, LC3 and p62/SQSTM1) were shown to be elevated in severe SMA mouse models, suggesting dysregulated autophagy induction as a compensatory mechanism in response to disease progression (Oliván et al., 2016). Injection of tetanus toxic heavy chain (TTC) – a recombinant protein known to display neurotrophic capabilities – in SMA mice resulted in neuroprotective effects (Oliván et al., 2016). Interestingly, TTC administration also downregulated Beclin 1, Atg5, LC3 and p62 expression to wildtype levels which implied a return to constitutive autophagy function (Oliván et al., 2016) and highlighted autophagy regulators as potential therapeutic targets. Furthermore, Bcl-2 – a protein derived from the same family as the aforementioned Bcl-XL – is known to regulate autophagy by binding to Beclin 1 and inhibiting the pathway (Marquez and Xu, 2012). This is noteworthy as SMN has been shown to directly interact with Bcl-2 (Iwahashi et al., 1997), further demonstrating the importance of examining the functional interactions of SMN with key autophagy players.

Recent findings suggest an important role for microRNAs (miRNAs) - small RNAs tasked with regulating post-transcriptional gene expression in the pathogenesis of several motor neuron diseases including SMA (Magri et al., 2018). A handful of miRNAs implicated in SMA have also been shown to have a regulatory effect in the autophagic pathway. For example, miRNA-206, a

miRNA involved in skeletal muscle that drives development and regenerative pathways at the neuromuscular junction, was upregulated in SMA and potentially delayed motor neuron degeneration, albeit not enough to rescue motor neuron integrity (Valsecchi et al., 2015, 2020). miRNA-206 overexpression in severe SMA mice resulted in improved motor neuron function and lifespan in mammalian models (Valsecchi et al., 2015, 2020). These findings prove to be highly relevant as evidence has suggested that miRNA-206 overexpression also resulted in increased autophagy in head and neck squamous cell carcinoma cells (Li et al., 2020). Similarly, it was found that miRNA-9, which promotes neuronal function/differentiation by activating autophagy was decreased upon SMN depletion (Yuva-Aydemir et al., 2011; Zhang et al., 2015; Magri et al., 2018). Furthermore, miRNA-183, which constitutes a role in axon outgrown (Wang et al., 2017), was found to be overexpression in more severe SMA mice (Kye et al., 2014). Intriguingly, miRNA-183 was established as an inhibitor of the autophagic pathway (Huangfu et al., 2016; Yuan et al., 2018). Kye et al. (2014) suggested that reduced SMN protein levels alter miRNA expression and distribution in neurons, whereas inhibition of miRNA-183 rescued Smn-knockdown axonal phenotypes in rat-derived neurons. Moreover, overexpression of miRNA-23a, a regulator of oligodendrocyte differentiation, increased the lifespan of severe SMA mice and inhibited autophagy (Lin et al., 2013; Si et al., 2018; Kaifer et al., 2019). Similarly, it was found that increased miRNA-146, a regulator of the inflammatory response, induced autophagy, while upregulation of this miRNA was observed in SMA mice (Cheng et al., 2013; Sison et al., 2017; Roy, 2021). Lastly, more severe SMA mice showed a marked reduction of miRNA-132 - which was known to promote dendritic growth and synaptic function - in the spinal cord (Catapano et al., 2016). In contrast, miRNA-132 levels were increased in more severe SMA mice skeletal muscles (Catapano et al., 2016). Interestingly, miRNA-132 overexpression was able to inhibit autophagy and its knockdown resulted in increased LC3 and reduced p62, indicative of autophagy induction (Ucar et al., 2012). Together, these findings clearly highlight the effect of SMN depletion on autophagy regulators. The aforementioned studies reveal the extent to which abnormal miRNA expression is related to disease. Future studies could employ the use of miRNA mimics and inhibitors which are capable of enhancing or rescuing the downregulation of targets, respectively. Additionally, these miRNA mimics and inhibitors should be observed for their effects on the autophagic pathway in the context of SMA. Interestingly. miRNA-155 inhibition which is known to alleviate autophagic flux defects in a pancreatitis mouse model (Wan et al., 2019) was also able to prolong survival in *SOD1* mutant mice (Koval et al., 2013; Seto et al., 2018; Gallant-Behm et al., 2019), highlighting that miRNAs could also serve as potential therapeutic targets for SMA.

Mitophagy

A hallmark of neurodegenerative disorders including SMA is the observed structural and functional mitochondrial defects prior to symptom development (Miller et al., 2016); thus, mitophagy – mitochondrial degradation via the macroautophagy pathway - should also be considered. Deguise et al. (2016) observed autophagic vacuoles (autophagosomes and autolysosomes) containing mitochondria in severe SMA mice, suggesting mitophagy to be activated. Importantly, muscle tissue in severe SMA mice revealed an accumulation of dysfunctional mitochondria with reduced clearance as well as a downregulation of mitochondria and lysosomal expressed genes (Chemello et al., 2023). The same study highlighted that apart from reduced mitochondrial clearance, proteins that mark mitochondria for mitophagy (i.e., PINK and Parkin) as well as p62 were also elevated indicating a decline in autophagic flux. Furthermore, Chemello et al. (2023) noted a downregulation of genes involved in lysosomal biogenesis, which may underlie a defect in autophagosome-lysosome fusion. Additionally, type I, II and III SMA patient muscle tissue analysis revealed reduced mitochondrial DNA content (Berger et al., 2003; Ripolone et al., 2015), confirming mitochondrial defects in human samples.

Mitochondria play a key role in the activation of apoptosis (Xiong et al., 2014) and it has been shown that accumulation of autophagosomes resulted in the activation of the apoptotic pathway and subsequently, cell death (Mariño et al., 2014). Piras et al. (2017) hypothesized that the increase in autophagosomes and autolysosomes may be responsible for the degeneration of lower motor neurons in SMNdelta7 severe mice as the increase in autophagosomes is likely to result in increased apoptotic cell death. Moreover, an increase in apoptotic nuclei and reduced levels of antiapoptotic proteins have been observed in more severe SMA mice and patient's motor neurons, while inhibition of apoptosis has been shown to block motor neuron cell death in SMA stem cell models (Sareen et al., 2012; Sansa et al., 2021). The observed mitochondrial damage is correlated with the severity of the disease; more severe SMA mice present with lower numbers of active mitochondria (Torres-Benito et al., 2011), suggesting that autophagy may in part influence disease phenotype. Therefore, it is possible that the presence of defective mitochondria results in autophagy activation which presents with reduced flux due to the downregulation of lysosomal genes. Thus, autophagosomes accumulate and subsequently signal the apoptotic pathway, resulting in motor neuron death. Ultimately, this may suggest that impaired autophagic flux – and not increased autophagy - could be the causative agent underlying autophagy-related development of symptoms in SMA (**Figure 4**).

The information presented herein highlights the autophagy networks perturbed in SMA and identifies these as a gateway to explore potential therapeutic interventions. While the potential of autophagy modulation holds significant promise, it is necessary to navigate through the appropriate considerations to overcome the boundaries of clinical applicability.

Autophagy as a therapeutic target for SMA: considerations and limitations

It is paramount for SMA researchers to initially consider the stage of autophagy that is mainly affected in SMA. Given the contradictory findings regarding (a) autophagic flux and (b) the lack of verdict on whether autophagy is in fact upregulated in SMA, future research should be aimed at elucidating these discrepancies.

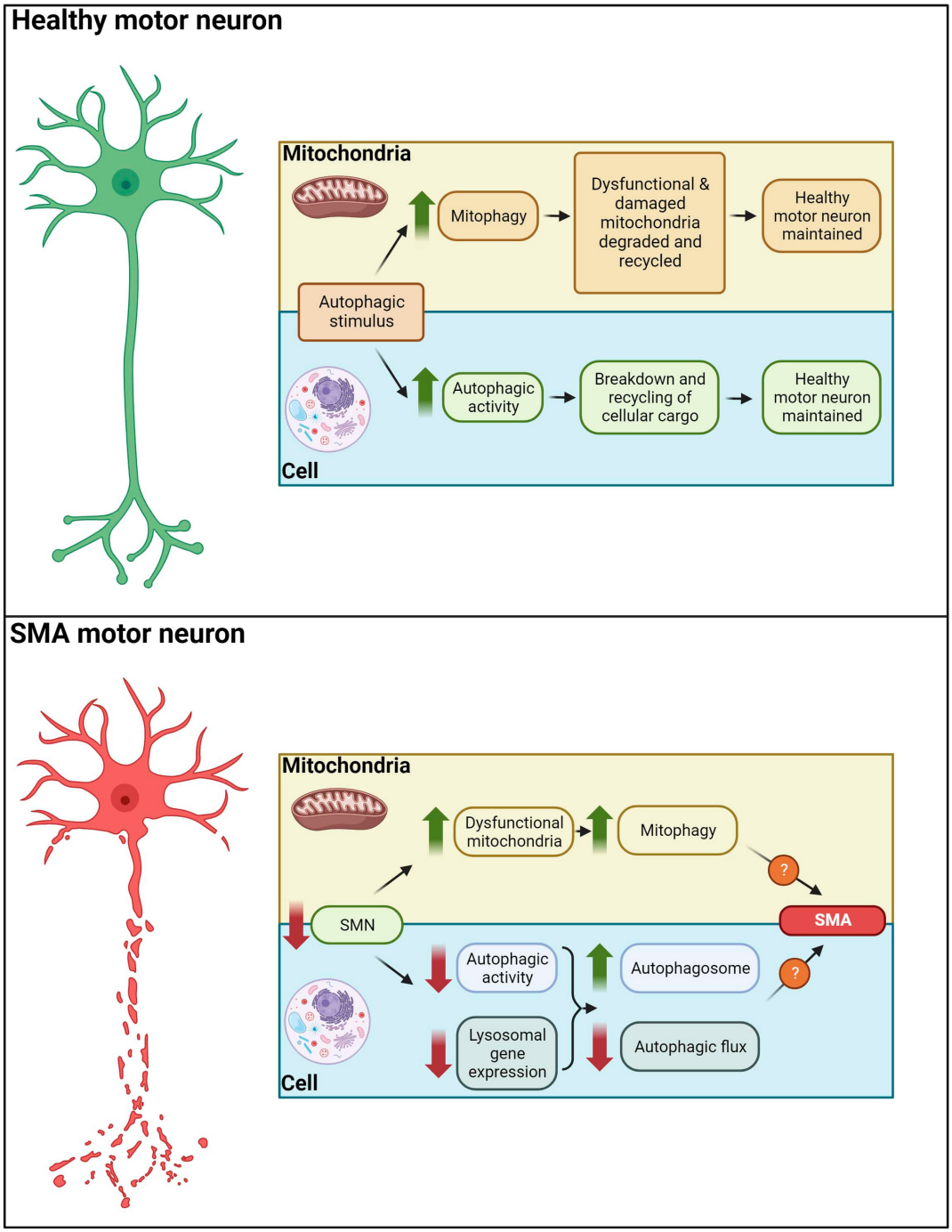

FIGURE 4
Autophagy in healthy and SMA motor neurons. In healthy motor neurons autophagic stimuli would lead to an increased mitophagy/autophagic activity, degradation and recycling of cellular cargo. In SMA motor neurons, decreased SMN levels result in dysfunctional mitochondria, reduced autophagic activity and downregulation of lysosomal gene expression. These aberrations drive autophagosome accumulation and diminished autophagic flux, potentially leading to apoptotic and non-apoptotic cell death in motor neurons of SMA patients.

It would be beneficial to study fluorescent probes (i.e., mRFP-EGFP-LC3B) that are degraded by the autolysosome and show specificity for autophagic flux (Chapin et al., 2015). Moreover, the tissue-specificity of autophagic dysregulation in SMA could present a barrier in translating research evidence into clinical practice for SMA patients. Particularly, SMA patient-derived motor neurons displayed a reduced flux while skeletal muscle from SMA mice showed the opposite phenotype, and as such, the development of autophagy-targeted therapy for SMA must account for the varying levels of autophagic activity in different tissues (Sansa et al., 2021). This is equally as relevant when considering the different models used in these studies. For example, severe SMA mice indicated no change in flux according to Piras et al. (2017), although Rodriguez-Muela et al. (2018) documented reduced flux

in the same model. On the other hand, more severe SMA mice and type I-III patient fibroblasts exhibited an impaired one (Sansa et al., 2021). Together, this suggests that further analysis is needed to elucidate the autophagic flux defects in severe SMA mice.

It would be of benefit to identify whether the observed therapeutic effects in the context of SMA are a result of autophagic inhibition or a rescue of flux defects in order to consider the stage of autophagy the intended therapy should be acting on. This is of particular importance when considering the literature findings of using the autophagic inhibitor 3-methyladenine (Piras et al., 2017), which we previously mentioned can play a dual role in modulating autophagy (Wu et al., 2010).

Besides, many of the known autophagic activators like rapamycin are known to act through mTOR inhibition; mTOR is also involved in autophagy independent pathways, such as lipid and nucleotide synthesis, protein synthesis, cell growth and immunosuppression (Saxton and Sabatini, 2017). For example, SMA patients present with a higher susceptibility to infection (Deguise and Kothary, 2017) and given the immunosuppression which follows prolonged mTOR inhibition, it may be more advantageous to consider compounds capable of activating autophagy independent of mTOR inhibition. Alternatively, clinicians would be required to regularly monitor liver and renal functions as well as cholesterol and triglycerides, a commonplace practice for patients taking rapamycin for the treatment of other diseases (Kahan et al., 2000).

When identifying potential new agents for treating SMA, one important consideration is that they should be capable of penetrating the blood-brain barrier. Furthermore, sex dependent limitations of treatments for SMA patients must be considered. This is specifically relevant in SMA where the protective capabilities of genetic modifiers such as PLS3 are known to be sex specific (Yanyan et al., 2014). For example, rapamycin-mediated increase in lifespan has been shown to be higher in female than in male mice across various doses (Miller et al., 2014). Therefore, future research should aim at highlighting any potential sex-specific differences following administration of autophagy modulators.

Finally, the identification of any autophagy-targeted treatment(s) should be considered complimentary to the current therapeutic strategies for SMA and administered at the earliest possible stage of the disease. As such, any potential treatments should be studied in combination with current SMA therapies to identify possible interactions.

Conclusions

We have summarized the growing body of evidence which underlies the dysregulation of autophagy in SMA, characterized mainly by an increase in autophagosome number. We speculate that it is the late, degradative stage of autophagy which seems impaired in SMA due to a failure in the lysosome-autophagosome docking and fusion step. It is important to consider the stage at which autophagy becomes dysfunctional in SMA patients before autophagy-targeted treatments can be considered. Subsequently, addressing the outlined limitations of autophagy-targeted treatments would be pivotal in designing specific and accurate treatments for SMA patients. Future research directions should aim to identify (a) the effect of SMN depletion on autophagic flux and (b) the relationship between SMN and the most important autophagy regulators known to be impacted in SMA. We advocate for a redirected research focus in order to unravel the discrepancies regarding autophagic flux which may in turn identify novel modifiers of the disease and lead to more effective therapeutic strategies in SMA.

Author contributions

SR: Writing—original draft, Writing—review and editing. MD: Writing—review and editing.

Funding

The author(s) declare that no financial support was received for the research, authorship, and/or publication of this article.

Acknowledgments

Figures created with BioRender.com.

Conflict of interest

The authors declare that the research was conducted in the absence of any commercial or financial relationships that could be construed as a potential conflict of interest.

Publisher's note

References

Acsadi, G., Lee, I., Li, X., Khaidakov, M., Pecinova, A., Parker, G., et al. (2009). Mitochondrial dysfunction in a neural cell model of spinal muscular atrophy. *J. Neurosci. Res.* 87, 2748–2756. doi: 10.1002/jnr.22106

Axe, E., Walker, S., Manifava, M., Chandra, P., Roderick, H., Habermann, A., et al. (2008). Autophagosome formation from membrane compartments enriched in phosphatidylinositol 3-phosphate and dynamically connected to

the endoplasmic reticulum. *J. Cell Biol.* 182, 685–701. doi: 10.1083/jcb.200803137

Bandyopadhyay, U., and Cuervo, A. (2007). Chaperone-mediated autophagy in aging and neurodegeneration: lessons from alpha-synuclein. *Exp. Gerontol.* 42, 120–128. doi: 10.1016/j.exger.2006.05.019

Barmada, S., Serio, A., Arjun, A., Bilican, B., Daub, A., Ando, D., et al. (2014). Autophagy induction enhances TDP43 turnover and survival in neuronal ALS models. *Nat. Chem. Biol.* 10, 677–685. doi: 10.1038/nchembio.1563

Barrett, D., Bilic, S., Chyung, Y., Cote, S., Iarrobino, R., Kacena, K., et al. (2021). A randomized phase 1 safety, pharmacokinetic and pharmacodynamic study of the novel myostatin inhibitor apitegromab (SRK-015): a potential treatment for spinal muscular atrophy. *Adv. Ther.* 38, 3203–3222. doi: 10.1007/s12325-021-01757-z

Béchade, C., Rostaing, P., Cisterni, C., Kalisch, R., La Bella, V., Pettmann, B., et al. (1999). Subcellular distribution of survival motor neuron (SMN) protein: possible involvement in nucleocytoplasmic and dendritic transport. *Eur. J. Neurosci.* 11, 293–304. doi: 10.1046/j.1460-9568.1999.00428.x

Berdyński, M., Miszta, P., Safranow, K., Andersen, P., Morita, M., Filipek, S., et al. (2022). SOD1 mutations associated with amyotrophic lateral sclerosis analysis of variant severity. *Sci. Rep.* 12:103. doi: 10.1038/s41598-021-03891-8

Berger, A., Mayr, J., Meierhofer, D., Fötschl, U., Bittner, R., Budka, H., et al. (2003). Severe depletion of mitochondrial DNA in spinal muscular atrophy. *Acta Neuropathol.* 105, 245–251. doi: 10.1007/s00401-002-0638-1

Berger, Z., Ravikumar, B., Menzies, F., Oroz, L., Underwood, B., Pangalos, M., et al. (2006). Rapamycin alleviates toxicity of different aggregate-prone proteins. *Hum. Mol. Genet.* 15, 433–442. doi: 10.1093/hmg/ddi458

Blokhuis, A., Groen, E., Koppers, M., van den Berg, L., and Pasterkamp, R. (2013). Protein aggregation in amyotrophic lateral sclerosis. *Acta Neuropathol.* 125, 777–794. doi: 10.1007/s00401-013-1125-6

Bowerman, M., Beauvais, A., Anderson, C., and Kothary, R. (2010). Rho-kinase inactivation prolongs survival of an intermediate SMA mouse model. *Hum. Mol. Genet.* 19, 1468–1478. doi: 10.1093/hmg/ddq021

Bowerman, M., Murray, L., Boyer, J., Anderson, C., and Kothary, R. (2012). Fasudil improves survival and promotes skeletal muscle development in a mouse model of spinal muscular atrophy. *BMC Med.* 10:24. doi: 10.1186/1741-7015-10-24

Budini, M., Buratti, E., Morselli, E., and Criollo, A. (2017). Autophagy and its impact on neurodegenerative diseases: new roles for TDP-43 and C9orf72. *Front. Mol. Neurosci.* 10:170. doi: 10.3389/fnmol.2017.00170

Burghes, A., and Beattie, C. (2009). Spinal muscular atrophy: why do low levels of survival motor neuron protein make motor neurons sick? *Nat. Rev. Neurosci.* 10, 597–609. doi: 10.1038/nrn2670

Burman, C., and Ktistakis, N. (2010). Autophagosome formation in mammalian cells. *Semin. Immunopathol.* 32, 397–413. doi: 10.1007/s00281-010-0222-z

Caccamo, A., Majumder, S., Deng, J., Bai, Y., Thornton, F., and Oddo, S. (2009). Rapamycin rescues TDP-43 mislocalization and the associated low molecular mass neurofilament instability. *J. Biol Chem.* 284, 27416–27424. doi: 10.1074/jbc.M109.031278

Cartegni, L., and Krainer, A. (2002). Disruption of an SF2/ASF-dependent exonic splicing enhancer in SMN2 causes spinal muscular atrophy in the absence of SMN1. *Nat. Genet.* 30, 377–384. doi: 10.1038/ng854

Cashman, N., Durham, H., Blusztajn, J., Oda, K., Tabira, T., Shaw, I., et al. (1992). Neuroblastoma x spinal cord (NSC) hybrid cell lines resemble developing motor neurons. *Dev. Dyn.* 194, 209–221. doi: 10.1002/aja.1001940306

Catapano, F., Zaharieva, I., Scoto, M., Marrosu, E., Morgan, J., Muntoni, F., et al. (2016). Altered levels of MicroRNA-9, -206, and -132 in spinal muscular atrophy and their response to antisense oligonucleotide therapy. *Mol. Ther. Nucleic Acids* 5, e331. doi: 10.1038/mtna.2016.47

Chand, D., Mohr, F., McMillan, H., Tukov, F., Montgomery, K., Kleyn, A., et al. (2021). Hepatotoxicity following administration of onasemnogene abeparvovec (AVXS-101) for the treatment of spinal muscular atrophy. *J. Hepatol.* 74, 560–566. doi: 10.1016/j.jhep.2020.11.001

Chang, T., Shravage, B., Hayes, S., Powers, C., Simin, R., Wade Harper, J., et al. (2013). Uba1 functions in Atg7- and Atg3-independent autophagy. *Nat. Cell Biol.* 15, 1067–1078. doi: 10.1038/ncb2804

Chapin, H. C., Okada, M., Merz, A., and Miller, D. (2015). Quantifying autophagy's magnitude in normal. *Aging* 7, 419–434. doi: 10.18632/aging.100765

Chemello, F., Pozzobon, M., Tsansizi, L., Varanita, T., Quintana-Cabrera, R., Bonesso, D., et al. (2023). Dysfunctional mitochondria accumulate in a skeletal muscle knockout model of Smn1, the causal gene of spinal muscular atrophy. *Cell Death Dis.* 14:162. doi: 10.1038/s41419-023-05573-x

Cheng, H., Sivachandran, N., Lau, A., Boudreau, E., Zhao, J., Baltimore, D., et al. (2013). MicroRNA-146 represses endothelial activation by inhibiting pro-inflammatory pathways. *EMBO Mol. Med.* 5, 1017–1034. doi: 10.1002/emmm.201202318

Comley, L., Nijssen, J., Frost-Nylen, J., and Hedlund, E. (2016). Cross-disease comparison of amyotrophic lateral sclerosis and spinal muscular atrophy reveals conservation of selective vulnerability but differential neuromuscular junction pathology. *J. Comp. Neurol.* 524, 1424–1442. doi: 10.1002/cne.23917

Coratti, G., Cutrona, C., Pera, M., Bovis, F., Ponzano, M., Chieppa, F., et al. (2021). Motor function in type 2 and 3 SMA patients treated with Nusinersen: a critical review and meta-analysis. *Orphanet. J. Rare Dis.* 16:430. doi: 10.1186/s13023-021-02065-z

Corson, L., Strain, J., Culotta, V., and Cleveland, D. (1998). Chaperone-facilitated copper binding is a property common to several classes of familial amyotrophic lateral sclerosis-linked superoxide dismutase mutants. *Proc. Natl. Acad. Sci. U. S. A.* 95, 6361–6366. doi: 10.1073/pnas.95.11.6361

Cowan, C., Fan, M., Fan, J., Shehadeh, J., Zhang, L., Graham, R., et al. (2008). Polyglutamine-modulated striatal calpain activity in YAC transgenic huntington disease mouse model: impact on NMDA receptor function and toxicity. *J. Neurosci.* 28, 12725–12735. doi: 10.1523/JNEUROSCI.4619-08.2008

Cozzi, M., and Ferrari, V. (2022). Autophagy dysfunction in ALS: From transport to protein degradation. *J. Mol. Neurosci.* 72, 1456–1481. doi: 10.1007/s12031-022-02029-3

Crawford, T., and Pardo, C. (1996). The neurobiology of childhood spinal muscular atrophy. *Neurobiol. Dis.* 3, 97–110. doi: 10.1006/nbdi.1996.0010

Custer, S., and Androphy, E. (2014). Autophagy dysregulation in cell culture and animals models of spinal muscular atrophy. *Mol. Cell Neurosci.* 61, 133–140. doi: 10.1016/j.mcn.2014.06.006

Das, G., Shravage, B., and Baehrecke, E. (2012). Regulation and function of autophagy during cell survival and cell death. *Cold Spring Harb. Perspect. Biol.* 4, a008813. doi: 10.1101/cshperspect.a008813

Day, J., Howell, K., Place, A., Long, K., Rossello, J., Kertesz, N., et al. (2022). Advances and limitations for the treatment of spinal muscular atrophy. *BMC Pediatr.* 22:632. doi: 10.1186/s12887-022-03671-x

de la Fuente, S., Sansa, A., Periyakaruppiah, A., Garcera, A., and Soler, R. (2019). Calpain inhibition increases SMN protein in spinal cord motoneurons and ameliorates the spinal muscular atrophy phenotype in mice. *Mol. Neurobiol.* 56, 4414–4427. doi: 10.1007/s12035-018-1379-z

Deguise, M., Boyer, J., McFall, E., Yazdani, A., De Repentigny, Y., and Kothary, R. (2016). Differential induction of muscle atrophy pathways in two mouse models of spinal muscular atrophy. *Sci. Rep.* 6:28846. doi: 10.1038/srep28846

Deguise, M., and Kothary, R. (2017). New insights into SMA pathogenesis: immune dysfunction and neuroinflammation. *Ann. Clin. Transl. Neurol.* 4, 522–530. doi: 10.1002/acn3.423

Dimitriadi, M., Sleigh, J. N., Walker, A., Chang, H. C., Sen, A., Kalloo, G., et al. (2010). Conserved genes act as modifiers of invertebrate SMN loss of function defects. *PLoS Genetics* 6:e1001172. doi: 10.1371/journal.pgen.1001172

Dominguez, E., Marais, T., Chatauret, N., Benkhelifa-Ziyyat, S., Duque, S., Ravassard, P., et al. (2010). Intravenous SCAAV9 delivery of a codon-optimized SMN1 sequence rescues SMA mice. *Hum. Mol. Genet.* 20, 681–693. doi: 10.1093/hmg/ddq514

Edens, B., Ajroud-Driss, S., Ma, L., and Ma, Y. (2015). Molecular mechanisms and animal models of spinal muscular atrophy. *Biochim. Biophys. Acta* 1852, 685–692. doi: 10.1016/j.bbadis.2014.07.024

Fallini, C., Bassell, G., and Rossoll, W. (2012). Spinal muscular atrophy: the role of SMN in axonal mRNA regulation. *Brain Res.* 1462, 81–92. doi: 10.1016/j.brainres.2012.01.044

Farrar, M., and Kiernan, M. (2015). The genetics of spinal muscular atrophy: progress and challenges. *Neurotherapeutics* 12, 290–302. doi: 10.1007/s13311-014-0314-x

Feng, Z., Ling, K., Zhao, X., Zhou, C., Karp, G., Welch, E., et al. (2016). Pharmacologically induced mouse model of adult spinal muscular atrophy to evaluate effectiveness of therapeutics after disease onset. *Hum. Mol. Genet.* 25, 964–975. doi: 10.1093/hmg/ddv629

Finkel, R., McDermott, M., Kaufmann, P., Darras, B., Chung, W., Sproule, D., et al. (2014). Observational study of spinal muscular atrophy type I and implications for clinical trials. *Neurology* 83, 810–817. doi: 10.1212/WNL.0000000000000741

Finkel, R., Mercuri, E., Darras, B., Connolly, A., Kuntz, N., Kirschner, J., et al. (2017). Nusinersen versus sham control in infantile-onset spinal muscular atrophy. *N. Engl. J. Med.* 377, 1723–1732. doi: 10.1056/NEJMoa1702752

Fischer, U., Liu, Q., and Dreyfuss, G. (1997). The SMN-SIP1 complex has an essential role in spliceosomal snRNP biogenesis. *Cell* 90, 1023–1029. doi: 10.1016/s0092-8674(00)80368-2

Franck, A., Lainé, J., Moulay, G., Lemerle, E., Trichet, M., Gentil, C., et al. (2019). Clathrin plaques and associated actin anchor intermediate filaments in skeletal muscle. *Mol. Biol. Cell* 30, 579–590. doi: 10.1091/mbc.E18-11-0718

Fuentes, J., Strayer, M., and Matera, A. (2010). Molecular determinants of survival motor neuron (SMN) protein cleavage by the calcium-activated protease, calpain. *PLoS One* 5:e15769. doi: 10.1371/journal.pone.0015769

Fujita, N., Itoh, T., Omori, H., Fukuda, M., Noda, T., and Yoshimori, T. (2008). The Atg16L complex specifies the site of LC3 lipidation for membrane biogenesis in autophagy. *Mol. Biol. Cell* 19, 2092–2100. doi: 10.1091/mbc.e07-12-1257

Fulceri, F., Ferrucci, M., Lazzeri, G., Paparelli, S., Bartalucci, A., Tamburini, I., et al. (2011). Autophagy activation in glutamate-induced motor neuron loss. *Arch. Ital. Biol.* 149, 101–111. doi: 10.4449/aib.v149i1.1259

Gallant-Behm, C., Piper, J., Lynch, J., Seto, A., Hong, S., Mustoe, T., et al. (2019). A MicroRNA-29 Mimic (Remlarsen) Represses Extracellular Matrix Expression and Fibroplasia in the Skin. *J. Invest. Dermatol.* 139, 1073–1081. doi: 10.1016/j.jid.2018.11.007

Garcera, A., Bahi, N., Periyakaruppiah, A., Arumugam, S., and Soler, R. (2013). Survival motor neuron protein reduction deregulates autophagy in spinal cord motoneurons in vitro. *Cell Death Dis.* 4, e686.

Garcera, A., Mincheva, S., Gou-Fabregas, M., Caraballo-Miralles, V., Lladó, J., Comella, J., et al. (2011). A new model to study spinal muscular atrophy: neurite degeneration and cell death is counteracted by BCL-X(L) Overexpression in motoneurons. *Neurobiol. Dis.* 42, 415–426. doi: 10.1016/j.nbd.2011.02.003

Giesemann, T., Rathke-Hartlieb, S., Rothkegel, M., Bartsch, J., Buchmeier, S., Jockusch, B., et al. (1999). A role for polyproline motifs in the spinal muscular atrophy protein SMN. Profilins bind to and colocalize with smn in nuclear gems. *J. Biol. Chem.* 274, 37908–37914. doi: 10.1074/jbc.274.53.37908

Gou-Fabregas, M., Garcera, A., Mincheva, S., Perez-Garcia, M., Comella, J., and Soler, R. (2009). Specific vulnerability of mouse spinal cord motoneurons to membrane depolarization. *J. Neurochem.* 110, 1842–1854. doi: 10.1111/j.1471-4159.2009.06278.x

Grice, S., and Liu, J. (2011). Survival motor neuron protein regulates stem cell division, proliferation, and differentiation in Drosophila. *PLoS Genet.* 7:e1002030. doi: 10.1371/journal.pgen.1002030

Gruzman, A., Wood, W., Alpert, E., Prasad, M., Miller, R., Rothstein, J., et al. (2007). Common molecular signature in SOD1 for both sporadic and familial amyotrophic lateral sclerosis. *Proc. Natl. Acad. Sci. U. S. A.* 104, 12524–12529. doi: 10.1073/pnas.0705044104

Hergesheimer, R., Chami, A., de Assis, D., Vourc'h, P., Andres, C., Corcia, P., et al. (2019). The debated toxic role of aggregated TDP-43 in amyotrophic lateral sclerosis: a resolution in sight? *Brain* 142, 1176–1194. doi: 10.1093/brain/awz078

Hetz, C., Thielen, P., Matus, S., Nassif, M., Court, F., Kiffin, R., et al. (2009). XBP-1 deficiency in the nervous system protects against amyotrophic lateral sclerosis by increasing autophagy. *Genes Dev.* 23, 2294–2306. doi: 10.1101/gad.1830709

Hosseinibarkooie, S., Schneider, S., and Wirth, B. (2017). Advances in understanding the role of disease-associated proteins in spinal muscular atrophy. *Expert. Rev. Proteomics* 14, 581–592. doi: 10.1080/14789450.2017.1345631

Hsieh-Li, H., Chang, J., Jong, Y., Wu, M., Wang, N., Tsai, C., et al. (2000). A mouse model for spinal muscular atrophy. *Nat. Genet.* 24, 66–70. doi: 10.1038/71709

Hua, Y., Sahashi, K., Hung, G., Rigo, F., Passini, M., Bennett, C., et al. (2010). Antisense correction of SMN2 splicing in the CNS rescues necrosis in a type III SMA mouse model. *Genes Dev.* 24, 1634–1644. doi: 10.1101/gad.1941310

Huangfu, L., Liang, H., Wang, G., Su, X., Li, L., Du, Z., et al. (2016). miR-183 regulates autophagy and apoptosis in colorectal cancer through targeting of UVRAG. *Oncotarget* 7, 4735–4745. doi: 10.18632/oncotarget.6732

Itakura, E., Kishi, C., Inoue, K., and Mizushima, N. (2008). Beclin 1 forms two distinct phosphatidylinositol 3-kinase complexes with mammalian Atg14 and UVRAG. *Mol. Biol. Cell* 19, 5360–5372. doi: 10.1091/mbc.e08-01-0080

Iwahashi, H., Eguchi, Y., Yasuhara, N., Hanafusa, T., Matsuzawa, Y., and Tsujimoto, Y. (1997). Synergistic anti-apoptotic activity between Bcl-2 and SMN implicated in spinal muscular atrophy. *Nature* 390, 413–417. doi: 10.1038/37144

Jung, C., Jun, C., Ro, S., Kim, Y., Otto, N., Cao, J., et al. (2009). ULK-Atg13-FIP200 complexes mediate mTOR signaling to the autophagy machinery. *Mol. Biol. Cell* 20, 1992–2003. doi: 10.1091/mbc.e08-12-1249

Kahan, B., Napoli, K., Kelly, P., Podbielski, J., Hussein, I., Urbauer, D., et al. (2000). Therapeutic drug monitoring of sirolimus: correlations with efficacy and toxicity. *Clin. Transplant.* 14, 97–109. doi: 10.1034/j.1399-0012.2000.140201.x

Kaifer, K., Villalón, E., O'Brien, B., Sison, S., Smith, C., Simon, M., et al. (2019). AAV9-mediated delivery of miR-23a reduces disease severity in Smn2B/-SMA model mice. *Hum. Mol. Genet.* 28, 3199–3210. doi: 10.1093/hmg/ddz142

Kaiser, M., Maletzki, I., Hülsmann, S., Holtmann, B., Schulz-Schaeffer, W., Kirchhoff, F., et al. (2006). Progressive loss of a glial potassium channel (KCNJ10) in the spinal cord of the SOD1 (G93A) transgenic mouse model of amyotrophic lateral sclerosis. *J. Neurochem.* 99, 900–912. doi: 10.1111/j.1471-4159.2006.04131.x

Kashima, T., and Manley, J. L. (2003). A negative element in SMN2 exon 7 inhibits splicing in spinal muscular atrophy. *Nat. Genet.* 34, 460–463. doi: 10.1038/ng1207

Kataura, T., Sedlackova, L., Otten, E., Kumari, R., Shapira, D., Scialo, F., et al. (2022). Autophagy promotes cell survival by maintaining NAD levels. *Dev. Cell* 57, 2584–2598.

Kaushik, S., and Cuervo, A. (2018). The coming of age of chaperone-mediated autophagy. *Nat. Rev Mol. Cell Biol.* 19, 365–381. doi: 10.1038/s41580-018-0001-6

Kim, J., Jha, N., Awano, T., Caine, C., Gollapalli, K., Welby, E., et al. (2023). A spinal muscular atrophy modifier implicates the SMN protein in SNARE complex assembly at neuromuscular synapses. *Neuron* 111, 1423–1439. doi: 10.1016/j.neuron.2023.02.004

Kirisako, T., Ichimura, Y., Okada, H., Kabeya, Y., Mizushima, N., Yoshimori, T., et al. (2000). The reversible modification regulates the membrane-binding state of Apg8/Aut7 essential for autophagy and the cytoplasm to vacuole targeting pathway. *J. Cell Biol.* 151, 263–276. doi: 10.1083/jcb.151.2.263

Klionsky, D. J., Abdel-Aziz, A. M., Abdelfatah, S., Abdellatif, M., Abdoli, A., Abel, S., et al. (2012). Guidelines for the use and interpretation of assays for monitoring autophagy. *Autophagy* 8, 445–544.

Kolb, S. J., and Kissel, J. T. (2015). Spinal muscular atrophy. *Neurol. Clin.* 33, 831–846. doi: 10.1016/j.ncl.2015.07.004

Koval, E. D., Shaner, C., Zhang, P., du Maine, X., Fischer, K., Tay, J., et al. (2013). Method for widespread microRNA-155 inhibition prolongs survival in ALS-model mice. *Hum. Mol. Genet.* 22, 4127–4135. doi: 10.1093/hmg/ddt261

Kumar, A. V., Mills, J., and Lapierre, L. R. (2022). Selective Autophagy Receptor p62/SQSTM1, a Pivotal Player in Stress and Aging. *Front. Cell Dev. Biol.* 10:793328. doi: 10.3389/fcell.2022.793328

Kye, M., Niederst, E., Wertz, M., Gonçalves Ido, C., Akten, B., Dover, K., et al. (2014). SMN regulates axonal local translation via miR-183/mTOR pathway. *Hum. Mol. Genet.* 23, 6318–6331. doi: 10.1093/hmg/ddu350

Lambert-Smith, I., Saunders, D., and Yerbury, J. (2020). The pivotal role of ubiquitin-activating enzyme E1 (UBA1) in neuronal health and neurodegeneration. *Int. J. Biochem. Cell Biol.* 123:105746. doi: 10.1016/j.biocel.2020.105746

Lauria, F., Bernabò, P., Tebaldi, T., Groen, E., Perenthaler, E., Maniscalco, F., et al. (2020). SMN-primed ribosomes modulate the translation of transcripts related to spinal muscular atrophy. *Nat. Cell Biol.* 22, 1239–1251. doi: 10.1038/s41556-020-00577-7

Lee, J., Shin, J., Lee, J., and Choi, E. (2015). Role of autophagy in the pathogenesis of amyotrophic lateral sclerosis. *Biochim. Biophys. Acta* 1852, 2517–2524. doi: 10.1016/j.bbadis.2015.08.005

Lee, S., Sato, Y., and Nixon, R. (2011). Lysosomal proteolysis inhibition selectively disrupts axonal transport of degradative organelles and causes an Alzheimer's-like axonal dystrophy. *J. Neurosci.* 31, 7817–7830. doi: 10.1523/JNEUROSCI.6412-10.2011

Levine, B., and Kroemer, G. (2008). Autophagy in the pathogenesis of disease. *Cell* 132, 27–42. doi: 10.1016/j.cell.2007.12.018

Li, T., Feng, Z., Wang, Y., Zhang, H., Li, Q., Qin, Y., et al. (2020). antioncogenic effect of microRNA-206 on neck squamous cell carcinoma through inhibition of proliferation and promotion of apoptosis and autophagy. *Hum. Gene Ther.* 31, 1260–1273. doi: 10.1089/hum.2020.090

Li, W., Li, J., and Bao, J. (2012). Microautophagy: lesser-known self-eating. *Cell Mol. Life Sci.* 69, 1125–1136. doi: 10.1007/s00018-011-0865-5

Lin, S., Huang, Y., Zhang, L., Heng, M., Ptácek, L., and Fu, Y. (2013). MicroRNA-23a promotes myelination in the central nervous system. *Proc. Natl. Acad. Sci. U. S. A.* 110, 17468–17473. doi: 10.1073/pnas.1317182110

Lörincz, P., and Juhász, G. (2020). Autophagosome-Lysosome Fusion. *J. Mol. Biol.* 432, 2462–2482. doi: 10.1016/j.jmb.2019.10.028

Lorson, C., Hahnen, E., Androphy, E., and Wirth, B. (1999). A single nucleotide in the SMN gene regulates splicing and is responsible for spinal muscular atrophy. *Proc. Natl. Acad. Sci. U. S. A.* 96, 6307–6311. doi: 10.1073/pnas.96.11.6307

Łusakowska, A., Wójcik, A., Frączek, A., Aragon-Gawińska, K., Potulska-Chromik, A., Baranowski, P., et al. (2023). Long-term nusinersen treatment across a wide spectrum of spinal muscular atrophy severity: a real-world experience. *Orphanet. J. Rare Dis.* 18:230. doi: 10.1186/s13023-023-02769-4

MacLeod, M., Taylor, J., Lunt, P., Mathew, C., and Robb, S. (1999). Prenatal onset spinal muscular atrophy. *Eur. J. Paediatr. Neurol.* 3, 65–72. doi: 10.1053/ejpn.1999.0184

Magri, F., Vanoli, F., and Corti, S. (2018). miRNA in spinal muscular atrophy pathogenesis and therapy. *J. Cell Mol. Med.* 22, 755–767. doi: 10.1111/jcmm.13450

Mariño, G., Niso-Santano, M., Baehrecke, E., and Kroemer, G. (2014). Self-consumption: the interplay of autophagy and apoptosis. *Nat. Rev. Mol. Cell Biol.* 15, 81–94. doi: 10.1038/nrm3735

Marquez, R. T., and Xu, L. (2012). Bcl-2:Beclin 1 complex: multiple, mechanisms regulating autophagy/apoptosis toggle switch. *Am. J. Cancer Res.* 2, 214–221.

Martinet, W., Agostinis, P., Vanhoecke, B., Dewaele, M., and De Meyer, G. (2009). Autophagy in disease: A double-edged sword with therapeutic potential. *Clin. Sci.* 116, 697–712. doi: 10.1042/CS20080508

Mendell, J. R., Al-Zaidy, S., Shell, R., Arnold, W., Rodino-Klapac, L., Prior, T., et al. (2017). Single-Dose Gene-Replacement Therapy for Spinal Muscular Atrophy. *N. Engl. J. Med.* 377, 1713–1722. doi: 10.1056/nejmoa1706198

Menzies, F. M., Moreau, K., Puri, C., Renna, M., and Rubinsztein, D. (2012). Measurement of Autophagic Activity in Mammalian Cells. *Curr. Protoc. Cell Biol.* 54, 15. doi: 10.1002/0471143030.cb1516s54

Meyer, K., Ferraiuolo, L., Schmelzer, L., Braun, L., McGovern, V., Likhite, S., et al. (2015). Improving single injection CSF delivery of AAV9-mediated gene therapy for

SMA: a dose-response study in mice and nonhuman primates. *Mol. Ther.* 23, 477–487. doi: 10.1038/mt.2014.210

Miller, N., Shi, H., Zelikovich, A., and Ma, Y. (2016). Motor neuron mitochondrial dysfunction in spinal muscular atrophy. *Hum. Mol. Genet.* 25, 3395–3406. doi: 10.1093/hmg/ddw262

Miller, R., Harrison, D., Astle, C., Fernandez, E., Flurkey, K., Han, M., et al. (2014). Rapamycin-mediated lifespan increase in mice is dose and sex dependent and metabolically distinct from dietary restriction. *Aging Cell* 13, 468–477. doi: 10.1111/acel.12194

Mizushima, N., and Levine, B. (2010). Autophagy in mammalian development and differentiation. *Nat. Cell Biol.* 12, 823–830. doi: 10.1038/ncb0910-823

Mizushima, N., Levine, B., Cuervo, A., and Klionsky, D. (2008). Autophagy fights disease through cellular self-digestion. *Nature* 451, 1069–1075. doi: 10.1038/nature06639

Mizushima, N., Yamamoto, A., Matsui, M., Yoshimori, T., and Ohsumi, Y. (2004). In vivo analysis of autophagy in response to nutrient starvation using transgenic mice expressing a fluorescent autophagosome marker. *Mol. Biol Cell* 15, 1101–1111. doi: 10.1091/mbc.e03-09-0704

Mizushima, N., Yoshimori, T., and Ohsumi, Y. (2011). The role of Atg proteins in autophagosome formation. *Annu. Rev. Cell Dev. Biol.* 27, 107–132. doi: 10.1146/annurev-cellbio-092910-154005

Mohamud, Y., Shi, J., Qu, J., Poon, T., Xue, Y., Deng, H., et al. (2018). Enteroviral Infection Inhibits Autophagic Flux via Disruption of the SNARE Complex to Enhance Viral Replication. *Cell Rep.* 22, 3292–3303. doi: 10.1016/j.celrep.2018.02.090

Monani, U., Coovert, D., and Burghes, A. (2000). Animal models of spinal muscular atrophy. *Hum. Mol. Genet.* 9, 2451–2457. doi: 10.1093/hmg/9.16.2451

Monani, U., and De Vivo, D. (2014). Neurodegeneration in spinal muscular atrophy: from disease phenotype and animal models to therapeutic strategies and beyond. *Fut. Neurol.* 9, 49–65. doi: 10.2217/fnl.13.58

Monani, U., Lorson, C., Parsons, D., Prior, T., Androphy, E., Burghes, A., et al. (1999). A single nucleotide difference that alters splicing patterns distinguishes the SMA gene SMN1 from the copy gene SMN2. *Hum. Mol. Genet.* 8, 1177–1183. doi: 10.1093/hmg/8.7.1177

Montagnac, G., Meas-Yedid, V., Irondelle, M., Castro-Castro, A., Franco, M., Shida, T., et al. (2013). αTAT1 catalyses microtubule acetylation at clathrin-coated pits. *Nature* 502, 567–570. doi: 10.1038/nature12571

Mu, Y., Yan, X., Li, D., Zhao, D., Wang, L., Wang, X., et al. (2018). NUPR1 maintains autolysosomal efflux by activating SNAP25 transcription in cancer cells. *Autophagy* 14, 654–670. doi: 10.1080/15548627.2017.1338556

Nguyen, D., Thombre, R., and Wang, J. (2019). Autophagy as a common pathway in amyotrophic lateral sclerosis. *Neurosci. Lett.* 697, 34–48. doi: 10.1016/j.neulet.2018.04.006

Nilsson, P., and Saido, T. (2014). Dual roles for autophagy: degradation and secretion of Alzheimer's disease Aβ peptide. *Bioessays* 36, 570–578. doi: 10.1002/bies.201400002

Ning, K., Drepper, C., Valori, C., Ahsan, M., Wyles, M., Higginbottom, A., et al. (2010). PTEN depletion rescues axonal growth defect and improves survival in SMN-deficient motor neurons. *Hum. Mol. Genet.* 19, 3159–3168. doi: 10.1093/hmg/ddq226

Nishio, H., Niba, E., Saito, T., Okamoto, K., Takeshima, Y., and Awano, H. (2023). Spinal muscular atrophy: the past, present, and future of diagnosis and treatment. *Int. J. Mol. Sci.* 24, 11939. doi: 10.3390/ijms241511939

Nixon, R. (2013). The role of autophagy in neurodegenerative disease. *Nat. Med.* 19, 983–997. doi: 10.1038/nm.3232

Noda, T., and Ohsumi, Y. (1998). Tor, a phosphatidylinositol kinase homologue, controls autophagy in yeast. *J. Biol. Chem.* 273, 3963–3966. doi: 10.1074/jbc.273.7.3963

Ogbonmide, T., Rathore, R., Rangrej, S., Hutchinson, S., Lewis, M., Ojilere, S., et al. (2023). Gene Therapy for Spinal Muscular Atrophy (SMA): A Review of Current Challenges and Safety Considerations for Onasemnogene Abeparvovec (Zolgensma). *Cureus* 15, e36197. doi: 10.7759/cureus.36197

O'Hern, P., Garcia, E. L., Hao, L. T., Hart, A. C., Matera, A. G., and Beattie, C. E. (2017). Nonmammalian animal models of spinal muscular atrophy. *Spinal Musc. Atrophy* 2017, 221–239. doi: 10.1016/B978-0-12-803685-3.00014-8

Ohsumi, Y. (2001). Molecular dissection of autophagy: two ubiquitin-like systems. *Nat. Rev. Mol. Cell Biol.* 2, 211–216. doi: 10.1038/35056522

Oliván, S., Calvo, A., Rando, A., Herrando-Grabulosa, M., Manzano, R., Zaragoza, P., et al. (2016). Neuroprotective effect of non-viral gene therapy treatment based on tetanus toxin c-fragment in a severe mouse model of spinal muscular atrophy. *Front. Mol. Neurosci.* 9:76. doi: 10.3389/fnmol.2016.00076

Oprea, G., Kröber, S., McWhorter, M., Rossoll, W., Müller, S., Krawczak, M., et al. (2008). Plastin 3 is a protective modifier of autosomal recessive spinal muscular atrophy. *Science* 320, 524–527. doi: 10.1126/science.1155085

Paik, J. (2022). Risdiplam: A Review in Spinal Muscular Atrophy. *CNS Drugs* 36, 401–410. doi: 10.1007/s40263-022-00910-8

Pankiv, S., and Johansen, T. (2010). FYCO1: linking autophagosomes to microtubule plus end-directing molecular motors. *Autophagy* 6, 550–552. doi: 10.4161/auto.6.4.11670

Passini, M., Bu, J., Richards, A., Kinnecom, C., Sardi, S., Stanek, L., et al. (2011). Antisense oligonucleotides delivered to the mouse CNS ameliorate symptoms of severe spinal muscular atrophy. *Sci. Transl. Med.* 3:72ra18. doi: 10.1126/scitranslmed.3001777

Pattingre, S., Tassa, A., Qu, X., Garuti, R., Liang, X., Mizushima, N., et al. (2005). Bcl-2 antiapoptotic proteins inhibit Beclin 1-dependent autophagy. *Cell* 122, 927–939. doi: 10.1016/j.cell.2005.07.002

Periyakaruppiah, A., de la Fuente, S., Arumugam, S., Bahí, N., Garcera, A., and Soler, R. (2016). Autophagy modulators regulate survival motor neuron protein stability in motoneurons. *Exp. Neurol.* 283, 287–297.

Piras, A., Schiaffino, L., Boido, M., Valsecchi, V., Guglielmotto, M., De Amicis, E., et al. (2017). Inhibition of autophagy delays motoneuron degeneration and extends lifespan in a mouse model of spinal muscular atrophy. *Cell Death Dis.* 8:3223. doi: 10.1038/s41419-017-0086-4

Poirier, A., Weetall, M., Heinig, K., Bucheli, F., Schoenlein, K., Alsenz, J., et al. (2018). Risdiplam distributes and increases SMN protein in both the central nervous system and peripheral organs. *Pharmacol. Res. Perspect.* 6, e00447. doi: 10.1002/prp2.447

Powis, R., Karyka, E., Boyd, P., Côme, J., Jones, R., Zheng, Y., et al. (2016). Systemic restoration of UBA1 ameliorates disease in spinal muscular atrophy. *JCI Insight* 1, e87908. doi: 10.1172/jci.insight.87908

Ragagnin, A., Shadfar, S., Vidal, M., Jamali, M., and Atkin, J. (2019). Motor Neuron Susceptibility in ALS/FTD. *Front. Neurosci.* 13:532. doi: 10.3389/fnins.2019.00532

Ramser, J., Ahearn, M., Lenski, C., Yariz, K., Hellebrand, H., von Rhein, M., et al. (2008). Rare missense and synonymous variants in UBE1 are associated with X-linked infantile spinal muscular atrophy. *Am. J. Hum. Genet.* 82, 188–193. doi: 10.1016/j.ajhg.2007.09.009

Ravikumar, B., Vacher, C., Berger, Z., Davies, J., Luo, S., Oroz, L., et al. (2004). Inhibition of mTOR induces autophagy and reduces toxicity of polyglutamine expansions in fly and mouse models of Huntington disease. *Nat. Genet.* 36, 585–595. doi: 10.1038/ng1362

Riessland, M., Kaczmarek, A., Schneider, S., Swoboda, K., Löhr, H., Bradler, C., et al. (2017). Neurocalcin delta suppression protects against spinal muscular atrophy in humans and across species by restoring impaired endocytosis. *Am. J. Hum. Genet.* 100, 297–315. doi: 10.1016/j.ajhg.2017.01.005

Ripolone, M., Ronchi, D., Violano, R., Vallejo, D., Fagiolari, G., Barca, E., et al. (2015). Impaired muscle mitochondrial biogenesis and myogenesis in spinal muscular atrophy. *JAMA Neurol.* 72, 666–675. doi: 10.1001/jamaneurol.2015.0178

Rodriguez-Muela, N., Parkhitko, A., Grass, T., Gibbs, R., Norabuena, E., Perrimon, N., et al. (2018). Blocking p62-dependent SMN degradation ameliorates spinal muscular atrophy disease phenotypes. *J. Clin. Invest.* 128, 3008–3023. doi: 10.1172/JCI95231

Rose, F., Mattis, V., Rindt, H., and Lorson, C. (2009). Delivery of recombinant follistatin lessens disease severity in a mouse model of spinal muscular atrophy. *Hum. Mol. Genet.* 18, 997–1005. doi: 10.1093/hmg/ddn426

Rossoll, W., Jablonka, S., Andreassi, C., Kröning, A., Karle, K., Monani, U., et al. (2003). Smn, the spinal muscular atrophy-determining gene product, modulates axon growth and localization of beta-actin mRNA in growth cones of motoneurons. *J. Cell Biol.* 163, 801–812. doi: 10.1083/jcb.200304128

Roy, S. (2021). Regulation of autophagy by miRNAs in human diseases. *Nucleus* 64, 317–329. doi: 10.1007/s13237-021-00378-9

Rubinsztein, D., and Nixon, R. (2010). Rapamycin induces autophagic flux in neurons. *Proc. Natl. Acad. Sci. U. S. A.* 107, E181. doi: 10.1073/pnas.1014633107

Sansa, A., Hidalgo, I., Miralles, M., delaFuente, S., Perez-Garcia, M., and Munell, F. (2021). . Spinal Muscular Atrophy autophagy profile is tissue-dependent: differential regulation between muscle and motoneurons. *Acta Neuropathol. Commun.* 9:122. doi: 10.1186/s40478-021-01223-5

Sareen, D., Ebert, A., Heins, B., McGivern, J., Ornelas, L., and Svendsen, C. (2012). Inhibition of apoptosis blocks human motor neuron cell death in a stem cell model of spinal muscular atrophy. *PLoS One* 7:e39113. doi: 10.1371/journal.pone.0039113

Sarkar, S., Korolchuk, V., Renna, M., Imarisio, S., Fleming, A., Williams, A., et al. (2011). Complex inhibitory effects of nitric oxide on autophagy. *Mol. Cell.* 43, 19–32. doi: 10.1016/j.molcel.2011.04.029

Sasaki, S. (2011). Autophagy in spinal cord motor neurons in sporadic amyotrophic lateral sclerosis. *J. Neuropathol. Exp. Neurol.* 70, 349–359. doi: 10.1097/NEN.0b013e3182160690

Saxton, R., and Sabatini, D. (2017). mTOR signaling in growth, metabolism, and disease. *Cell* 168, 960–976. doi: 10.1016/j.cell.2017.02.004

Seto, A., Beatty, X., Lynch, J., Hermreck, M., Tetzlaff, M., Duvic, M., et al. (2018). Cobomarsen, an oligonucleotide inhibitor of miR-155, co-ordinately regulates multiple survival pathways to reduce cellular proliferation and survival in cutaneous T-cell lymphoma. *Br. J. Haematol.* 183, 428–444. doi: 10.1111/bjh.15547

Shababi, M., Lorson, C., and Rudnik-Schöneborn, S. (2014). Spinal muscular atrophy: a motor neuron disorder or a multi-organ disease? *J. Anat.* 224, 15–28. doi: 10.1111/joa.12083

Shang, L., Chen, S., Du, F., Li, S., Zhao, L., and Wang, X. (2011). Nutrient starvation elicits an acute autophagic response mediated by Ulk1 dephosphorylation and its subsequent dissociation from AMPK. *Proc. Natl. Acad. Sci. U. S. A.* 108, 4788–4793. doi: 10.1073/pnas.1100844108

Sharma, M., McFarlane, C., Kambadur, R., Kukreti, H., Bonala, S., and Srinivasan, S. (2015). Myostatin: expanding horizons. *IUBMB Life* 67, 589–600. doi: 10.1002/iub.1392

Shimizu, S., Honda, S., Arakawa, S., and Yamaguchi, H. (2014). Alternative macroautophagy and mitophagy. *Int. J. Biochem. Cell Biol.* 50, 64–66. doi: 10.1016/j.biocel.2014.02.016

Si, X., Cao, D., Chen, J., Nie, Y., Jiang, Z., Chen, M., et al. (2018). miR-23a downregulation modulates the inflammatory response by targeting ATG12-mediated autophagy. *Mol. Med. Rep.* 18, 1524–1530. doi: 10.3892/mmr.2018.9081

Singh, N., Singh, N., Androphy, E., and Singh, R. (2006). Splicing of a critical exon of human Survival Motor Neuron is regulated by a unique silencer element located in the last intron. *Mol. Cell Biol.* 26, 1333–1346. doi: 10.1128/MCB.26.4.1333-1346.2006

Singh, R., and Singh, N. (2018). Mechanism of splicing regulation of spinal muscular atrophy genes. *Adv. Neurobiol.* 20, 31–61. doi: 10.1007/978-3-319-89689-2_2

Sison, S., Patitucci, T., Seminary, E., Villalon, E., Lorson, C., and Ebert, A. (2017). Astrocyte-produced miR-146a as a mediator of motor neuron loss in spinal muscular atrophy. *Hum. Mol. Genet.* 26, 3409–3420. doi: 10.1093/hmg/ddx230

Sivaramakrishnan, M., McCarthy, K., Campagne, S., Huber, S., Meier, S., Augustin, A., et al. (2017). Binding to SMN2 pre-mRNA-protein complex elicits specificity for small molecule splicing modifiers. *Nat. Commun.* 8:1476. doi: 10.1038/s41467-017-01559-4

Song, C., Guo, J., Liu, Y., and Tang, B. (2012). Autophagy and its comprehensive impact on ALS. *Int. J. Neurosci.* 122, 695–703. doi: 10.3109/00207454.2012.714430

Summers, C., and Valentine, R. (2020). Acute Heat Exposure Alters Autophagy Signaling in C2C12 Myotubes. *Front. Physiol.* 10:1521. doi: 10.3389/fphys.2019.01521

Thomas, N., and Dubowitz, V. (1994). The natural history of type I (severe) spinal muscular atrophy. *Neuromuscul. Disord.* 4, 497–502. doi: 10.1016/0960-8966(94)90090-6

Torres-Benito, L., Neher, M., Cano, R., Ruiz, R., and Tabares, L. (2011). SMN requirement for synaptic vesicle, active zone and microtubule postnatal organization in motor nerve terminals. *PLoS One.* 6:e26164. doi: 10.1371/journal.pone.0026164

Torres-Benito, L., Schneider, S., Rombo, R., Ling, K., Grysko, V., Upadhyay, A., et al. (2019). NCALD antisense oligonucleotide therapy in addition to nusinersen further ameliorates spinal muscular atrophy in mice. *Am. J. Hum. Genet.* 105, 221–230. doi: 10.1016/j.ajhg.2019.05.008

Ucar, A., Gupta, S., Fiedler, J., Erikci, E., Kardasinski, M., Batkai, S., et al. (2012). The miRNA-212/132 family regulates both cardiac hypertrophy and cardiomyocyte autophagy. *Nat. Commun.* 3:1078. doi: 10.1038/ncomms2090

Valori, C., Ning, K., Wyles, M., Mead, R., Grierson, A., Shaw, P., et al. (2010). Systemic delivery of scAAV9 expressing SMN prolongs survival in a model of spinal muscular atrophy. *Sci. Transl. Med.* 2:35ra42. doi: 10.1126/scitranslmed.3000830

Valsecchi, V., Anzilotti, S., Serani, A., Laudati, G., Brancaccio, P., Guida, N., et al. (2020). miR-206 Reduces the Severity of Motor Neuron Degeneration in the Facial Nuclei of the Brainstem in a Mouse Model of SMA. *Mol. Ther.* 28, 1154–1166. doi: 10.1016/j.ymthe.2020.01.013

Valsecchi, V., Boido, M., De Amicis, E., Piras, A., and Vercelli, A. (2015). Expression of Muscle-Specific MiRNA 206 in the Progression of Disease in a Murine SMA Model. *PLoS One* 10:e0128560. doi: 10.1371/journal.pone.0128560

Verhaart, I., Robertson, A., Wilson, I., Aartsma-Rus, A., Cameron, S., Jones, C., et al. (2017). Prevalence, incidence and carrier frequency of 5q-linked spinal muscular atrophy - a literature review. *Orphanet. J. Rare Dis.* 12:124. doi: 10.1186/s13023-017-0671-8

Wan, J., Yang, X., Ren, Y., Li, X., Zhu, Y., Haddock, A., et al. (2019). Inhibition of miR-155 reduces impaired autophagy and improves prognosis in an experimental pancreatitis mouse model. *Cell Death Dis.* 10:303. doi: 10.1038/s41419-019-1545-x

Wang, W., Lu, G., Su, X., Lyu, H., and Poon, W. (2017). MicroRNA-182 Regulates Neurite Outgrowth Involving the PTEN/AKT Pathway. *Front. Cell Neurosci.* 11:96. doi: 10.3389/fncel.2017.00096

Wei, Y. (2014). Autophagic induction of amyotrophic lateral sclerosis-linked Cu/Zn superoxide dismutase 1 G93A mutant in NSC34 cells. *Neural. Regen. Res.* 9, 16–24. doi: 10.4103/1673-5374.125325

Williams, A., Sarkar, S., Cuddon, P., Ttofi, E., Saiki, S., Siddiqi, F., et al. (2008). Novel targets for Huntington's disease in an mTOR-independent autophagy pathway. *Nat. Chem. Biol.* 4, 295–305. doi: 10.1038/nchembio.79

Wirth, B. (2021). Spinal Muscular Atrophy: In the Challenge Lies a Solution. *Trends Neurosci.* 44, 306–322. doi: 10.1016/j.tins.2020.11.009

Wong, E., and Cuervo, A. (2010). Autophagy gone awry in neurodegenerative diseases. *Nat. Neurosci.* 13, 805–811. doi: 10.1038/nn.2575

Wu, Y. T., Tan, H., Shui, G., Bauvy, C., Huang, Q., Wenk, M., et al. (2010). Dual role of 3-methyladenine in modulation of autophagy via different temporal patterns of inhibition on class I and III phosphoinositide 3-kinase. *J. Biol. Chem.* 285, 10850–10861. doi: 10.1074/jbc.M109.080796

Xiong, S., Mu, T., Wang, G., and Jiang, X. (2014). Mitochondria-mediated apoptosis in mammals. *Protein Cell* 5, 737–749. doi: 10.1007/s13238-014-0089-1

Yamamoto, A., Tagawa, Y., Yoshimori, T., Moriyama, Y., Masaki, R., and Tashiro, Y. (1998). Bafilomycin A1 prevents maturation of autophagic vacuoles by inhibiting fusion between autophagosomes and lysosomes in rat hepatoma cell line, H-4-II-E cells. *Cell Struct. Funct.* 23, 33–42. doi: 10.1247/csf.23.33

Yamashima, T. (2013). Reconsider Alzheimer's disease by the 'calpain-cathepsin hypothesis'–a perspective review. *Prog. Neurobiol.* 105, 1–23. doi: 10.1016/j.pneurobio.2013.02.004

Yang, J., Kim, W., and Kim, D. (2023). Autophagy in cell survival and death. *Int. J. Mol. Sci.* 24:4744. doi: 10.3390/ijms24054744

Yanyan, C., Yujin, Q., Jinli, B., Yuwei, J., Hong, W., and Fang, S. (2014). Correlation of PLS3 expression with disease severity in children with spinal muscular atrophy. *J. Hum. Genet.* 59, 24–27. doi: 10.1038/jhg.2013.111

Yorimitsu, T., and Klionsky, D. (2005). Autophagy: molecular machinery for self-eating. *Cell Death Differ.* 12, 1542–1552. doi: 10.1038/sj.cdd.4401765

Yuan, Y., Zhang, Y., Han, L., Sun, S., and Shu, Y. (2018). miR-183 inhibits autophagy and apoptosis in gastric cancer cells by targeting ultraviolet radiation resistance-associated gene. *Int. J. Mol. Med.* 42, 3562–3570. doi: 10.3892/ijmm.2018.3871

Yuva-Aydemir, Y., Simkin, A., Gascon, E., and Gao, F. (2011). MicroRNA-9: functional evolution of a conserved small regulatory RNA. *RNA Biol.* 8, 557–564. doi: 10.4161/rna.8.4.16019

Zerres, K., and Rudnik-Schöneborn, S. (1995). Natural history in proximal spinal muscular atrophy. Clinical analysis of 445 patients and suggestions for a modification of existing classifications. *Arch. Neurol.* 52, 518–523. doi: 10.1001/archneur.1995.00540290108025

Zerres, K., Rudnik-Schöneborn, S., Forrest, E., Lusakowska, A., Borkowska, J., and Hausmanowa-Petrusewicz, I. (1997). A collaborative study on the natural history of childhood and juvenile onset proximal spinal muscular atrophy (type II and III SMA): 569 patients. *J. Neurol. Sci.* 146, 67–72. doi: 10.1016/s0022-510x(96)00284-5

Zhang, G., Wang, J., Jia, Y., Han, R., Li, P., and Zhu, D. (2015). MicroRNA-9 promotes the neuronal differentiation of rat bone marrow mesenchymal stem cells by activating autophagy. *Neural Regen. Res.* 10, 314–320. doi: 10.4103/1673-5374.143439

Zhang, Z., Pinto, A., Wan, L., Wang, W., Berg, M., Oliva, I., et al. (2013). Dysregulation of synaptogenesis genes antecedes motor neuron pathology in spinal muscular atrophy. *Proc. Natl. Acad. Sci. U. S. A.* 110, 19348–19353. doi: 10.1073/pnas.1319280110

frontiers | Frontiers in Cellular Neuroscience

TYPE Original Research
PUBLISHED 19 January 2024
DOI 10.3389/fncel.2023.1327361

OPEN ACCESS

EDITED BY
Danyllo Oliveira,
University of São Paulo, Brazil

REVIEWED BY
Maria Catarina Silva,
Massachusetts General Hospital and Harvard Medical School, United States
Karina Oliveira,
Albert Einstein Israelite Hospital, Brazil

*CORRESPONDENCE
Lee L. Rubin
✉ lee_rubin@harvard.edu

†PRESENT ADDRESS
Alban Ordureau,
Cell Biology Program, Sloan Kettering Institute, Memorial Sloan Kettering Cancer Center, New York, NY, United States

‡These authors share first authorship

RECEIVED 24 October 2023
ACCEPTED 15 December 2023
PUBLISHED 19 January 2024

CITATION
Watts ME, Giadone RM, Ordureau A, Holton KM, Harper JW and Rubin LL (2024) Analyzing the ER stress response in ALS patient derived motor neurons identifies druggable neuroprotective targets. *Front. Cell. Neurosci.* 17:1327361. doi: 10.3389/fncel.2023.1327361

Analyzing the ER stress response in ALS patient derived motor neurons identifies druggable neuroprotective targets

Michelle E. Watts[1,2‡], Richard M. Giadone[1,2‡], Alban Ordureau[3†], Kristina M. Holton[1,2], J. Wade Harper[3] and Lee L. Rubin[1,2*]

[1]Department of Stem Cell and Regenerative Biology, Harvard University, Cambridge, MA, United States, [2]Harvard Stem Cell Institute, Harvard University, Cambridge, MA, United States, [3]Department of Cell Biology, Harvard Medical School, Boston, MA, United States

Amyotrophic lateral sclerosis (ALS) is a degenerative motor neuron (MN) disease with severely limited treatment options. Identification of effective treatments has been limited in part by the lack of predictive animal models for complex human disorders. Here, we utilized pharmacologic ER stressors to exacerbate underlying sensitivities conferred by ALS patient genetics in induced pluripotent stem cell (iPSC)-derived motor neurons (MNs). In doing so, we found that thapsigargin and tunicamycin exposure recapitulated ALS-associated degeneration, and that we could rescue this degeneration via MAP4K4 inhibition (MAP4K4i). We subsequently identified mechanisms underlying MAP4K4i-mediated protection by performing phosphoproteomics on iPSC-derived MNs treated with ER stressors ±MAP4K4i. Through these analyses, we found JNK, PKC, and BRAF to be differentially modulated in MAP4K4i-protected MNs, and that inhibitors to these proteins could also rescue MN toxicity. Collectively, this study highlights the value of utilizing ER stressors in ALS patient MNs to identify novel druggable targets.

KEYWORDS

ALS, ER stress, iPSCs, motor neurons, proteomics, phosphoproteomics

1 Introduction

Amyotrophic lateral sclerosis (ALS) is a fatal neurodegenerative disorder characterized by selective death of motor neurons (MNs) (Brown and Al-Chalabi, 2017). The loss of this cell type in the brain and spinal cord manifests in symptoms of muscle weakness and atrophy, which progress rapidly to paralysis and respiratory failure approximately 1–5 years after diagnosis (Hardiman et al., 2017). Currently, there are only 4 FDA approved treatments for the disease (riluzole, edaravone, and the recently approved relyvrio and tofersen). However, none of these extend life expectancy beyond several months nor improve muscle function in all patient cohorts (Jaiswal, 2019), and only tofersen acts via a widely accepted disease-associated mechanism. Developing efficacious therapeutics for ALS has been particularly challenging in part due to the inaccessibility of human tissue for study. Moreover, animal models fail to recapitulate the variable genetic drivers observed

in patients, including coding and non-coding elements, thereby limiting their effectiveness and therapeutic translatability (Petrov et al., 2017).

To overcome this limitation, several studies have employed patient-specific induced pluripotent stem cell (iPSC)-based culture systems to understand ALS pathogenesis as well as evaluate the ability of pre-clinical therapeutic candidates to attenuate disease phenotypes (Dimos et al., 2008; Wainger et al., 2014; Fujimori et al., 2018). iPSC lines have been generated from individuals with a variety of mutations in genetic drivers of the disease (e.g., FUS, C9ORF72, TDP-43, SOD1) as well as more common sporadic forms (Boulting et al., 2011; Burkhardt et al., 2013; Sareen et al., 2013; Kiskinis et al., 2014; Ichiyanagi et al., 2016). Through these models, the field has recapitulated a number of disease-relevant phenotypes in iPSC-derived neuronal cell types, including: altered neurite morphology (Egawa et al., 2012; Chen et al., 2014; Fujimori et al., 2018), disease-specific transcriptional signatures (Workman et al., 2023), increased excitotoxicity (Wainger et al., 2014; Shi et al., 2018), accumulation of intracellular aggregates (Egawa et al., 2012; Naumann et al., 2018; Sun et al., 2018; Shi et al., 2019; Hung et al., 2023), mRNA mis-processing (Melamed et al., 2019), increased apoptotic activity (Kiskinis et al., 2014; Naujock et al., 2016; Wu et al., 2019; Abo-Rady et al., 2020), and increased sensitivity to stressors (Yang et al., 2013; Zhang et al., 2013; Shi et al., 2018). Utilizing these models, it may be possible to identify convergent mechanisms driving MN death in ALS patients, perhaps enabling the development of broadly efficacious therapeutics.

A hallmark of ALS is the accumulation of aggregated proteins, particularly TDP-43 (Brown and Al-Chalabi, 2017). Accumulation of aggregated proteins in the ER lumen can lead to activation of several signaling pathways, including the unfolded protein response (UPR) (Matus et al., 2011). Specifically, the ER chaperone BiP dissociates from three transmembrane receptors (ATF6, IRE1, and PERK) and binds to misfolded proteins. This initial dissociation of BiP leads to activation of downstream signaling events, including proteolytic cleavage of ATF6 in the Golgi, phosphorylation of ATF4 downstream of PERK and eIF2α phosphorylation, and splicing of XBP1 mRNA (downstream of IRE1 activation). Ultimately, these events lead to induction of transcription factors that translocate into the nucleus and activate downstream transcriptional networks with adaptive/cytoprotective or pro-apoptotic outputs including: upregulation of chaperone genes downstream of ATF6, ER associated degradation (ERAD) components via XBP1, and pro-apoptotic machinery via PERK (Hetz et al., 2020). MNs, with characteristically long axonal projections exhibit increased demand on ER-Golgi secretory pathways, ultimately resulting in high levels of basal ER stress. Further, in the case of ALS MNs, several studies demonstrate pathogenic aggregation of disease-associated proteins (e.g., FUS, TDP-43, and SOD1) contributes to increased UPR activity. Coupled with increased basal activation of ER stress, this leads to increased sensitivity to apoptotic signaling, and ultimately death of vulnerable MN subpopulations, implicating proteostasis dysfunction in the pathobiology of ALS (Saxena et al., 2009; Ruegsegger and Saxena, 2016; Rozas et al., 2017; Webster et al., 2017).

Another hallmark of ALS, one often overlooked in cell culture models, includes differential MN vulnerability, where upper MNs in the motor cortex of the brain and lower MNs in the brainstem and spinal cord are disproportionately damaged in patients relative to other CNS cell types (Ferraiuolo et al., 2011; Ragagnin et al., 2019). Studies utilizing stem cell-based differentiation platforms have predominately focused on minimizing heterogeneity in their cultures, potentially overlooking important differences in cell type-specific responses to proteostatic perturbations.

To address these challenges and better recapitulate the MN-specific vulnerability observed in patients with ALS, we employed an established MN differentiation protocol producing cells of lower motor column (LMC) identity, including: MNs, ventral spinal interneurons, and a small number of astroglia (Maury et al., 2015; Neel et al., 2023). We then exposed these cells to chemical inducers of ER stress to exacerbate underlying ER stress signaling. We hypothesized that stressors preferentially affecting the MN cell types within these heterogenous cultures may reflect selective damage of MNs within the diverse spinal cord niche. Through these efforts, we observed that 2 mechanistically distinct ER stressors, thapsigargin (a SERCA inhibitor) and tunicamycin (an N-linked glycosylation inhibitor) synchronously recapitulated the activation of early disease-associated UPR signaling events, along with gross MN toxicity and neurite degradation (henceforth referred to as late-stage MN-specific degenerative phenotypes) in both healthy and ALS patient MNs. We then validated the fidelity of this approach to identify neuroprotective drugs by reproducing the ability of several pharmacological MAP4K4 inhibitors, originally identified by our group, to rescue this ALS MN toxicity. To discover additional neuroprotective effectors downstream of MAP4K4 inhibition, we subsequently performed phosphoproteomics on iPSC-derived MNs after exposure to thapsigargin, with or without protection by MAP4K4 inhibition. In doing so, we identified PKC and BRAF as signaling components downstream of MAP4K4 inhibition, and further showed that commercial inhibitors of these targets also exhibited neuroprotective effects. Collectively, these data demonstrate the effectiveness of utilizing chemical ER stress to exacerbate ALS disease phenotypes in patient-derived cells and that synergizing this platform with proteomics assays allows for identification of druggable targets for neurodegenerative diseases.

2 Results

2.1 ER stress preferentially induced death in MN, but not non-MN, ALS iPSC-derived cell populations

Many studies have implicated ER stress as an underlying mechanism of MN death in ALS, demonstrating changes in solubility and localization of intracellular aggregates upon treatment with ER stress-inducing compounds such as thapsigargin, tunicamycin, and MG132 (Walker et al., 2013; Bhinge et al., 2017; Medinas et al., 2018); however, few have investigated toxicity or unbiased proteomic/phosphoproteomic changes upon perturbation. To investigate the extent to which proteostatic stress initiates preferential MN degeneration in human cells, we first evaluated MN cultures derived from a non-diseased, healthy control 1016A hiPSC line. hiPSCs were differentiated into MNs following an established 15-day embryoid body (EB)-based protocol that recapitulates neurectoderm induction with

dual SMAD inhibition, caudalization with retinoic acid (RA), ventralization with Sonic Hedgehog pathway activation, and MN maturation with the neurotrophic factors (BDNF, GDNF), and γ-secretase inhibitor DAPT (**Figure 1A**; Maury et al., 2015). Following this protocol, ∼80% of cells were neurons (based on the expression of βIII-Tubulin; TUJ1 +), ∼30% of which expressed the mature MN marker Isl1/2 (Isl1/2 + , TUJ1 +) (**Figures 1B, C**). ISL1/2 and TUJ1 double-positive cells were considered MNs, while the remaining populations were considered non-MN cells (**Figure 1B**).

Since preferential death of MNs in ALS occurs in the spinal cord, comprised of diverse cell types, we then compared the response of MN and non-MN populations in our cultures to challenge with proteotoxic stressors. In doing so, we found that 2 mechanistically distinct ER stressors, thapsigargin and tunicamycin, were preferentially toxic to the MN population compared to the non-MN population, in both a dose- and time-dependent manner (**Figures 1C–E**). As cellular response to stress can be influenced by culture parameters, we confirmed that this preferential MN toxicity was maintained at a variety of culture densities and MN maturation statuses (**Supplementary Figure 1A**). Moreover, exposure to the proteasome inhibitor MG132 did not result in preferential MN cell death under the conditions employed here, demonstrating that selective MN death did not result from all forms of proteostatic stress (**Supplementary Figures 1B–E**), but rather implicated ER stress specifically in preferential MN vulnerability.

We next sought to assess whether induction of ER stress could also potentiate differential cell-type toxicity in MN cultures derived from ALS patients. We used two established ALS patient iPSC lines, each with a heterozygous familial ALS (fALS) mutation–TDP-43$^{G298S/+}$ (47D) and SOD1$^{L144F/+}$ (29D) (Boulting et al., 2011; Alami et al., 2014). These fALS patient iPSCs demonstrated comparable pluripotent stem cell properties and differentiation capacities to the 1016A control iPSC line (Neel et al., 2023). Furthermore, both types of fALS patient MNs also similarly displayed enhanced MN vulnerabilities to the ER stressors compared to the non-MN populations (**Figure 1F**). The observation that both healthy and fALS MN cultures displayed preferential MN degeneration compared to non-MN cell types, adds support to the premise that MNs are intrinsically more vulnerable to ER stressors than other cell types, a result consistent with ALS mouse and hESC stem cell models (Saxena et al., 2009; Thams et al., 2019). Finally, both stressors could be applied to synchronously accelerate MN degeneration in healthy and ALS MN cultures (**Figure 1G**). We observed a tendency for the ALS MNs to show increased vulnerability to the ER stressors, especially at the highest concentrations of thapsigargin and tunicamycin tested (**Figure 1G**). As there might be additional polygenic risk factors other than the single fALS mutation in these lines that contribute to this enhanced vulnerability, we cannot exclusively attribute this exacerbated sensitivity to either single fALS mutation itself. However, corroboratory data using isogenic SOD1-A4V-hESC-derived MNs has been reported to show that isogenic ALS MNs have significantly increased sensitivity to an ER stressor like thapsigargin (CPA) compared to the isogenic control MNs (Thams et al., 2019). Together, these data add support to the hypothesis that ALS MNs have enhanced vulnerability to ER stress. Moreover, simultaneously inducing MN degeneration in both healthy and fALS MN cultures enabled the development of a pharmacological human MN survival assay that encompassed both genetic and non-genetic drivers of disease.

2.2 Early UPR signaling preceded destruction of neurites and apoptotic signaling

Thapsigargin and tunicamycin are known inducers of the UPR, a signaling pathway adapted to handle intracellular protein misfolding and hypothesized to contribute to underlying differential MN vulnerability in ALS (Kanekura et al., 2009; Saxena et al., 2009; Saxena and Caroni, 2011; Matus et al., 2013). Although UPR signaling provides an adaptive mechanism to limit ER burden and accumulation of misfolded proteins, prolonged signaling drives apoptosis via the PERK pathway.

To understand the relationship between UPR activation and initiation of preferential death in MNs, we temporally tracked UPR induction in healthy 1016A iPSC-derived MNs upon exposure to 1 μM thapsigargin and tunicamycin. We found that thapsigargin induced phosphorylation of eIF2α to block protein translation 30 min after stressor challenge, with a maximum response after 1 h (**Figure 2A**, *S1E*). Tunicamycin addition also led to phosphorylation of eIF2α, although the activation was somewhat slower and less robust, reaching a maximum only 4 h post-exposure (**Figure 2A**, *S1E*). We then detected splicing of XBP1 (downstream of IRE1 signaling) for thapsigargin and tunicamycin between 2 and 4 h after treatment (**Figure 2A**, *S1F*). Upregulation of the ER resident chaperone BiP was rapidly initiated, with increases at the mRNA level between 1 and 4 h after each stressor addition, and increases in protein levels by 8 and 24 h (**Figures 2A, B**, *S1G*). The induction of the pro-apoptotic transcription factor CHOP displayed a similar expression pattern to BiP upregulation, with mRNA increases between 1 and 4 h after each stressor treatment, and increases in protein levels by 8 and 24 h (**Figures 2A, B**, *S1H*).

ER stress signaling after 8–24 h exposure to thapsigargin and tunicamycin resulted in the cleavage of caspase 3 (**Figure 2A**, *S1I*) and coincided with an increase in the percentage of TUNEL + MNs (**Figure 2C**). About half of the MN death caused by thapsigargin and tunicamycin treatment was also prevented by the addition of a pan-caspase apoptosis inhibitor Z-VAD-FMK, demonstrating that the selective MN toxicity was due in part to apoptosis (**Figure 2D**). Furthermore, apoptotic death was coincident with and often preceded by degeneration of neurites extending from the neuronal soma, which was observed with both live cell imaging (Supplementary Video Files 1–3) and high throughput neurite tracking software (**Figure 2E**). Moreover, like the healthy control MNs, the ALS iPSC-derived MNs similarly induced UPR responsive genes (e.g., ATF6, BiP, CHOP, IRE1) after thapsigargin exposure (**Supplementary Figure 1J**). Taken together, these data generate a temporal guide of ER stress activation in iPSC-derived MNs, suggesting prolonged ER stress (>8 h) leads to death of vulnerable MN populations via apoptosis. Additionally, these results indicate a dosing paradigm in which potential protective compounds could be evaluated for their ability to attenuate ER

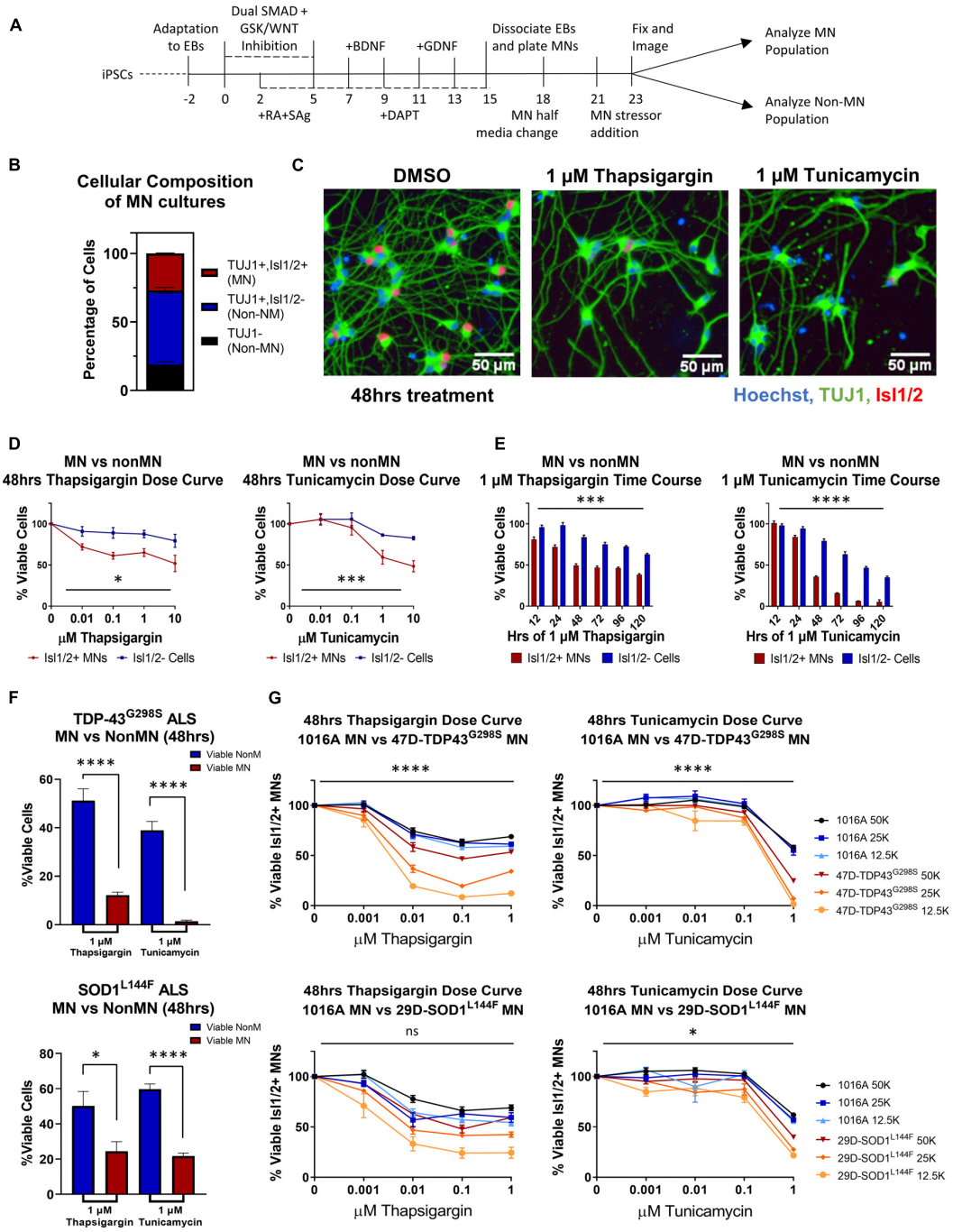

FIGURE 1
ER stressors induce preferential MN death. **(A)** Schematic of MN differentiation protocol and stressor assay. **(B)** Quantification of cell types in iPSC-derived MN cultures (1016A healthy control line). MN populations include Isl1/2 + , TUJ1 + immunostained cells, non-MN populations include Isl1/ 2-, TUJ1 + neuronal populations and TUJ1- non-neuronal cells. Nb = 4, nt = 6. **(C)** Representative immunofluorescent images of iPSC-derived derived MN cultures (1016A healthy control line) in control (DMSO) or ER stress (1 µM compound, 48 h) conditions. **(D)** Quantification of *iPSC-derived* MN and non-MN viability 48 h after treatment with increasing concentrations of ER stressors (1016A healthy control line). Nb > 3, nt > 2, two-way ANOVA; Thapsigargin- $p = 0.015$, Tunicamycin- $p = 0.000127$. **(E)** Quantification of *iPSC-derived* MN and non-MN viability after treatment with 1 µM ER stressors for various lengths of time (1016A healthy control line). Nb = 3, nt = 6, two-way ANOVA; Thapsigargin- $p = 0.000215$, Tunicamycin- $p = 1.64 \times 10^{-33}$. **(F)** Comparison of viable non-MNs and viable MNs after TDP-43^{G298S} mutant or SOD1^{L144F} mutant fALS iPSC-derived MN cultures were treated with 48 h 1 µM ER stressors. Nb = 3, nt > 2, 2 tailed unpaired student's *t*-test; 47D-Thapsigargin- $p = 1.526 \times 10^{-5}$, 47D-Tunicamycin- $p = 1.450 \times 10^{-6}$, 29D-Thapsigargin- $p = 0.02698$, 29D-Tunicamycin- $p = 6.07742 \times 10^{-7}$. **(G)** Quantification of viable MNs from a healthy patient line (1016A) and ALS patient lines (47D-TDP-43^{G298S} or 29D-SOD1^{L144F}) after 48 h of ER stressor exposure. A total of 4 different concentrations of each stressor were tested, in 3 different densities of each line. Nb = 3, nt = 2, three-way ANOVA comparing interaction of cell density and stressor dosage between ALS and control; 47D-Thapsigargin- $p = 5.81 \times 10^{-11}$, 47D-Tunicamycin- $p = 1.37 \times 10^{-17}$, 29D-Thapsigargin- $p = 0.515$, 29D-Tunicamycin- $p = 0.016$. Biological replicate experiments denoted as Nb, each with technical replicate experiments nt. Data are mean value ± SEM. *$p < 0.05$, **$p < 0.01$, ***$p < 0.001$, and ****$p < 0.0001$.

10.3389/fncel.2023.1327361

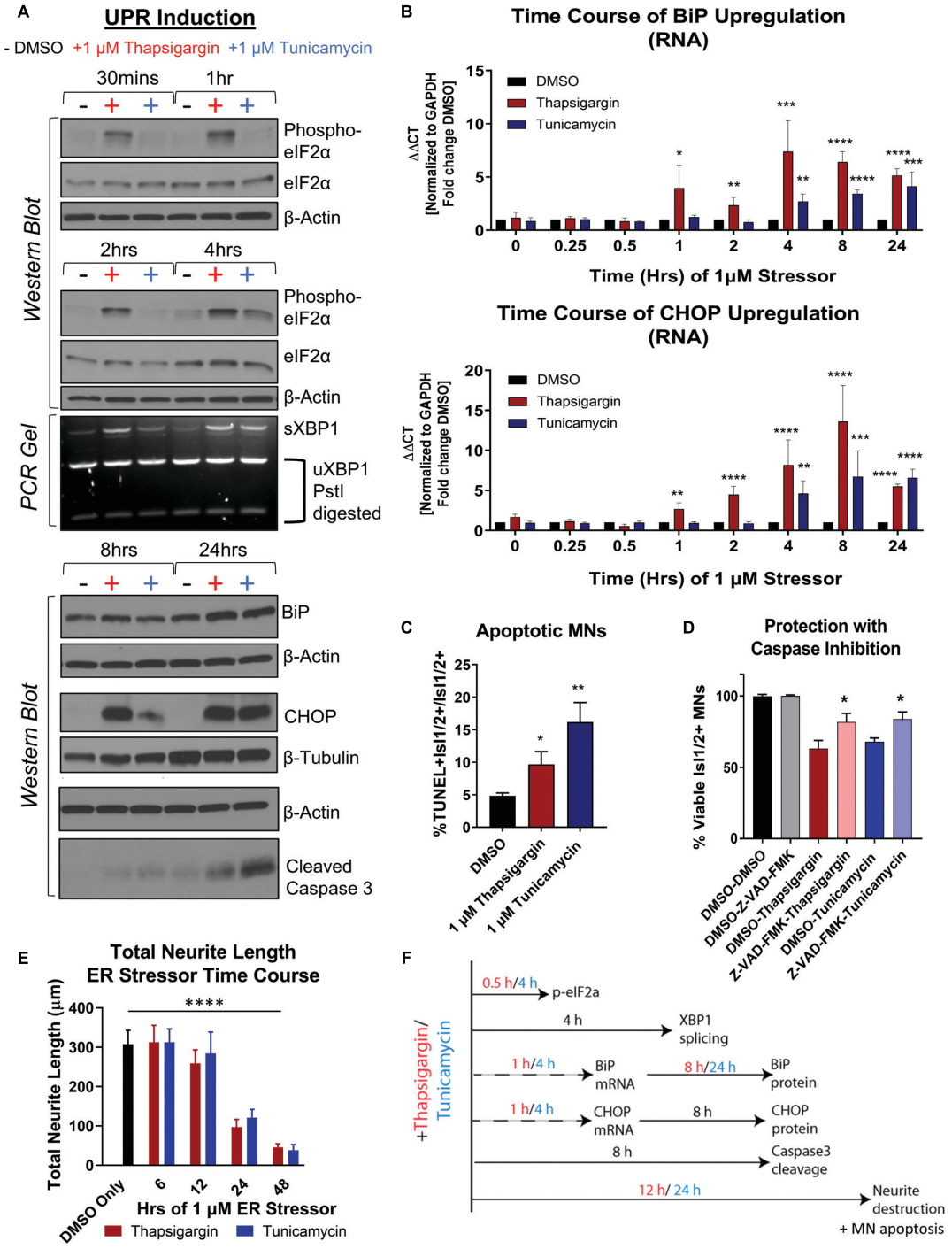

FIGURE 2
Unfolded protein response signaling drives neuritic damage and MN apoptosis. **(A)** Western blot and splicing-PCR analyses of iPSC-derived MN cultures (1016A healthy control line) treated with either DMSO, 1 μM thapsigargin or 1 μM tunicamycin for various times. Nb = 3. **(B)** qRT-PCR analyses of iPSC-derived MN cultures (1016A healthy control line) treated with DMSO, 1 μM thapsigargin or 1 μM tunicamycin for various points. ΔΔCt values are graphed, normalizing target gene qPCR Ct values (BiP or CHOP) to housekeeping gene Ct values (GAPDH) and then calculating the fold change of this normalized Ct value to control conditions such that DMSO = 1 at all-time points. Nb = 3, nt = 3, *$p < 0.05$, **$p < 0.01$, ***$p < 0.001$, ****$p < 0.0001$ one-way ANOVA. **(C)** The percentage of apoptotic MNs (1016A healthy control line) in control (DMSO), 1 μM thapsigargin, or 1 μM tunicamycin stress conditions, quantified by the number of TUNEL + MNs (Isl1/2 +) per total MN numbers (Isl1/2 +). Nb = 3, nt > 4, 2 tailed unpaired student's *t*-test; Thapsigargin- $p = 0.02853$, Tunicamycin- $p = 0.0011$. **(D)** Quantification of MN viability in 1016A healthy control iPSC-derived cultures treated with either control vehicle (DMSO), stressors alone (1 μM thapsigargin or tunicamycin), or stressors with a pan-caspase inhibitor (100 μM Z-VAD-FMK). Nb = 3, nt > 2, 2 tailed unpaired student's *t*-test; Thapsigargin- $p = 0.011583$, Tunicamycin- $p = 0.018997$. **(E)** Quantification of total neurite length (μm) after 1016A healthy control iPSC-derived MNs were exposed to 1 μM ER stressors for increasing amounts of time. Nb = 3, nt = 6, *$p < 0.05$, **$p < 0.01$, ***$p < 0.001$, ****$p < 0.0001$ one-way ANOVA with Tukey's hsd *post-hoc* test. **(F)** Temporal schematic of UPR-associated signaling events occurring post-treatment with thapsigargin or tunicamycin in iPSC-derived MNs. Biological replicate experiments denoted as Nb, each with technical replicate experiments nt. Data are mean value ± SEM.

stress-associated toxicity. The observed temporal order of UPR-associated signaling events post-addition of thapsigargin and tunicamycin is summarized in **Figure 2F**.

2.3 Pharmacologic inhibition of MAP4K4 preserved ALS patient MN viability to a greater extent than current ALS therapeutics

We next sought to determine the extent to which the above defined ER stress MN platform could be rescued with current therapeutics. To do this, we assessed the protective effects of two FDA approved treatments for ALS, riluzole and edaravone, in healthy control 1016A MNs exposed to 1 μM thapsigargin stress. Interestingly, we found that none of the concentrations of riluzole and edaravone tested (10 nM–10 μM) protected from the toxicity caused by ER stress, as measured by the number of viable MNs and neurite architecture (**Figures 3A, B**). Failure of these compounds to confer MN protection could be due either to (1) the elicited ER stress being too profound for rescue, (2) misaligned kinetics of stressor and drug in a co-treatment paradigm, or (3) the distinct non-ER related mechanism of action of these drugs. To rule out the first point that our ER stress assay was unresolvable, we performed the same ER stress experiment, but this time added kenpaullone, a kinase inhibitor found originally by our group to broadly protect murine and human MNs in various cellular culture systems (Yang et al., 2013; Reinhardt et al., 2019; Thams et al., 2019). Consistent with these previous studies, we found that treatment with kenpaullone dramatically improved human MN survival in response to both ER stressors, in healthy control 1016A, TDP-43, and SOD1 fALS patient iPSC-derived MNs (**Figure 3C**). This preservation of MN viability coincided with the maintenance of TUJ1 + neuritic networks (**Figure 3D**). As MN death via thapsigargin and tunicamycin could be attenuated, these data implied that the ER stress assays were not unresolvable, that MN protectants could indeed be identified, and that riluzole and edaravone were not functionally protective against the ER stress. To the possibilities that ER stressor/ALS drug kinetics were not optimized or that the ALS drugs work in non-ER related assays or specific ALS patient cohorts, corroboratory data in a large (∼50) ALS iPSC-derived cohort using extended maturation times (>45 days in culture) to reveal ALS MN neurite regression, cytotoxicity, and FUS + or phosphorylated-TDP-43 + protein aggregates, has also demonstrated that riluzole and edaravone fail to protect against these degenerative phenotypes in ALS MNs (Fujimori et al., 2018). Together, this study and our work support the interpretation that riluzole and edaravone do not robustly protect human MNs, and that the inefficacy of these drugs are not likely due to the stressor employed, drug kinetics/dynamics, or a differential response from certain ALS patient lines.

As kenpaullone had such a pronounced ability to protect patient MNs, but has multiple cellular targets (Leost et al., 2000; Yang et al., 2013) and is unlikely to be CNS penetrant (Kitabayashi et al., 2019), we aimed to gain further insight into its protective effects in the hopes of identifying additional, druggable targets for MN degeneration in ALS. Previous work indicated that MAP4K4 was among the kinases inhibited by kenpaullone (Yang et al., 2013) and that inhibition of MAP4K4 alone was sufficient to protect against trophic factor withdrawal-induced ALS MN degeneration (Wu et al., 2019). Therefore, we next tested whether treatment with a more selective compound inhibitor of MAP4K4 (MAP4K4 inhibitor 29), (Crawford et al., 2014) would also confer protection from ER stress. We found that MAP4K4 inhibitor 29 indeed protected viability and neurite morphology in response to both ER stressors, in control 1016A, TDP-43, and SOD1 fALS patient MNs, similar to kenpaullone (**Figures 3C, D**). In addition to confirming the robustness of our platform for modeling ER stress-associated MN toxicity and finding neuroprotective drugs, these results provide further evidence that inhibition of MAPK4K is protective of MNs.

2.4 Pharmacological MAP4K4 inhibition protected MNs against ER stress-associated toxicity despite UPR induction

Since exposure to thapsigargin and tunicamycin rapidly upregulates UPR-associated signaling pathways eventually leading to cell death, we sought to explore whether kenpaullone and MAP4K4 inhibition protected against ER stress by directly blocking these signaling cascades. To test this, we exposed healthy control 1016A iPSC-derived MNs to thapsigargin in the presence or absence of kenpaullone or MAP4K4 inhibitor 29 and evaluated protein level expression of the chaperone BiP and the stress induced transcription factor CHOP via Western blot. We observed sustained upregulation of both BiP and CHOP in cultures treated with kenpaullone or the MAP4K4 inhibitor (**Figure 3E**), consistent with a mechanism independent of blocked UPR induction.

2.5 Phosphoproteomic analyses identified JNK, PKC, and BRAF as convergent cellular perturbations of protective MAP4K4 inhibitors

Results thus far demonstrated the ability of kenpaullone and a MAP4K4 inhibitor to protect against MN death under various conditions, corroborating Wu et al. (2019). However, MAP4K4 shares a high degree of structural similarity to other upstream MAP kinases, including MINK1, with nearly 100% sequence homology at the kinase ATP-binding pocket. Moreover, studies have demonstrated that small molecule inhibitors of MAP4K4 also target additional kinases including MINK1 and TNIK (Larhammar et al., 2017; Bos et al., 2019). As a result, we sought to further define the landscape underlying pharmacological MN protection conferred by MAP4K4 inhibition in the presence of prolonged ER stress. To do so, we performed global phosphoproteomic analyses on healthy control 1016A iPSC-derived MN cultures treated with thapsigargin in the presence or absence of kenpaullone or MAP4K4 inhibitor 29 (**Supplementary Figure 2A**). To best capture more late stage degenerative signaling pathways, while still ensuring detection of protective signaling pathways in populations of surviving cells, total protein lysates from MN cultures were

10.3389/fncel.2023.1327361

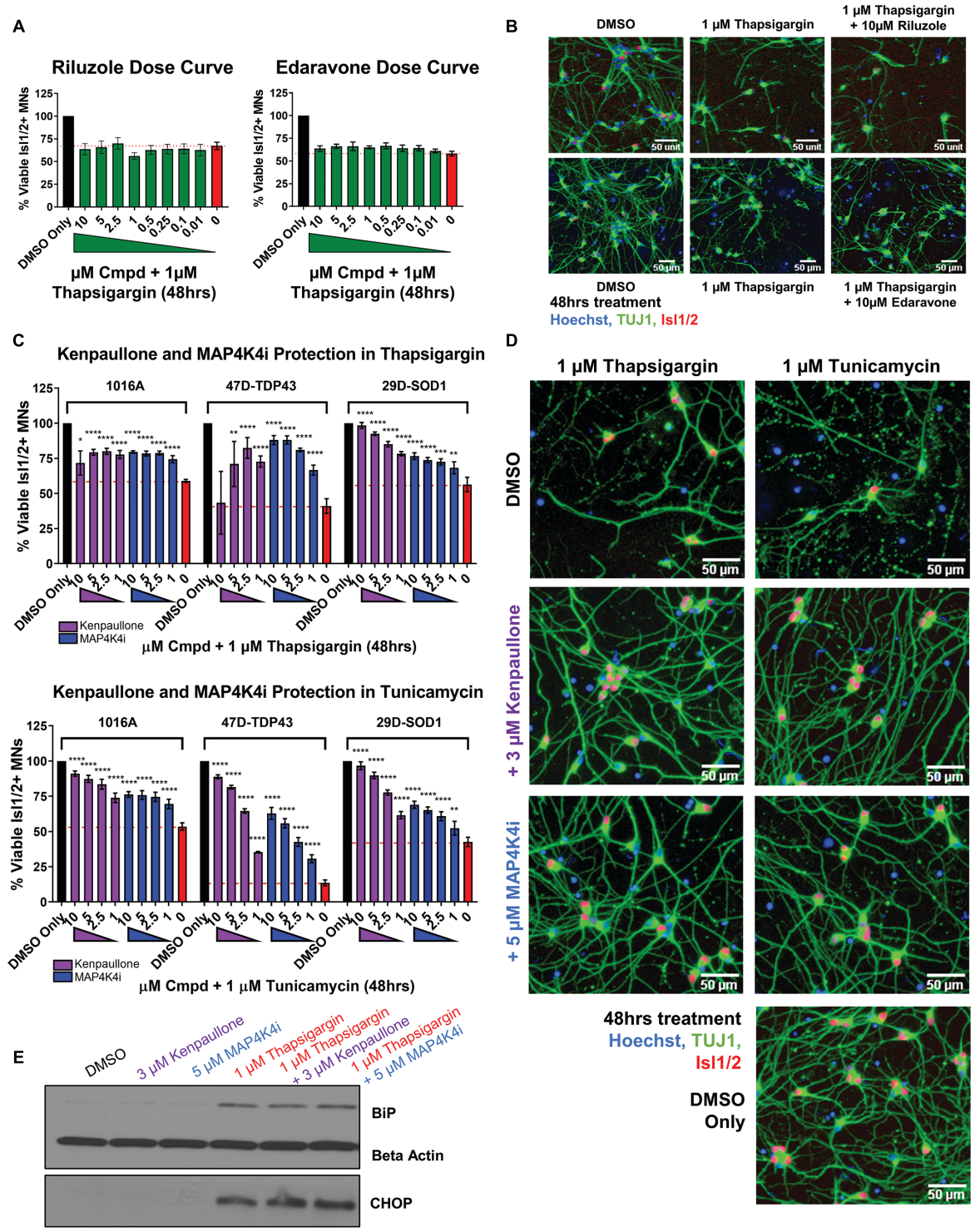

FIGURE 3

MAP4K4 inhibitors preserve MN viability better than the current FDA approved ALS drugs without reducing UPR induction. **(A)** Quantification of MN viability in 1016A healthy control iPSC-derived cultures treated for 48 h with various doses of Riluzole or Edaravone in 1 μM thapsigargin. Nb = 3, nt = 3. **(B)** Representative immunofluorescent staining of 1016A healthy control iPSC derived MNs in control (DMSO), thapsigargin, or Riluzole/Edaravone thapsigargin treated conditions. **(C)** Quantification of healthy patient MN viability (1016A) or ALS patient MN viability (47-TDP-43^{G298S} mutant or 29D-SOD1^{L144F} mutant) after 48 h treatment with various doses of kenpaullone or MAP4K4 inhibitor 29 in ER stress conditions (1 μM thapsigargin or tunicamycin). Nb = 3, nt = 3, *$p < 0.05$, **$p < 0.01$, ***$p < 0.001$, ****$p < 0.0001$ one-way ANOVA with Tukey's hsd *post-hoc* test. **(D)** Representative immunofluorescent images of ALS TDP-43^{G298S} mutant patient derived MN cultures in control (DMSO), ER stress, or ER stress and kenpaullone/MAP4K4 inhibitor 29 rescued conditions. **(E)** Western blot analyses of BiP and CHOP in 1016A healthy control iPSC-derived MN cultures treated with either DMSO vehicle, 3 μM kenpaullone, 5 μM MAP4K4i, 1 μM thapsigargin, or kenpaullone/MAP4K4i in thapsigargin. Nb = 3. Biological replicate experiments denoted as Nb, each with technical replicate experiments nt. Data are mean value ± SEM.

collected at 24 and 48 h, after treatment with a low dose of thapsigargin (0.1 vs. 1 μM) (**Supplementary Figure 2A**).

From 2 biological replicate experiments, a total of 67,357 and 59,708 peptides, and 28,399 and 28,973 phosphopeptides were quantified. This corresponded to 6,697 unique proteins, 2,764 unique phosphoproteins and 7,999 non-redundant phosphorylation sites, with the changes in phospho-site abundance being normalized to protein levels when possible (**Supplementary Table 1** and Supplementary Data Set 1). We first observed that thapsigargin treatment alone drove the largest alterations in the proteome and phosphoproteome (**Figure 4A**, *S2B*). Significantly upregulated proteins in thapsigargin treated conditions included the ER chaperone BiP (HSPA5) and the pro-apoptotic protein Bcl-2 binding protein 3 (BBC3), consistent with our results showing thapsigargin induces UPR-driven apoptosis in human MNs (**Figures 2**, **4A**). Gene ontology analysis of significantly upregulated proteins (FDR < 0.05) in thapsigargin-stressed cells revealed enriched terms including "response to endoplasmic reticulum stress" and "positive regulation of cytosolic calcium ion concentration" (**Figure 4B**), consistent with known effects of thapsigargin as an inhibitor of the ER calcium ATPase pump (cytosol to ER calcium transporter).

In addition to thapsigargin, we observed that kenpaullone exposure significantly perturbed the phosphoproteome (**Figure 4C**, *S2C*). As expected, known targets of kenpaullone, including phosphorylated MAP4K4 and GSK3β/α, were notably decreased with kenpaullone treatment alone (**Figure 4C**). Moreover, gene ontology terms of the significantly dysregulated proteins from kenpaullone treatment largely indicated changes in neuron extension processes, including: "positive regulation of axon extension," "neuron projection development," "dendrite morphogenesis," and "microtubule cytoskeleton organization" (**Figure 4D**), with the main drivers of these changes including the microtubule plus-end tracking protein CLASP2, the neuronal guidance microtubule assembly protein DPYSL2, and the microtubule associated proteins MAP1B and MAPT (**Figure 4C**). Since cultures treated with the more selective MAP4K4 inhibitor 29 did not exhibit changes in these microtubule proteins, it is likely that these phosphoproteomic changes were due to kenpaullone's dual inhibition of GSK3β and CDK5, rather than MAP4K4 inhibition, consistent with previously published work (Reinhardt et al., 2019). Downregulation of "apoptotic signaling pathways" was also observed in the gene ontology terms (**Figure 4D**), further supporting the pro-survival effect observed with kenpaullone treatment.

As treatment with the MAP4K4 inhibitor resulted in few, if any, statistically significant changes in individual proteins, we next utilized pathway enrichment analyses on the total datasets to interrogate how incremental changes in functional groups of proteins might be conferring protection by MAP4K4 inhibitor 29. Unbiased hierarchical clustering of kinase-substrate enrichment analyses revealed several kinase pathways commonly downregulated by both kenpaullone and MAP4K4 inhibitor 29 (**Figure 4E**), including an expected decrease in the JNK pathway (annotated as MAPK8/9/10), a known downstream pro-apoptotic target of MAP4K4 signaling. Additionally, several unexpected targets were commonly altered between kenpaullone and MAP4K4 inhibitor 29 treatment, including protein kinase family members (PRKD1, PRKCG, PRKC1, PRKCB, PRKCE) as well as RAFs (BRAF, ARAF, RAF1), suggesting that these proteins might also play a neuroprotective role in MNs. Since Kenpaullone and MAP4K4 inhibitors both demonstrate a similar degree of MN protection, we were most interested in pursuing protective targets that were shared between the two compounds. This ultimately led us to pursue the JNK, PKC and RAF targets further. However, there remains a wealth of information in the proteomics dataset that can continue to be interrogated for identification of functional MN protectants. We have categorized all protective processes and targets implicated for each compound into discrete functional groups in **Supplementary Table 2**.

2.6 Small molecule inhibitors to JNK, PKC, and BRAF prevented ER stress-associated MN death

To next assess if the shared pathways dysregulated by kenpaullone and MAP4K4 inhibitor 29 were functionally consequential in MN survival, we tested selective small molecule inhibitors of JNK (SP600125), PKC (Enzastaurin), and BRAF (GDC-0879) in an 8-point dose response survival curve on healthy control 1016A MNs treated with thapsigargin stress. In line with our work and that of others implicating JNK signaling in ALS MN degeneration (Bhinge et al., 2017; Wu et al., 2019), we observed that the JNK inhibitor SP600125, as well as the PKC inhibitor Enzastaurin and the BRAF inhibitor GDC-0879, all preserved MN viability and TUJ1 + neurite networks to levels comparable to those obtained with kenpaullone or MAP4K4 inhibitor 29 (**Figures 5A, B**). These small molecule inhibitors also significantly protected MN numbers and neurite morphology in the presence of tunicamycin stress (**Figures 5C, D**), indicating the protection was not thapsigargin-specific.

3 Discussion

Amyotrophic lateral sclerosis is an extremely complex MN disease with few therapeutic options. Recent advances in generating MNs from healthy control and ALS patient iPSCs have greatly helped address limitations of traditional rodent models and improved drug discovery by enabling scalable production of affected cells for high-throughput drug screening (Dimos et al., 2008; Fujimori et al., 2018). Here, we sought to build upon traditional iPSC models of ALS by inducing chemical ER stress in ALS patient MN cultures, and subsequently employing mass spectrometry to identify pathways altered downstream of ER stress-induced toxicity. In doing so, we observed that chemical ER stressors led to activation of the UPR, neurite degeneration, and preferential MN death, in both healthy control and ALS patient MN cultures. We further found that these culture systems could predict neuroprotective targets discovered in other ALS models, and identified several novel neuroprotective agents, including a PKC inhibitor Enzastaurin and an FDA approved BRAF inhibitor GDC-0879.

One hallmark of ALS sometimes overlooked in cell culture models, includes differential MN vulnerability, where upper MNs in the motor cortex of the brain and lower MNs in the

10.3389/fncel.2023.1327361

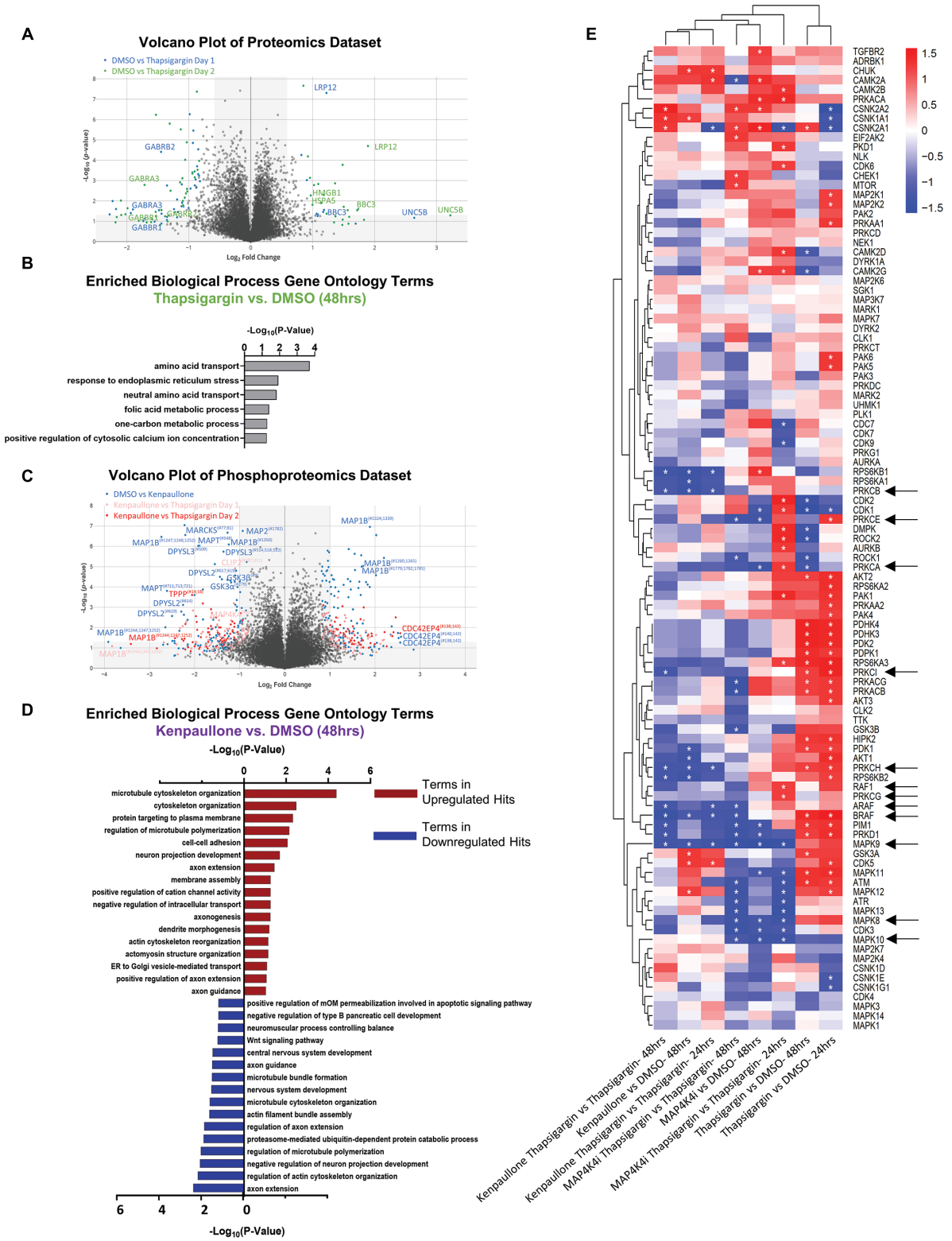

FIGURE 4

Proteomic and phosphoproteomic analyses of degenerating MNs protected with MAP4K4 inhibitors. **(A)** Volcano plot of all proteins quantified in the proteomics dataset. Individual proteins are represented as single dots. **(B)** Gene ontology analyses of significantly upregulated proteins in response to thapsigargin treatment. **(C)** Volcano plot of all phosphoproteins quantified in the phosphoproteomics dataset. Individual phosphoproteins are represented as single dots, with round shapes indicating normalized phosphoprotein levels (to protein levels), and diamond shapes indicating non-normalized phosphoprotein levels (due to lack of non-phosphorylated protein quantification). Selected phosphoproteins are annotated with the phosphorylation site position indicated as a superscript. **(D)** Gene ontology analyses of the significantly upregulated phosphoproteins or downregulated phosphoproteins in response to kenpaullone treatment. **(E)** Unbiased hierarchical clustering of kinases whose phosphosubstrates were perturbed with compound treatments [identified by kinase-substrate enrichment analyses (KSEA)]. z-scores of each experiment are plotted, with asterisks denoting FDR q-values < 0.05. Red boxes indicate upregulated kinase substrates; blue boxes indicate downregulated kinase substrates. *FDR q-values <0.05.

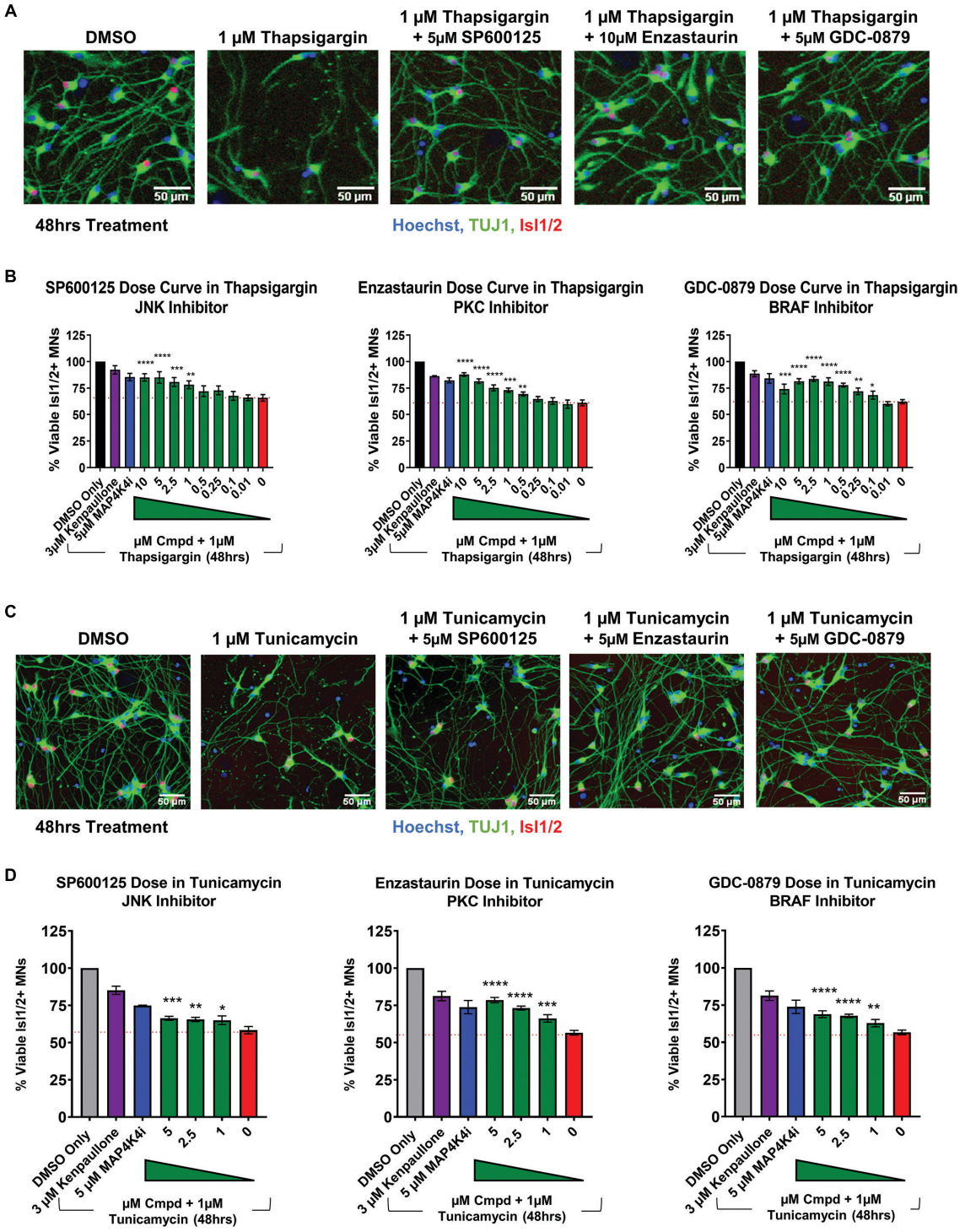

FIGURE 5
Small molecule inhibitors to JNK, PKC, and BRAF are MN protective compounds. **(A)** Representative immunofluorescent images of healthy control 1016A iPSC-derived MN cultures in control (DMSO), thapsigargin stress, or small-molecule-inhibitor-rescued conditions. **(B)** Quantification of MN viability in healthy control 1016A iPSC-derived MN cultures after 48 h treatment with various doses of small molecule inhibitors in 1 µM thapsigargin. A total of 3 µM kenpaullone or 5 µM MAP4K4i in thapsigargin stress were used as positive controls, DMSO vehicle only as a negative control. Nb ≥ 3, nt = 3, *$p < 0.05$, **$p < 0.01$, ***$p < 0.001$, ****$p < 0.0001$ one-way ANOVA with Tukey's hsd *post-hoc* test. **(C)** Representative immunofluorescent images of healthy control 1016A iPSC-derived MN cultures treated with control vehicle (DMSO), 1 µM tunicamycin, or 1 µM tunicamycin with 5 µM small molecule-inhibitors. **(D)** Quantification of MN viability in healthy control 1016A iPSC-derived MN cultures after 48 h treatment with various doses of small molecule inhibitors in 1 µM tunicamycin. A total of 3 µM kenpaullone or 5 µM MAP4K4i in tunicamycin stress were used as positive controls, DMSO vehicle only as a negative control. Please note that values for tunicamycin, kenpaullone and MAP4K4i rescue in Enzastaurin and GDC-0879 dose curves are the same as these experiments were performed on the same plate. Nb = 3, nt = 3, *$p < 0.05$, **$p < 0.01$, ***$p < 0.001$, ****$p < 0.0001$ one-way ANOVA with Tukey's hsd *post-hoc* test. Biological replicate experiments denoted as Nb, each with technical replicate experiments nt. Data are mean value ± SEM.

brainstem and spinal cord are disproportionately damaged in patients relative to other CNS cell types (Ferraiuolo et al., 2011; Ragagnin et al., 2019). To recapitulate this phenomenon in our model, we employed a MN differentiation protocol known to produce MNs as well as non-MN cell types of LMC identity, including interneurons and glia. Consistent with our reasoning, utilizing the heterogeneous culture of cells produced by this differentiation protocol, we observed that 2 mechanistically distinct ER stressors were both preferentially toxic to MNs compared to non-MN cell types in healthy and ALS patient cultures, demonstrating our model recapitulates this differential sensitivity and supports the proposition that perturbed ER homeostasis underlies intrinsic MN vulnerability in disease. Furthermore, as this MN selective phenotype was not observed with MG132, this indicates that different forms of proteostatic stress result in differential MN sensitivities.

Several studies suggest ER stress may underlie preferential toxicity of MNs relative to other neuronal populations in CNS disorders other than ALS. One example is Spinal Muscular Atrophy (SMA), a degenerative MN disease caused by a deficiency of the Survival of Motor Neuron (SMN) protein due to mutations in the SMN1 gene (Ng et al., 2015). Similar to ALS, in SMA, MNs are the most affected cell population–despite SMN being expressed equally across cell types. Previous work has demonstrated that SMA iPSC-derived MNs exhibited increased levels of UPR signaling components (e.g., ATF6, sXBP1, PERK, CHOP) compared to healthy control iPSC-derived MNs, and that inhibiting ER stress rescued SMA MN toxicity and other disease-associated phenotypes (e.g., SMN levels) (Ng et al., 2015). Together, these data as well as those reported here provide support for the hypothesis that MNs are intrinsically more vulnerable to ER stress, and that this vulnerability may underlie the cell-type specific degeneration observed in ALS, SMA, and other MN diseases.

As ALS is commonly sporadic with complex environmental and age-related dysfunctions significantly contributing to disease, it was important that selective vulnerability of MNs not only be observed in ALS MNs but in healthy control MNs as well. We reasoned that inducing human MN degeneration, even in MNs not affected with a defined fALS mutation, would aid in the identification of neuroprotective agents that would be effective against multiple forms of MN disease (Yang et al., 2013). Demonstrating that thapsigargin and tunicamycin universally caused an ALS-associated phenotype of preferential MN degeneration in all human MN cultures in an accelerated and reproducible timeline enabled development of a drug discovery platform compatible for high throughput drug screening assays compared to extended culture systems typically used.

To be useful for ALS drug discovery, screening-based assays must demonstrate an ability to predict neuroprotective drugs. We demonstrated this potential in our ER stressor assays using kenpaullone, a published MN protective agent identified by our group (Yang et al., 2013) and validated by others (Reinhardt et al., 2019; Thams et al., 2019), as well as a small molecule inhibitor to MAP4K4, one of kenpaullone's targets (Yang et al., 2013; Crawford et al., 2014). We found that both compounds were able to increase control, SOD1 and TDP-43 fALS MN viability and neurite morphology, and that this rescue was greater than that of riluzole or edaravone, 2 FDA approved drugs for ALS. The inefficacy of riluzole and edaravone to confer neuroprotection is important to note. Our results are indeed largely consistent with those from the Okano group (Yang et al., 2013; Fujimori et al., 2018) who also demonstrated that these ALS treatments failed to protect against ALS MN neurite regression, cytotoxicity, and FUS + or phosphorylated-TDP-43 + protein aggregates following extended culture maturation times (∼ 40–70 days). The inefficacy of both compounds in these platforms is unlikely due to a limitation of either assay to detect protective compounds with mechanistically distinct actions. Since riluzole and edaravone both only modestly prolong patient survival and improve motor function, these data leave open the possibility that drugs with more robust *in vitro* MN protective activity may benefit patients more than the existing ALS treatments (Andrews et al., 2020; Samadhiya et al., 2022; Witzel et al., 2022).

In this study, we combined the scalability of human stem cell-based MN cultures with mass spectrometry to capture the entire proteomic and phosphoproteomic temporal landscape in MNs exposed to degenerative stress or protective small molecules. In doing so, we observed expected molecular changes, including decreased JNK and cJUN signaling with both MN protective agents kenpaullone and MAP4K4 inhibitor 29, and that pharmacological reduction of this signaling pathway with a JNK inhibitor (SP600125) was protective. Moreover, we discovered that protein kinase family members (PRKD1, PRKCG, PRKC1, PRKCB, PRKCE) and RAFs were also significantly dysregulated with kenpaullone and MAP4K4 inhibitor 29, and identified Enzastaurin (a PKC inhibitor), and GDC-0879 (a B-RAF inhibitor), as protective in our ER stress MN assay. Enzastaurin has been determined to be well-tolerated in clinical trials (Ma and Rosen, 2007; Bourhill et al., 2017), and GDC-0879 is already in clinical development for certain cancers, highlighting the notion that current drugs may be re-purposed for ALS therapeutics.

In a variety of studies, PKC and BRAF have been associated with neuronal viability in a context-dependent manner (Nishizuka, 1986; Kolch, 2001; Tanaka and Koike, 2001; Wiese et al., 2001; Zhu et al., 2004; Frebel and Wiese, 2006). Here, in ALS patient-specific iPSC-derived MNs, we observed a neuroprotective effect for PKC inhibition via Enzastaurin, that we speculate to be via activation of the AKT pro-survival pathway based on data from rat cerebellar granule cell neurons (Zhu et al., 2004). BRAF is a proto-oncogene with reported roles in embryonic MN and sensory neuron survival in response to neurotrophic factors (Wiese et al., 2001; Davies et al., 2002). Compound inhibitors to BRAF, including GDC-087, target the $BRAF^{V600E/K}$ tumors, exhibiting paradoxical activation of the MEK/ERK pro-survival pathway in cells with $BRAF^{WT}$ via RAF transactivation (Agianian and Gavathiotis, 2018; Sieber et al., 2018; Uenaka et al., 2018). Here, we speculate that BRAF inhibition with GDC-0879 protects patient MNs challenged with ER stress due to restored activation of MAPK/ERK pro-survival signaling.

Ultimately, these data demonstrate that pharmacologic ER stress induces toxicity in iPSC-derived cultures by initiating the UPR and apoptosis, resulting in neurite degeneration and MN death (**Figure 6A**). By combining this model of MN toxicity with proteomics and phosphoproteomics, we identified druggable targets capable of protecting ALS MNs from ER stress-associated toxicity, including PKC and BRAF signaling components (**Figure 6B**). Despite this, however, understanding the precise mechanisms by which small molecules utilized in this study (MAP4K4, BRAF, JNK, and PKC inhibitors) attenuate MN

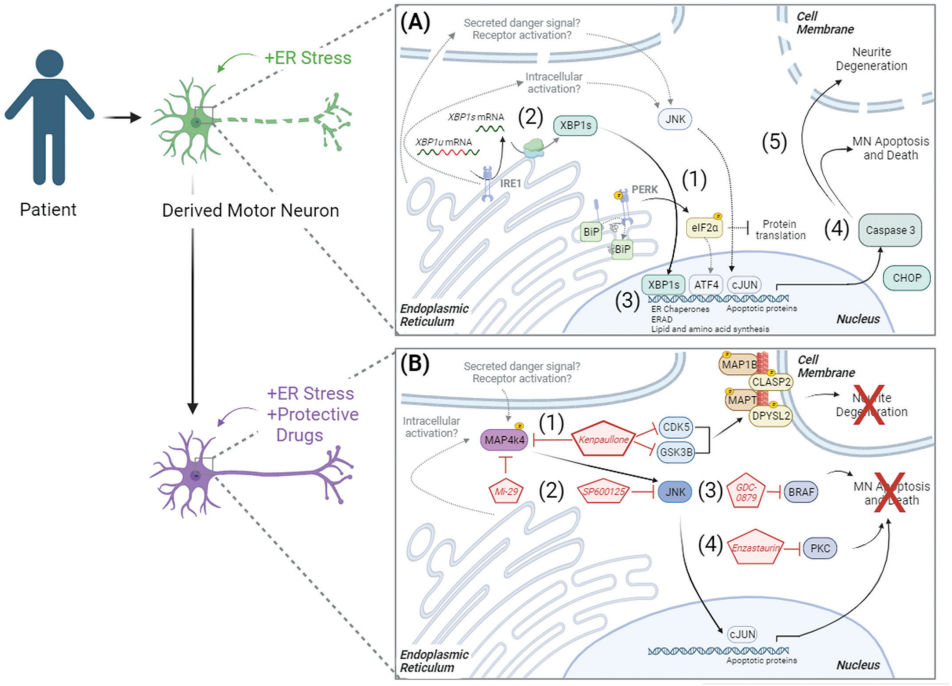

FIGURE 6
Model of ER stress induced preferential MN degeneration and pharmacological protection. ER stress induced preferential MN degeneration in both healthy and ALS patient MN cultures, and small molecule inhibitors to intracellular signaling pathways could protect against this MN degeneration. **(A)** In conditions of ER stress, the unfolded protein response was activated, with (1) PERK-mediated phosphorylation of eIF2α and (2) IRE1-mediated splicing of XBP1 upregulating protein folding chaperones BIP (3), ER associated degradation (ERAD) proteins, and lipid and amino acid biosynthesis. With chronic/prolonged UPR signaling, apoptotic proteins like CHOP were upregulated and caspase 3 was cleaved (4), driving neurite degeneration and MN apoptosis (5). **(B)** In the presence of neuroprotective compounds, ER stress induced MN death was attenuated. (1) Kenpaullone mediated MN protection through the dual inhibition of GSK3β and CDKs, which reduced the aberrant hyperphosphorylation of microtubule associated proteins, as well as through the inhibition of MAP4K4. (2) MAP4K4 inhibition by kenpaullone or the more selective MAP4K4 inhibitor 29 (Mi-29) promoted MN protection by attenuating the pro-apoptotic JNK/cJUN pathway. Specific inhibition of JNK with SP600125 additionally conferred MN protection. PKC and BRAF were additional proteins commonly dysregulated by the protective agents kenpaullone and MAP4K4 inhibitor 29, and a BRAF inhibitor GDC-0879 (3) and a PKC inhibitor Enzastaurin (4) also functionally promoted MN protection. Proteins and pathways experimentally determined in this publication are colored with black arrows. Proteins and pathways not experimentally detected in this publication, but with literature support, are non-colored with dashed gray arrows.

damage downstream of ER stress requires further exploration. For example, it remains unclear how MAP4K4 is activated in instances of ER stress and MN death. We hypothesize either an intracellular activation mechanism related to UPR signaling and/or an extracellular activation mechanism via a secreted protein or receptor activation (Figure 6B, lower panel). Moreover, the neuroprotective mechanisms underlying Enzastaurin and GDC-0879 remain unclear. Despite these opportunities for future investigation, these data demonstrate the utility of exacerbating ER stress in patient-derived MNs in a scalable manner to identify pathways underlying MN toxicity in disease and identify novel neuroprotective compounds.

4. Materials and methods

4.1 hiPSC culture

All human induced pluripotent stem cell (hiPSC) culture was performed with approval by the institutional review board and the Harvard Committee on the Use of Human Subjects. hiPSC cultures were maintained at 37°C with 5% CO_2 in a Thermo Fisher Scientific biological incubator. hiPSCs were cultured with supplemented StemFlex medium (Thermo Fisher Scientific) on Matrigel-coated (BD Biosciences) tissue culture plates. Cells were fed every other day and passaged at ∼80% confluency using 5 min of room temperature 0.5 mM EDTA (Life Technologies) followed by mechanical disruption with a cell lifter. All cell lines were confirmed genotypically correct, karyotypically normal by analysis of 20 metaphase spreads by Cell Line Genetics or WiCell Cytogenetics, and free of mycoplasma contamination using the LookOut Mycoplasma PCR Detection Kit (Sigma Aldrich) or the MycoAlert PLUS Mycoplasma Detection Kit (Lonza).

4.2 MN differentiation and dissociation

hiPSCs were differentiated into MNs as described previously (Maury et al., 2015; Neel et al., 2023). Briefly, confluent (60–90%) hiPSC cultures were first detached from Matrigel (BD Biosciences) coated plates and dissociated into single cells using 37°C Accutase (Stem Cell Technologies) for ∼5 min. Accutase was quenched and single cells were seeded for differentiation in suspension at a density of 1×10^6 cells/mL in complete mTeSR media (Stem

Cell Technologies) supplemented with 10 ng/mL FGF2 (Peprotech) and 10 μM ROCK-inhibitor Y-27632 (Stemgent). A total of 24 h after seeding, cells were filtered through a 100 μm cell strainer (VWR) and additional, equal volume complete mTeSR media (Stem Cell Technologies) was added. A total of 48 h after seeding (differentiation day 0), mTeSR media was replaced with N2B27 MN differentiation media, composed of a v:v mixture of DMEM/F12 and Neurobasal media (Life Technologies), supplemented with 1% N2 (Life Technologies), 2% B27 (Life Technologies), 1% Pen-Strep (Life Technologies), 1% Glutamax (Life Technologies), 0.1% beta-mercaptoethanol (βME, Life Technologies), and 20 μM ascorbic acid (Sigma Aldrich). Day 0 and day 1 of differentiation, N2B27 MN differentiation media was supplemented with 10 μM SB-431542 (R&D Systems), 100 nM LDN-193189 (ReproCELL), and 3 μM CHIR-99021 (ReproCELL). Day 2 and Day 4, differentiation media was supplemented with 10 μM SB-431542, 100 nM LDN-193189, 3 μM CHIR-99021, 1 μM retinoic acid (Sigma Aldrich), and 1 μM smoothened agonist (DNSK International, LLC). Day 5, differentiation media was supplemented with 1 μM retinoic acid, and 1 μM smoothened agonist, Day 7 with 1 μM retinoic acid, 1 μM smoothened agonist, and 20 ng/mL brain derived neurotrophic factor (BDNF, R&D Systems). Day 9, differentiation media was supplemented with 1 μM retinoic acid, 1 μM smoothened agonist, 20 ng/mL BDNF, and 10 μM DAPT (R&D Systems). Day 11 and 13, differentiation media was supplemented with 1 μM retinoic acid, 1 μM smoothened agonist, 20 ng/mL BDNF, 10 μM DAPT, and 20 ng/mL glial derived neurotrophic factor (GDNF, R&D Systems).

Day 15 of differentiation, embryoid bodies (EBs) were collected, washed once with 1x phosphate buffer solution (PBS) without calcium and magnesium (VWR), and dissociated with 0.25% Trypsin-EDTA (Life Technologies) and 50 μg/mL DNase1 (Worthington Biochemical) for 5 min at 37°C with movement. Trypsin was quenched with fetal bovine serum (FBS, Sigma Aldrich), and centrifuged at 400 × *g* for 5 min. The cell pellet was then resuspended in dissociation buffer, consisting of 5% fetal bovine serum (FBS, Sigma Aldrich), 25 mM glucose, 1% Glutamax, in 1x PBS without calcium and magnesium, and mechanically triturated using a p1000 pipet. Dissociated single cells were pelleted by centrifugation (400 × *g*, 5 min) and resuspended in complete MN media, consisting of Neurobasal media supplemented with 1% N2, 2% B27, 1% Pen-Strep, 1% Glutamax, 1% Non-essential amino acids (Life Technologies), 0.1% βME, 20 μM ascorbic acid, 20 ng/mL BDNF, GDNF, and CNTF (ciliary neurotrophic factor, R&D Systems), and 10 μM UFDU [v:v Uridine (Sigma Aldrich):Fluorodeoxyuridine (Sigma Aldrich)]. Resuspended dissociated single cells were filtered through a 40 μm cell strainer, counted with a 1:1 trypan blue dilution using an automated cell counter, and plated at the desired density on tissue culture treated plates coated with 1X borate buffer (Life Technologies), 25 μg/mL poly-ornithine (Sigma Aldrich), 5 μg/mL mouse laminin (Life Technologies), and 10 μg/mL fibronectin (VWR).

4.3 ER stressor assays

For survival analyses, dissociated MNs were plated in complete MN media at a density of 50,000 cells/well (unless otherwise indicated) in the inner 60 wells of borate/poly-ornithine/laminin/fibronectin coated 96-well plates (Perkin Elmer). Outer wells were filled with water to avoid evaporation effects. A total of 3 days after plating, 3/4 media was removed and replaced with fresh complete MN media. A total of 6 days after plating, all media was removed, and MN cultures were treated simultaneously with ER stressor media or ER stressors with protective compounds. Unless otherwise indicated in dose response curves, 1 μM of thapsigargin (Sigma Aldrich) or 1 μM tunicamycin (Sigma Aldrich) were used for standard stressor conditions, and 3 μM of kenpaullone (Tocris) and 5 μM of MAP4K4 inhibitor 29 (Genentech) in 1 μM ER stressor media were protective positive controls. A total of 0.1% DMSO (Sigma Aldrich) complete MN media was the negative control, and total concentration of DMSO was equal to 0.1% in all wells. MNs were incubated with stressors, protective compounds, and test compounds, for 48 h and fixed with 4% paraformaldehyde (PFA, VWR) prior to quantitative analysis of Isl1/2 (Abcam), TUJ1 (Biolegend) and Hoechst (Life Technologies) staining as described in Immunofluorescent staining and high content image analysis methods section. All cell counts were expressed as a percentage of surviving DMSO-control cells.

For gene expression analyses, dissociated MNs were plated in complete MN media at a density of 2×10^6 cells/well of 6-well plates coated with borate, poly-ornithine, laminin, and fibronectin. A total of 3 or 6 days after plating, media was removed and MN cultures were treated with 1 μM thapsigargin, tunicamycin, MG132 stressor media, alone or with 3 μM of kenpaullone (Tocris) or 5 μM of MAP4K4 inhibitor 29 (Genentech). Equal concentration DMSO was used as a negative control. Samples were collected at the appropriate timepoints for RNA and protein expression analyses as described in Protein extraction and western blotting and RNA isolation, reverse transcription, and quantitative PCR methods sections.

4.4 Immunofluorescent staining and high content image analysis

Cells were fixed for 15 min at room temperature with 4% paraformaldehyde (PFA, Sigma Aldrich) in PBS, achieved by adding equal volume 8% PFA to equal volume culture media. Fixed cells were gently washed once with PBS, then blocked with 10% normal goat serum, 0.1% Triton X-100 in 1x PBS for 30 min at room temperature. Blocked cells were then incubated for 1 h at room temperature with primary antibodies anti-Isl1/2 (Abcam ab109517, 1:2000) and anti-TUJ1 (Biolegend 801202, 1:2000, or Novus Biologicals NB100-1612, 1:2000). Following primary antibody incubation, cells were gently washed once with PBS, and incubated for 1 h at room temperature with 2 μg/mL Hoechst (Life Technologies H3569) and species-matched, fluorophore-conjugated secondary antibodies (Life Technologies Alexa-488, -546, -555, or -647, 1:1000) diluted in 10% normal goat serum, 0.1% Triton X-100, in PBS. Immunofluorescent labeled cells were gently washed twice with PBS before image acquisition.

High content screening systems [Operetta (PerkinElmer) or ImageXpress (Molecular Devices)] were used for all image acquisition. Images were acquired automatically using a 10x or

20x objective, a solid-state laser light source, and a sCMOS (scientific complementary metal-oxide-semiconductor) camera, corresponding to 9–12 evenly distributed fields per well of each 96-well plate. Using these parameters, at least 2,000 cells were imaged per well of each 96-well plate, with typically >5,000 cells/well with normal assay conditions. Quantitative analyses of these images were then performed using the Columbus/Harmony image analysis software (PerkinElmer). Manually designed scripts were written to define a viable cell population, which consisted of intact, Hoechst-stained nuclei larger than ∼45 μm^2 (range 37–55) in surface area and with intensities lower than the threshold brightness of pyknotic nuclei (**Supplementary Figures 3A, B**). From this viable cell population, the neuron-specific βIII-Tubulin marker was used to define the neuronal population and neurite morphologies (as described below, **Supplementary Figure 4**). From the viable population, nuclear Isl1/2 antibody staining was used to define the MN population, using intensity thresholds that accurately reflect positive nuclear staining (**Supplementary Figure 3C**). With these set parameters, total numbers of nuclei, viable neurons, and viable MNs were then quantified automatically across the plate, ensuring unbiased measurements for all test conditions. Images were visually inspected during analysis and script generation, and after analysis to ensure data validity. All cell counts were then expressed as a percentage of surviving DMSO-control cells.

For neurite detection, the CSIRO neurite analysis 2 method (Harmony/Columbus, PerkinElmer) was used on βIII-Tubulin (TUJ1) staining of total Hoechst + nuclei populations. This generated a mask that traced and segmented neuritic processes extending from individual neurons (**Supplementary Figure 4**). Scripts were optimized per plate to achieve accurate neurite tracking, with the following parameters typically used- smoothing width at ∼2–3 px was used to suppress noise and obtain a single maximum intensity across the neurites with gaussian filtering; linear windows at ∼11px specified the dimension in pixels used to find local βIII-Tubulin intensity maxima and contrast parameters between 1 and 2.5 were used to decrease background noise. Small, spurious objects were eliminated by removal of small diameter objects >3 px, and extraneous lateral projections were cleaned using a debarb length of <9–15 px. Gap closure distance and tree length were optimized to ensure gaps between detected neurites were closed, without making false connections, and that neurite bodies were linked to their corresponding mother cell. All output counts were the values per neuron, averaged per well.

Representative images displayed in figures were cropped using FIJI/ImageJ. All automatic contrast settings in Harmony/Columbus were first disabled. Images were then selected for each condition, saved from the database, and imported into FIJI/ImageJ. A region of interest (ROI) was generated and used for each image per condition, allowing the preservation of equal image scale. Cropped images were then saved as final high-resolution TIFs.

4.5 Automated live cell imaging

Dissociated MNs were plated in complete MN media at a density of 50, 25, and 12.5 K cells/well in the inner 60 wells of borate/poly-ornithine/laminin/fibronectin coated 96-well plates (Greiner). Outer wells were filled with water to avoid evaporation effects. A total of 3 days after plating, 3/4 of the media was removed and replaced with fresh complete MN media. A total of 6 days after plating, and before treatment, the MN culture plate was entered into the Nikon BioStation CT for an initial image acquisition. A 10x objective was used to acquire phase images across the plate with a 4 × 4 stitched tiling capture area equivalent to 3.08 mm × 3.08 mm per well. After an initial image acquisition, the plate was removed, and MN culture media was replaced with stressor media as indicated in ER stressor assays methods section. The plate was then returned to the Nikon BioStation CT for image acquisition every 6 h for 48 h. Final images were then saved as time-lapse video files using CL-Quant software (Nikon) and FIJI/ImageJ was used to select and crop a region of interest for representative video files.

4.6 Protein extraction and western blotting

Protein from 2×10^6 cells was harvested on ice after 1 PBS wash using the Pierce RIPA lysis and extraction buffer (25 mM Tris–HCl, pH 7.6, 150 mM NaCl, 1% NP-40, 1% sodium deoxycholate, 0.1% SDS, Life Technologies) containing fresh protease and phosphatase inhibitors (Life Technologies). Collected samples sat on ice for an additional 30 min and were pulled through a 28G insulin syringe for complete lysis. Protein concentrations were then determined using the Pierce BCA Protein Assay Kit (Thermo Fisher Scientific). Equal amounts of protein samples (5–20 μg) were diluted in RIPA buffer and βME-Laemmli buffer (Bio-Rad Laboratories) to equal volumes and boiled for 7 min at 95°C. Denatured samples were then loaded and run on Criterion TGX (Tris-Glycine eXtended) precast gels (Bio-Rad) for ∼15 min at 80 V, and then ∼45 min at 150 V. Migrated proteins were transferred from the gels to PVDF membranes using the *Trans*-Blot Turbo Transfer System (Bio-Rad) and run settings of 2.5A, 25V, for 7 min. Equal loading and complete transfer were checked with Ponceau S (Sigma Aldrich) staining for 30 min, shaking. After removing Ponceau, membranes were blocked for 45 min with shaking in 5% non-fat milk diluted in 1x TBS-T or SuperBlock T20 (Life Technologies) for phosphoproteins. Blocked membranes were incubated with primary antibodies overnight at 4°C, with shaking, using the following primary antibodies: Phospho-eIF2α (Cell Signaling Technology 9721S, 1:1000), eIF2α (Cell Signaling Technology 9722S, 1:1000), GRP78 BiP (Abcam ab21685, 1:1000), CHOP (Cell Signaling Technology 2895T, 1:1000), Cleaved Caspase-3 (Cell Signaling Technology 9664S, 1:1000), Actin (Cell Signaling Technology 3700S, 1:5000), β-Tubulin (Abcam ab6046, 1:10,000), GAPDH (Life Technologies AM4300, 1:5000).

Primary antibody solutions were removed after overnight incubation, and membranes washed 3 times with 1x TBS-T for 5 min. Membranes were then incubated for 1 h, shaking, with species-matched secondary antibodies conjugated to horse radish peroxidase (Goat anti-Rabbit IgG (H + L) HRP, Life Technologies 31460, 1:5,000; Goat anti-Mouse IgG (H + L) HRP, Life Technologies 31430, 1:5000), diluted in block (5% milk or SuperBlock). Following 3 TBS-T washes, chemiluminescent signal was produced using the SuperSignal West Dura Extended Duration Substrate (Thermo Fisher Scientific) and membrane

signal was detected on film. All films were scanned using an EPSON scanner without automatic intensity contrast adjustments. Scanned images were cropped and measured for pixel intensity using FIJI/ImageJ. Figure quantifications display fold changes normalized for background film intensity and loading control protein.

4.7 RNA isolation, reverse transcription, and quantitative PCR

Total RNA was isolated from 2 × 10^6 cells with Trizol (Life Technologies) according to manufacturer's instructions. Briefly, cells were washed once with 1x PBS, on ice, and lysed with 250 μL Trizol Reagent and mechanical disruption using a cell lifter. A total of 50 μL of chloroform was added to the Trizol-cell extract, and samples were centrifuged at 12,000 × *g* at 4°C for 15 min. The aqueous phase was collected into a clean Eppendorf tube and 125 μL isopropanol, 15 μg GlycoBlue Coprecipitant (Life Technologies) were added. Samples were incubated for 10 min at room temperature, and then centrifuged at 12,000 × *g* at 4°C for 10 min. The RNA pellet was washed twice with 250 μL 75% ethanol, air-dried, and resuspended in 30 μL of 1x DNase1 buffer (Life Technologies). A total of 1 μL of amplification grade DNase 1 was then added and incubated for 15 min at room temperature to degrade contaminating genomic DNA. A total of 1 μL of 25 mM EDTA was added to each sample and incubated at 65°C for 10 min to quench the reaction.

Total RNA concentrations were analyzed using a nanodrop, and equal amounts of sample RNA were used to synthesize cDNA using the iScript Reverse Transcription Supermix for RT-qPCR (Bio-Rad). Per reaction, 4 μL of 5X iScript RT supermix was combined with 0.5–1 μg of total RNA, with water to a final volume of 20 μL. Sample reactions were then run through the following thermocycler conditions- 5 min at 25°C, 20 min at 46°C, and 1 min at 95°C.

Quantitative PCR (qPCR) was then performed on cDNA samples using Fast SYBR Green (Life Technologies). Per reaction, 5 μL of 2X Fast SYBR Green Master Mix was combined with 1 μL (50 ng) of cDNA sample, 1 μL of 10 μM forward and reverse primer solution, and 3 μL water. The following primer pairs were designed for target transcripts using Primer3Plus and validated using NCBI Blast and Geneious software (GAPDH forward 5′-TGACTTCAACAGCGACACCCA-3′, GAPDH reverse 5′-CACCCTGTTGCTGTAGCCAAA-3′; BiP forward 5′-TCTTCAGGAGCAAATGTCTTTGT-3′; BiP reverse 5′-CAT CAAGTTCTTGCCGTTCA-3′; CHOP forward 5′-AGGGCTAAC ATTCTTACCTCTTCA-3′, CHOP reverse 5′-GATGAAAATGGG GGTACCTATG-3′; ATF6 forward 5′-CTTTTAGCCCGGGACT CTTT-3′; ATF6 reverse 5′-TCAGCAAAGAGAGCAGAATCC-3′; IRE1 forward 5′-TCTGTCGCTCACGTCCTG-3′; IRE1 reverse 5′-GAAGCATGTGCTCAAACACC-3′). Technical triplicate reactions were set up for each sample and target primer in MicroAmp Optical 384-well Reaction Plates (Life Technologies), and reactions were run and analyzed on a Quant Studio 12 K Flex Real-Time PCR system (Thermo Fisher Scientific) following the standard Fast SYBER Green protocol. Melt curves for each target primer pair were analyzed to ensure amplification and quantification of a single PCR product. Differential gene expression was then determined using the ΔΔCT method and visualized as fold change values.

4.8 XBP1 splicing analysis

For XBP1 splicing analysis, 2 μl (100 ng) of cDNA samples were combined with 12.5 μl Phusion Hot Start Flex 2X Master Mix (New England Biolabs), 2.5 μL of 10 μM forward and reverse primer solution (forward: 5′-GGGGCTTGGTATATATGTGG-3′, reverse: 5′- CCTTGTAGTTGAGAACCAGG-3′) and water to a final reaction volume of 25 μl. Reactions were run with the following thermocycler conditions: 1 cycle of 98°C for 30 s; 40 cycles of 98°C for 10 s, 60°C for 30 s, and 72°C for 30 s; and 1 cycle of 72°C for 5 min. A total of 2 μg of resulting PCR products were then digested with Pst1-HF restriction enzyme (New England Biolabs) to cleave the unspliced XBP1 template. Digested PCR reactions were then run on a 2% agarose gel containing ethidium bromide at 135 V. Bands were observed using a ChemiDoc XRS + (Bio-Rad) and measured for pixel intensity using FIJI/ImageJ.

4.9 TUNEL assay

The Click-iT Plus TUNEL Assay for *in situ* Apoptosis Detection using an Alexa Fluor 647 dye (Life Technologies) was performed according to manufacturer's instructions. Cells were first fixed for 15 min at room temperature using 4% PFA diluted in 1x PBS. Samples were then permeabilized with 0.25% Triton X-100 in 1x PBS for 20 min at room temperature and washed twice with deionized water. Terminal deoxynucleotidyl transferase (TdT) reaction buffer was added to cells for 10 min at 37°C. TdT reaction buffer supplemented with TdT enzyme and EdUTP were then added for 60 min at 37°C for labeling of double-stranded DNA breaks. Following this incubation, cells were washed twice with 3% BSA in 1x PBS for 5 min each, and the Click-iT plus TUNEL reaction cocktail was added to cells at 37°C protected from light. Following 30 min of florescent labeling of EdUTP with click chemistry, the reaction mixture was removed, and cells were washed twice for 5 min with 3% BSA in 1x PBS. Cells were then stained with Hoechst, and immunofluorescent Isl1/2, and TUJ1 antibodies as normal for image acquisition and analysis of TUNEL + MNs.

4.10 ER stress/protection assay and sample collection for proteomic and phosphoproteomic analyses

3 × 10^6 patient derived MNs were plated in complete MN media on borate/poly-ornithine/laminin/fibronectin coated 6-well tissue culture plates. A total of 3-day old cultures were treated with 0.1 μM thapsigargin, 3 μM kenpaullone, 5 μM MAP4K4 inhibitor 29 or 0.1 μM thapsigargin with 3 μM kenpaullone or 5 μM MAP4K4 inhibitor 29. A total of 24 and 48 h after compound treatment, MN cultures were washed 3 times with chilled PBS, on ice, and total protein was collected using 200 μL/well of freshly

prepared lysis buffer containing 6 M urea (Life Technologies), 50 mM EPPS (Sigma Aldrich), 1% triton X-100 (Sigma Aldrich), 5 mM tris (2-carboxyethyl) phosphine (Thermo Fisher Scientific), 20 mM chloroacetamide (Sigma Aldrich), with 1x protease and phosphatase inhibitors (Life Technologies). Mechanical disruption with a cell lifter was used to collect the protein lysates into Eppendorf tubes which were then flash frozen in liquid nitrogen and stored at −80°C until mass spectrometry analysis.

4.11 Proteomics–Sample preparation and digestion

Protein concentrations from sample lysates were determined using the Bradford assay (Thermo Fisher Scientific). Proteins denatured in 1% SDS were subjected to disulfide bond reduction with 5 mM tris (2-carboxyethyl) phosphine (room temperature, 15 min) and alkylation with 20 mM chloroacetamide (room temperature, 20 min). Methanol-chloroform precipitation was then performed, adding 400 μL of 100% methanol to the 100/100 μL protein sample, vortexing 5 s, and then adding 100 μL of 100% chloroform and vortexing 5 s. A total of 300 μL of water was added to the sample, vortexed 5 s, and centrifuged for 1 min at 14,000 × *g* to generate distinct phase separations. The aqueous phase and organic phases were removed, leaving behind the protein disk that was washed twice with 400 μL 100% methanol, and centrifuged at 21,000 × *g* for 2 min at room temperature. Samples were resuspended in 100 mM EPPS, pH 8.5, containing 0.1% RapiGest and digested at 37°C for 2 h with LysC protease at a 200:1 protein-to-protease ratio. Trypsin was then added at a 100:1 protein-to-protease ratio and the reaction was incubated for 6 h at 37°C.

Tandem mass tag labeling of each sample was performed by adding 10 μl of the 20 ng/μL stock of TMT reagent along with acetonitrile to achieve a final acetonitrile concentration of approximately 30% (v/v). Following incubation at room temperature for 1 h, labeling efficiency of a small aliquot was tested, and the reaction was then quenched with hydroxylamine to a final concentration of 0.5% (v/v) for 15 min. The TMT-labeled samples were pooled together at a 1:1 ratio. The sample was vacuum centrifuged to near dryness, resuspended in 5% formic acid for 15 min, centrifuged at 10000 × *g* for 5 min at room temperature and subjected to C18 solid-phase extraction (SPE) (Sep-Pak, Waters).

4.12 Proteomics–TMT-labeled phosphopeptide enrichment

Phosphopeptides were enriched using Pierce Fe-NTA phosphopeptide enrichment kit (Thermo Fisher Scientific, A32992) following the provided protocol. In brief, combined TMT-labeled dried peptides were enriched for phosphopeptides, while the unbound peptides (flow through) and washes were combined and saved for total proteome analysis. The enriched phosphopeptides were dried down and fractionated according to manufacturer's instructions using High pH reversed-phase peptide fractionation kit (Thermo Fisher Scientific, 84868) for a final 6 fractions and subjected to C18 StageTip desalting prior to MS analysis.

4.13 Proteomics–Off-line basic pH reversed-phase (BPRP) fractionation

Unbound TMT-labeled peptides (flow through from phosphopeptide enrichment step) and washes were dried down and resuspended in 100 μl of 10 mM NH4HCO3 pH 8.0 and fractionated using BPRP HPLC (Paulo et al., 2016). Briefly, samples were offline fractionated over a 90 min run, into 96 fractions by high pH reverse-phase HPLC (Agilent LC1260) through an aeris peptide xb-c18 column (Phenomenex; 250 mm x 3.6 mm) with mobile phase A containing 5% acetonitrile and 10 mM NH_4HCO_3 in LC-MS grade H_2O, and mobile phase B containing 90% acetonitrile and 10 mM NH_4HCO_3 in LC-MS grade H_2O (both pH 8.0). The 96 resulting fractions were then pooled in a non-continuous manner into 24 fractions [as outlined in **Supplementary Figure 5** of (Paulo et al., 2016) and 12 fractions (even numbers) were used for subsequent mass spectrometry analysis]. Fractions were vacuum centrifuged to near dryness. Each consolidated fraction was desalted via StageTip, dried again via vacuum centrifugation, and reconstituted in 5% acetonitrile, 1% formic acid for LC-MS/MS processing.

4.14 Proteomics–Liquid chromatography and tandem mass spectrometry

Mass spectrometry data were collected using an Orbitrap Fusion Lumos mass spectrometer (Thermo Fisher Scientific, San Jose, CA, USA) coupled to a Proxeon EASY-nLC1200 liquid chromatography (LC) pump (Thermo Fisher Scientific). Peptides were separated on a 100 μm inner diameter microcapillary column packed in house with ∼35 cm of Accucore 150 resin (2.6 μm, 150 Å, Thermo Fisher Scientific, San Jose, CA, USA) with a gradient consisting of 5%–16% (0–78 min), 16–22% (78–98 min), 22–28% (98–110 min) (ACN, 0.1% FA) over a total 120 min at ∼500 nL/min. For analysis, we loaded 1/2 of each fraction onto the column. Each analysis used the Multi-Notch MS3-based TMT method (McAlister et al., 2014). The scan sequence began with an MS1 spectrum (Orbitrap analysis; resolution 120,000 at 200 Th; mass range 400-1400 m/z; automatic gain control (AGC) target 1×10^6; maximum injection time 50 ms). Precursors for MS2 analysis were selected using a Top 10 method. MS2 analysis consisted of collision-induced dissociation (quadrupole ion trap analysis; Turbo scan rate; AGC 2.0×10^4; isolation window 0.7 Th; normalized collision energy (NCE) 35; maximum injection time 150 ms) with MultiStage Activation (MSA) for neutral loss of 97.9763. Monoisotopic peak assignment was used, and previously interrogated precursors were excluded using a dynamic window (150 s ± 7 ppm). Following acquisition of each MS2 spectrum, a synchronous-precursor-selection (SPS) MS3 scan was collected on the top 10 most intense ions in the MS2 spectrum (McAlister et al., 2014). MS3 precursors were fragmented by high energy collision-induced dissociation (HCD) and analyzed using the Orbitrap (NCE 65; AGC 1.5×10^5; maximum injection time 250 ms, resolution was 50,000 at 200 Th).

Mass spectrometry data were collected using an Orbitrap Fusion Lumos mass spectrometer (Thermo Fisher Scientific, San Jose, CA, USA) coupled to a Proxeon EASY-nLC1200 liquid chromatography (LC) pump (Thermo Fisher Scientific). Peptides were separated on a 100 μm inner diameter microcapillary column packed in house with ~35 cm of Accucore 150 resin (2.6 μm, 150 Å, Thermo Fisher Scientific, San Jose, CA, USA) with a gradient consisting of 5%–22% (0–125 min), 22–28% (125–140 min) (ACN, 0.1% FA) over a total 150 min run at ~500 nL/min. For analysis, we loaded 1/10 of each fraction onto the column. Each analysis used the Multi-Notch MS3-based TMT method (McAlister et al., 2014), to reduce ion interference compared to MS2 quantification. The scan sequence began with an MS1 spectrum (Orbitrap analysis; resolution 120,000 at 200 Th; mass range 350-1400 m/z; automatic gain control (AGC) target 5×10^5; maximum injection time 50 ms). Precursors for MS2 analysis were selected using a Top10 method. MS2 analysis consisted of collision-induced dissociation [quadrupole ion trap analysis; Turbo scan rate; AGC 2.0×10^4; isolation window 0.7 Th; normalized collision energy (NCE) 35; maximum injection time 35 ms]. Monoisotopic peak assignment was used, and previously interrogated precursors were excluded using a dynamic window (150 s ± 7 ppm), and dependent scan was performed on a single charge state per precursor. Following acquisition of each MS2 spectrum, a synchronous-precursor-selection (SPS) MS3 scan was collected on the top 10 most intense ions in the MS2 spectrum (McAlister et al., 2014). MS3 precursors were fragmented by high energy collision-induced dissociation (HCD) and analyzed using the Orbitrap (NCE 65; AGC 3×10^5; maximum injection time 150 ms, resolution was 50,000 at 200 Th).

4.15 Proteomics–Data analysis

Mass spectra were processed using a Sequest-based (v.28, rev. 12) in-house software pipeline (Huttlin et al., 2010). Spectra were converted to mzXML using a modified version of ReAdW.exe. Database searching included all entries from the UniProt Human Reference Proteome database (2017–SwissProt and TrEMBL). Sequences of common contaminant proteins (for example, trypsin, keratins and so on) were appended and the database was concatenated with one composed of all size-sorted protein sequences in reverse order. Searches were performed using a mass tolerance of 20 p.m. for precursors and a fragment-ion tolerance of 0.9 Da, and a maximum of two missed cleavages per peptide was allowed. TMT tags on lysine residues and peptide N termini (+ 229.163 Da) and carbamidomethylation of cysteine residues (+ 57.021 Da) were set as static modifications (except when testing for labeling efficiency, in which case the TMT modifications are set to variable), while oxidation of methionine residues (+ 15.995 Da) was set as a variable modification. Peptide-spectrum matches (PSMs) were adjusted to a 1% false discovery rate (FDR) and PSM filtering was performed using a linear discriminant analysis, as described previously (Huttlin et al., 2010), while considering the following parameters: Xcorr and Diff Seq. Delta Score, missed cleavages, peptide length, charge state, and precursor mass accuracy. Using the Picked FDR method (Savitski et al., 2015), proteins were filtered to the target 1% FDR level. Moreover, protein assembly was guided by principles of parsimony to produce the smallest set of proteins necessary to account for all observed peptides. For TMT-based reporter ion quantitation, we extracted the summed signal-to-noise (S:N) ratio for each TMT channel and found the closest matching centroid to the expected mass of the TMT reporter ion (integration tolerance of 0.003 Da). Proteins were quantified by summing reporter ion counts across all matching PSMs using in-house software, as described previously (Huttlin et al., 2010). PSMs with poor quality, MS3 spectra with more than 8 TMT reporter ion channels missing, or isolation specificity less than 0.7 (or 0.6 for phosphorylation dataset), or with TMT reporter summed signal-to-noise ratio that were less than 150 (100 for phosphorylation dataset) or had no MS3 spectra were excluded from quantification.

For phosphorylation dataset search, phosphorylation (+ 79.966 Da) on Serine, Threonine or Tyrosine and deamidation (+ 0.984 Da) on Asparagine or Glutamine were set as additional variable modifications. Phosphorylation site localization was determined using the AScore algorithm (Beausoleil et al., 2006). AScore is a probability-based approach for high-throughput protein phosphorylation site localization. Specifically, a threshold of 13 corresponded to 95% confidence in site localization.

The MS TMT proteomic data have been deposited to the MassIVE repository with the dataset identifier MSV000093190. Protein quantification values were exported for further analysis in Microsoft Excel and Perseus (Tyanova et al., 2016) and statistical test and parameters used are indicated in the corresponding Supplementary Data Set 1. Briefly, Welch's *t*-test analysis was performed to compare two datasets, using s0 parameter (a minimal fold change cut-off) and correction for multiple comparison was achieved by the permutation-based FDR method, both functions that are built-in in Perseus software. For whole cell proteome (**Figure 4A**, *S2B*) analysis, each reporter ion channel was summed across all quantified proteins and normalized assuming equal protein loading of all samples. For phosphopeptide dataset (**Figure 4C**, *S2C*), peptide abundance was normalized to the protein abundance when available.

4.16 Gene ontology analyses

Gene ontology enrichment analyses were performed using the Database for Annotation, Visualization, and Integrated Discovery (DAVID) v6.8. Differentially expressed genes that reached a false discovery rate *q*-value significance threshold <0.05 were analyzed for enrichment compared to the total protein list quantified using default stringency parameters. GOTERM_BP_DIRECT terms with corresponding $-\log_{10}$ (*p*-values) from the functional annotation chart results were graphed.

4.17 Kinase-substrate enrichment analyses

Kinase-substrate enrichment analyses were performed on Supplementary Data Set 1 using the KSEA software, available as the R package "KSEAapp" on CRAN: CRAN.R-project.org/package = KSEAapp/and online at https://casecpb.shinyapps.io/ksea/ (Wiredja et al., 2017). The $\log_2$

(fold change) of phosphoproteins in each treatment-comparison group were used as input, and kinase-substrate annotations were derived from both PhosphoSitePlus and NetworKIN datasets. The resulting output displayed a z-score for each kinase, which described the collective phosphorylation status of its substrates, such that a kinase with a negative score had substrates that were generally dephosphorylated with the test group, and vice versa for a kinase with a positive score. *P*-values for kinase z-scores were then determined by assessing the one-tailed probability of having a more extreme score than the one measured, followed by a Benjamini-Hochberg false discovery rate correction for multiple hypothesis testing. Kinase z-scores with $p < 0.05$ were determined significant, and unbiased hierarchical clustering was performed to determine the relative similarity of kinase scores between each treatment group.

4.18 DNA extraction and genotyping PCR

Genomic DNA was extracted using the Wizard Genomic DNA Purification Kit (Promega). Approximately 2×10^6 cells were lysed using nuclei lysis solution and mechanical trituration by pipetting. RNase solution was added to the nuclear lysate and incubated for 15 min at 37°C. Protein Precipitation Solution was added, vortexed briefly, and centrifuged for 4 min at 16,000 × *g*. Sample solutions were mixed gently by inversion until white thread-like strands of DNA were visible. Samples were centrifuged for 1 min at 16,000 × *g*, and the DNA pellet was washed with 70% ethanol before centrifuging again (1 min, 16,000 × *g*). The DNA pellet was air dried for 15 min and resuspended with DNA rehydration solution for 1 h at 65°C or overnight at 4°C. Total DNA concentrations were analyzed using a nanodrop.

Polymerase chain reaction (PCR) was performed using the Phusion Hot Start Flex 2X Master Mix (New England Biolabs). Reactions were set up according to the manufacturer's instructions (TDP-43^{G298S} forward 5′- CGACTGAAATATCACTGCTGCTG-3′, TDP-43^{G298S} reverse 5′- GGATGCTGATCCCCAACCAA-3′; SOD1^{L144F} forward 5′- GTTATTTTTCTAATATTATGAGG-3′, SOD1^{L144F} reverse 5′- GTTTTATAAAACTATACAAATCTTCC-3′. Thermocycler conditions were the following- 1 cycle of 98°C for 30 s; 30 cycles of 98°C for 10 s, 45–72°C for 30 s (depending on melting temperature of primer pairs determined by NEB Tm calculator),[1] 72°C for 30 s/kb; and 1 cycle of 72°C for 10 min. PCR products were run at 135V on a 1% agarose gel containing ethidium bromide and bands were observed using a ChemiDoc XRS + (Bio-Rad). Sequencing of PCR products was performed by Psomagen and resulting sequencing files were analyzed with Geneious software using NCBI gene data.

4.19 Statistical analyses

All statistical analyses were performed using rstatix: Pipe-Friendly Framework for Basic Statistical Tests, R package version 0.6.0. https://CRAN.R-project.org/package=rstatix (Kassambara, 2020). Data were determined to be normally distributed using the Shapiro Wilk test and variance was determined equal between groups using Levene's test. For comparisons of 2 groups, a 2 tailed, unpaired student's *t*-test was used. For comparisons of 3 or more groups, an analysis of variance (ANOVA) was used followed by Tukey's HSD *post-hoc* tests. $p < 0.05$ was considered statistically significant and denoted in graphs with a $^*p < 0.01$ **, $p < 0.001$ ***, and $P < 0.0001$ ****.

1 https://tmcalculator.neb.com

Data availability statement

The data presented in the study are deposited in the MassIVE repository, with accession number MSV000093190.

Ethics statement

All hiPSC culture work was performed with approval by the Institutional Review Board and the Harvard Committee on the Use of Human Subjects, and determined to not be human subjects research.

Author contributions

MW: Conceptualization, Data curation, Formal Analysis, Funding acquisition, Investigation, Methodology, Writing – original draft, Writing – review and editing. RG: Data curation, Formal Analysis, Investigation, Validation, Writing – review and editing. AO: Data curation, Formal Analysis, Investigation, Writing – review and editing, Visualization. KH: Data curation, Formal Analysis, Investigation, Visualization, Writing – review and editing. JH: Funding acquisition, Project administration, Resources, Supervision, Writing – review and editing. LR: Conceptualization, Funding acquisition, Project administration, Resources, Supervision, Writing – review and editing.

Funding

The author(s) declare financial support was received for the research, authorship, and/or publication of this article. This study received funding from Biogen, Harvard Brain Science Initiative, and Google and also supported by the NIH (R37 NS083524 to JH, R01 NS110395 to JH, and F32 AG079593 to RG). The funders were not involved in the study design, collection, analysis, interpretation of data, the writing of this article or the decision to submit it for publication.

Acknowledgments

We thank Dr. Chen Wu and Dr. Silvia Piccinotti for helpful suggestions and discussions. **Figure 6** was created with BioRender.com.

Conflict of interest

JH was a founder and consultant for Caraway Therapeutics and a founding scientific advisor for Interline Therapeutics. LR was a founder of Elevian, Rejuveron, and Vesalius Therapeutics, a member of their scientific advisory boards and a private equity shareholder. All are interested in formulating approaches intended to treat diseases of the nervous system and other tissues. He is also on the advisory board of Alkahest, a Grifols company, focused on the plasma proteome, and scientific advisory board member of ProjenX and Corsalex. None of these companies provided any financial support for the work in this manuscript. However, both ProjenX and Corsalex are focused on treating ALS, including via modulating targets that are described in this manuscript.

The remaining authors declare that the research was conducted in the absence of any commercial or financial relationships that could be construed as a potential conflict of interest.

Publisher's note

Supplementary material

The Supplementary Material for this article can be found online at: https://www.frontiersin.org/articles/10.3389/fncel.2023.1327361/full#supplementary-material

References

Abo-Rady, M., Kalmbach, N., Pal, A., Schludi, C., Janosch, A., Richter, T., et al. (2020). Knocking out C9ORF72 exacerbates axonal trafficking defects associated with hexanucleotide repeat expansion and reduces levels of heat shock proteins. *Stem Cell Rep*. 14, 390–405. doi: 10.1016/j.stemcr.2020.01.010

Agianian, B., and Gavathiotis, E. (2018). Current insights *of* BRAF inhibitors in cancer. *J. Med. Chem*. 61, 5775–5793. doi: 10.1021/acs.jmedchem.7b01306

Alami, N. H., Smith, R. B., Carrasco, M. A., Williams, L. A., Winborn, C. S., Han, S. S. W., et al. (2014). Axonal transport of TDP-43 mRNA granules is impaired by ALS-causing mutations. *Neuron* 81, 536–543. doi: 10.1016/j.neuron.2013.12.018

Andrews, J. A., Jackson, C. E., Heiman-Patterson, T. D., Bettica, P., Brooks, B. R., and Pioro, E. P. (2020). Real-world evidence of riluzole effectiveness in treating amyotrophic lateral sclerosis. *Amyotroph Lateral Scler Frontotemp. Degener.* 21, 509–518. doi: 10.1080/21678421.2020.1771734

Beausoleil, S. A., Villén, J., Gerber, S. A., Rush, J., and Gygi, S. P. (2006). A probability-based approach for high-throughput protein phosphorylation analysis *and* site localization. *Nat. Biotechnol.* 24, 1285–1292. doi: 10.1038/nbt1240

Bhinge, A., Namboori, S. C., Zhang, X., VanDongen, A. M. J., and Stanton, L. W. (2017). Genetic Correction of SOD1 mutant iPSCs reveals ERK and JNK activated AP1 as a driver of neurodegeneration in *Amyotrophic* lateral sclerosis. *Stem Cell Rep*. 8, 856–869. doi: 10.1016/j.stemcr.2017.02.019

Bos, P. H., Lowry, E. R., Costa, J., Thams, S., Garcia-Diaz, A., Zask, A., et al. (2019). Development of MAP4 kinase inhibitors as motor neuron-protecting agents. *Cell Chem. Biol*. 26, 1703–1715.e37. doi: 10.1016/j.chembiol.2019.10.005

Boulting, G. L., Kiskinis, E., Croft, G. F., Amoroso, M. W., Oakley, D. H., Wainger, B. J., et al. (2011). A functionally characterized test set of human induced pluripotent stem cells. *Nat. Biotechnol.* 29, 279–286. doi: 10.1038/nbt.1783

Bourhill, T., Narendran, A., and Johnston, R. N. (2017). Enzastaurin: A lesson *in* drug development. *Crit. Rev. Oncol. Hematol.* 112, 72–79. doi: 10.1016/j.critrevonc.2017.02.003

Brown, R. H., and Al-Chalabi, A. (2017). Amyotrophic lateral sclerosis. *N. Engl. J. Med.* 377, 162–172. doi: 10.1056/NEJMra1603471

Burkhardt, M. F., Martinez, F. J., Wright, S., Ramos, C., Volfson, D., Mason, M., et al. (2013). A cellular model for sporadic ALS using patient-derived induced pluripotent stem cells. *Mol. Cell Neurosci.* 56, 355–364. doi: 10.1016/j.mcn.2013.07.007

Chen, H., Qian, K., Du, Z., Cao, J., Petersen, A., Liu, H., et al. (2014). Modeling ALS with iPSCs reveals that mutant SOD1 misregulates neurofilament balance in motor neurons. *Cell Stem Cell* 14, 796–809. doi: 10.1016/j.stem.2014.02.004

Crawford, T. D., Ndubaku, C. O., Chen, H., Boggs, J. W., Bravo, B. J., Delatorre, K., et al. (2014). Discovery *of* selective 4-Amino-pyridopyrimidine inhibitors of MAP4K4 using fragment-based lead identification *and* optimization. *J. Med. Chem.* 57, 3484–3493. doi: 10.1021/jm500155b

Davies, H., Bignell, G. R., Cox, C., Stephens, P., Edkins, S., Clegg, S., et al. (2002). Mutations of the BRAF gene in human cancer. *Nature* 417, 949–954. doi: 10.1038/nature00766

Dimos, J. T., Rodolfa, K. T., Niakan, K. K., Weisenthal, L. M., Mitsumoto, H., Chung, W., et al. (2008). Induced pluripotent stem cells generated from patients with ALS can be differentiated into motor neurons. *Science* 321, 1218–1221. doi: 10.1126/science.1158799

Egawa, N., Kitaoka, S., Tsukita, K., Naitoh, M., Takahashi, K., Yamamoto, T., et al. (2012). Drug screening for ALS using patient-specific induced pluripotent stem cells. *Sci. Transl. Med.* 4:145ra104. doi: 10.1126/scitranslmed.3004052

Ferraiuolo, L., Kirby, J., Grierson, A. J., Sendtner, M., and Shaw, P. J. (2011). *Molecular* pathways of motor neuron injury in amyotrophic lateral sclerosis. *Nat. Rev. Neurol.* 7, 616–630. doi: 10.1038/nrneurol.2011.152

Frebel, K., and Wiese, S. (2006). Signalling molecules essential for neuronal survival and differentiation. *Biochem. Soc. Trans.* 34(Pt 6), 1287–1290. doi: 10.1042/BST0341287

Fujimori, K., Ishikawa, M., Otomo, A., Atsuta, N., Nakamura, R., Akiyama, T., et al. (2018). Modeling sporadic ALS in iPSC-derived motor neurons identifies a potential therapeutic agent. *Nat. Med.* 24, 1579–1589. doi: 10.1038/s41591-018-0140-5

Hardiman, O., Al-Chalabi, A., Chio, A., Corr, E. M., Logroscino, G., Robberecht, W., et al. (2017). Amyotrophic lateral sclerosis. *Nat. Rev. Dis. Primers* 3:17071. doi: 10.1038/nrdp.2017.71

Hetz, C., Zhang, K., and Kaufman, R. J. (2020). Mechanisms, regulation and functions of the unfolded protein response. *Nat. Rev. Mol. Cell Biol.* 21, 421–438. doi: 10.1038/s41580-020-0250-z

Hung, S. T., Linares, G. R., Chang, W. H., Eoh, Y., Krishnan, G., Mendonca, S., et al. (2023). PIKFYVE inhibition mitigates disease in models of diverse forms of ALS. *Cell* 186, 786–802.e28. doi: 10.1016/j.cell.2023.01.005

Huttlin, E. L., Jedrychowski, M. P., Elias, J. E., Goswami, T., Rad, R., Beausoleil, S. A., et al. (2010). A tissue-specific atlas of mouse protein phosphorylation and expression. *Cell* 143, 1174–1189. doi: 10.1016/j.cell.2010.12.001

Ichiyanagi, N., Fujimori, K., Yano, M., Ishihara-Fujisaki, C., Sone, T., Akiyama, T., et al. (2016). Establishment of in vitro FUS-associated familial amyotrophic lateral *sclerosis* model using human induced pluripotent *stem* cells. *Stem Cell Rep.* 6, 496–510. doi: 10.1016/j.stemcr.2016.02.011

Jaiswal, M. K. (2019). Riluzole and edaravone: A tale of two amyotrophic lateral sclerosis drugs. *Med. Res. Rev.* 39, 733–748. doi: 10.1002/med.21528

Kanekura, K., Suzuki, H., Aiso, S., and Matsuoka, M. (2009). ER stress and unfolded protein response in amyotrophic lateral sclerosis. *Mol. Neurobiol.* 39, 81–89. doi: 10.1007/s12035-009-8054-3

Kassambara, A. (2020). *rstatix: Pipe-friendly framework for basic statistical tests*. Available online at: http://CRAN.R-project.org/package=rstatix (accessed February 01, 2023).

Kiskinis, E., Sandoe, J., Williams, L. A., Boulting, G. L., Moccia, R., Wainger, B. J., et al. (2014). Pathways disrupted in human ALS motor neurons identified through genetic correction of mutant SOD1. *Cell Stem Cell* 14, 781–795. doi: 10.1016/j.stem.2014.03.004

Kitabayashi, T., Dong, Y., Furuta, T., Sabit, H., Jiapaer, S., Zhang, J., et al. (2019). Identification of GSK3β inhibitor kenpaullone as a temozolomide enhancer against glioblastoma. *Sci. Rep.* 9:10049. doi: 10.1038/s41598-019-46454-8

Kolch, W. (2001). To be or not to be: A question of B-Raf? *Trends Neurosci.* 24, 498–500. doi: 10.1016/s0166-2236(00)01889-0

Larhammar, M., Huntwork-Rodriguez, S., Rudhard, Y., Sengupta-Ghosh, A., and Lewcock, J. W. (2017). *The* Ste20 family kinases MAP4K4, MINK1, and TNIK converge to regulate stress-induced JNK signaling *in* neurons. *J. Neurosci.* 37, 11074–11084. doi: 10.1523/JNEUROSCI.0905-17.2017

Leost, M., Schultz, C., Link, A., Wu, Y. Z., Biernat, J., Mandelkow, E. M., et al. (2000). Paullones are potent inhibitors *of* glycogen synthase kinase-3beta and cyclin-dependent kinase 5/p25. *Eur. J. Biochem.* 267, 5983–5994. doi: 10.1046/j.1432-1327.2000.01673.x

Ma, S., and Rosen, S. T. (2007). Enzastaurin. *Curr. Opin. Oncol.* 19, 590–595. doi: 10.1097/CCO.0b013e3282f10a00

Matus, S., Glimcher, L. H., and Hetz, C. (2011). Prote*in* folding stress in neurodegenerative diseases: A glimpse into the ER. *Curr. Opin. Cell Biol.* 23, 239–252. doi: 10.1016/j.ceb.2011.01.003

Matus, S., Valenzuela, V., Medinas, D. B., and Hetz, C. (2013). ER dysfunction and protein folding stress in ALS. *Int. J. Cell Biol.* 2013, 674751. doi: 10.1155/2013/674751

Maury, Y., Côme, J., Piskorowski, R. A., Salah-Mohellibi, N., Chevaleyre, V., Peschanski, M., et al. (2015). Combinatorial analysis *of* developmental cues efficiently converts human pluripotent stem cells into multiple neuronal subtypes. *Nat. Biotechnol.* 33, 89–96. doi: 10.1038/nbt.3049

McAlister, G. C., Nusinow, D. P., Jedrychowski, M. P., Wühr, M., Huttlin, E. L., Erickson, B. K., et al. (2014). MultiNotch MS3 enables accurate, sensitive, and multiplexed detection of differential expression across cancer cell line proteomes. *Anal. Chem.* 86, 7150–7158. doi: 10.1021/ac502040v

Medinas, D. B., Rozas, P., Martínez Traub, F., Woehlbier, U., Brown, R. H., Bosco, D. A., et al. (2018). Endoplasmic reticulum stress leads to accumulation *of* wild-type SOD1 aggregates associated with sporadic amyotrophic lateral sclerosis. *Proc. Natl. Acad. Sci. U.S.A.* 115, 8209–8214. doi: 10.1073/pnas.1801109115

Melamed, Z., López-Erauskin, J., Baughn, M. W., Zhang, O., Drenner, K., Sun, Y., et al. (2019). Premature polyadenylation-mediated loss of stathmin-2 is a hallmark of TDP-43-dependent neurodegeneration. *Nat. Neurosci.* 22, 180–190. doi: 10.1038/s41593-018-0293-z

Naujock, M., Stanslowsky, N., Bufler, S., Naumann, M., Reinhardt, P., Sterneckert, J., et al. (2016). 4-aminopyridine induced activity rescues hypoexcitable motor neurons from amyotrophic lateral sclerosis patient-derived induced pluripotent *stem* cells. *Stem Cells* 34, 1563–1575. doi: 10.1002/stem.2354

Naumann, M., Pal, A., Goswami, A., Lojewski, X., Japtok, J., Vehlow, A., et al. (2018). Impaired DNA damage response signaling by FUS-NLS mutations leads to neurodegeneration and FUS aggregate formation. *Nat. Commun.* 9:335. doi: 10.1038/s41467-017-02299-1

Neel, D. V., Basu, H., Gunner, G., Bergstresser, M. D., Giadone, R. M., Chung, H., et al. (2023). Gasdermin-E mediates mitochondrial damage in axons and neurodegeneration. *Neuron* 111, 1222–1240.e9. doi: 10.1016/j.neuron.2023.02.019

Ng, S. Y., Soh, B. S., Rodriguez-Muela, N., Hendrickson, D. G., Price, F., Rinn, J. L., et al. (2015). Genome-wide RNA-seq of human motor neurons implicates selective ER stress activation in spinal muscular atrophy. *Cell Stem Cell* 17, 569–584. doi: 10.1016/j.stem.2015.08.003

Nishizuka, Y. (1986). Studies and perspectives of protein kinase C. *Science* 233, 305–312. doi: 10.1126/science.3014651

Paulo, J. A., O'Connell, J. D., Everley, R. A., O'Brien, J., Gygi, M. A., and Gygi, S. P. (2016). Quantitative mass spectrometry-based multiplexing compares *the* abundance *of* 5000 S. cerevisiae proteins across 10 carbon sources. *J. Proteomics* 148, 85–93. doi: 10.1016/j.jprot.2016.07.005

Petrov, D., Mansfield, C., Moussy, A., and Hermine, O. (2017). ALS clinical trials review: 20 years of failure. Are we any closer to registering a *new* treatment? *Front. Aging Neurosci.* 9:68. doi: 10.3389/fnagi.2017.00068

Ragagnin, A. M. G., Shadfar, S., Vidal, M., Jamali, M. S., and Atkin, J. D. (2019). Motor *Neuron* susceptibility in ALS/FTD. *Front. Neurosci.* 13:532. doi: 10.3389/fnins.2019.00532

Reinhardt, L., Kordes, S., Reinhardt, P., Glatza, M., Baumann, M., Drexler, H. C. A., et al. (2019). Dual inhibition of GSK3β and CDK5 protects the cytoskeleton of neurons from neuroinflammatory-mediated *degeneration* in vitro and in vivo. *Stem Cell Rep.* 12, 502–517. doi: 10.1016/j.stemcr.2019.01.015

Rozas, P., Bargsted, L., Martínez, F., Hetz, C., and Medinas, D. B. (2017). The ER proteostasis network in ALS: Determining the differential motoneuron vulnerability. *Neurosci. Lett.* 636, 9–15. doi: 10.1016/j.neulet.2016.04.066

Ruegsegger, C., and Saxena, S. (2016). Proteostasis impairment in ALS. *Brain Res.* 1648(Pt B), 571–579. doi: 10.1016/j.brainres.2016.03.032

Samadhiya, S., Sardana, V., Bhushan, B., Maheshwari, D., Goyal, R., and Pankaj. (2022). Assessment *of* therapeutic response of edaravone and riluzole combination therapy in amyotrophic lateral sclerosis patients. *Ann. Indian Acad. Neurol.* 25, 692–697. doi: 10.4103/aian.aian_1083_21

Sareen, D., O'Rourke, J. G., Meera, P., Muhammad, A. K., Grant, S., Simpkinson, M., et al. (2013). Targeting RNA foci in iPSC-derived motor neurons from ALS patients with a C9ORF72 repeat expansion. *Sci. Transl. Med.* 5:208ra149. doi: 10.1126/scitranslmed.3007529

Savitski, M. M., Wilhelm, M., Hahne, H., Kuster, B., and Bantscheff, M. A. (2015). Scalable Approach for protein false discovery rate estimation in large proteomic data sets. *Mol. Cell Proteomics* 14, 2394–2404. doi: 10.1074/mcp.M114.046995

Saxena, S., and Caroni, P. (2011). Selective neuronal vulnerability in neurodegenerative diseases: From stressor thresholds to degeneration. *Neuron* 71, 35–48. doi: 10.1016/j.neuron.2011.06.031

Saxena, S., Cabuy, E., and Caroni, P. (2009). A role for motoneuron subtype-selective ER stress in disease manifestations of FALS mice. *Nat. Neurosci.* 12, 627–636. doi: 10.1038/nn.2297

Shi, Y., Hung, S. T., Rocha, G., Lin, S., Linares, G. R., Staats, K. A., et al. (2019). Identification *and* therapeutic rescue of autophagosome and glutamate receptor defects in C9ORF72 and sporadic ALS neurons. *JCI Insight* 5:e127736. doi: 10.1172/jci.insight.127736

Shi, Y., Lin, S., Staats, K. A., Li, Y., Chang, W. H., Hung, S. T., et al. (2018). Haploinsufficiency leads to neurodegeneration in C9ORF72 ALS/FTD human induced motor neurons. *Nat. Med.* 24, 313–325. doi: 10.1038/nm.4490

Sieber, J., Wieder, N., Clark, A., Reitberger, M., Matan, S., Schoenfelder, J., et al. (2018). GDC-0879, a BRAFV600E inhibitor, protects kidney podocytes from death. *Cell* Chem Biol 25, 175–184.e4. doi: 10.1016/j.chembiol.2017.11.006

Sun, X., Song, J., Huang, H., Chen, H., and Qian, K. (2018). Modeling hallmark pathology using motor neurons derived from the family *and* sporadic amyotrophic lateral sclerosis patient-specific iPS cells. *Stem Cell Res. Ther.* 9:315. doi: 10.1186/s13287-018-1048-1

Tanaka, S., and Koike, T. (2001). Activation of protein kinase C delays apoptosis of nerve growth factor-deprived rat sympathetic neurons through a Ca(2+)-influx dependent mechanism. *Neurosci. Lett.* 313, 9–12. doi: 10.1016/s0304-3940(01)02193-0

Thams, S., Lowry, E. R., Larraufie, M. H., Spiller, K. J., Li, H., Williams, D. J., et al. (2019). A stem cell-based screening platform identifies compounds that desensitize motor neurons to endoplasmic reticulum stress. *Mol. Ther.* 27, 87–101. doi: 10.1016/j.ymthe.2018.10.010

Tyanova, S., Temu, T., Sinitcyn, P., Carlson, A., Hein, M. Y., Geiger, T., et al. (2016). The Perseus computational platform for comprehensive analysis of (prote)omics data. *Nat. Methods* 13, 731–740. doi: 10.1038/nmeth.3901

Uenaka, T., Satake, W., Cha, P. C., Hayakawa, H., Baba, K., Jiang, S., et al. (2018). In silico drug screening by using genome-wide association study data repurposed dabrafenib, an anti-melanoma drug, for Parkinson's disease. *Hum. Mol. Genet.* 27, 3974–3985. doi: 10.1093/hmg/ddy279

Wainger, B. J., Kiskinis, E., Mellin, C., Wiskow, O., Han, S. S., Sandoe, J., et al. (2014). Intrinsic membrane hyperexcitability of amyotrophic lateral sclerosis patient-derived motor neurons. *Cell Rep.* 7, 1–11. doi: 10.1016/j.celrep.2014.03.019

Walker, A. K., Soo, K. Y., Sundaramoorthy, V., Parakh, S., Ma, Y., Farg, M. A., et al. (2013). ALS-associated TDP-43 induces endoplasmic reticulum stress, which drives cytoplasmic TDP-43 accumulation and stress granule formation. *PLoS One* 8:e81170. doi: 10.1371/journal.pone.0081170

Webster, C. P., Smith, E. F., Shaw, P. J., and De Vos, K. J. (2017). Prote*in* homeostasis in amyotrophic lateral sclerosis: Therapeutic opportunities? *Front. Mol. Neurosci.* 10:123. doi: 10.3389/fnmol.2017.00123

Wiese, S., Pei, G., Karch, C., Troppmair, J., Holtmann, B., Rapp, U. R., et al. (2001). Specific function of B-Raf in mediating survival of embryonic motoneurons and sensory neurons. *Nat. Neurosci.* 4, 137–142. doi: 10.1038/83960

Wiredja, D. D., Koyutürk, M., and Chance, M. R. (2017). The KSEA app: A web-based tool for kinase activity inference from quantitative phosphoproteomics. *Bioinformatics* 33, 3489–3491. doi: 10.1093/bioinformatics/btx415

Witzel, S., Maier, A., Steinbach, R., Grosskreutz, J., Koch, J. C., Sarikidi, A., et al. (2022). Safety and effectiveness of long-term intravenous administration of edaravone for treatment of patients with amyotrophic lateral sclerosis. *JAMA Neurol.* 79, 121–130. doi: 10.1001/jamaneurol.2021.4893

Workman, M. J., Lim, R. G., Wu, J., Frank, A., Ornelas, L., Panther, L., et al. (2023). Large-scale differentiation of iPSC-derived motor neurons from ALS and control subjects. *Neuron* 111, 1191–1204.e5. doi: 10.1016/j.neuron.2023.01.010

Wu, C., Watts, M. E., and Rubin, L. L. (2019). MAP4K4 activation mediates motor *neuron* degeneration in amyotrophic lateral sclerosis. *Cell Rep.* 26, 1143–1156.e5. doi: 10.1016/j.celrep.2019.01.019

Yang, Y. M., Gupta, S. K., Kim, K. J., Powers, B. E., Cerqueira, A., Wainger, B. J., et al. (2013). A small molecule screen in stem-cell-derived motor neurons identifies a kinase inhibitor as a candidate therapeutic for ALS. *Cell Stem Cell* 12, 713–726. doi: 10.1016/j.stem.2013.04.003

Zhang, Z., Almeida, S., Lu, Y., Nishimura, A. L., Peng, L., Sun, D., et al. (2013). Downregulation of microRNA-9 in iPSC-derived neurons of FTD/ALS patients with TDP-43 mutations. *PLoS One* 8:e76055. doi: 10.1371/journal.pone.0076055

Zhu, D., Jiang, X., Wu, X., Tian, F., Mearow, K., Lipsky, R. H., et al. (2004). Inhibition of protein kinase C promotes neuronal survival in low potassium through an Akt-dependent pathway. *Neurotox. Res.* 6, 281–289. doi: 10.1007/BF03033438

frontiers | Frontiers in Neurology

TYPE Original Research
PUBLISHED 26 January 2024
DOI 10.3389/fneur.2024.1325222

OPEN ACCESS

EDITED BY
Agnes Lumi Nishimura,
Queen Mary University of London,
United Kingdom

REVIEWED BY
Matthew S. Alexander,
University of Alabama at Birmingham,
United States
A. M. Jimenez-Garcia,
Nebrija University, Spain

*CORRESPONDENCE
Mariz Vainzof
✉ mvainzof@usp.br

RECEIVED 09 November 2023
ACCEPTED 15 January 2024
PUBLISHED 26 January 2024

CITATION
Vasconcelos FTGR, Ribeiro Júnior AF, Souza BW, Zogbi IA, Carvalho LML, Feitosa LN, Souza LS, Saldys NG, Ferrari MFR and Vainzof M (2024) Induced degeneration and regeneration in aged muscle reduce tubular aggregates but not muscle function.
Front. Neurol. 15:1325222.
doi: 10.3389/fneur.2024.1325222

Induced degeneration and regeneration in aged muscle reduce tubular aggregates but not muscle function

Felipe Tadeu Galante Rocha de Vasconcelos, Antonio Fernando Ribeiro Júnior, Brandow Willy Souza, Isabela de Aquino Zogbi, Laura Machado Lara Carvalho, Letícia Nogueira Feitosa, Lucas Santos Souza, Nathália Gagliardi Saldys, Merari de Fátima Ramires Ferrari and Mariz Vainzof*

Human Genome and Stem Cell Research Center, Department of Genetics and Evolutionary Biology, Biosciences Institute, University of São Paulo, São Paulo, Brazil

Introduction: Tubular aggregates (TA) are skeletal muscle structures that arise from the progressive accumulation of sarcoplasmic reticulum proteins. Cytoplasmic aggregates in muscle fibers have already been observed in mice and humans, mainly during aging and muscle disease processes. However, the effects of muscle regeneration on TA formation have not yet been reported. This study aimed to investigate the relationship between degeneration/regeneration and TA in aged murine models. We investigated the presence and quantity of TA in old males from two murine models with intense muscle degeneration and regeneration.

Methods: One murine lineage was a *Dmd*^{mdx} model of Duchenne muscular dystrophy ($n = 6$). In the other model, muscle damage was induced by electroporation in C57BL/6J wild-type mice, and analyzed after 5, 15, and 30 days post-electroporation (dpe; $n = 15$). Regeneration was evaluated based on the quantity of developmental myosin heavy chain (dMyHC)-positive fibers.

Results: The frequency of fibers containing TA was higher in aged C57BL/6J ($26 \pm 8.3\%$) than in old dystrophic *Dmd*^{mdx} mice ($2.4 \pm 2\%$). Comparing the data from induced degeneration/regeneration in normal mice revealed a reduced proportion of TA-containing fibers after 5 and 30 dpe. Normal aged muscle was able to regenerate and form dMyHC+ fibers, mainly at 5 dpe (0.1 ± 0.1 vs. $16.5 \pm 2.6\%$). However, there was no difference in force or resistance between normal and 30 dpe animals, except for the measurements by the Actimeter device, which showed the worst parameters in the second group.

Discussion: Our results suggest that TA also forms in the *Dmd*^{mdx} muscle but in smaller amounts. The intense degeneration and regeneration of the old dystrophic model resulted in the generation of new muscle fibers with a lower quantity of TA. Data from electroporated wild-type mice support the idea that muscle regeneration leads to a reduction in the amount of TA. We suggest that TA accumulates in muscle fibers throughout physiological aging and that regeneration leads to the formation of new fibers without these structures. In addition, these new fibers do not confer functional benefits to the muscle.

KEYWORDS

tubular aggregates, muscle regeneration, aging, muscular dystrophies, neuromuscular disease

1 Introduction

Tubular aggregates (TA) are skeletal muscle structures that arise from the progressive accumulation of sarcoplasmic reticulum (SR) proteins (1–5). Cytoplasmic aggregates of muscle fibers have been observed in both mice (6) and humans (3). These factors are relevant to aging and muscle disease processes. The pathophysiological mechanisms of many human neurodegenerative diseases, such as amyotrophic lateral sclerosis, Alzheimer's disease, Parkinson's disease, and Huntington's disease, are intrinsically related to protein aggregation and inclusion body formation (7). Thus, there is a strong link between condensate-forming proteins and age-related diseases, such as neurodegeneration and cancer (8).

In humans, TA are found in diseased skeletal muscles such as tubular aggregate myopathy (TAM) (9), Andersen–Tawil syndrome (10), and limb-girdle myasthenia (11). Major differences between TAM and TA are associated with other myopathies. TA are prevalent in both slow-twitch (type I) and fast-twitch (type II) muscle fibers in TAM, whereas they are only present in type II fibers as a secondary effect in other myopathies. TAM affects mostly men, and in isolated TA, the proportion of women presenting with them is greater, although men are generally more affected (12).

TA have also been found in wild-type aged mice of different strains within muscle fibers, especially type II, but only in male specimens (5), which makes these structures age-, fiber type- and sex-specific (1).

The effects of muscle regeneration on TA have not yet been reported. This study aimed to compare the presence of TA in normal and dystrophic aged muscles and assess whether TA negatively influences muscle function after induced regeneration.

2 Animals and methods

2.1 Animals

To evaluate the presence of TA, C57BL/6J ($n = 15$, 24 months of age) mice were subdivided into a control non-electroporated group (NE; $n = 6$) and three groups of animals submitted to electroporation in the calves and analyzed 5 days post-electroporation (dpe) ($n = 3$), 15 dpe ($n = 3$), and 30 dpe ($n = 3$). An additional group of naturally degenerated animals composed of *Dmd*^{mdx} mice (model for Duchenne muscular dystrophy) ($n = 6$, 18–24 months of age) was also included (Figure 1A). All animals were males.

In the functional evaluation (Figure 1B), 2 years-old C57BL/6J ($n = 8$) mice were subdivided into the NE control group ($n = 3$) and electroporated group ($n = 5$), composed of animals subjected to electroporation of calves according to a previously described protocol (13). Functional evaluations included strength, resistance, and global activity (Figure 2). These tests were performed at 0 dpe time zero in both groups and at 30 dpe in the second group (Figure 1B).

2.2 Experimental procedures

2.2.1 Global activity measurements

Actitrack equipment (Panlab, Barcelona, Spain; Figure 2) was used to measure the distance covered, speed, slow and fast movements, rest, and number of rearings. The velocity thresholds adopted were the equipment software standards (rest <2 cm/s, slow velocity between 2 and 5 cm/s, and fast velocity >5 cm/s). Each animal was monitored for 20 min with a 10 min break between animals. This assessment was repeated once daily for 4 days. On the fifth day, we performed the other tests as described below. For the second evaluation after 30 days, the Actitrack assessment was repeated for 3 days and the other tests were repeated on the fourth day.

2.2.2 Assessment of strength and endurance

The grip strength, hanging test involving two and four limbs, and rotarod test (Figure 2) were performed based on the TREAT-NMD protocols (14), which consider the conversion of measures in newtons into grams, and divided these values by the respective weights.

2.2.3 Sample collection

The animals were then anesthetized and euthanized. Gastrocnemius muscles were collected and stored in liquid nitrogen. Frozen tissues were cross-sectioned in a HM 505 E cryostat (Microm International GmbH, Walldorf, Germany) at 6–7 nm thickness for histological and immunofluorescence (IF) analyses.

2.2.4 Staining processes

Hematoxylin and eosin (HE) staining was performed using a standard protocol aimed at assessing tissue integrity. Gomori trichrome (GT) staining was performed to verify the presence of TA in the muscle fibers, as previously described (15). Muscle fiber cytoplasm stained green, nuclei purple, and TA a purple-reddish color.

2.2.5 IF of developmental myosin heavy chain

dMyHC is a protein present in immature fibers. It is a marker of muscular regeneration. Primary antibodies used for staining were a 1:30 dilution of mouse dMyHC-NCL, for developmental myosin staining (Novocastra NCL-MHCd, Leica Biosystems, Concord, ON, Canada) and a 1:100 dilution of rabbit anti-laminin (Z0097, Dako, San Diego, CA, United States) for extracellular matrix staining. The secondary antibodies used were a 1:200 dilution of Cy3 goat anti-mouse (A10521; Invitrogen, Carlsbad, CA, United States) and a 1:100 dilution of fluorescein isothiocyanate (FITC) goat anti-rabbit (F0511; Sigma-Aldrich, St. Louis, MO, United States). IF was visualized and analyzed using an Axio Imager.Z1 microscope (Zeiss, Jena, Germany).

2.2.6 Morphometric analysis

We photographed entirely each gastrocnemius section stained by Gomori Trichrome. It allows us to correctly identify the myofibers contour and the TA presence, so we can count them individually, which was done in a global manner using the Fiji software (16). On average, 2,370 fibers were analyzed per animal. After that, we calculated the proportion of myofibers containing TA over total number of fibers counted in muscle section.

2.3 Statistical analysis

The statistical software GraphPad Prism v8.2.1 (GraphPad Software Inc., Boston, MA, United States) was used. The Shapiro–Wilk normality test was performed for each experimental group

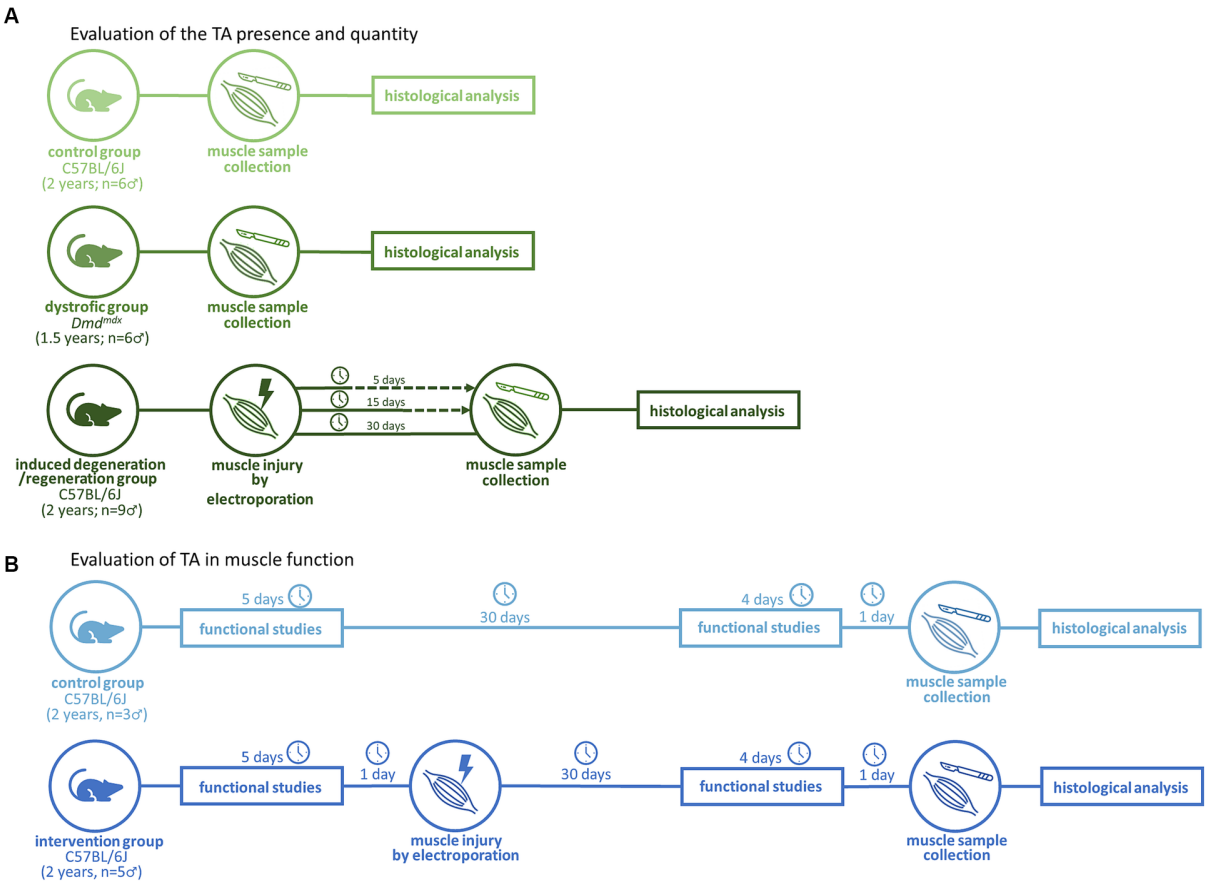

FIGURE 1
Experimental workflows for evaluation of the TA presence **(A)** and impact in muscle function **(B)**.

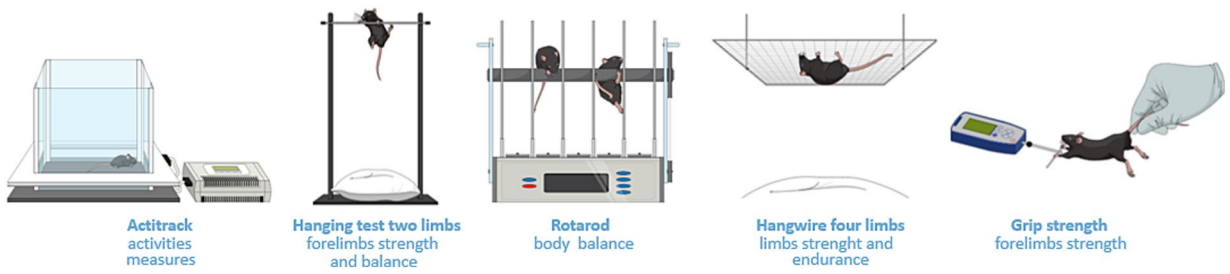

FIGURE 2
Methodologies for functional studies. Actitrack uses infrared sensors to record mouse movements, providing data that includes distance traveled and speed. The two-limb hanging test assesses forelimb strength and balance. The observer records the hanging time of the subject. The four-limb hanging test assesses strength and endurance by placing the mouse upside down, hanging from a grid. The rotarod test assesses body balance as the animal is positioned on a spinning metal cylinder. The grip strength test records the force produced by the animal while the researcher pulls its tail gently.

analyzed. If the distribution was normal, paired or unpaired student's *t* parametric tests were used to compare two experimental groups, while one-way ANOVA with Dunnett's correction was performed to compare more than two. If the distribution was not normal, the Mann–Whitney test (unpaired samples) or Wilcoxon test (paired samples; before vs. after) were used to compare two groups, while Kruskal–Wallis was perfomed to compare more than two groups. The confidence interval adopted for the statistics was 95%.

3 Results

3.1 TA are present, but in decreased quantity in dystrophic aged muscles

TA were detected in both aged normal and dystrophic *Dmd*^{mdx} mice (Figure 3). However, more aggregates were evident in normal C57BL/6J mice than in *Dmd*^{mdx} mice (26 ± 8.3% vs. 2.4 ± 2%, $p = 0.0007$, *t*-test; Figure 3C).

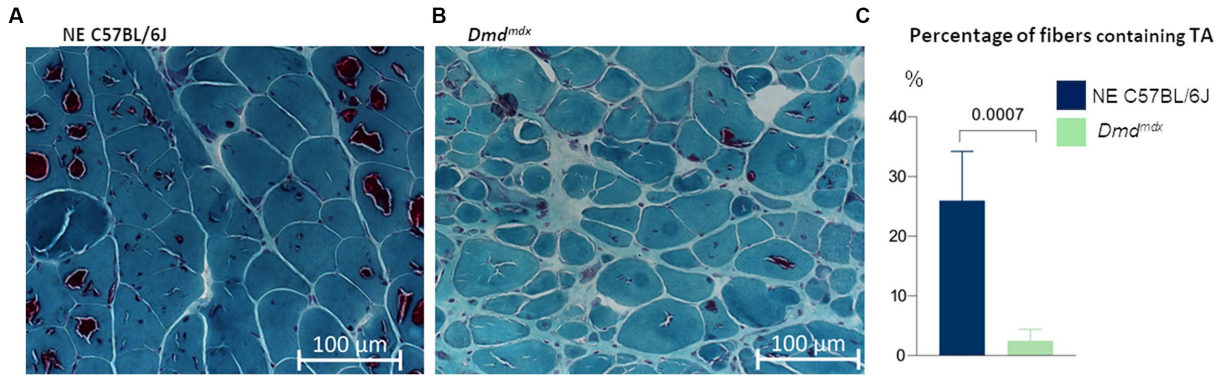

FIGURE 3
Gastrocnemius muscle from aged mice, stained with modified Gomori trichrome. TA are present in all experimental groups. There were more fibers containing TA in **(A)** C57BL/6J mice (n = 6) than in **(B)** Dmd^{mdx} mice (n = 6, t-test).

3.2 Induced degeneration causes decrease in number of TA after regeneration

Comparison of the data from normal aged animals with induced degeneration-regeneration revealed a reduction in the proportion of fibers containing TA at all times post-electroporation. One-way ANOVA with Dunnett's correction analysis showed that reductions were statistically significant after 5 dpe (3.7 ± 5%, $p = 0.0177$) and 30 dpe (7.7 ± 5.7%, $p = 0.0435$) (Figure 4). TA were different sizes and present as single or multiple units in each muscle fiber, and with or without internal content (staining inside the TA or only on the outer edge, respectively). In fibers with internalized nuclei (newly formed fibers), TA were not identified, although they were still present within nearby fibers.

3.3 Regeneration profile in old mice

dMyHC-positive fibers were scarce in NE old C57BL/6J animals (0.1 ± 0.1%; Figure 5A) and *Dmd*^{mdx} mice (0.3 ± 0.4%; Figure 5E), with no statistically significant difference between them (Mann–Whitney—$p = 0.3864$; Figure 5F). The lesion induced regeneration, with increase of dMyHC-positive fibers at 5 dpe (16.5 ± 2.6%; Figure 5B). The difference between NE and 5dpe C57BL/6J is statistically significant (Kruskal–Wallis with Dunnett's correction—$p = 0.0424$; Figure 5F). From 15 dpe there was a reduction in dMyHC-positive fibers (1.8 ± 1.7%; Figure 5C). Thirty dpe animals (0.1 ± 0.1% - Figure 5D) presented a complete regeneration, with similar values to those of NE C57BL/6J. Comparison of 15 dpe and 30 dpe with NE animals showed no significant differences (Kruskal–Wallis with Dunnett's correction—Figure 5F).

3.4 Decreased TA after muscle regeneration is not related to muscle functional improvement

The observation of less TA in regenerated muscles of aged normal mice after induced degeneration prompted the hypothesis that regeneration inducing the formation of new fibers with less TA could modify the functional capacity of the muscle. To verify this hypothesis, we repeated the experiment and induced degeneration in normal aged muscles and functionally evaluated these animals before and 30 days after injury and regeneration. Again, more fibers with TA were observed in NE animals (35.3 ± 12%) compared to electroporated animals at 30 dpe (23.8 ± 5.3%). The global activity measurements obtained using Actitrack equipment revealed statistically significant poorer performance of the electroporated animals compared to NE subjects. As shown in Figure 6, the indices of mean velocity (A), distance (B), slow movement (C), fast movement (D), and rearing (E) were significantly lower in the electroporated mice (30 dpe), whereas rest time (F) was higher in this group (paired t-tests). The animals were also evaluated using four tests for force and resistance: grip strength, rotarod, hanging with two limbs, and hanging with four limbs. No differences between the control and intervention groups were evident using paired t or Wilcoxon tests (Figure 7).

4 Discussion

In this study, we aimed to compare the capacity of the old muscle to regenerate, both in chronic model of degeneration, as observed in muscular dystrophies, as compared to acute degeneration, induced by muscle demage by electroporation. The number of positive dMyHCs was quantified to verify the efficiency of regeneration and formation of new muscle fibers in genetically degenerated dystrophin-deficient mice (*Dmd*^{mdx}) and in normal muscles under induced degeneration. As observed in young normal mice subjected to electrical muscle injury (17, 18), new fibers positive for dMyHC clearly increased at 5 dpe. dMyHC-positive fibers were reduced in number at 15 dpe and reached normal values after 30 dpe. The findings indicate that aged normal muscle preserves its regenerative capacity and formation of new muscle fibers in a pattern similar to that observed in young normal animals. In contrast, old *Dmd*^{mdx} mice showed a small increase in the number of positive new fibers. This result is different from the significantly greater prevalence of regenerated fibers observed in young *Dmd*^{mdx} mice (17%) (17).

TA inside aged muscle fibers are more likely to form during muscular physiological senescence. TA are repositories of proteins that have accumulated for a long time (several months in mice or years

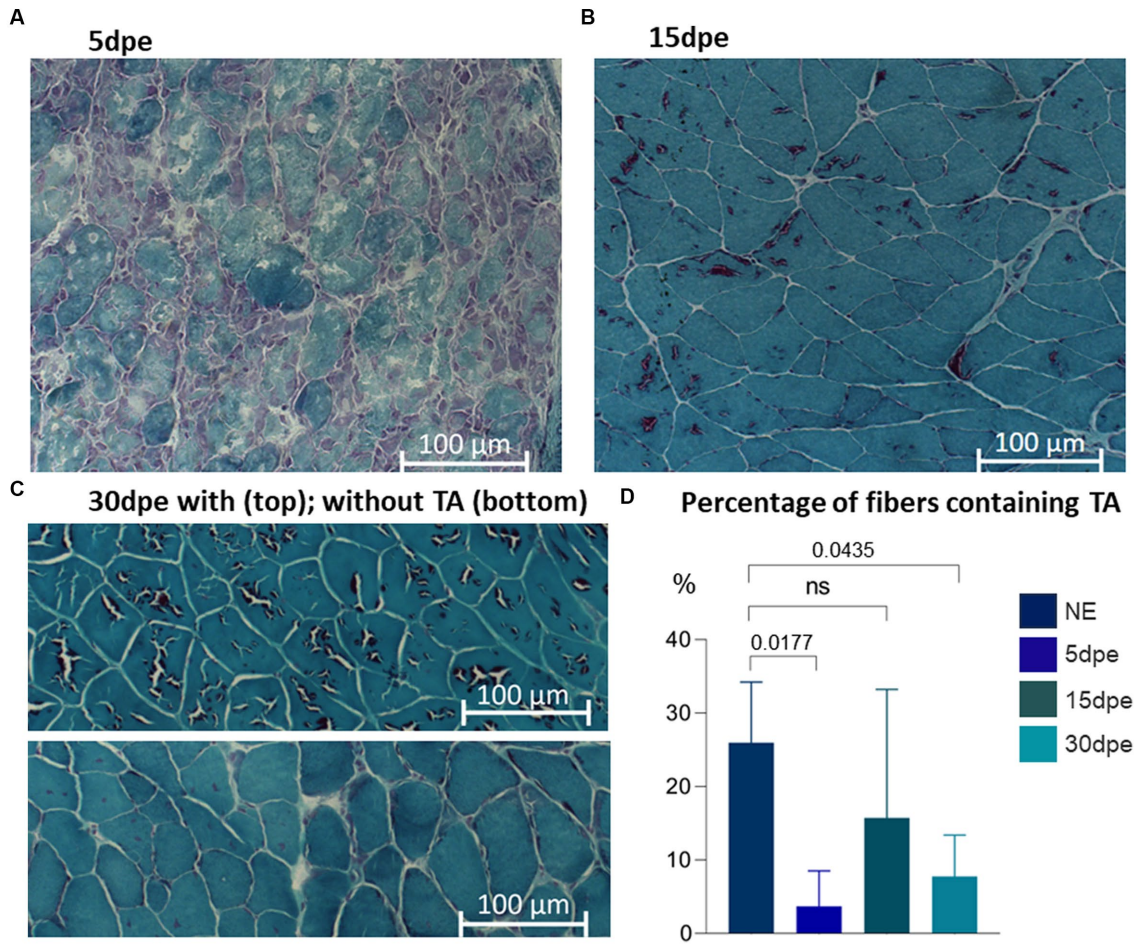

FIGURE 4
Gastrocnemius muscle from aged mice stained with modified Gomori trichrome. TA are present in all experimental groups. Intense degeneration is evident at **(A)** 5 dpe. After muscle regeneration, TA are present in some muscle fibers at **(B)** 15 and **(C)** 30 dpe. The proportion of fibers containing TA was less at 5 and 30 dpe (one-way ANOVA with Dunnett's correction).

in humans). Acute injury, such as electroporation, or chronic injury, such as dystrophic state, leads to a degeneration-regeneration process in which severely damaged fibers are removed from muscle and satellite cells are recruited. The cells differentiate into myoblasts and fuse with each other to form new fibers or with a lesioned fiber to repair the fiber (19). In the present study, new fibers lacked TA. In the first round of experiments, both degeneration-regeneration groups of mice (*Dmd*^{mdx} and electroporated C57BL/6J) presented fewer fibers containing TA than the control group (NE C57BL/6J mice). These findings indicate that recently formed muscle fibers do not contain TA, possibly due to the short post-regeneration time.

The identification of TA is technically challenging. Previous studies using different staining protocols to visualize TA have generated inconsistent results (20). For example, TA stained positively with nicotinamide adenine dinucleotide dehydrogenase-tetrazolium reductase (NADH-TR) (21) but negatively in another study (6). Details are lacking concerning the mechanism of TA genesis, chemical content, and functional consequences. However, some relevant knowledge is known. For example, SR proteins such as calsequestrin (1, 2, 5), Serca1 (1, 2, 6) and Stim1 (22, 23) are found in TA. All these SR proteins are involved in calcium homeostasis (2, 23). Schiaffino et al. (5) proposed the origin of TA in the SR, and compared protein aggregation in muscle with that in neurodegenerative diseases, and discussed the rearrangement of endoplasmic reticulum membranes in non-muscle cells in a similar form to that observed in muscle. The authors suggested that hypoxia led to the formation of TA. Orai1 plasma membrane calcium channel protein (23) was also identified in muscle TA (2, 6, 22). Due to the protein composition of TA, it is possible that correct calcium homeostasis influences TA formation. It would be interesting to verify whether the abnormal elevation of intracellular calcium concentration in dystrophin-deficient muscle, which contributes to disease progression in Duchenne muscular dystrophy (24), could be related to a lower amount of TA in *Dmd*^{mdx} dystrophic muscle.

TA have been demonstrated in different mouse strains (C57BL/6J, BALB/c, DBA/2, 129Sv, and 129Ola) since 5 months of age, with a subsequent increased prevalence within fibers to almost 80% in old gastrocnemius mice (18 months) (6). In addition, male mice fed a resveratrol-enriched diet from 12 to 18 months of age showed a reduction in TA and an improvement in capillarization per fiber (25). Despite the broad observation of TA in wild-type inbred mouse strains (6), TA has also been previously found in dystrophic mice (*Lama2*^{dy} model for congenital merosin-deficient muscular dystrophy 1A) (26). TA were observed in heterozygous, but not homozygous,

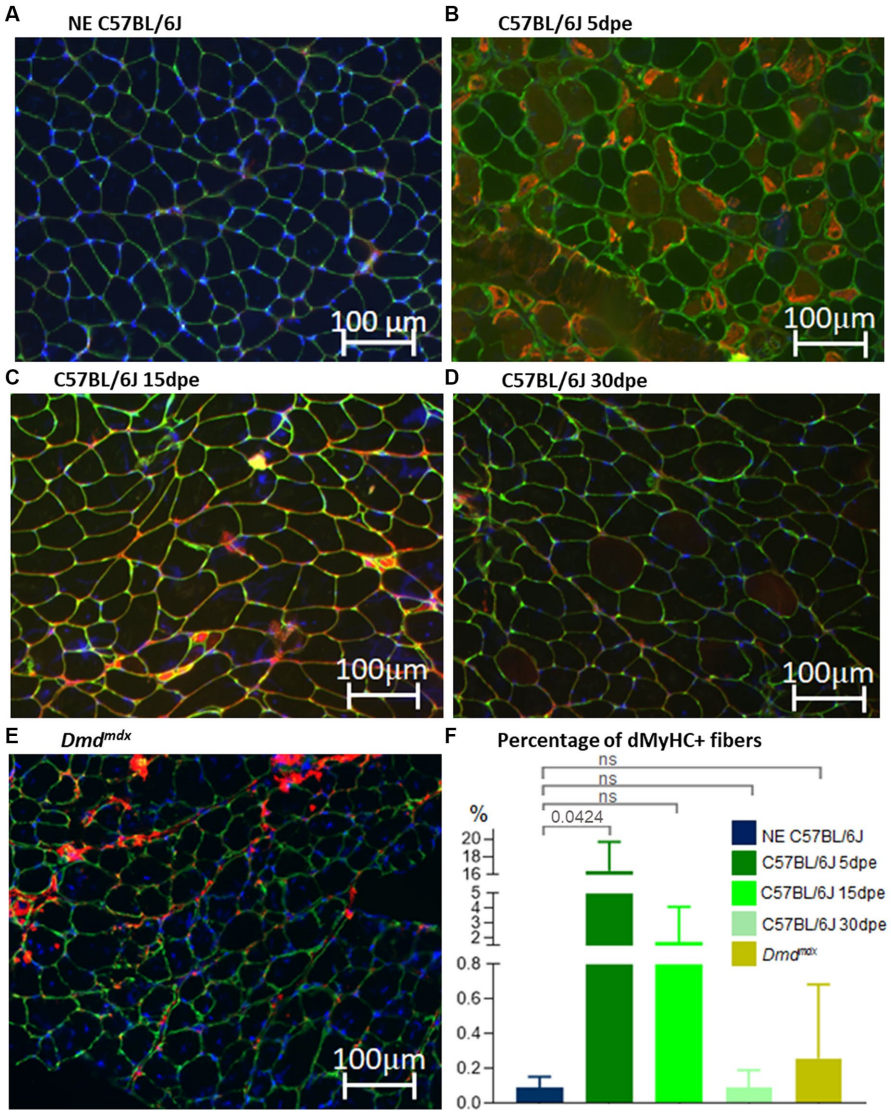

FIGURE 5
Gastrocnemius muscle sections of C57BL/6J before (NE, **A**) and after electroporation (5, 15, and 30 dpe, **B–D**) and in Dmd^{mdx} mice **(E)**. IF was performed using antibodies against dMyHC (red stain inside muscle fibers) and laminin (green stain). Nuclei are stained in blue by dapi (4′,6-diamidino-2-phenylindol). **(F)** Denotes the percentage of positive dMyHC fibers between experimental groups. The only significant difference was between NE C57BL/6J and 5 dpe mice (Kruskal–Wallis with Dunnett's correction).

mice; in the latter, degeneration-regeneration is more intense. In the present study, the presence of TA was observed in another dystrophic model (*Dmd*^{mdx}), specifically in old animals, but in a lesser quantity that observed in old NE C57BL/6J mice. These findings reinforce the hypothesis that TA requires time to accumulate in the sarcoplasm because the intense degeneration-regeneration process in dystrophic animals results in the formation of new fibers that do not have aggregate.

TA have also been observed in human muscle diseases. Funk et al. (12) reported TA in 103 myopathic patients with variable clinical findings and age of onset ranging from childhood to old age. TA presented in subsarcolemmal regions and stained positively for SERCA1 and SERCA2 in both fiber types. Interestingly, the TA stained positive for tau, a protein associated with neurodegenerative diseases. Jain et al. (9) reported four adult patients with TAM; TA appeared in type 1 fibers in two patients and in type 2 fibers in the other two. TA were positively stained by HE, GT, and NADH-TR but were not stained by SDH and Cox stains. All patients presented with muscle weakness. Vivekanandam et al. (10) reported TA (as subsarcolemmal structures) in two of five biopsies of Andersen–Tawil syndrome, which affects most patients with episodic muscle weakness. Limb-girdle myasthenia is another example of a disease in which TA could be present, with a reported patient with clinical signs at 5 years of age. TA in his muscle was revealed at 23 years of age by biopsy (11). In all these reported cases (9–12), TA did not seem to be the cause of the disease. The eventual contribution of TA to pathophysiology or even to the worsening of clinical signs has not yet been investigated.

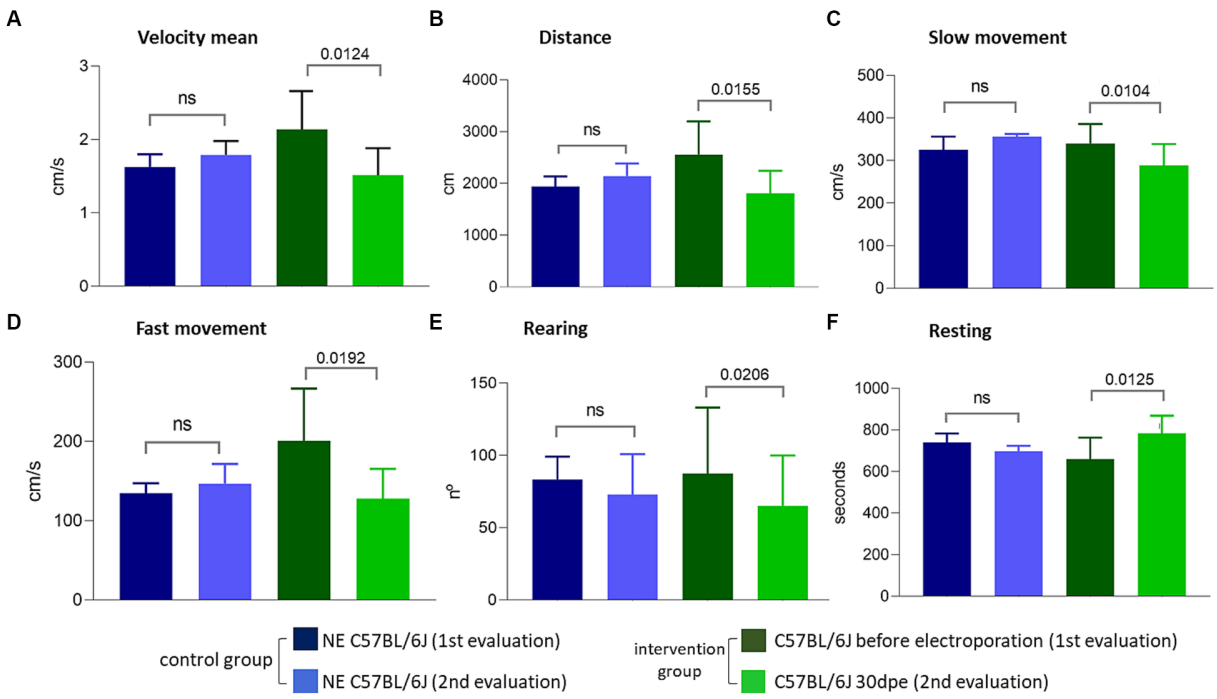

FIGURE 6
Evaluations performed using the Actitrack equipment. All comparisons **(A–F)** between the intervention group before electroporation and 30 dpe were statistically significant (paired *t*-test, $p < 0.05$), compatible with a worsening of the phenotype caused by electroporation.

The functional assessments in the present study measured the physical aptitude of aged mice with more or less TA within muscle fibers. The aim was to see if the absence of TA in new fibers could affect muscle function. However, we did not consider that this *in vivo* experimental design could be influenced by other changes in the tissue caused by the injury, such as loss of muscle mass and consequent loss of strength, fiber type change, and diminished motor units (motor neuron and the myofibers activated by it) (27, 28). The experimental design could not assess the presence of TA as the only variable among the analyzed groups. Moreover, the absence of differences in these tests may have been due to the limited number of animals used.

A possible strategy for TA reduction is exercise (22). Exercise improves health, especially for the elderly population. This has global importance, given that it is expected to be 1 billion people ≥60 years of age worldwide by 2030 (29). During aging, progressively increasing cellular death and malfunction result in sarcopenia and osteoporosis, featuring loss of muscle and bone mass, respectively (30). Locomotor skills can be impaired, reducing the autonomy of the older population in their daily activities. A better understanding of age-related dysfunctions, such as the aggregation of intracellular structures, would help in tracing targets for therapies and other strategies to improve healthier aging.

5 Conclusion

TA form over time, appears in aging normal murine muscles. TA reduction in injured conditions may be due to the degeneration-regeneration process in muscles, with loss of damaged muscle fibers and formation of new fibers that do not present protein aggregation. These new regenerated fibers do not improve the functiona capacity of the aged muscle.

Data availability statement

The raw data supporting the conclusions of this article will be made available by the authors, without undue reservation.

Ethics statement

The animal study was approved by Comissão de Ética no Uso de Animais em Pesquisa, Instituto de Biociencias, Universidade de São Paulo. The study was conducted in accordance with the local legislation and institutional requirements.

Author contributions

FV: Conceptualization, Data curation, Formal analysis, Validation, Writing – original draft, Writing – review & editing, Investigation, Methodology. AJ: Data curation, Investigation, Writing – review & editing. BS: Writing – review & editing, Methodology. IA: Methodology, Writing – review & editing. LC: Writing – review & editing. LF: Writing – review & editing, Methodology. LS: Methodology, Writing – review & editing. NS: Methodology, Writing – review & editing. MF: Writing – review & editing, Formal analysis. MV: Formal analysis, Writing – review & editing, Conceptualization,

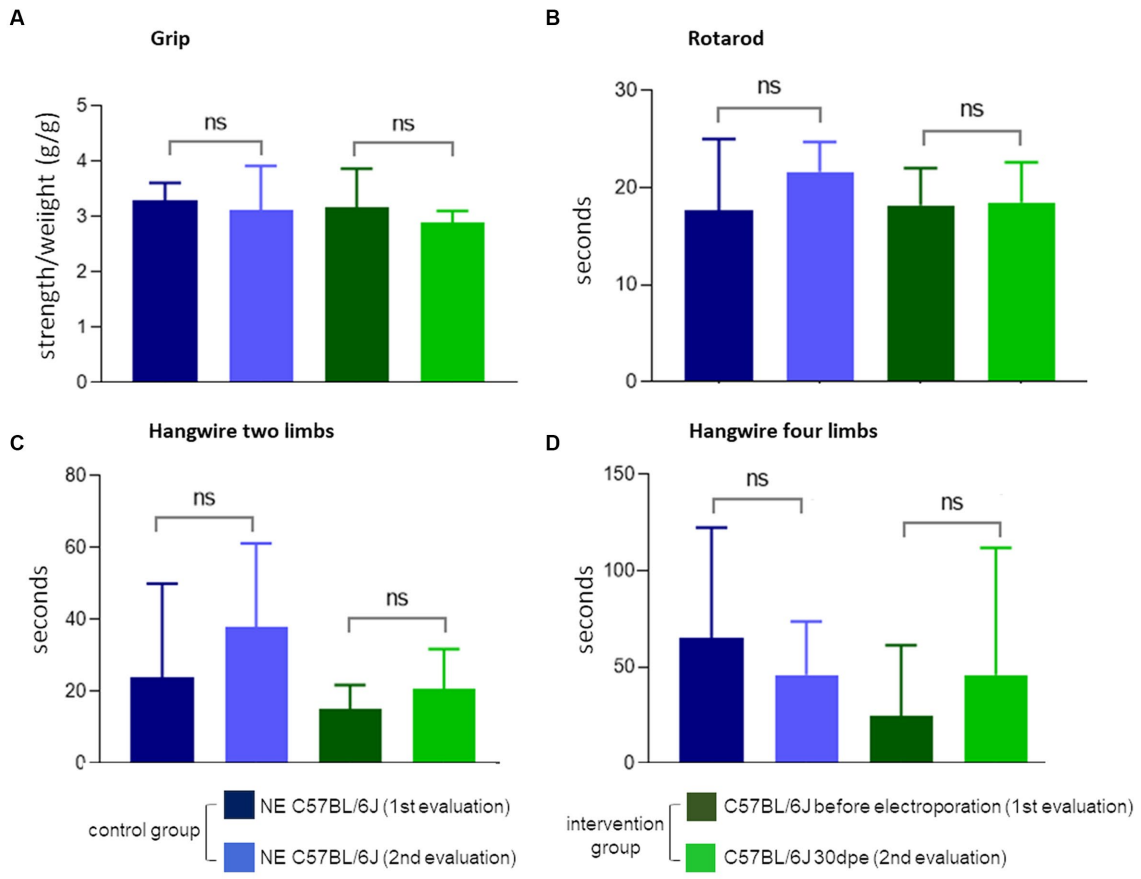

FIGURE 7
Force and balance measures. None of the four tests **(A–D)** showed the difference between normal NE C57Bl and 30 dpe post-injury animals (paired *t* or Wilcoxon tests).

Data curation, Funding acquisition, Project administration, Supervision, Validation, Writing – original draft.

Funding

The author(s) declare financial support was received for the research, authorship, and/or publication of this article. Financial support for the reseach was provided by the FAPESP (2013/08028-1 and 2014/50931-3), CNPq (465355/2014-5), and CAPES (fellowship no 88882.377407/2019-01, for FTGRV).

Acknowledgments

The authors are grateful to Rosimeire dos Santos, Job Carvalho, Heloisa Bueno, and André Santos for technical support.

Conflict of interest

The authors declare that the research was conducted in the absence of any commercial or financial relationships that could be construed as a potential conflict of interest.

Publisher's note

All claims expressed in this article are solely those of the authors and do not necessarily represent those of their affiliated organizations, or those of the publisher, the editors and the reviewers. Any product that may be evaluated in this article, or claim that may be made by its manufacturer, is not guaranteed or endorsed by the publisher.

References

1. Boncompagni S, Protasi F, Franzini-Armstrong C. Sequential stages in the age-dependent gradual formation and accumulation of tubular aggregates in fast twitch muscle fibers: SERCA and calsequestrin involvement. *Age*. (2012) 34:27–41. doi: 10.1007/s11357-011-9211-y

2. Chevessier F, Marty I, Paturneau-Jouas M, Hantaï D, Verdière-Sahuqué M. Tubular aggregates are from whole sarcoplasmic reticulum origin: alterations in calcium binding protein expression in mouse skeletal muscle during aging. *Neuromuscul Disord*. (2004) 14:208–16. doi: 10.1016/j.nmd.2003.11.007

3. Chevessier F, Bauché-Godard S, Leroy JP, Koenig J, Paturneau-Jouas M, Eymard B, et al. The origin of tubular aggregates in human myopathies. *J Pathol*. (2005) 207:313–23. doi: 10.1002/path.1832

4. Engel WK, Bishop DW, Cunningham GG. Tubular aggregates in type II muscle fibers: ultrastructural and histochernical correlation. *J Ultrastruct Res*. (1970) 31:507–25. doi: 10.1016/s0022-5320(70)90166-8

5. Schiaffino S. Tubular aggregates in skeletal muscle: just a special type of protein aggregates? *Neuromuscul Disord*. (2012) 22:199–207. doi: 10.1016/j.nmd.2011.10.005

6. Agbulut O, Destombes J, Thiesson D, Butler-Browne G. Age-related appearance of tubular aggregates in the skeletal muscle of almost all male inbred mice. *Histochem Cell Biol*. (2000) 114:477–81. doi: 10.1007/s004180000211

7. Alberti S, Hyman AA. Biomolecular condensates at the nexus of cellular stress, protein aggregation disease and ageing. *Nat Rev Mol Cell Biol*. (2021) 22:196–213. doi: 10.1038/s41580-020-00326-6

8. Ross CA, Poirier MA. Protein aggregation and neurodegenerative disease. *Nat Med*. (2004) 10:S10–7. doi: 10.1038/nm1066

9. Jain D, Sharma MC, Sarkar C, Suri V, Sharma SK, Singh S, et al. Tubular aggregate myopathy: a rare form of myopathy. *J Clin Neurosci*. (2008) 15:1222–6. doi: 10.1016/j.jocn.2007.11.010

10. Vivekanandam V, Männikkö R, Skorupinska I, Germain L, Gray B, Wedderburn S, et al. Andersen–Tawil syndrome: deep phenotyping reveals significant cardiac and neuromuscular morbidity. *Brain*. (2022) 145:2108–20. doi: 10.1093/brain/awab445

11. Yang LH, Zhao L, Yuan MC, Hua YZ, Yang J, Lin WY, et al. Novel compound heterozygous GFPT1 mutations in a family with limb-girdle myasthenia with tubular aggregates. *Neuromuscul Disord*. (2019) 29:549–53. doi: 10.1016/j.nmd.2019.05.008

12. Funk F, Ceuterick-de Groote C, Martin J-J, Meinhardt A, Taratuto AL, De Bleecker J, et al. Morphological spectrum and clinical features of myopathies with tubular aggregates. *Histol Histopathol*. (2013) 28:1041–54. doi: 10.14670/HH-28.1041

13. Almeida CF, Vainzof M. Skeletal muscle injury by electroporation: a model to study degeneration/regeneration pathways in muscle In: *Nucleic acid detection and structural investigations*. New York city, USA: Springer (2020). 157–69.

14. Aartsma-Rus A, van Putten M. Assessing functional performance in the mdx mouse model. *J Vis Exp*. (2014) 85:1–11. doi: 10.3791/51303

15. Dubowitz V, Sewry CA, Oldfors A. *Muscle biopsy a pratical approach*. Amsterdam, Netherlands: Saunders (2013). 572 p.

16. Schneider CA, Rasband WS, Eliceiri KW. NIH image to image J: 25 years of image analysis. *Nat Methods*. (2012) 9:671–5. doi: 10.1038/nmeth.2089

17. Ribeiro AF, Souza LS, Almeida CF, Ishiba R, Fernandes SA, Guerrieri DA, et al. Muscle satellite cells and impaired late stage regeneration in different murine models for muscular dystrophies. *Sci Rep*. (2019) 9:11842. doi: 10.1038/s41598-019-48156-7

18. F Almeida C, Bitoun M, Vainzof M. Satellite cells deficiency and defective regeneration in dynamin 2-related centronuclear myopathy. *FASEB J*. (2021) 35:e21346. doi: 10.1096/fj.202001313RRR

19. Almeida CF, Fernandes SA, Ribeiro Junior AF, Keith Okamoto O, Vainzof M. Muscle satellite cells: exploring the basic biology to rule them. *Stem Cells Int*. (2016) 2016:1–14. doi: 10.1155/2016/1078686

20. Pavlovičová M, Novotová M, Zahradník I. Structure and composition of tubular aggregates of skeletal muscle fibres. *Gen Physiol Biophys*. (2003) 22:425–40.

21. Rosenberg NL. Tubular aggregates. *Arch Neurol*. (1985) 42:973. doi: 10.1001/archneur.1985.04060090055014

22. Boncompagni S, Pecorai C, Michelucci A, Pietrangelo L, Protasi F. Long-term exercise reduces formation of tubular aggregates and promotes maintenance of Ca^{2+} entry units in aged muscle. *Front Physiol*. (2021) 11:601057. doi: 10.3389/fphys.2020.601057

23. Michelucci A, García-Castañeda M, Boncompagni S, Dirksen RT. Role of STIM1/ORAI1-mediated store-operated Ca^{2+} entry in skeletal muscle physiology and disease HHS public access. *Cell Calcium*. (2018) 76:101–15. doi: 10.1016/j.ceca.2018.10.004

24. Mareedu S, Million ED, Duan D, Babu GJ. Abnormal calcium handling in Duchenne muscular dystrophy: mechanisms and potential therapies. *Front Physiol*. (2021) 12:647010. doi: 10.3389/fphys.2021.647010

25. Toniolo L, Formoso L, Torelli L, Crea E, Bergamo A, Sava G, et al. Long-term resveratrol treatment improves the capillarization in the skeletal muscles of ageing C57BL/6J mice. *Int J Food Sci Nutr*. (2021) 72:37–44. doi: 10.1080/09637486.2020.1769569

26. Craig ID, Allen IV. Tubular aggregates in murine dystrophy heterozygotes. *Muscle Nerve*. (1980) 3:134–40. doi: 10.1002/mus.880030206

27. Gollapudi SK, Michael JJ, Chandra M. Striated muscle dynamics In: *Reference module in biomedical sciences*. Amsterdam, Netherlands: Elsevier (2014)

28. Doherty TJ. Invited review: aging and sarcopenia. *J Appl Physiol*. (2003) 95:1717–27. doi: 10.1152/japplphysiol.00347.2003

29. WHO. Ageing and health. Available at: https://www.who.int/news-room/fact-sheets/detail/ageing-and-health. (2022).

30. Tagliaferri C, Wittrant Y, Davicco MJ, Walrand S, Coxam V. Muscle and bone, two interconnected tissues. *Ageing Res Rev*. (2015) 21:55–70. doi: 10.1016/j.arr.2015.03.002

frontiers | Frontiers in Cellular Neuroscience

TYPE Original Research
PUBLISHED 21 February 2024
DOI 10.3389/fncel.2024.1340240

OPEN ACCESS

EDITED BY
Agnes Lumi Nishimura,
Queen Mary University of London,
United Kingdom

REVIEWED BY
Sonam Parakh,
Macquarie University, Australia
Satish Bodakuntla,
National Institutes of Health (NIH),
United States

*CORRESPONDENCE
Valérie Bercier
valerie.bercier@kuleuven.be

†These authors share first authorship
‡These authors share last authorship

RECEIVED 17 November 2023
ACCEPTED 22 January 2024
PUBLISHED 21 February 2024

CITATION
Van Schoor E, Strubbe D, Braems E, Weishaupt J, Ludolph AC, Van Damme P, Thal DR, Bercier V and Van Den Bosch L (2024) TUBA4A downregulation as observed in ALS *post-mortem* motor cortex causes ALS-related abnormalities in zebrafish. *Front. Cell. Neurosci.* 18:1340240. doi: 10.3389/fncel.2024.1340240

TUBA4A downregulation as observed in ALS *post-mortem* motor cortex causes ALS-related abnormalities in zebrafish

Evelien Van Schoor [1,2,3†], Dufie Strubbe [2,3†], Elke Braems [2,3], Jochen Weishaupt [4], Albert C. Ludolph [4,5], Philip Van Damme [2,3,6], Dietmar Rudolf Thal [1,7‡], Valérie Bercier [2,3*‡] and Ludo Van Den Bosch [2,3‡]

[1]Laboratory of Neuropathology, Department of Imaging and Pathology, KU Leuven (University of Leuven) and Leuven Brain Institute (LBI), Leuven, Belgium, [2]Laboratory of Neurobiology, Department of Neurosciences, KU Leuven (University of Leuven) and Leuven Brain Institute (LBI), Leuven, Belgium, [3]Center for Brain and Disease Research, VIB, Leuven, Belgium, [4]Department of Neurology, Ulm University, Ulm, Germany, [5]Deutsches Zentrum für Neurodegenerative Erkrankungen, Ulm, Germany, [6]Department of Neurology, University Hospitals Leuven, Leuven, Belgium, [7]Department of Pathology, University Hospitals Leuven, Leuven, Belgium

Disease-associated variants of *TUBA4A* (alpha-tubulin 4A) have recently been identified in familial ALS. Interestingly, a downregulation of TUBA4A protein expression was observed in familial as well as sporadic ALS brain tissue. To investigate whether a decreased TUBA4A expression could be a driving factor in ALS pathogenesis, we assessed whether *TUBA4A* knockdown in zebrafish could recapitulate an ALS-like phenotype. For this, we injected an antisense oligonucleotide morpholino in zebrafish embryos targeting the zebrafish *TUBA4A* orthologue. An antibody against synaptic vesicle 2 was used to visualize motor axons in the spinal cord, allowing the analysis of embryonic ventral root projections. Motor behavior was assessed using the touch-evoked escape response. In *post-mortem* ALS motor cortex, we observed reduced TUBA4A levels. The knockdown of the zebrafish *TUBA4A* orthologue induced a motor axonopathy and a significantly disturbed motor behavior. Both phenotypes were dose-dependent and could be rescued by the addition of human wild-type *TUBA4A* mRNA. Thus, *TUBA4A* downregulation as observed in ALS *post-mortem* motor cortex could be modeled in zebrafish and induced a motor axonopathy and motor behavior defects reflecting a motor neuron disease phenotype, as previously described in embryonic zebrafish models of ALS. The rescue with human wild-type *TUBA4A* mRNA suggests functional conservation and strengthens the causal relation between TUBA4A protein levels and phenotype severity. Furthermore, the loss of TUBA4A induces significant changes in post-translational modifications of tubulin, such as acetylation, detyrosination and polyglutamylation. Our data unveil an important role for *TUBA4A* in ALS pathogenesis, and extend the relevance of *TUBA4A* to the majority of ALS patients, in addition to cases bearing *TUBA4A* mutations.

KEYWORDS

amyotrophic lateral sclerosis, TUBA4A, microtubules, axonal pathology, zebrafish

1 Introduction

Amyotrophic lateral sclerosis (ALS) is a fatal neurodegenerative disorder characterized by progressive paralysis resulting from the selective loss of upper and lower motor neurons. Patients usually die 2–5 years after disease onset due to respiratory failure. ALS has an incidence of 1–2 individuals per 100.000 each year. About 90% of patients display sporadic ALS, with no family history of the disease. In the remaining 10%, the disease is transmitted within families, referred to as familial ALS (Taylor et al., 2016). The most common disease-causing mutations are found in fused in sarcoma (*FUS*), superoxide dismutase 1 (*SOD1*), chromosome 9 open reading frame 72 (*C9orf72*) and transactive response DNA-binding protein (*TARDBP*) (Al-Chalabi and Hardiman, 2013; Taylor et al., 2016).

In addition, several genes with a role in cytoskeletal dynamics and axonal transport are linked to ALS, amongst which dynactin subunit 1 (*DCTN1*), kinesin family member 5A (*KIF5A*) and spastin (*SPAST*) (Castellanos-Montiel et al., 2020). This suggests that there might be a direct causative relationship between defects in cytoskeletal integrity and neurodegeneration. More recently, Smith et al. found mutated variants in the alpha-tubulin 4A (*TUBA4A*) gene in ALS patients, based on exome sequencing data from a large cohort of ALS patients and controls. These mutated variants are associated with classical spinal onset ALS, and in some cases also frontotemporal dementia (FTD)-like symptoms (Smith et al., 2014). We confirmed the importance of *TUBA4A* variants in ALS in an independent Belgian cohort (Perrone et al., 2017).

TUBA4A encodes one of nine known α-tubulin isotypes, with all variants expressed from different genes. The structures of α- and β-tubulin are highly conserved throughout eukaryotes, nevertheless, the range of human diseases associated with mutations in different tubulin isotypes indicates that specific isotypes have different functional specifications (Breuss et al., 2017). This is supported by the fact that the expression of different isotypes differs depending on cell type and tissue. For example, *TUBA8A* is mainly expressed in testes and skeletal muscle, while *TUBA4A* is highly expressed in the nervous system (Braun et al., 2010; Clark et al., 2016).

Functionally, α-tubulin assembles with β-tubulin to form stable tubulin heterodimers, which dynamically polymerize into sheets of longitudinal polarized protofilaments, building the cylindrical, hollow microtubules (Tischfield et al., 2011; Chakraborti et al., 2016). Stable microtubules are important for a wide range of functions in long extending axons, and serve as the tracks along which motor proteins (such as dynein and kinesin) move cargoes with the help of adaptor proteins (Clark et al., 2016). Hereby, microtubule stability and function is influenced by the presence of different post-translational modifications (PTMs) of tubulin (Boiarska and Passarella, 2021). Most PTMs are reversible and occur on the C-terminal tail of tubulins, except for lysine (K40) acetylation which is located on the luminal surface or microtubules (Sferra et al., 2020).

Motor neurons are the most asymmetric cells in nature, with axons reaching a meter in length in humans. Therefore, they have a crucial requirement for proper cytoskeletal functioning. A disruption of cytoskeleton integrity could affect cell morphology, axonal branching, the establishment of neuromuscular junctions, and many other critical cell functions. In addition, it could prevent molecular motors from transporting the necessary cargoes, with a potentially deleterious effect on neuronal function (Clark et al., 2016; Taylor et al., 2016; Castellanos-Montiel et al., 2020). Interestingly, it was reported that sporadic ALS patients have a downregulation of α-tubulin subunits in affected brain regions (Jiang et al., 2005; Helferich et al., 2018; Maraldi et al., 2019). However, whether these alterations in α-tubulin expression in the majority of ALS patients can also drive ALS disease pathogenesis is still unknown.

In this study, we confirmed a decrease in TUBA4A protein expression in *post-mortem* tissue from ALS patients compared to controls. We mimicked this decrease in zebrafish using antisense oligonucleotide morpholinos (AMO) directed against *tuba8l2* (ENSDARG00000031164), the single zebrafish orthologue for *TUBA4A,* which is 94% conserved at the protein level. This decreased expression of tuba8l2 did not affect total levels of alpha-tubulin, but led to abnormalities in the axons of spinal cord motor neurons, as well as motor behavior deficits consistent with published models of ALS (Kabashi et al., 2011, Swinnen et al., 2018). Both phenotypes were dose-dependent and could be rescued by the addition of human wild-type *TUBA4A* mRNA. Additionally, while we did not observe changes in microtubule polymerization, we found significant changes in post-translational modifications of tubulin in our zebrafish knockdown model. Overall, our data point toward a central role of *TUBA4A* in ALS pathogenesis, aside from cases bearing *TUBA4A* mutations.

2 Material and Methods

2.1 Human autopsy cases

Brain and spinal cord tissues were collected in accordance with the applicable laws in Belgium (UZ Leuven) and Germany (Ulm). The recruitment protocols for collecting the brains were approved by the ethical committees of the University of Ulm (Germany) and UZ Leuven (Belgium). This study was approved by the UZ Leuven ethical committee (Belgium) (S60803, S55312). Tissues were collected with an average *post-mortem* interval of 45 h. After autopsy, the right hemisphere was dissected in coronal planes and frozen at −80°C. The left hemisphere was fixed in 4% phosphate-buffered formaldehyde (PFA) (F8775, Sigma-Aldrich, St Louis, MO, US). Ten sporadic ALS cases and twelve non-neurodegenerative controls were included in this study (Online

Abbreviations: ALS, Amyotrophic lateral sclerosis; AMO, Antisense oligonucleotide morpholinos; C9orf72, Chromosome 9 open reading frame 72; CaP, Caudal primary; DAB, 3,3′-Diaminobenzidine; DCTN1, Dynactin subunit 1; DPRs, dipeptide repeat proteins; FBS, Fetal Bovine Serum; FTD, Frontotemporal dementia; FUS, Fused in sarcoma; GAPDH, Glyceraldehyde-3-phosphate dehydrogenase; HA, Hemagglutinin; hpf, Hours post fertilization; HRP, Horseradish peroxidase; KIF5A, Kinesin family member 5A; MAPs, Microtubule-associated proteins; MTL, Medial temporal lobe; NF-H, Neurofilament H; NFT, Neurofibrillary tangle; PBS, Phosphate-buffered saline; PFN1, Profilin 1; PFA, Phosphate-buffered formaldehyde; PRPH, Peripherin; pTDP-43, Phosphorylated transactive response DNA-binding protein 43kDa; PTMs, Post-translational modifications; SDS-PAGE, Sodium dodecyl sulfate-polyacrylamide gel electrophoresis; SOD1, Superoxide dismutase 1; SPAST, Spastin; SV2, Synaptic vesicle 2; TARDBP, Transactive response DNA-binding protein; TBCB, Tubulin-folding cofactor B; TBS, Tris-buffered saline; TEER, Touch-evoked escape response; TUBA4A, Alpha-tubulin 4A.

resource **Supplementary Table 1**). The diagnosis of ALS was based on clinical assessment according to the consensus criteria for ALS (Brooks et al., 2000; de Carvalho et al., 2008; de Carvalho and Swash, 2009). The *post-mortem* diagnosis of ALS was pathologically confirmed by assessment of the pTDP-43 pathology. Braak NFT stage (Braak et al., 2006) and AβMTL phase (Thal et al., 2000) were determined based on immunohistochemical stainings with antibodies against Aβ and p-tau.

2.2 Human tissue immunohistochemistry

Histological examination was performed on 5 μm thick sections cut from formalin-fixed, paraffin-embedded tissue of frontal, pre- and post-central, and temporal cortex, hippocampus and spinal cord. Sections were stained with antibodies against pTDP-43, TUBA4A (C-term), pTau$^{(S202/T205)}$ and Aβ_{17-24} (Online resource **Supplementary Table 2**). Stainings were performed with the BOND-MAX automated IHC/ISH Stainer (Leica Biosystems, Wetzlar, Germany) using the Bond Polymer Refine Detection kit (DS9800, Leica Biosystems). Briefly, slides were deparaffinized and epitopes were retrieved with low or high pH buffer. After incubation with Peroxidase-Blocking Reagent (DS9800, Leica Biosystems), slides were incubated with primary antibodies for 30 min, followed by secondary antibody incubation. DAB was used for visualization, followed by counterstaining with hematoxylin. Dehydration was carried out in an autostainer, followed by mounting in an automated cover-slipper (Leica Biosystems). Images were acquired using the Leica DM2000 LED microscope coupled to a Leica DFC 7000 T camera. Images were processed using ImageJ and combined into figures using Inkscape.

2.3 Human tissue protein extraction

For biochemistry of human tissues, the right hemispheres were cut in approx. 1 cm thick slabs and frozen at −80°C. Fifty mg of motor cortex and spinal cord was weighed and mechanically homogenized in 0.5 ml 2% SDS in TBS (Tris-buffered saline) with Nuclease (88701, Pierce^{TM} Universal Nuclease, Thermo Fisher Scientific) and a cocktail of protease/phosphatase inhibitors (78440, Halt, Thermo Fisher Scientific) using a micropestle (CXH7.1, Carl Roth, Karlsruhe, Germany). Samples were sonicated, followed by a centrifugation at 13,000 g for 30 min. The resulting supernatant was used. Protein concentrations were determined using the Pierce BCA Protein Assay Kit (23225, Thermo Fisher Scientific).

2.4 Zebrafish protein extraction

Zebrafish embryos were collected at 48 h post fertilization (hpf) and were manually dechorionated using forceps and the yolk was removed. The embryos were homogenized in RIPA buffer (R0278, Sigma-Aldrich) supplemented with protease and phosphatase inhibitors (78440, Halt, Thermo Fisher Scientific) using a micropestle on a rotor. After centrifugation (3 min, 13 000 g), the supernatant was collected and protein concentrations were determined using the Pierce BCA Protein Assay Kit (23225, Thermo Fisher Scientific).

2.5 Human tissue and zebrafish western blotting

For western blotting, 10 μg (human central nervous system lysates) or 20 μg (zebrafish lysates) of protein was loaded on a Bis-Tris 4–12% gradient SDS-PAGE (WG1402BOX, Invitrogen, Thermo Fisher Scientific) in MOPS-SDS running buffer (J62847.K2, Alfa Aesar, Haverhill, MA, USA), electrophoresed at 150 V for 60 min, and transferred to a nitrocellulose membrane (GE10600001, Semidry transfer, Biorad, Hercules, CA, USA). Membranes were blocked with 5% non-fat dried milk (A0830.1000, AppliChem, Darmstadt, Germany) in phosphate-buffered saline (PBS) 0.1% Tween-20 (PBST). Primary antibodies and the corresponding dilutions are listed in **Supplementary Table 2** (Online resource). Secondary antibodies were goat anti-rabbit IgG-HRP or goat anti-mouse IgG-HRP (1:10 000, P044801-2 and P044701-2, polyclonal, Dako). Blots were developed with SuperSignal West Pico or Dura plus ECL reagent (34580 and 34075, Thermo Fisher Scientific). Digital images were acquired using the Amersham Imager 600 (GE Healthcare, Chicago, IL, USA). All blots were stripped (21063, Restore Western Blot Stripping Buffer, Thermo Fisher Scientific) of bound antibodies and reprobed with GAPDH to control for equal protein loading. Band intensities were measured using ImageJ and were normalized to GAPDH.

2.6 Antisense oligonucleotide morpholino design and *TUBA4A* mRNA transcription

An ATG blocking morpholino (AMO) against *tuba8l2*, the single human *TUBA4A* orthologue in Danio rerio (morpholino sequence 5'-TTGGAGTTGGATTTGTTTTTTGCCG-3') was designed and generated by Gene Tools (Philomath, USA). The standard control AMO provided by Gene Tools was used as negative control (morpholino sequence 5'-CCTCTTACCTCAGTTACAATTTATA-3'). A human wild-type TUBA4A HA-tagged encoding plasmid was kindly provided by Dr. J. Landers (Smith et al., 2014). To produce mRNA, plasmids were linearized by restriction digestion, transcribed with mMESSAGE mMACHINE T7 kit (AM1344, Ambion, Huntingdon, UK) and the resulting mRNA purified with the MEGAclear Kit (AM1908, Ambion). The mRNA concentration was measured by spectrophotometry (Nanodrop, Thermo Fisher Scientific). mRNA quality and length were verified by RNA gel electrophoresis.

2.7 Zebrafish injections

All zebrafish breeding was approved by the Ethical Committee for Animal Experimentation of the KU Leuven (P125/2014). Zebrafish were reared and incubated at 28.5°C. All experiments were performed on embryos younger than five days post fertilization, implying that these experiments are in line with the principle of 3Rs as these are not regulated as animal studies. One- to two-cell stage zebrafish embryos from the AB strain were injected

with the indicated amounts of morpholino and/or mRNA diluted in aqua ad iniectabilia (3521664, B. Braun, Melsungen, Germany) and supplemented with phenol red for verification of injection volume.

2.8 Zebrafish SV2 immunohistochemistry and analysis

At 30 hpf, embryos were manually dechorionated and deyolked, and fixed overnight at 4°C in 4% PFA in PBS. Fish were permeabilized with acetone for 1 h at −20°C, followed by blocking with 1% bovine serum albumin (BSA) (A7030, Sigma-Aldrich)/1% dimethyl sulfoxide (DMSO) (D2650, Sigma-Aldrich)/PBS for 1h at RT and immunostained with mouse anti-synaptic vesicle 2 (SV2) (1:200; online resource **Supplementary Table 2**) and secondary Alexa Fluor 555 anti-mouse antibody (1:500, A-31570, Thermo Fisher Scientific) as previously described (Swinnen et al., 2018). For axonal length analysis, 10–15 embryos per condition per experiment were analyzed using a Leica DM 3000 LED microscope and the tracking tool in Lucia software (version 4.60, Laboratory Imaging, resolution 2448 x 2048 pixels). Five predefined and consecutive ventral root projections (i.e. the 8^{th} up to the 12^{th} axon) were measured by a blinded observer. Each axon was measured starting from the beginning of the ventral root projection until the end of any observable staining. Data were normalized to the control condition. A total of 10–15 embryos were used per condition per experiment with three biological replicates, which has previously been shown to be adequate to measure an effect (Swinnen et al., 2018).

2.9 Zebrafish touch-evoked escape response (TEER)

Embryos were manually dechorionated at 30 hpf. 10–15 embryos were used per condition per experiment with three biological replicates, which has previously been shown to be adequate to measure an effect (Bercier et al., 2019). At 48 hpf, zebrafish embryos were individually placed in a 150 mm petri dish filled with 28.5°C embryo medium. After 30 s of habituation, an escape response was elicited by a light brush on the tail and recorded at 30 Hz with a Sony HDR-AS30V camera (resolution 1920 x 1080 pixels) until the end of the escape response (Kabashi et al., 2011). The videos were analyzed in ImageJ using the Manual Tracking plugin and the total distance, the maximal instant velocity and the average velocity were calculated by a blinded observer. Data were normalized to the control condition.

2.10 EB3 comet assay

Analysis of microtubule polymerization events was performed according to the previously described EB3 comet assay (Bercier et al., 2019), where EB3-GFP is expressed in single caudal primary (CaP) motor neurons by microinjection of the pUAS-EB3-GFP plasmid in the Tg(mnx1:GAL4) line (Zelenchuk and Brusés, 2011). Time-lapse imaging was performed at 48 hpf on live, agarose-embedded embryos with a spinning disk confocal microscope (Nikon NiE microscope, Yokogawa CSU-X spinning-disk module and Teledyne Photometrics Prime 95B camera, NIS-Elements software, Nikon Instruments Europe B.V.). Imaging was performed using a 60x LWD water-immersion lens (Nikon Fluor 60x/NA 1.00 WD 2.0) where an image was acquired every 500 ms for a total duration of 5 min. The average length of the imaged arbor segments did not differ between conditions. Kymograms were extracted from time-lapse series on linear segments of CaP distal arbors using the Kymograph Tool (Montpellier RIO Imaging, CNRS, France). Each pixel on the Y-axis represents one timepoint projected against neurite length on the X-axis. Kymogram analysis was performed to determine the duration and distance of single comets as well as the average speed of polymerization and the number of polymerization events (i.e., comet density).

2.11 Statistical analysis

Statistical analyses were performed using Graphpad Prism 9.0 software. Normality was assessed using the Shapiro-Wilk test. Variance homogeneity was assessed using the F-test (for two groups) or the Bartlett's test (for more than two groups). A Mann-Whitney test or unpaired t-test was used to compare two groups. A one-way ANOVA or Kruskal-Wallis test followed by Dunn's or Dunnett's multiple comparisons was used to determine the significant difference between multiple groups. Data are presented as mean ± SD or median ± IQR. Significance levels are indicated as follows: $^{*}p < 0.05$, $^{**}p < 0.01$, $^{***}p < 0.001$, $^{****}p < 00001$.

3 Results

3.1 ALS *post-mortem* motor cortex shows decreased TUBA4A expression

To investigate possible alterations in the expression of the TUBA4A protein in ALS, we performed western blot on SDS-soluble extracts from motor cortex from ALS and control cases using a TUBA4A-specific antibody. A significant decrease in the total protein expression of TUBA4A in ALS compared to control motor cortex was observed ($p = 0.0066$; unpaired t-test; **Figures 1a, b**; online resource **Supplementary Figure 1a**). In the spinal cord, there was a trend toward decreased TUBA4A levels in ALS cases compared to controls, although significance was not reached ($p = 0.1349$; unpaired t-test; online resource **Supplementary Figures 1b, c**). In addition, we evaluated the TUBA4A expression pattern by immunohistochemistry in ALS and control cases and observed a dense staining of the cell body and neurites in the motor cortex (**Figure 1c**) and in the spinal cord (online resource **Supplementary Figure 2**), both in ALS cases and controls. No TUBA4A inclusions were observed microscopically in the motor cortex or the spinal cord (**Figure 1c**, online resource **Supplementary Figure 2**). These results from *post-mortem* human tissue showed that TUBA4A protein levels were reduced in sporadic ALS patient tissue without changes in protein distribution.

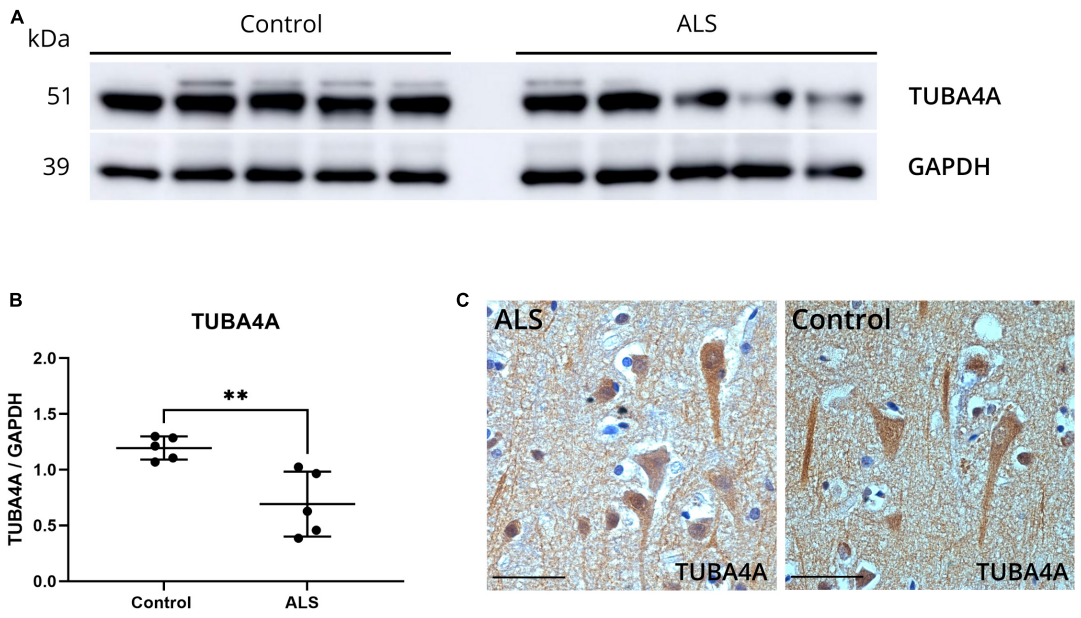

FIGURE 1
ALS *post-mortem* motor cortex exhibits TUBA4A downregulation. **(a)** Western blot on SDS-soluble lysates derived from the motor cortex of control ($n = 5$) and ALS ($n = 5$) cases using an antibody against TUBA4A (C-term). GAPDH was used as a loading control. **(b)** Quantification of the expression of TUBA4A as a ratio to GAPDH in the motor cortex. Unpaired t-test. **(c)** Immunohistochemical staining of the motor cortex of a representative ALS and control case with an antibody against TUBA4A (C-term). Scale bar represents 50 μm. $^{**}p < 0.01$.

3.2 Knockdown of zebrafish *TUBA4A* orthologue induces dose-dependent axonal abnormalities and motor behavior deficits in zebrafish

To determine the potential significance of TUBA4A downregulation, we investigated whether the knockdown of *tuba8l2* is deleterious to motor axons of zebrafish embryos. This is the single zebrafish *TUBA4A* orthologue (ENSDARG00000031164), which is 94% conserved at the protein level when compared to human *TUBA4A*, and shown to be expressed throughout all anatomical structures in embryonic stages (at least until pec-fin stage at 72 hpf (Thisse and Thisse, 2004). We designed a morpholino directed against the ATG start codon of *tuba8l2* (**Figure 2a**) and injected different doses in one- to two-cell stage zebrafish oocytes. The highest dose of 0.160 mM was determined through a dose-response where we observed a high increase in morphological abnormalities together with a fast drop in survival at doses above 0.200 mM. The dose of 0.160 mM led to morphologically normal embryos (**Figure 4a**) and a standard control morpholino was injected at a dose equaling the highest dose of the *tuba8l2* morpholino (0.160 mM). We then assessed tuba8l2 protein levels by western blot at 48 hpf using a specific antibody against TUBA4A (C-term). We detected a dose-dependent knockdown of tuba8l2 levels, with the highest knockdown of 54% at 0.160 mM of morpholino (mean ratio to control: 0.46), a knockdown of 41% at a dose of 0.125 mM (mean ratio to control: 0.59) and a 12% knockdown when we injected 0.050 mM morpholino (mean ratio to control: 0.88) (**Figures 2b, c**; online resource **Supplementary Figure 3**). Importantly, the morpholino injection and subsequent reduction in tuba8l2 did not affect the levels of total α-tubulin, as shown by western blot with an antibody against α-tubulin (**Figures 2d, e**; online resource **Supplementary Figure 3**) suggesting compensation by other isotypes.

To assess the effect of the specific knockdown of *tuba8l2* on motor neuron axonal morphology, we performed SV2 immunohistochemistry to visualize the ventral roots projections of the spinal cord motor neurons at 30 hpf (**Figure 2f**) (Swinnen et al., 2018). We observed a significant reduction in axonal length in the 0.160 mM *tuba8l2* morpholino condition compared to the control morpholino condition ($p < 0.0001$; one-way ANOVA with Dunnett's multiple comparisons; **Figure 2g**). This effect was dose-dependent, as shown by the 0.125 mM and 0.050 mM morpholino conditions ($p < 0.0001$ and $p = 0.045$, respectively; one-way ANOVA with Dunnett's multiple comparisons; **Figure 2g**).

To assess whether *tuba8l2* knockdown in zebrafish also had an effect on motor function, we performed a touch-evoked escape response (TEER) assay at 48 hpf as previously described (Kabashi et al., 2011). We compared non-injected, control morpholino injected and *tuba8l2* morpholino injected conditions, with an example escape trace of the AMO control condition depicted in **Figure 3d**. This assay showed that reduction of tuba8l2 led to a shorter escape, as shown by a significant decrease in total distance travelled (0.160 mM: $p < 0.0001$; 0.125 mM: $p = 0.0001$; Kruskal-Wallis test with Dunn's multiple comparisons; **Figure 3a**). Furthermore, we observed a significant reduction in the average velocity (**Figure 3b**) and instant maximal velocity (**Figure 3c**) in the 0.160 mM ($p < 0.0001$; one-way ANOVA with Dunnett's multiple comparisons) and the 0.125 mM ($p < 0.0001$; one-way ANOVA with Dunnett's multiple comparisons) *tuba8l2* morpholino-injected embryos compared to control morpholino. In

10.3389/fncel.2024.1340240

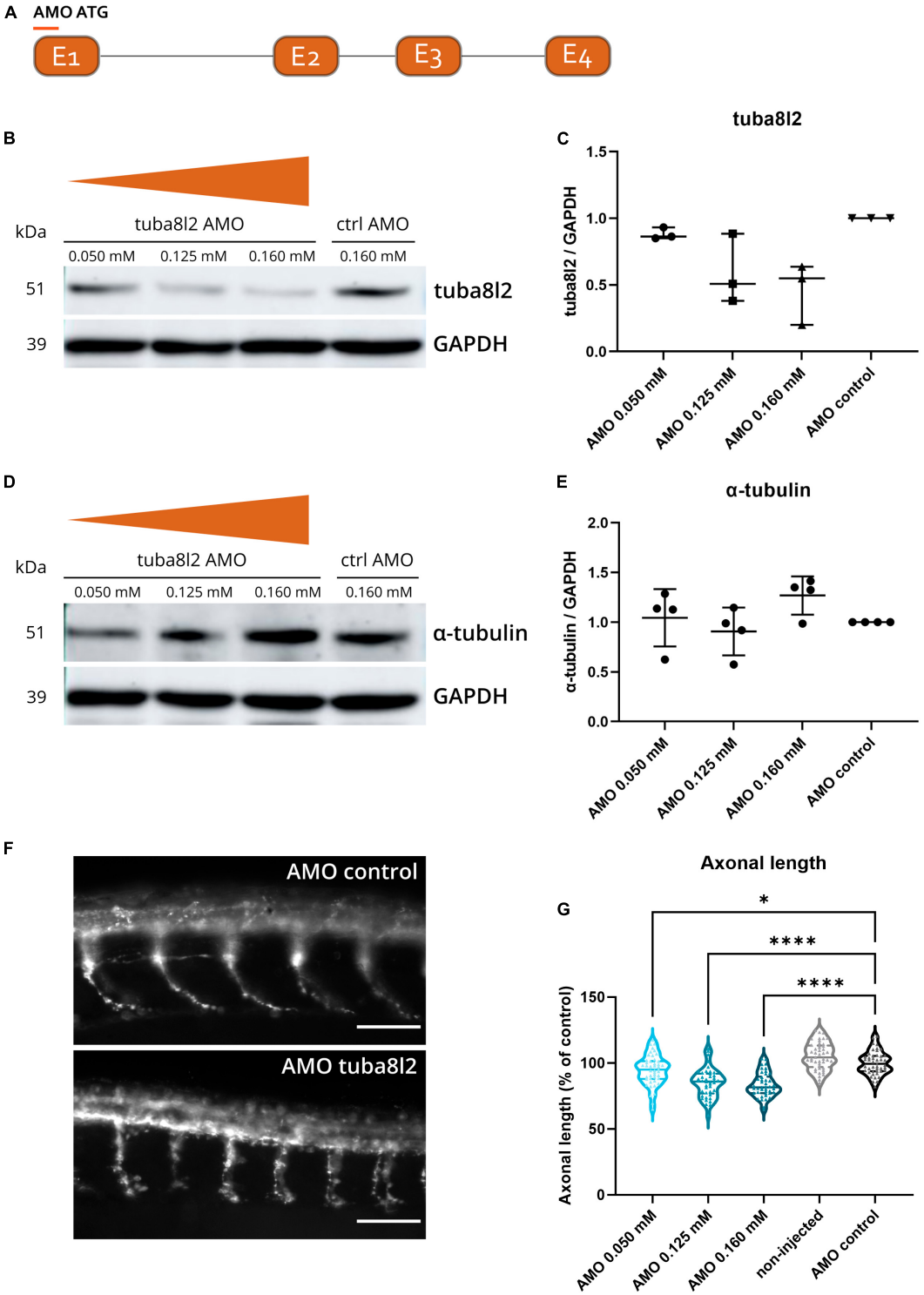

FIGURE 2
Specific *tuba8l2* knockdown in zebrafish induces axonal abnormalities. **(a)** An ATG morpholino was designed against the *Danio rerio TUBA4A* orthologue *tuba8l2*. **(b–e)** Western blot was performed at 48 hpf after injection of different doses of ATG morpholino against *tuba8l2* (0.160 mM, 0.125 mM and 0.050 mM) as well as the injection of a control morpholino (0.160 mM). $N = 3$ experiments; $n = 10–15$ zebrafish per group per experiment. Quantification of tuba8l2 panel **(c)** and α-tubulin panel **(e)** protein levels relative to GAPDH for the different injection conditions. **(f,g)** Visualization of motor axons by SV2 immunohistochemistry at 30 hpf after injection of different doses of ATG morpholino against *tuba8l2* (0.160 mM, 0.125 mM and 0.050 mM) or a control morpholino (0.160 mM). A non-injected condition was also included. Scale bar represents 50 μm $p < 0.0001$ (0.160 mM versus AMO control), $p < 0.0001$ (0.125 mM versus AMO control) and $p < 0.0450$ (0.050 mM versus AMO control); one-way ANOVA with Dunnett's multiple comparisons. Axonal length was measured for $N = 3$ experiments; $n = 10–15$ zebrafish embryos per group per experiment; with every data point representing the average length of the five measured axons for each zebrafish embryo. *$p < 0.05$; ****$p < 0.0001$. AMO, morpholino; hpf, hours post fertilization.

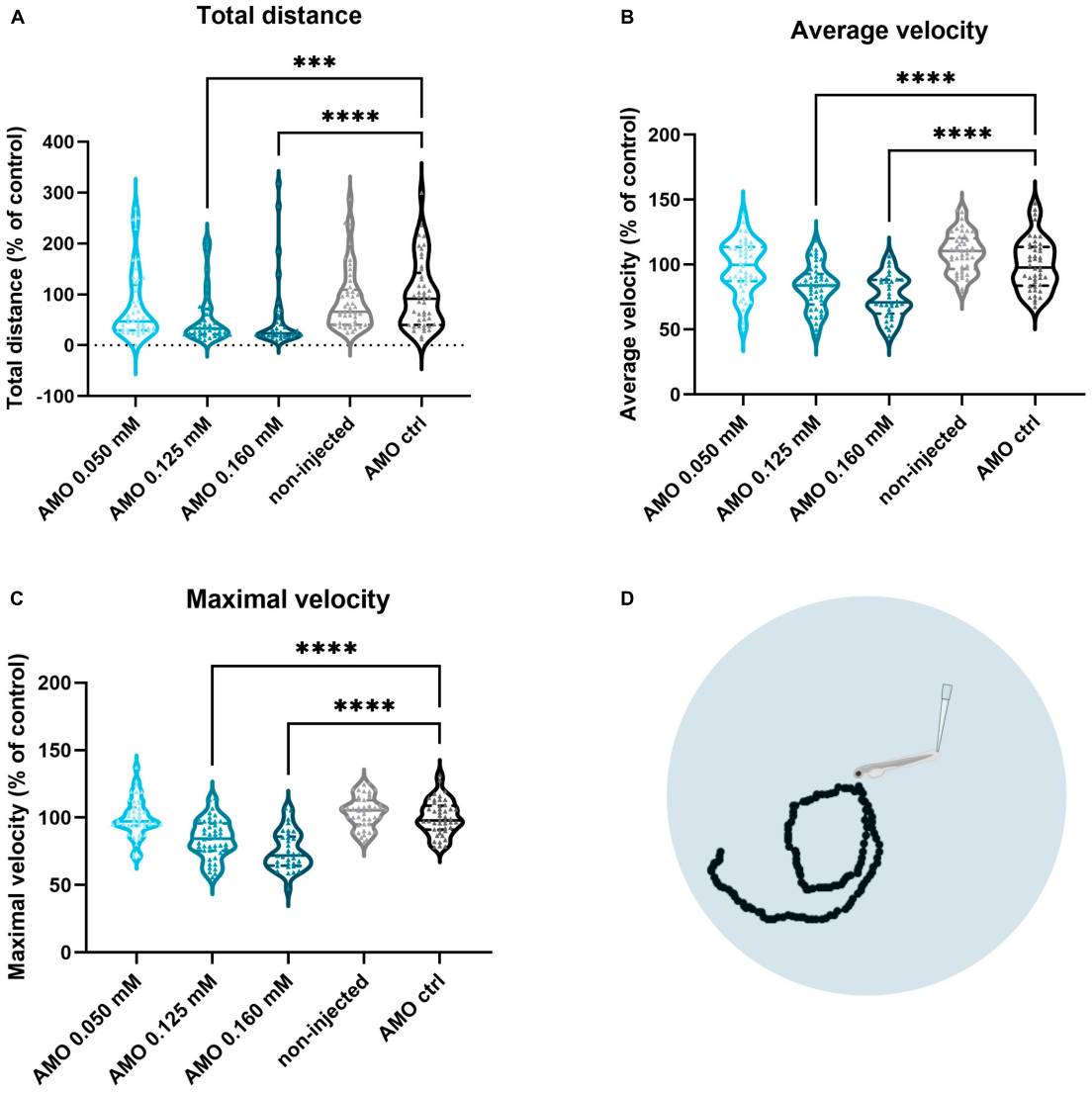

FIGURE 3
Zebrafish motor behavior deficits are induced by *tuba8l2* knockdown. Zebrafish were subjected to a touch-evoked escape response (TEER) assay at 48 hpf after injection of different doses of ATG morpholino against *tuba8l2* (0.160 mM, 0.125 mM, 0.050 mM), or a control morpholino (0.160 mM). In addition, non-injected embryos were included in the analysis. **(a)** Total distance for 0.160 mM ($p < 0.0001$), 0.125 mM ($p = 0.0001$) and 0.050 mM ($p = 0.1936$) compared to AMO control condition. **(b)** Average velocity for 0.160 mM ($p < 0.0001$), 0.125 mM ($p < 0.0001$) and 0.050 mM ($p = 0.9814$) compared to AMO control condition. **(c)** Maximal instant velocity 0.160 mM ($p < 0.0001$), 0.125 mM ($p < 0.0001$) and 0.050 mM ($p = 0.9983$) compared to AMO control condition. Kruskal-Wallis test with Dunn's multiple comparisons panel **(a)** or one-way ANOVA with Dunnett's multiple comparisons panels **(b,c)**; $N = 3$ experiments; $n = 10–15$ zebrafish embryos per group per experiment; with each data point representing an individual zebrafish embryo. **(d)** Visual example of the tracking of an escape response in the AMO control condition using the TEER assay in zebrafish embryos at 48 hpf. ***$p < 0.001$; ****$p < 0.0001$. AMO, morpholino; hpf, hours post fertilization.

conclusion, we find that the specific knockdown of the zebrafish orthologue of *TUBA4A* led to a dose-dependent axonopathy and motor behavior phenotype similar to what has previously been described for zebrafish ALS models.

3.3 Axonal phenotype and motor behavior defects are rescued by human *TUBA4A* mRNA

To confirm that the observed phenotypes are indeed a direct consequence of the specific knockdown of *tuba8l2*, and to confirm functional conservation between zebrafish and human orthologues, we assessed the rescue of these phenotypes through the co-expression of human wild-type TUBA4A. To achieve this, we injected zebrafish eggs with human HA-tagged *TUBA4A* mRNA at the highest non-toxic dose of 300 ng/μl, and collected the embryos for western blot at 48 hpf. An anti-HA antibody confirmed the expression of the HA-TUBA4A protein at 48 hpf in the *TUBA4A* mRNA-injected condition, which was absent in the control condition (Online resource; **Supplementary Figure 4**). Next, we co-injected *TUBA4A* mRNA with the highest *tuba8l2* morpholino dose (i.e.,0.160 mM) (**Figure 4a**). We analyzed the effect on spinal cord motor neurons, as aforementioned, by

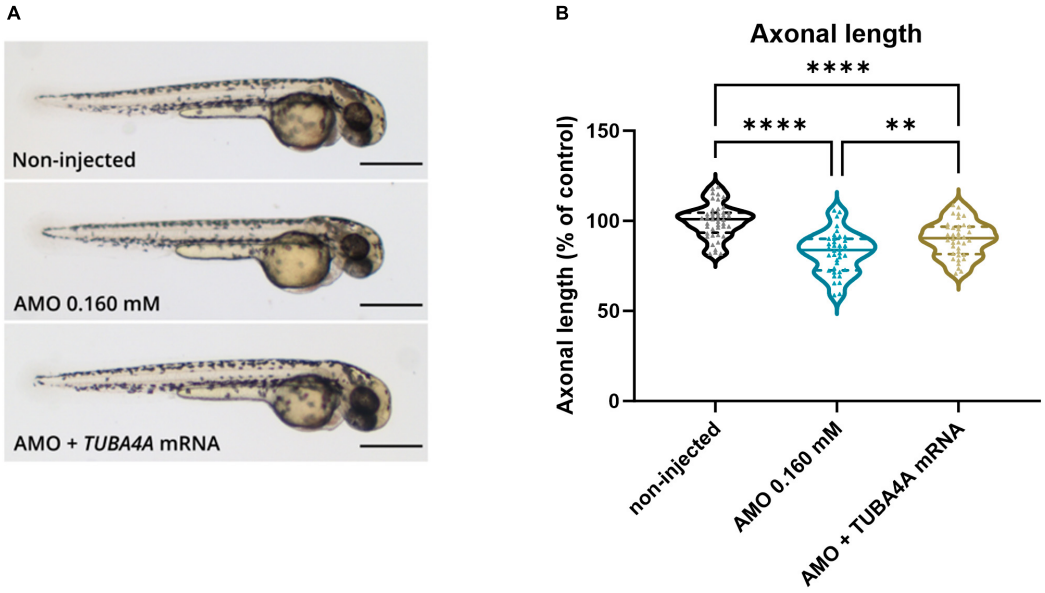

FIGURE 4
Rescue of axonal length defects by the addition of human wild-type *TUBA4A* mRNA. Zebrafish embryos were injected with an ATG morpholino against zebrafish *tuba8l2* (0.160 mM) with or without the injection of human wild-type *TUBA4A* mRNA (300 ng/μl). Non-injected embryos were also included in the analysis. **(a)** Representative whole body images of zebrafish embryos for the different conditions at 48 hpf (scale bar represents 500 μm). **(b)** At 30 hpf, axonal length was measured for all conditions, with $p = 0.0051$ (AMO 0.160 mM versus AMO 0.160 mM + *TUBA4A* mRNA), $p < 0.0001$ (AMO 0.160 mM versus non-injected) and $p < 0.0001$ (non-injected versus AMO 0.160 mM + *TUBA4A* mRNA); one-way ANOVA with Dunnett's multiple comparisons. Axonal length was measured for N = 3 experiments; $n = 10–15$ zebrafish per group per experiment; with every data point representing the average length of the five measured axons for each zebrafish embryo. $^{**}p < 0.01$; $^{****}p < 0.0001$. AMO, morpholino; hpf, hours post fertilization.

measuring axonal length using SV2 immunohistochemistry at 30 hpf. This showed a rescue of the phenotype by the co-injection of wild-type *TUBA4A* mRNA (Figure 4; $p = 0.0051$; one-way ANOVA with Dunnett's multiple comparisons).

When we performed the TEER assay at 48 hpf, we also observed a complete rescue of the phenotype when looking at the total distance travelled (Figure 5a; $p < 0.0001$; Kruskal-Wallis test with Dunn's multiple comparisons), and a partial rescue of the phenotype for the average swimming velocity (Figure 5b; $p < 0.0001$; Kruskal-Wallis test with Dunn's multiple comparisons) and the instant maximal swimming velocity (Figure 5c; $p < 0.0001$; Kruskal-Wallis test with Dunn's multiple comparisons). Representative escape traces for 10 embryos per group are depicted in Figure 5d. We showed that the observed axonopathy and behavioral phenotype induced by the knockdown of *tuba8l2* could be rescued by co-expression of human *TUBA4A* mRNA, confirming both the conservation between orthologues and the specificity of our knockdown approach.

3.4 Knockdown of zebrafish *tuba8l2* does not alter microtubule polymerization

Microtubule growth rates are known to be affected by the amount of soluble, free tubulin (Stepanova et al., 2003). Since TUBA4A is highly expressed in neurons, knockdown of this specific α-tubulin isotype could alter microtubule assembly and thus be responsible for the observed phenotypes. We therefore investigated changes in microtubule polymerization by performing an EB3 comet assay. Indeed, EB3 is a plus-end tracking protein (+TIP) known to bind the plus-end of growing microtubules in order to regulate their dynamics (Stepanova et al., 2003). These assembly events, called 'comets', can be quantified by imaging the association of an EB3 fusion protein with the growing microtubule via time-lapse imaging. We performed a live, *in vivo* comet assay in single CaP motor neurons of 48 hpf zebrafish embryos injected with pUAS-EB3-GFP, in the mnx1:GAL4 background (Figure 6e: composite z-stack projection of one CaP motor neuron), as performed previously (Bercier et al., 2019). We quantified the comet metrics (i.e., distance, duration and velocity) on kymograms extracted from time-lapse imaging (Figure 6f) in *tuba8l2* AMO and control AMO injected embryos, but did not observe any significant changes in the kinetics of polymerization events (Figures 6a–c; respectively, $p = 0.8230$, unpaired *t*-test $p = 0.7340$, $p = 0.4605$, Mann-Whitney test). In addition, reduction of tuba8l2 did not affect the number of events, as quantified by the comet density (Figure 6d; $p = 0.3741$, Mann-Whitney test). Overall, a reduction of tuba8l2, without changes in total α-tubulin (Figures 2d, e), did not affect microtubule polymerization rates or kinetics in 48 hpf zebrafish motor neurons.

3.5 Changes in post-translational modifications of tubulin are induced by knockdown of *tuba8l2*

As we observed no significant changes in microtubule growth after knockdown of the *TUBA4A* zebrafish orthologue *tuba8l2*,

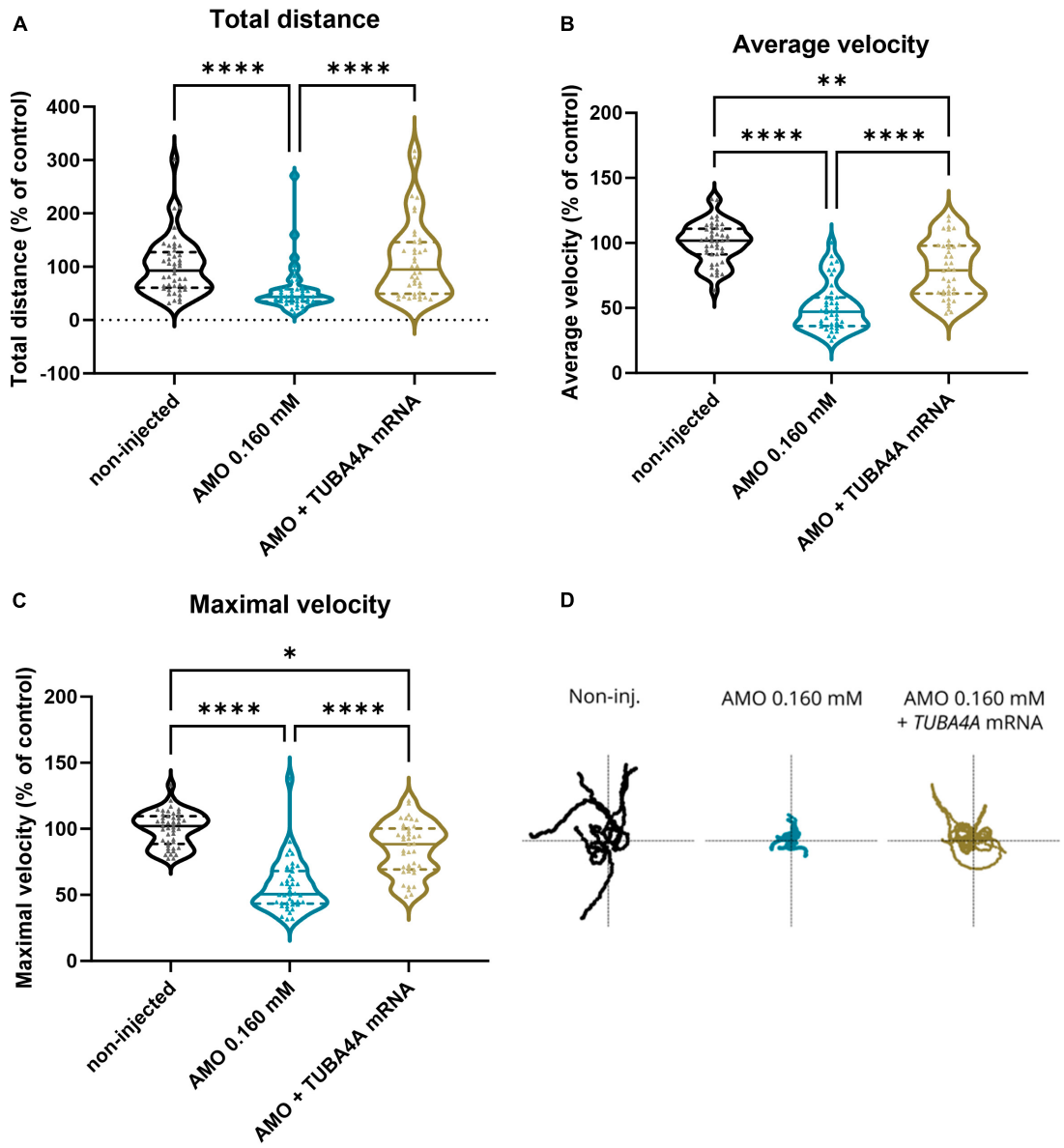

FIGURE 5
Rescue of motor behavior deficits by the addition of human wild-type *TUBA4A* mRNA. Zebrafish embryos were subjected to a touch-evoked escape response (TEER) assay at 48 hpf after injection with an ATG morpholino against zebrafish *tuba8l2* (0.160 mM) with or without the injection of wild-type human *TUBA4A* mRNA (300 ng/μl). Non-injected embryos were also included in the analysis. **(a)** Total distance for AMO 0.160 mM + *TUBA4A* mRNA compared to non-injected (non-significant) and AMO 0.160 mM condition ($p < 0.0001$), and non-injected ($p < 0.0001$) compared to AMO 0.160 mM condition. **(b)** Average velocity for AMO 0.160 mM + *TUBA4A* mRNA compared to non-injected ($p = 0.0018$) and AMO 0.160 mM condition ($p < 0.0001$), and non-injected ($p < 0.0001$) compared to AMO 0.160 mM condition. **(c)** Maximal instant velocity for AMO 0.160 mM + *TUBA4A* mRNA compared to non-injected ($p = 0.0110$) and AMO 0.160 mM condition ($p < 0.0001$), and non-injected ($p < 0.0001$) compared to AMO 0.160 mM condition. Kruskal-Wallis test with Dunn's multiple comparisons; $N = 3$ experiments; $n = 10–15$ zebrafish embryos per group per experiment; which each data point representing an individual zebrafish embryo. **(d)** Representative escape traces from 10 zebrafish embryos per group shown as a visual example. *$p < 0.05$, **$p < 0.01$, and ****$p < 0.0001$. AMO, morpholino; hpf, hours post fertilization.

we decided to look further into microtubule PTMs. Indeed, the isotype composition of microtubules can not only influence their stability, but also their PTMs which often decorate the C-terminal tail of tubulins regulating a range of functions (Janke and Magiera, 2020). More specifically, we investigated acetylated α-tubulin, detyrosinated α-tubulin, and polyglutamylated tubulin levels because all three have been shown to play a role in microtubule functionality (Bodakuntla et al., 2021; Cappelletti et al., 2021; Sanyal et al., 2021).

First, we performed western blotting on total lysate from 48 hpf zebrafish embryos injected with *tuba8l2* AMO compared to control AMO (Figures 7a–c). We found that both acetylated as well as detyrosinated α-tubulin levels were significantly decreased upon knockdown of *tuba8l2* (Figures 7d, e; respectively, $p = 0017$, $p = 0.0001$ unpaired *t*-test). For polyglutamylated tubulin on the other hand, there was more variation although a general trend toward decreased levels could be observed (Figure 7f, $p = 0.2014$ unpaired *t*-test). These results suggest that a reduction in tuba8l2

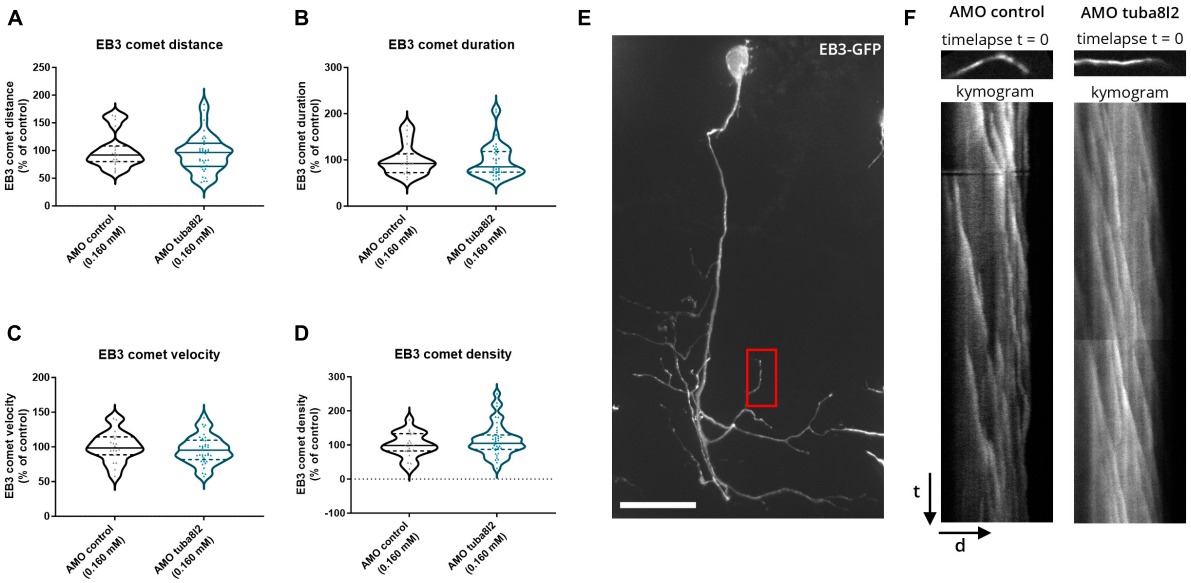

FIGURE 6
Zebrafish microtubule polymerization is not affected by *tuba8l2* knockdown. At 48 hpf, an EB3 comet assay was performed in single CaP motor neurons after co-injection of an ATG morpholino against *tuba8l2* (0.160 mM) or a control morpholino (0.160 mM). **(a–d)** Quantification of the comet run metrics extracted from kymograms show no difference in microtubule growth kinetics. **(a)** Average comet distance for AMO 0.160 mM ($p = 0.8230$) compared to AMO control condition. **(b)** Average comet duration for AMO 0.160 mM ($p = 0.7340$) compared to AMO control condition. **(c)** Average comet velocity for AMO 0.160 mM ($p = 0.4605$) compared to AMO control condition. **(d)** Average comet density for AMO 0.160 mM ($p = 0.3741$). Unpaired *t*-test **(a)** or Mann-Whitney test **(b,c,d)**; $N = 3$ experiments; $n = 20–37$ zebrafish embryos with each data point representing an individual zebrafish embryo. **(e)** Representative image (composite z-stack projection) of EB3-GFP in AMO control zebrafish embryo. Red box: representative area for the comet analysis in a distal segment in the CaP. **(f)** Representative kymograms represent microtubule growth extracted through time-lapse imaging (500 ms/5 min) of EB3-GFP comets in single CaP motor neurons distal arbors at 48 hpf. Each pixel on the *Y*-axis represents one timepoint image (time) projected against the neurite length (distance) on the *X*-axis. AMO, morpholino; hpf, hours post fertilization; CaP, caudal primary; scale bar, 25 μm; t, time (5 min); d, distance (average: 17 μm segments).

affects microtubule PTMs, which are known to be involved in neurodegeneration, and therefore potentially affect the functions they regulate, such as interactions with molecular motors for axonal transport, protection from disassembly and/or from mechanical aging (Janke and Magiera, 2020; Moutin et al., 2021).

4 Discussion

In this study, we showed that a reduction of TUBA4A protein expression, as observed in *post-mortem* tissue of sporadic ALS patients, leads to an ALS-related phenotype in embryonic zebrafish via knockdown of the zebrafish orthologue of *TUBA4A* (*tuba8l2*). Moreover, we observed a decreased axonal length of spinal motor neurons and a behavioral phenotype, which were dose-dependent and rescued by the addition of wild-type human *TUBA4A* mRNA, demonstrating the specificity of our approach and conservation of the orthologue. We hereby investigated the mechanism by which the reduction of tuba8l2 could induce these phenotypes and found no change in microtubule polymerization while we did find alterations in post-translational modifications of tubulin, known to be involved in neurodegeneration. These results extend the importance of *TUBA4A*, a familial ALS disease gene, to sporadic ALS cases, suggesting that alterations in its expression may indeed be a contributing factor in ALS pathophysiology.

Mutations in various tubulin isotypes are associated with disease, supporting a functional specification of alternative isotypes (Breuss et al., 2017). Interestingly, *TUBA4A* is the isotype with the highest expression in the human motor cortex after birth (Leandro-García et al., 2010; Sferra et al., 2020) and its expression in the brain dramatically increases with age. This could explain why *TUBA4A* dysregulation may contribute to adult-onset neurodegenerative disease, contrary to mutations in other tubulin isotypes involved in neurodevelopmental disorders (Tischfield et al., 2011; Chakraborti et al., 2016; Castellanos-Montiel et al., 2020). Previously, C-terminal mutations in *TUBA4A* were shown to be associated with classical spinal onset ALS, and to be associated in some cases with FTD-like symptoms (Smith et al., 2014; Perrone et al., 2017). The C-terminal part of TUBA4A is important for its interaction with β-tubulin and microtubule-associated proteins (MAPs), which regulate microtubule stability (Wall et al., 2016). C-terminally mutated TUBA4A proteins were shown to be ineffective at forming tubulin dimers *in vitro*, and displayed a decreased incorporation into protofibrils, inhibiting microtubule network stability (Smith et al., 2014). These mutations, would therefore represent a toxic gain-of-function due to the production of mutant protein products. On the other hand, N-terminal *TUBA4A* mutations were identified in patients presenting with FTD, possibly with extrapyramidal symptoms (Perrone et al., 2017; Mol et al., 2021). We and others have shown that these mutations led to reduced TUBA4A levels in central nervous system tissues, suggesting a loss-of-function mechanism (Mol et al., 2021; Okada et al., 2021; Van Schoor et al., 2022).

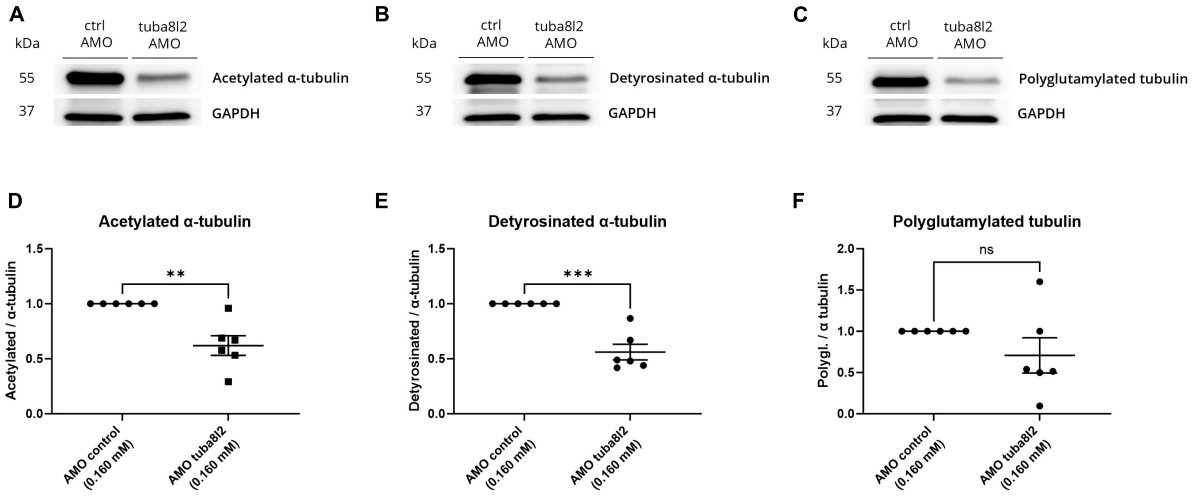

FIGURE 7
Specific *tuba8l2* knockdown in zebrafish induces changes in post-translational modifications of tubulin. **(a–f)** Western blot was performed on whole fish lysate from 48 hpf embryos injected with ATG morpholino against *tuba8l2* (0.160 mM) vs. control morpholino (0.160 mM). $N = 6$ experiments; $n = 10–30$ zebrafish per group per experiment. **(a–c)** Representative western blot for acetylated α-tubulin **(a)**, detyrosinated α-tubulin **(b)** and polyglutamylated tubulin **(c)**. **(d–f)** Quantification of acetylated α-tubulin **(d)** ($p = 0017$), detyrosinated α-tubulin **(e)** ($p < 0.0001$) and polyglutamylated tubulin **(f)** ($p = 0.2014$) protein levels relative to α-tubulin after normalization to GAPDH for the different injection conditions. Data represent mean ± SEM. Unpaired *t*-test: ** $p < 0.01$, *** $p < 0.001$. AMO, morpholino; hpf, hours post fertilization; ctrl, control.

Interestingly, a downregulation of TUBA4A protein expression was also reported in the brain of sporadic ALS patients (Helferich et al., 2018), which we confirmed in this study via western blotting of motor cortex tissue. In addition, we detected a trend toward a decreased TUBA4A expression in the spinal cord of sporadic ALS patients, though the high variability between samples prevented statistical significance. Furthermore, qualitative IHC analysis indicated no differences in the cellular localization of TUBA4A between ALS and control cases, and no TUBA4A aggregates were detected, in line with a previous study (Smith et al., 2014). Altogether, these data suggest that alterations in expression of *TUBA4A* are of importance in sporadic ALS pathogenesis.

Downregulation of TUBA4A can occur through the miR-1825/*TBCB*/*TUBA4A* pathway, previously reported to be dysregulated in sporadic and familial ALS. Indeed, it was demonstrated that miR-1825 downregulation in ALS patient tissue led to increased tubulin-folding cofactor B (TBCB) levels, which led to the sequestration of TUBA4A and induced a decrease in its expression (Helferich et al., 2018). This gives an indication of the possible upstream events leading to decreased TUBA4A levels in ALS, aside from N-terminal *TUBA4A* mutations (Van Schoor et al., 2022). Importantly, we here demonstrate the causality of TUBA4A downregulation by showing that knockdown of the *TUBA4A* orthologue *tuba8l2* in zebrafish embryos led to ALS-associated abnormalities, namely spinal axonopathy and behavioral deficits. These phenotypes were previously also shown to be triggered by pathological protein products such as mutant SOD1 (Van Hoecke et al., 2012) and mutant TDP-43 (Laird et al., 2010), as well as by the pathological hallmarks of patients with *C9orf72* mutations, i.e., dipeptide repeat proteins (DPRs) and sense and anti-sense repeat RNA (Swinnen et al., 2018), among others. Importantly, the severity of the observed phenotypes was dose-dependent, did not affect total α-tubulin levels and could be rescued by co-expression of human TUBA4A, which alone caused a reduction of endogenous tuba8l2 (Online resource; **Supplementary Figure 4**). This suggests that the TUBA4A level is specifically important for neuronal health and that its reduction can contribute to ALS pathobiology.

Since a reduction of TUBA4A might affect cytoskeletal integrity in neurons, we investigated microtubule polymerization in our zebrafish model. However, we did not observe changes in the number of polymerization events or the kinetics at which they occur. We then assessed the levels of known PTMs in whole fish lysate and found decreased levels of acetylated α-tubulin, detyrosinated α-tubulin, and trends indicating decreased polyglutamylated tubulin. Indeed, aside from the composition of specific tubulin isotypes, microtubule specification also occurs through tubulin post-translational modifications (PTMs). Specifically, neuronal microtubules mainly undergo detyrosination of the C-terminal tyrosine, acetylation at K40 and polyglutamylation (Moutin et al., 2021). These PTMs are fine-tuned, unevenly distributed and are known to accumulate as neurons differentiate and mature (Sferra et al., 2020). Importantly, out of nine α-tubulins isotypes, only TUBA8 and TUBA4A lack the C-terminal tyrosine residue which undergoes detyrosination (Janke and Magiera, 2020; Sanyal et al., 2021). As a result, the integration of TUBA4A in microtubules mimics enzymatically detyrosinated α-tubulin, linked with increased stability (Janke and Magiera, 2020), and is enriched in the axonal microtubules of neurons (Boiarska and Passarella, 2021; Moutin et al., 2021; Sanyal et al., 2021). A reduction in TUBA4A could therefore lead to decreased levels in detyrosinated α-tubulin, in line with what we have observed. Furthermore, acetylation is present along the entire axonal microtubule cytoskeleton, while tyrosination is predominantly present at the growing, actively polymerizing ends of microtubules. Axonal microtubules are thus presumed to be long-lived, having highly acetylated and detyrosinated tubulins (Janke and Magiera, 2020). According to our findings in the zebrafish model, the reduction of *TUBA4A* by knockdown of

orthologue *tuba8l2* results in decreased levels of both acetylated and detyrosinated α-tubulin. While we could not achieve statistical significance for the polyglutamylated tubulin levels, our results do suggest a decrease which could have an additional negative impact on microtubule functionality. Indeed, polyglutamylation does not only modulate the binding of MAPs and molecular motors, it is also shown to be necessary in modulating synaptic transmission-related transport. Furthermore, alterations in this PTM were previously associated with neurodegeneration (Magiera et al., 2018; Moutin et al., 2021; Hausrat et al., 2022).

In ALS, the dying-back hypothesis implies that abnormalities in axon connectivity and synaptic function long precede somatic cell death (Fischer et al., 2004; Nijssen et al., 2017). Defects in cytoskeleton integrity and microtubule-dependent transport mechanisms can thus result in axonal trafficking disruption and dysfunctional neuromuscular junctions (Castellanos-Montiel et al., 2020; Sanyal et al., 2021; Stoklund Dittlau et al., 2021). Due to the physical length of motor neuron axons, cortical and spinal motor neurons are thought to be particularly vulnerable to this dying-back mechanism (Clark et al., 2016). Apart from *TUBA4A*, other genes involved in cytoskeleton integrity have also been linked with ALS, namely *DCTN1*, *KIF5A*, *PRPH*, *NF-H*, *PFN1* and *SPAST* (Chakraborti et al., 2016; Guo et al., 2020). This stresses the causative relation between cytoskeletal defects and neurodegeneration in the context of ALS. Therefore, our results are consistent with the hypothesis that a downregulation of TUBA4A expression leads to aberrant cytoskeletal function, explaining the observed axonal phenotype and motor behavior in zebrafish.

In conclusion, we showed an ALS-related axonopathy and behavioral phenotype in zebrafish embryos following downregulation of the zebrafish orthologue for *TUBA4A* via knockdown of *tuba8l2*. While we did observe changes in tubulin PTMs, we did not observe changes in microtubule polymerization. This could be due to the fact that expression of total α-tubulin was not affected by the reduction of tuba8l2 (Wethekam and Moore, 2022). Overall, these data support that, apart from ALS cases bearing a *TUBA4A* mutation, dysregulated TUBA4A expression plays an important role in sporadic ALS disease pathogenesis, and stresses the importance of microtubule dysfunction in ALS.

4.1 Limitations of this study

In this study, we assessed axonal and behavioral phenotypes in embryonic zebrafish stages (until 48 hpf). An important limitation of the use of zebrafish to model a motor neuron disorder such as ALS is the absence of corticospinal upper motor neurons projecting to the spinal cord in zebrafish. The use of embryonic zebrafish also has its limitations to model an adult onset neurodegenerative disease. However, zebrafish experiments offer an advantage over standard cell culture models as it gives the possibility to study effects on motor behavior in addition to axonal pathology, which is not possible *in vitro*. Moreover, the zebrafish orthologue *tuba8l2* shows 94% conservation compared to human *TUBA4A* at the protein level, and we showed that TUBA4A can compensate for the loss of tuba8l2 in our rescue experiments. This suggests functional conservation between the two orthologues, with both genes able to regulate motor axon morphology and motor behavior. Although the use of morpholino-based knockdown in zebrafish can be an important avenue to explore emerging pathogenic pathways in neurodegenerative disorders, like any model, it has its limitations. Thus, research including other *in vivo* and patient-relevant *in vitro* models is needed to further unravel the downstream consequences of TUBA4A downregulation, and how this contributes to ALS-related neurodegeneration.

Data availability statement

The raw data supporting the conclusions of this article will be made available by the authors, without undue reservation.

Ethics statement

Brain and spinal cord tissues were collected in accordance with the applicable laws in Belgium (UZ Leuven) and Germany (Ulm). The recruitment protocols for collecting the brains were approved by the ethical committees of the University of Ulm (Germany) and of UZ Leuven (Belgium) and consent was obtained.

Author contributions

EVS: Conceptualization, Data curation, Formal Analysis, Investigation, Methodology, Visualization, Writing–original draft, Writing–review and editing. DS: Formal Analysis, Investigation, Methodology, Validation, Visualization, Writing–original draft, Writing–review and editing. EB: Formal Analysis, Investigation, Methodology, Visualization, Writing–review and editing. JW: Resources, Writing–review and editing. ACL: Resources, Writing–review and editing. PVD: Conceptualization, Funding acquisition, Resources, Writing–review and editing. DRT: Conceptualization, Funding acquisition, Resources, Supervision, Writing–review and editing. VB: Conceptualization, Formal Analysis, Methodology, Supervision, Visualization, Writing–original draft, Writing–review and editing. LVDB: Conceptualization, Funding acquisition, Supervision, Writing–review and editing.

Funding

The author(s) declare financial support was received for the research, authorship, and/or publication of the article. EVS is funded by an SB Fellowship of the Research Foundation–Flanders (FWO) (1S46219N). DS is funded by a fundamental FWO fellowship (11D4523N). EB is funded by a fundamental FWO Fellowship (1145619N). VB is funded by a postdoctoral FWO Fellowship (12Y9120N). PVD holds a senior clinical investigatorship of FWO and is supported by the E. von Behring Chair for Neuromuscular and Neurodegenerative Disorders, the KU Leuven ALS funds "Een hart voor ALS," "Laeversfonds voor ALS onderzoek," and "Valéry Perrier Race against ALS fund." LVDB

is supported by the Generet Award for rare diseases 2022. PVD and LVDB are supported by the ALS Liga Belgium. PVD, LVDB and DRT received C1-internal funds from KU Leuven (C14-17-107, C14/22/132). DRT is additionally funded by the FWO-Odysseus grant G0F8516N and FWO grant G065721N.

Acknowledgments

We thank Alicja Ronisz and Simona Ospitalieri for technical support. We also thank Dr. John Landers for providing the wild-type TUBA4A plasmid. We thank Klara Gawor for statistical support.

Conflict of interest

ACL serves on the Advisory Board of Roche Pharma (Basel, Switserland) and Biogen (Cambridge, MA, USA), and on the data and safety monitoring board of Zeneus pharma (Bray, UK). ACL received consulting fees from AB Science (Paris, France), Desitin (Buckinghamshire, UK), Novartis (Basel, Switserland) and Teva (Jerusalem, Israel). PVD participated in advisory board meetings of Biogen (Cambridge, MA, USA), Cytokinetics (San Francisco, CA, USA), Ferrer (Barcelona, Spain), UCB (Brussels, Belgium), Argenx (Ghent, Belgium), Muna Therapeutics (Copenhagen, Denmark), Alector (San Francisco, CA, USA), Augustine Therapeutics (Leuven, Belgium), Alexion Therapeutics (Boston, MA, USA) and QurAlis (Cambridge, MA, USA). DRT received speaker honorary or travel reimbursement from Biogen (USA), UCB (Brussels, Belgium), and collaborated with Novartis Pharma AG (Basel, Switzerland), Probiodrug [Halle (Saale), Germany, GE Healthcare Amersham, UK], and Janssen Pharmaceutical Companies (Beerse, Belgium). LVDB is scientific founder and head of the Scientific Advisory Board of Augustine Therapeutics (Leuven, Belgium). The funders had no role in the design of the study; in the collection, analyses or interpretation of data; in the writing of the manuscript, or in the decision to publish the results.

Publisher's note

All claims expressed in this article are solely those of the authors and do not necessarily represent those of their affiliated organizations, or those of the publisher, the editors and the reviewers. Any product that may be evaluated in this article, or claim that may be made by its manufacturer, is not guaranteed or endorsed by the publisher.

Supplementary material

The Supplementary Material for this article can be found online at: https://www.frontiersin.org/articles/10.3389/fncel.2024.1340240/full#supplementary-material

References

Al-Chalabi, A., and Hardiman, O. (2013). The epidemiology of ALS: a conspiracy of genes, environment and time. *Nat. Rev. Neurol.* 9, 617–628. doi: 10.1038/nrneurol.2013.203

Bercier, V., Hubbard, J. M., Fidelin, K., Duroure, K., Auer, T., Revenu, C., et al. (2019). Dynactin1 depletion leads to neuromuscular synapse instability and functional abnormalities. *Mol. Neurodegeneration* 14:27. doi: 10.1186/s13024-019-0327-3

Bodakuntla, S., Janke, C., and Magiera, M. M. (2021). Tubulin polyglutamylation, a regulator of microtubule functions, can cause neurodegeneration. *Neurosci. Lett.* 746:135656. doi: 10.1016/j.neulet.2021.135656

Boiarska, Z., and Passarella, D. (2021). Microtubule-targeting agents and neurodegeneration. *Drug Discov. Today* 26, 604–615. doi: 10.1016/j.drudis.2020.11.033

Braak, H., Alafuzoff, I., Arzberger, T., Kretzschmar, H., and Del Tredici, K. (2006). Staging of Alzheimer disease-associated neurofibrillary pathology using paraffin sections and immunocytochemistry. *Acta Neuropathol.* 112, 389–404. doi: 10.1007/s00401-006-0127-z

Braun, A., Breuss, M., Salzer, M. C., Flint, J., Cowan, N. J., and Keays, D. A. (2010). Tuba8 is expressed at low levels in the developing mouse and human brain. *Am. J. Hum. Genet.* 86, 819–822. doi: 10.1016/j.ajhg.2010.03.019

Breuss, M. W., Leca, I., Gstrein, T., Hansen, A. H., and Keays, D. A. (2017). Tubulins and brain development – The origins of functional specification. *Mol. Cell. Neurosci.* 84, 58–67. doi: 10.1016/j.mcn.2017.03.002

Brooks, B. R., Miller, R. G., Swash, M., Munsat, T. L., and World Federation of Neurology Research Group on Motor Neuron Diseases (2000). El escorial revisited: revised criteria for the diagnosis of amyotrophic lateral sclerosis. *Amyotroph. Lateral Scler.* 1, 293–299. doi: 10.1080/146608200300079536

Cappelletti, G., Calogero, A. M., and Rolando, C. (2021). Microtubule acetylation: a reading key to neural physiology and degeneration. *Neurosci. Lett.* 755:135900. doi: 10.1016/j.neulet.2021.135900

Castellanos-Montiel, M. J., Chaineau, M., and Durcan, T. M. (2020). The neglected genes of ALS: cytoskeletal dynamics impact synaptic degeneration in ALS. *Front. Cell. Neurosci.* 14:594975. doi: 10.3389/fncel.2020.594975

Chakraborti, S., Natarajan, K., Curiel, J., Janke, C., and Liu, J. (2016). The emerging role of the tubulin code: from the tubulin molecule to neuronal function and disease. *Cytoskeleton* 73, 521–550. doi: 10.1002/cm.21290

Clark, J. A., Yeaman, E., Blizzard, C., Chuckowree, J., and Dickson, T. (2016). A case for microtubule vulnerability in amyotrophic lateral sclerosis: altered dynamics during disease. *Front. Cell. Neurosci.* 10:204. doi: 10.3389/fncel.2016.00204

de Carvalho, M., Dengler, R., Eisen, A., England, J. D., Kaji, R., Kimura, J., et al. (2008). Electrodiagnostic criteria for diagnosis of ALS. *Clin. Neurophysiol.* 119, 497–503. doi: 10.1016/j.clinph.2007.09.143

de Carvalho, M., and Swash, M. (2009). Awaji diagnostic algorithm increases sensitivity of El Escorial criteria for ALS diagnosis. *Amyotroph. Lateral Scler.* 10, 53–57. doi: doi.org/10.1080/17482960802521126

Fischer, L. R., Culver, D. G., Tennant, P., Davis, A. A., Wang, M., Castellano-Sanchez, A., et al. (2004). Amyotrophic lateral sclerosis is a distal axonopathy: evidence in mice and man. *Exp. Neurol.* 185, 232–240. doi: 10.1016/j.expneurol.2003.10.004

Guo, W., Stoklund Dittlau, K., and Van Den Bosch, L. (2020). Axonal transport defects and neurodegeneration: molecular mechanisms and therapeutic implications. *Semin. Cell Dev. Biol.* 99, 133–150. doi: 10.1016/j.semcdb.2019.07.010

Hausrat, T. J., Janiesch, P. C., Breiden, P., Lutz, D., Hoffmeister–Ullerich, S., Hermans-Borgmeryer, I., et al. (2022). Disruption of tubulin-alpha4a polyglutamylation prevents aggregation of hyper-phosphorylated tau and microglia activation in mice. *Nat. Commun.* 13:4192. doi: 10.1038/s41467-022-31776-5

Helferich, A. M., Brockmann, S. J., Reinders, J., Deshpande, D., Holzmann, K., Brenner, D., et al. (2018). Dysregulation of a novel miR-1825/TBCB/TUBA4A pathway in sporadic and familial ALS. *Cell. Mol. Life Sci.* 75, 4301–4319. doi: 10.1007/s00018-018-2873-1

Janke, C., and Magiera, M. M. (2020). The tubulin code and its role in controlling microtubule properties and functions. *Nat. Rev. Mol. Cell Biol.* 21, 307–326. doi: 10.1038/s41580-020-0214-3

Jiang, Y. M., Yamamoto, M., Kobayashi, Y., Yoshihara, T., Liang, Y., Terao, S., et al. (2005). Gene expression profile of spinal motor neurons in sporadic amyotrophic lateral sclerosis. *Ann. Neurol.* 57, 236–251. doi: 10.1002/ana.20379

Kabashi, E., Bercier, V., Lissouba, A., Liao, M., Brustein, E., Rouleau, G. A., et al. (2011). FUS and TARDBP but not SOD1 interact in genetic models of amyotrophic lateral sclerosis. *PLoS Genet.* 7:e1002214. doi: 10.1371/JOURNAL.PGEN.1002214

Laird, A. S., Van Hoecke, A., De Muynck, L., Timmers, M., Van Den Bosch, L., Van Damme, P., et al. (2010). Progranulin is neurotrophic in vivo and protects against a mutant TDP-43 induced axonopathy. *PLoS one* 5:e13368. doi: 10.1371/journal.pone.0013368

Leandro-García, L. J., Landa, I., Montero-Conde, C., López-Jiménez, E., Letón, R., Cascón, A., et al. (2010). Tumoral and tissue-specific expression of the major human beta-tubulin isotypes. *Cytoskeleton* 67, 214–223. doi: 10.1002/cm.20436

Magiera, M. M., Bodakuntla, S., Žiak, J., Lacomme, S., Marques Sousa, P., Leboucher, S., et al. (2018). Excessive tubulin polyglutamylation causes neurodegeneration and perturbs neuronal transport. *EMBO J.* 37:e100440. doi: 10.15252/embj.2018100440

Maraldi, T., Beretti, F., Anselmi, L., Franchin, C., Arrigoni, G., Braglia, L., et al. (2019). Influence of selenium on the emergence of neuro tubule defects in a neuron-like cell line and its implications for amyotrophic lateral sclerosis. *Neurotoxicology* 75, 209–220. doi: 10.1016/j.neuro.2019.09.015

Mol, M. O., Wong, T. H., Melhem, S., Basu, S., Viscusi, R., Galjart, N., et al. (2021). Novel TUBA4A variant associated with familial frontotemporal dementia. *Neurol. Genet.* 7:e596. doi: 10.1212/NXG.0000000000000596

Moutin, M. J., Bosc, C., Peris, L., and Andrieux, A. (2021). Tubulin post-translational modifications control neuronal development and functions. *Dev. Neurobiol.* 81, 253–272. doi: 10.1002/dneu.22774

Nijssen, J., Comley, L. H., and Hedlund, E. (2017). Motor neuron vulnerability and resistance in amyotrophic lateral sclerosis. *Acta Neuropathol.* 133, 863–885. doi: 10.1007/s00401-017-1708-8

Okada, K., Hata, Y., Ichimata, S., Yoshida, K., Oku, Y., Asahi, T., et al. (2021). An autopsy case of pure nigropathy with TUBA4A nonsense mutation. *Neuropathol. Appl. Neurobiol.* 47, 891–893. doi: 10.1111/nan.12712

Perrone, F., Nguyen, H. P., Van Mossevelde, S., Moisse, M., Sieben, A., Santens, P., et al. (2017). Investigating the role of ALS genes CHCHD10 and TUBA4A in Belgian FTD-ALS spectrum patients. *Neurobiol. Aging* 51, 177.e9-177.e16. doi: 10.1016/j.neurobiolaging.2016.12.008

Sanyal, C., Pietsch, N., Ramirez Rios, S., Peris, L., Carrier, L., and Moutin, M. J. (2021). The detyrosination/re-tyrosination cycle of tubulin and its role and dysfunction in neurons and cardiomyocytes. *Sem. Cell Dev. Biol.* 137, 46–62. doi: 10.1016/j.semcdb.2021.12.006

Sferra, A., Nicita, F., and Bertini, E. (2020). Microtubule dysfunction: a common feature of neurodegenerative diseases. *Int. J. Mol. Sci.* 21:7354. doi: 10.3390/ijms21197354

Smith, B. N., Ticozzi, N., Fallini, C., Gkazi, A. S., Topp, S., Kenna, K., et al. (2014). Exome-wide rare variant analysis identifies TUBA4A mutations associated with familial ALS. *Neuron* 84, 324–331. doi: 10.1016/j.neuron.2014.09.027

Stepanova, T., Slemmer, J., Hoogenraad, C. C., Lansbergen, G., Dortland, B., De Zeeuw, C., et al. (2003). Visualization of microtubule growth in cultured neurons via the use of EB3-GFP (end-binding Protein 3-green fluorescent protein). *J. Neurosci.* 23, 2655–2664. doi: 10.1523/JNEUROSCI.23-07-02655.2003

Stoklund Dittlau, K., Krasnow, E. N., Fumagalli, L., Vandoorne, T., Baatsen, P., Kerstens, A., et al. (2021). Human motor units in microfluidic devices are impaired by FUS mutations and improved by HDAC6 inhibition. *Stem. Cell Rep.* 16, 2213–2227. doi: 10.1016/j.stemcr.2021.03.029

Swinnen, B., Bento-Abreu, A., Gendron, T. F., Boeynaems, S., Bogaert, E., Nuyts, R., et al. (2018). A zebrafish model for C9orf72 ALS reveals RNA toxicity as a pathogenic mechanism. *Acta Neuropathol.* 135, 427–443. doi: 10.1007/s00401-017-1796-5

Taylor, J. P., Brown, R. H., and Cleveland, D. W. (2016). Decoding ALS: from genes to mechanism. *Nature* 539, 197–206. doi: 0.038/nature20413

Thal, D. R., Rüb, U., Schultz, C., Sassin, I., Ghebremedhin, E., Del Tredici, K., et al. (2000). Sequence of Aβ-protein deposition in the human medial temporal lobe. *J. Neuropathol. Exp. Neurol.* 59, 733–748. doi: 10.1093/jnen/59.8.733

Thisse, B., and Thisse, C. (2004). *Fast Release Clones: a High Throughput Expression Analysis., ZFIN Direct Data Submission*. Available Online at: https://zfin.org/ZDB-PUB-040907-1 (accessed November 10, 2023).

Tischfield, M. A., Cederquist, G., Gupta, M., and Engle, E. (2011). Phenotypic spectrum of the tubulin-related disorders and functional implications of disease-causing mutations. *Curr. Opin. Genet. Dev.* 21, 286–294. doi: 10.1016/j.gde.2011.01.003

Van Hoecke, A., Schoonaert, L., Lemmens, R., Timmers, M., Staats, K. A., Laird, A., et al. (2012). EPHA4 is a disease modifier of amyotrophic lateral sclerosis in animal models and in humans. *Nat. Med.* 18, 1418–1422. doi: 10.1038/nm.2901

Van Schoor, E., Vandenbulcke, M., Bercier, V., Vandenberghe, R., van der Zee, J., Van Broeckhoven, C., et al. (2022). Frontotemporal lobar degeneration case with an N-Terminal TUBA4A mutation exhibits reduced TUBA4A levels in the brain and TDP-43 pathology. *Biomolecules* 12:440. doi: 10.3390/biom12030440

Wall, K. P., Pagratis, M., Armstrong, G., Balsbaugh, J. L., Verbeke, E., Pearson, C. G., et al. (2016). Molecular determinants of tubulin's C-terminal tail conformational ensemble. *ACS Chem. Biol.* 11, 2981–2990. doi: 10.1021/acschembio.6b00507

Wethekam, L. C., and Moore, J. K. (2022). Asymmetric requirement for α-tubulin over β-tubulin. *J. Cell Biol.* 222:e202202102. doi: 10.1101/2022.02.17.480930

Zelenchuk, T. A., and Brusés, J. L. (2011). In vivo labeling of zebrafish motor neurons using an mnx1 enhancer and Gal4/UAS. *Genesis* 49, 546–554. doi: 10.1002/dvg.20766

frontiers | Frontiers in Neuroscience

TYPE Original Research
PUBLISHED 15 May 2024
DOI 10.3389/fnins.2024.1375892

OPEN ACCESS

EDITED BY
Agnes Lumi Nishimura,
Queen Mary University of London,
United Kingdom

REVIEWED BY
Ivana Munitic,
University of Rijeka, Croatia
Wenting Guo,
NeuroStra Institute, France

*CORRESPONDENCE
Xueping Chen
✉ chenxueping0606@sina.com
Huifang Shang
✉ hfshang2002@163.com

RECEIVED 24 January 2024
ACCEPTED 30 April 2024
PUBLISHED 15 May 2024

CITATION
Fu J, Lai X, Wei Q, Chen X and Shang H (2024) Associations of cerebrospinal fluid profiles with severity and mortality risk of amyotrophic lateral sclerosis.
Front. Neurosci. 18:1375892.
doi: 10.3389/fnins.2024.1375892

Associations of cerebrospinal fluid profiles with severity and mortality risk of amyotrophic lateral sclerosis

Jiajia Fu[1,2,3], Xiaohui Lai[1], Qianqian Wei[1,2,3], Xueping Chen[1,2,3]* and Huifang Shang[1,2,3]*

[1]Department of Neurology, West China Hospital, Sichuan University, Chengdu, China, [2]Rare Disease Center, West China Hospital, Sichuan University, Chengdu, China, [3]Laboratory of Neurodegenerative Disorders, West China Hospital, Sichuan University, Chengdu, China

Background: The relationship between routine cerebrospinal fluid (CSF) testing and the disease phenotype of amyotrophic lateral sclerosis (ALS) is unclear, and there are some contradictions in current studies.

Methods: This study aimed to analyze the relationship between CSF profiles and disease phenotype in ALS patients. We collected 870 ALS patients and 96 control subjects admitted to West China Hospital of Sichuan University. CSF microprotein, albumin, IgG, index of IgG (IgG_{index}), albumin quotient (Q_{ALB}), and serum IgG were examined.

Results: In ALS patients, CSF IgG, and Q_{ALB} were significantly increased, while CSF IgG_{index} was decreased, compared with control subjects. Approximately one-third of ALS patients had higher CSF IgG levels. The multiple linear regression analysis identified that CSF IgG_{index} was weakly negatively associated with ALS functional rating scale revised (ALSFRS-R) scores ($\beta = -0.062$, $p = 0.041$). This significance was found in male ALS but not in female ALS. The Cox survival analyses found that upregulated CSF IgG was significantly associated with the increased mortality risk in ALS [HR = 1.219 (1.010–1.470), $p = 0.039$].

Conclusion: In the current study, the higher CFS IgG was associated with increased mortality risk of ALS. CSF IgG_{index} may be associated with the severity of ALS. These findings may be sex-specific.

KEYWORDS

amyotrophic lateral sclerosis, cerebrospinal fluid profiles, disease phenotype, IgG, Q_{ALB} (CSF albumin/serum albumin)

Introduction

Amyotrophic lateral sclerosis (ALS) is a neurodegenerative disease characterized by loss of upper motor neurons and lower motor neurons resulting in progressive muscle atrophy and paralysis (Yang et al., 2022; Akçimen et al., 2023). The ALS phenotype varies across different ethnicities and regions. The average age of onset in ALS cohorts is around 66 years in Germany, 52 years in northern China, and 55 years in southwestern China (Rosenbohm et al., 2018; Chen et al., 2021; Wei et al., 2022). Currently, the majority of research suggests that ALS is associated with various factors such as immunity and infection, metallic elements, genetics, environmental

factors, and many others (Li C. et al., 2022; Yang et al., 2022, 2023). However, the etiology and pathogenesis of ALS are highly complex and remain unknown. There are regional and racial differences in ALS patients. The research of biomarkers in cerebrospinal fluid (CSF) is one of the most active areas of ALS. Most previous studies focused on comparing the differences between healthy controls (HCs) and ALS patients, and most found that CSF IgG levels, CSF protein levels, and the quotient of CSF albumin and blood albumin (Q_{ALB}) in ALS patients were higher than those in controls (Gårde et al., 1971; Leonardi et al., 1984; Norris et al., 1993; Assialioui et al., 2022). However, the associations between CSF profiles and the disease phenotype of ALS are controversial. Some studies found that the CSF protein of patients with late-onset ALS was significantly higher than that of patients with early-onset ALS (Guiloff et al., 1979; Leonardi et al., 1984), while other studies found that the CSF protein of ALS patients gradually decreased with the increased age of onset (Guiloff et al., 1980; Norris et al., 1993). Some studies found that ALS patients with higher CSF IgG, CSF protein, and Q_{ALB} had short survival times (Guiloff et al., 1980; Li J. Y. et al., 2022; Klose et al., 2023). However, some studies did not find that CSF protein levels were associated with the survival of ALS (Norris et al., 1993; Li J. Y. et al., 2022). Besides, the associations with the disease phenotypes such as the stage of the disease or the progression rate turned out to be unapparent in the majority of the studies (Tarasiuk et al., 2012; Zhao et al., 2020). One recent study found CSF protein was significantly negatively associated with the ALS functional rating scale revised (ALSFRS-R) scores in female ALS, not in male ALS (Assialioui et al., 2022). These inconsistent findings of the CSF profiles may result from inherent limitations, including small sample size, varied applied methods, characteristics of enrolled ALS patients, ethnic differences of participants, and so on. Therefore, the relationship between CSF profiles and disease phenotypes needs further study.

As the basic laboratory examinations, CSF profiles might reflect the pathophysiological alterations along the disease course and provide insight into the pathogenesis of the disease. Therefore, in the present study, we analyzed the CSF profiles from a longitudinal cohort of ALS from Southwest China, trying to elucidate the relationship between the CSF profiles and the phenotype, severity, progression, and prognosis of the disease.

Methods

Patients and controls

Inclusion criteria

All ALS patients included in the study, from the Department of Neurology, West China Hospital of Sichuan University between 2009 and 2022, who received a diagnosis of probable or definite ALS based on the El Escorial revised criteria. Demographic and clinical characteristics, such as age of onset, sex, disease type, disease stage, site of onset, disease course, progression rate, ALSFRS-R scores, and survival status, were recorded for each patient. Control subjects were admitted to the hospital for suspected neurological diseases, and underwent lumbar puncture as part of routine diagnostic procedures; no medication was administered at the time of the lumbar puncture.

Exclusion criteria

In the present study, participants with acute infections or trauma were excluded. Furthermore, individuals with immune system-related conditions such as multiple sclerosis, systemic lupus erythematosus, etc., which could potentially impact immune-related factors, were also excluded. ALS patients who did not undergo complete follow-up were excluded from the primary analysis; their data was solely utilized for sensitivity analysis.

The disease course was defined as the interval between the first symptoms of the disease onset and the hospitalization when the CSF and serum were examined. The progression rate was calculated using the total revised ALSFRS-R and symptom duration at diagnosis. ALSFRS-R scores were spliced into three subgroups of severity: mild (37–48), moderate (25–36), and severe (0–24). All the ALS patients were followed up at about 3-month intervals, and it was possible to determine a slope of deterioration for the clinical features of these patients. For survival analysis, the database was closed in August 2023. The term "death" is defined as death, endotracheal intubation, tracheostomy, and date of death confirmed by relatives.

We received approval from the ethical standards committee on human experimentation at West China Hospital. Written informed consent for research was obtained from all patients and control subjects participating in the study. All procedures and protocols were carried out in accordance with the guidelines of the Declaration of Helsinki and the International Ethical Guidelines for Human Biomedical Research.

CSF analysis

Lumbar puncture was performed in all participants. All CSF samples were checked for blood contamination. No sample was excluded due to contamination. All tests were conducted by the Department of Experimental Medicine of West China Hospital. Albumin and IgG in CSF and serum were detected using Beckman Coulter IMMAGE800 automatic specific protein analyzer (United States, IMM-10013) and its original supporting reagents, and using the industry gold standard rate scattering method with high efficiency and accuracy. The reference ranges were all based on the biological reference intervals provided by BECKMAN COULTER and executed in accordance with the "Clinical Laboratory Testing Project Reference Interval Establishment Standard" formulated by the National Health Commission of the People's Republic of China (WCH-LM-IMM-EXT-SP-026-07 WS/T 402). The reference ranges of CSF microprotein, albumin, IgG, index of IgG (IgG_{index}), and serum IgG (s-IgG) were 0.15–0.45 g/L, 0.134–0.337 g/L, 0.005–0.041 g/L, 0.18–0.84, and 8.00–15.50 g/L. Q_{ALB} ($Q_{ALB} = Alb_{CSF}/Alb_S$) is the albumin quotient, recognized as an effective marker to evaluate the permeability of the blood–brain barrier (BBB) (Reiber and Peter, 2001). CSF IgG_{index} is calculated through the equation; $IgG_{index} = Q_{IgG}/Q_{ALB}$($Q_{IgG}$ = CSF IgG/s-IgG).

Statistics

The normal distribution of the data was assessed by visual inspection and Shapiro–Wilk tests. The levels of CSF profiles between ALS patients and control subjects were compared using the

Abbreviations: ALS, Amyotrophic lateral sclerosis; CSF, Cerebrospinal fluid; Q_{ALB}, Albumin quotient; IgG_{index}, Index of IgG; HCs, Healthy controls; ALSFRS-R, Amyotrophic lateral sclerosis functional rating scale revised; BBB, The blood–brain barrier; s-IgG, Serum IgG.

Mann–Whitney U test and Kruskal-Wallis nonparametric test for non-normal variables and the Student's test for normal variables. The chi-square test was used to evaluate differences in frequencies. Pearson's or Spearman's correlation coefficients were used to evaluate the associations between these parameters and clinical phenotypes. One-way analysis of variance was used for comparison among multiple groups, and LSD and Welch's ANOVA tests were used for pair-to-group comparison. Multiple regression analysis was applied to find these associations with adjustment for confounding factors. Survival analysis was performed with a stepwise Cox proportional hazard analysis. After propensity score matching of ALS and control participants based on age and sex in a 1:1 ratio, inter-group comparisons of CSF profiles were conducted once more. The results of non-normal data were presented as non-normal data as median (interquartile range). We utilized the Hodges–Lehmann estimation to compute the median difference along with the 95% CI. The significance level was set at $p < 0.05$. All statistical analyses were conducted with SPSS (v26; IBM SPSS Statistics for Windows, Armonk, NY) software and GraphPad Prism 9 (GraphPad Software, Inc. Boston, MA, United States).

Results

In the study, 957 ALS patients underwent CSF and serum examinations during hospitalization. Eighty-seven ALS patients were lost to follow-up and were excluded from the study (9.1%) (Supplementary Figure S1). The control group consisted of 96 patients diagnosed with primary headache (41.7%) and anxiety and depression status (58.3%). The median age of ALS patients was 57.26 (48.15–64.99) years, while that of the control group was 41.00 (26.00–52.00) years. The ALS group comprised 530 males and 340 females, whereas the control group consisted of 28 males and 68 females.

Among the included 870 ALS patients, 69.1% were classical phenotype, 77.0% were of limb onset, 23.0% were of bulbar onset, 26.2% were at stage I, 39.8% were at stage II, and 34.0% were at stage III. As of August 2023, 43.1% of the patients had taken riluzole for more than 3 months, and 70.3% of the patients had died (with a median survival time of 42.43 months). The characteristics of male ALS and female ALS patients are listed in Supplementary Table S1, and male ALS patients were found to be older and had more limb onset, higher mortality rate, and lower median survival time than female ALS patients (Supplementary Table S1).

We compared the CSF profiles between the 870 ALS patients and 96 control subjects, and found that CSF microprotein, albumin, IgG, and Q_{ALB} in ALS patients were higher than those in the control group, but CSF IgG_{index} was lower than that in the control group (Table 1), although the difference was small. In ALS patients, the proportions above the median of the CSF microprotein, IgG, albumin, and Q_{ALB} were significantly higher than those in controls (CSF microprotein: 56.9% vs. 13.5%; IgG: 53.6% vs. 26.0%; albumin: 53.5% vs. 19.8%; Q_{ALB}: 53.7% vs. 11.5%). In ALS patients, the proportion of the CSF microprotein exceeding the upper limit of the normal range was 32.6%, IgG was 26.1%, and albumin was 14.6%. Besides, we found that the difference in CSF microprotein, IgG, albumin, and Q_{ALB} remained significantly higher between ALS and controls in both male and female subgroups (Supplementary Tables S2, S3). However, the differences in the CSF IgG_{index} between female ALS and female control subjects were insignificant (Supplementary Table S3). Taking into account the significant differences in age and sex between ALS and control participants, propensity score matching was conducted based on age and sex, resulting in the selection of 69 ALS participants and 69 control participants in a 1:1 matching ratio. After matching, there were no significant differences in age and sex between the groups. However, the levels of CSF microprotein, IgG, albumin, and Q_{ALB} in the ALS group remained significantly higher than those in the control group, and the CSF IgG_{index} remained significantly lower than that in the control group, which were consistent with the results of the unmatched group comparisons (Table 1). In addition, in the subgroup analyses, we found that CSF microprotein, albumin, IgG, and Q_{ALB} were higher in male than in female participants (Supplementary Tables S4, S5).

The correlation analyses found that CSF IgG was correlated with survival status ($r = -0.075$, $p = 0.028$; Table 2), that is, the higher the CSF IgG, the higher the risk of death from ALS. CSF IgG_{index} was negatively correlated with ALSFRS-R ($r = -0.067$, $p = 0.048$; Table 2). CSF IgG, albumin, and Q_{ALB} were correlated with disease duration (CSF IgG: $r = -0.105$, $p = 0.002$; CSF albumin: $r = -0.146$, $p < 0.001$; Q_{ALB}: $r = 0.155$ $p < 0.001$; Table 2). Considering the influence of sex in CSF profiles, we stratified ALS patients according to sex and found that in male ALS patients, CSF IgG and albumin were correlated with survival status, and CSF IgG_{index} was negatively correlated with ALSFRS-R ($r = -0.109$, $p = 0.012$, Table 2), but these associations did not exist in female ALS. Besides, we found that the associations of CSF IgG, albumin, $Q_{ALB,}$ and disease duration were found only in female ALS, but not in male ALS (Table 2).

In addition, we classified ALS into tertiles based on ALSFRS-R scores to analyze the correlation between CSF IgG_{index} and disease severity. We found that CSF IgG_{index} had significant differences between tertiles. Moderate ALS patients had higher CSF IgG_{index} compared to mild ALS patients (0.504 vs. 0.490, $p = 0.006$; Figure 1).

In order to verify whether the relationship between CSF IgG_{index} and ALSFRS-R was affected by other factors, multiple regression analysis was applied, and the results showed that CSF IgG_{index} was weakly correlated with ALSFRS-R scores in ALS patients after adjusting age of onset, sex, BMI, disease stage, site of onset, disease duration, and riluzole use ($F = 30.624$, $p < 0.001$; CSF IgG_{index}: $\beta = -0.062$, $p = 0.041$; Table 3). In the subgroup analyses, these correlations still existed in male ALS patients ($\beta = -0.095$, $p = 0.015$; Supplementary Table S6), but not in female ALS patients ($\beta = -0.014$, $p = 0.784$; Supplementary Table S7).

Since a significant correlation between CSF IgG and survival status was identified in ALS patients, we conducted further subgroup analysis based on the normal range of CSF IgG, and found that the survival time was shorter and survival rate were lower in the subgroup with CSF IgG exceeding the upper limit of the normal range ($p < 0.001$; Figure 2). In order to adjust the effects of other factors, including age of onset, disease course, disease stage, and site of onset, Cox survival analyses were performed. CSF IgG exceeding the upper limit of the normal range was significantly associated with the increased mortality risk in ALS patients [HR = 1.219 (1.010–1.470), $p = 0.039$; Figure 3]. Besides, ALS patients in stages II and III might be associated with increased mortality risk compared to those in stage I [stage II: HR = 1.689 (1.374–2.076), $p < 0.001$; stage III: HR = 2.100 (1.688–2.611), $p < 0.001$; Figure 3]. Older age of onset might be associated with increased mortality risk [age of onset:

TABLE 1 Comparison of CSF profiles between ALS and control groups.

	Non-matched				Matched		
	ALS (*N* = 870)	Controls (*N* = 96)	Estimated median difference (95% CI)	*p*	ALS (*N* = 69)	Controls (*N* = 69)	*p*
Age	57.26 (48.15–64.99)	41.00 (26.00–52.00)		**<0.001**	46.64 (39.10–62.44)	49.00 (37.50–57.00)	0.907
Sex (female%)	340 (39.1)	68 (70.8)		**<0.001**	32 (61.5)	46 (66.7)	0.378
CSF microprotein (g/L)	0.390 (0.330–0.470)↑	0.300 (0.243–0.340)	−0.100 (−0.120, −0.080)	**<0.001**	0.36 (0.30–0.45) ↑	0.32 (0.25–0.36)	**<0.001**
Proportion of CSF microprotein exceeding median (0.380 g/L)	56.9%↑	13.5%		**<0.001**	44.9%↑	15.9%	**<0.001**
Proportion of CSF microprotein exceeding the upper limit (0.450 g/L)	32.6%	0.0%			24.6%	0.0%	
CSF IgG (g/L)	0.030 (0.023–0.042)↑	0.022 (0.017–0.030)	−0.008 (−0.011, −0.006)	**<0.001**	0.03 (0.02–0.04) ↑	0.02 (0.02–0.03)	**0.002**
Proportion of CSF IgG exceeding median (0.029 g/L)	53.6%↑	26.0%		**<0.001**	53.6%↑	29.0%	**0.003**
Proportion of CSF IgG exceeding the upper limit (0.041 g/L)	26.1%	0.0%			27.5%	0.0%	
CSF albumin (g/L)	0.214 (0.174–0.278)↑	0.160 (0.128–0.200)	−0.057 (−0.071, −0.044)	**<0.001**	0.15 (0.20–0.26) ↑	0.14 (0.17–0.20)	**<0.001**
Proportion of CSF albumin exceeding median (0.207 g/L)	53.5%↑	19.8%		**<0.001**	47.8% ↑	23.2%	**0.002**
Proportion of CSF albumin exceeding the upper limit (0.337 g/L)	14.6%	0.0%			11.6%	0.0%	
CSF IgG_{index}	0.494 (0.455–0.531) ↓	0.508 (0.467–0.543)	0.014 (0.000, 0.028)	**0.047**	0.50 (0.44–0.53) ↓	0.50 (0.45–0.56)	**0.029**
Proportion of CSF IgG_{index} exceeding median (0.495)	49.8%	55.2%		0.312	53.6%	50.7%	0.733
Proportion of CSF IgG_{index} exceeding the upper limit (0.840)	0.5%	0.0%			0.0%	0.0%	
Q_{ALB}	0.006 (0.005–0.007)↑	0.004 (0.003–0.005)	−1.659 (−2.009, −1.311)	**<0.001**	0.005 (0.004–0.007)↑	0.004 (0.003–0.005)	**<0.001**
Proportion of CSF Q_{ALB} exceeding median (0.005)	53.7%↑	11.5%		**<0.001**	52.2%↑	15.9%	**<0.001**
s-IgG (g/L)	11.200 (9.625–12.700)	10.950 (9.530–12.450)	−0.300 (−0.800, 0.220)	0.304	11.25 (9.64–13.63)	10.80 (9.50–12.10)	0.060
Proportion of s-IgG exceeding median (11.100 g/L)	52.3%	49.0%		0.576	53.9%	46.4%	0.516
Proportion of s-IgG exceeding the upper limit (15.500 g/L)	3.1%	0.0%			7.7%	0.0%	

Bold: $p < 0.05$. $Q_{ALB} = Alb_{CSF}/Alb_S$ (CSF albumin/serum albumin); s-IgG: serum IgG; **↑:** CSF profiles in ALS group were higher than that in control group; ↓: CSF profiles in ALS group were lower than that in control group.

10.3389/fnins.2024.1375892

TABLE 2 Correlation analysis between CSF profiles and clinical features of ALS.

r/P	Age	Sex	Disease stage	Site of onset	Disease duration	ALSFRS-R	Progression rate	Survival state
CSF microprotein	0.035/0.303	**−0.109/0.001**	**−0.071/0.036**	0.035/0.302	−0.021/0.535	0.010/0.777	0.012/0.728	−0.014/0.676
CSF IgG	−0.036/0.288	**−0.073/0.032**	−0.053/0.120	−0.032/0.348	**−0.105/0.002**	−0.011/0.738	−0.031/0.354	**−0.075/0.028**
CSF albumin	0.057/0.095	**−0.118/0.000**	−0.051/0.136	0.000/0.990	**−0.146/0.000**	0.015/0.655	−0.022/0.518	−0.040/0.240
CSF IgG_{index}	0.020/0.549	−0.036/0.286	0.044/0.197	−0.020/0.548	0.014/0.690	**−0.067/0.048**	−0.007/0.839	0.034/0.313
Q_{ALB}	**0.067/0.047**	**−0.109/0.001**	−0.047/0.164	0.000/0.992	**0.155/0.000**	0.013/0.712	−0.018/0.594	−0.001/0.979
Male ALS								
CSF microprotein	0.048/0.275		−0.053/0.223	0.019/0.657	0.007/0.886	−0.058/0.179	−0.002/0.972	−0.080/0.065
CSF IgG	0.037/0.396		−0.050/0.247	−0.054/0.218	−0.006/0.895	−0.067/0.126	−0.044/0.314	**−0.122/0.005**
CSF albumin	0.029/0.510		−0.017/0.697	0.007/0.879	0.004/0.926	−0.050/0.251	−0.009/0.828	**−0.113/0.009**
CSF IgG_{index}	−0.003/0.939		0.074/0.090	−0.013/0.773	−0.035/0.426	**−0.109/0.012**	−0.005/0.910	0.028/0.520
Q_{ALB}	0.054/0.213		−0.023/0.600	0.006/0.896	0.013/0.765	−0.049/0.264	−0.008/0.860	−0.072/0.097
Female ALS								
CSF microprotein	0.008/0.890		−0.068/0.212	0.031/0.565	−0.050/0.362	0.077/0.158	0.022/0.687	0.056/0.303
CSF IgG	0.032/0.557		−0.047/0.392	−0.021/0.705	**0.224/0.000**	0.044/0.419	−0.020/0.710	−0.024/0.655
CSF albumin	0.079/0.144		−0.082/0.133	−0.041/0.452	**0.246/0.000**	0.052/0.339	−0.033/0.547	0.042/0.442
CSF IgG_{index}	−0.057/0.297		0.002/0.996	−0.040/0.458	0.093/0.086	−0.005/0.923	−0.013/0.816	0.034/0.531
Q_{ALB}	0.085/0.116		−0.067/0.219	−0.036/0.506	**0.251/0.000**	0.044/0.423	−0.027/0.622	0.087/0.111

Bold: $p < 0.05$.

HR = 1.034 (1.027–1.042), $p < 0.001$; Figure 3], while longer disease duration and limb-onset compared to other onset regions may be associated with lower mortality risk [disease duration: HR = 0.947 (0.939–0.955), $p < 0.001$; site of onset: HR = 0.771 (0.639–0.931), $p = 0.007$; Figure 3].

Sensitivity analysis: First, we compared the levels of CSF profiles between the lost to follow-up ALS patients and ALS patients included in the analysis and found no significant differences between ALS patients who were lost to follow-up and ALS patients who completed follow-up (Supplementary Table S8). Secondly, we included the loss to follow-up ALS patients in the sensitivity analysis and found that it did not affect the results of the aforementioned analysis.

Discussion

The study found a significant association between CSF IgG and survival status in ALS patients. The survival time was shorter and survival rates were lower in the ALS with CSF IgG exceeding the upper limit of the normal range. CSF IgG_{index} may negatively correlate with ALSFRS-R scores, especially in male ALS.

The current study found approximately one-third of ALS patients had higher CSF IgG levels. A previous study found IgG isolated from ALS patients increased the mobility of primary astrocyte endosomes and lysosomes, suggesting that it may be involved in the endocytosis/autophagy pathway (Stenovec et al., 2011). A single intraperitoneal injection of serum IgG from ALS patients induced a selective increase in the excitatory amino acids aspartate and glutamate levels in the CSF of rats (La Bella et al., 1997). Furthermore, some studies showed that IgG isolated from ALS patients can bind to CD16 receptors on microglia or lymphocytes and immune synapses between microglia and neurons (Edri-Brami et al., 2012, 2015), and can activate the oxidative stress response of microglia and release inflammatory factors (Milošević et al., 2017). Therefore, CSF IgG in ALS patients may accelerate the mortality risk in ALS by activating microglia to release oxidative stress. However, future basic research is still needed to elucidate the role of increased CSF IgG.

$IgG_{index} = Q_{IgG}/Q_{ALB}$($Q_{IgG}$ = CSF IgG/s-IgG, $Q_{ALB} = Alb_{CSF}/Alb_S$). In our study, we found that in mild ALS, the CSF IgG_{index} was lower compared to the control group. We considered this may be due to the significant increase in Q_{ALB} in the ALS group compared to the control group. Therefore, as Q_{ALB} serves as the divisor in the formula ($IgG_{index} = Q_{IgG}/Q_{ALB}$), its significant increase may lead to a decrease in the quotient. However, the difference in Q_{ALB} between mild ALS and moderate ALS was not significant. In this situation, CSF IgG_{index} may better reflect changes in Q_{IgG}, as consistent with the finding of the negative association between CSF IgG_{index} and ALSFRS-R scores in ALS patients. That is, the more severe the ALS patient, the higher the CSF IgG_{index} may be, indicating potentially more intrathecal IgG synthesis. Therefore, as an accessible CSF biomarker, CSF IgG_{index} can only roughly reflect the situation of intrathecal synthesis, and compared to the most reliable indicator of intrathecal oligoclonal protein synthesis, OB, it definitely has its limitations.

Q_{ALB} is recognized as an effective marker to evaluate the permeability of the BBB (Reiber and Peter, 2001). The current finding of the significant increase in Q_{ALB} of ALS patients was consistent with some studies (Wu et al., 2020; Alarcan et al., 2023). Some researchers believed that the disruption of BBB was an early event in ALS, and most studies suggested that BBB disruption in neurodegenerative diseases mediates the invasion of immune cells from the blood, resulting in neurodegeneration (Aragón-González et al., 2022;

10.3389/fnins.2024.1375892

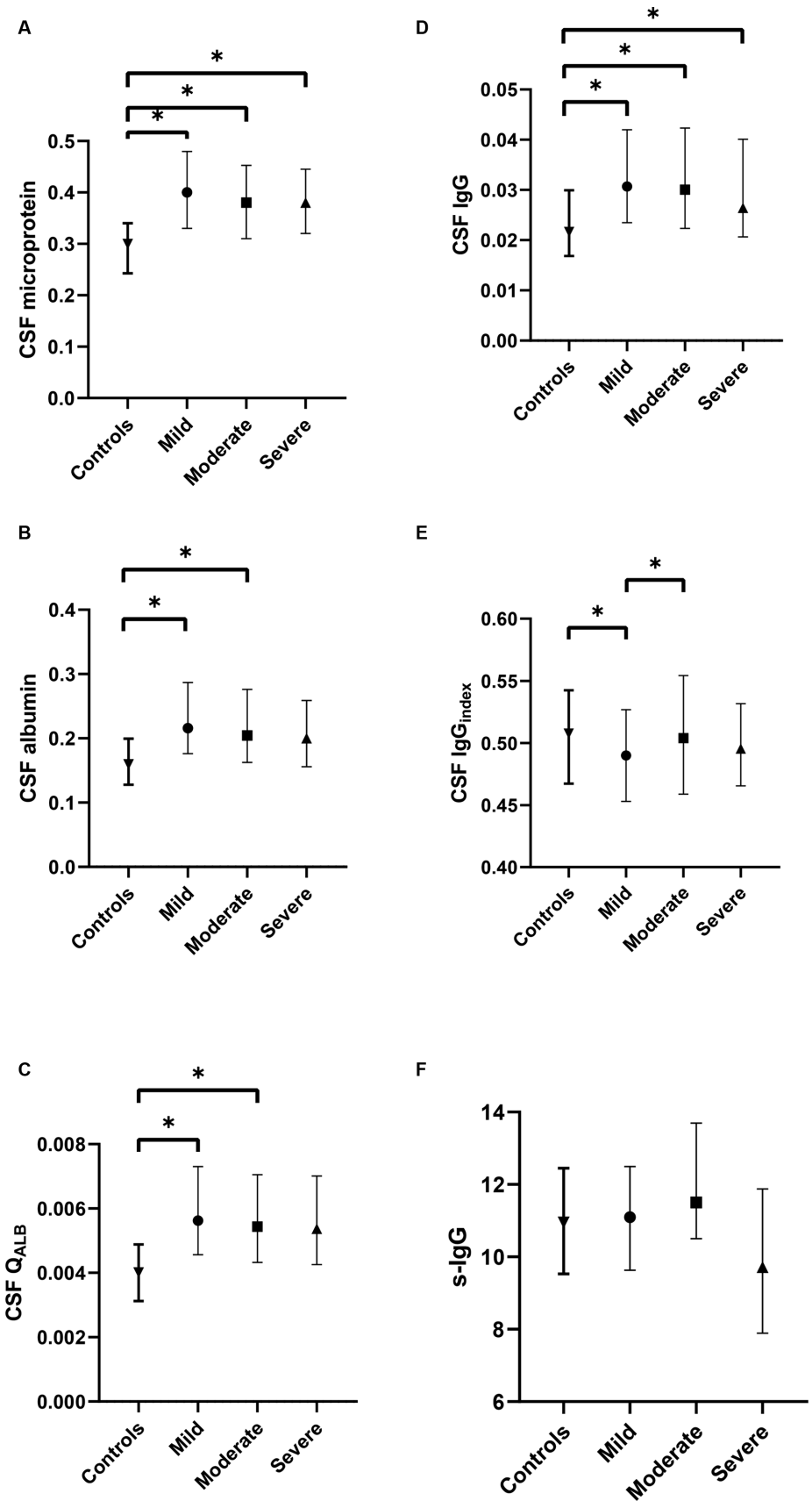

FIGURE 1
Comparison of CSF profiles among different subgroups of ALS and control group. **(A)** The difference in CSF microprotein, albumin, and IgG between mild, moderate, and severe ALS; **(B)** The difference in CSF albumin between mild, moderate, and severe ALS; **(C)** The difference in Q_{ALB} between mild, moderate, and severe ALS; **(D)** The difference in CSF IgG between mild, moderate, and severe ALS; **(E)** The difference in CSF IgG_{index} between mild, moderate, and severe ALS; **(F)** The difference in serum IgG between mild, moderate, and severe ALS. *$p < 0.05$.

TABLE 3 Multiple linear regression analysis of ALSFRS-R of CSF IgG_{Index}.

	Unnormalized coefficient		Normalized coefficient	*t*	*p*	95.0% Confidence interval	
	Beta	Standard error	Beta			Lower limit	Upper limit
Age of onset	−0.070	0.019	−0.114	−3.685	**<0.001**	−0.107	−0.033
Sex	−0.764	0.427	−0.055	−1.792	0.073	−1.602	0.073
BMI	−0.039	0.070	−0.017	−0.552	0.581	−0.176	0.099
Disease stage	−3.707	0.270	−0.424	−13.754	**<0.001**	−4.237	−3.178
Site of onset	−0.138	0.187	−0.023	−0.739	0.460	−0.505	0.229
Disease duration	−0.062	0.014	−0.133	−4.281	**<0.001**	−0.090	−0.033
Riluzole use	1.768	0.417	0.130	4.242	**<0.001**	0.950	2.586
CSF IgG_{index}	−5.091	2.481	−0.062	−2.052	**0.041**	−9.962	−0.220

Bold: $p < 0.05$.

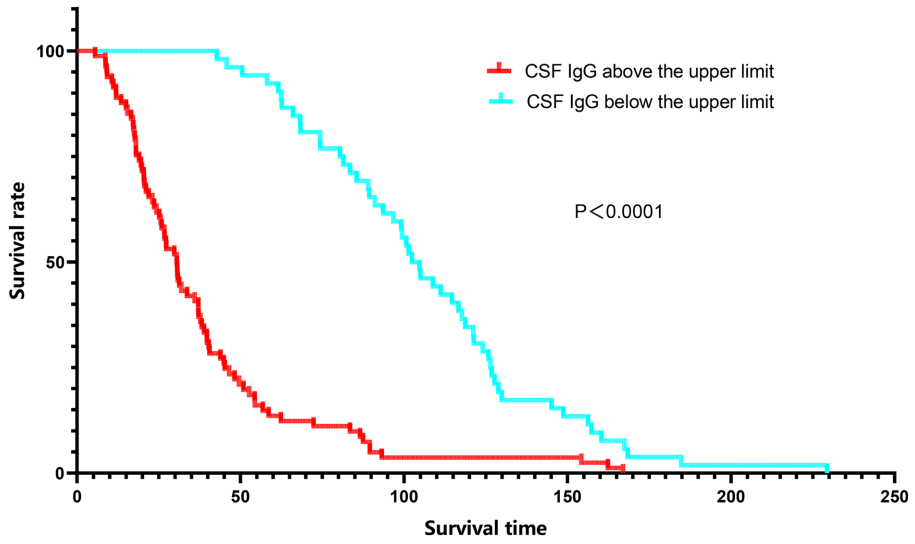

FIGURE 2
Kaplan–Meier survival curves of ALS patients according to CSF IgG stratifications. Red line: CSF IgG above the upper limit. Blue line: CSF IgG below the lower limit.

Beaman et al., 2022). However, Sweeney et al. suggested that decreased CSF reabsorption and/or production may elevate Q_{ALB}, leading to potential false-positive results in reflecting BBB breakdown (Sweeney et al., 2018). Therefore, further research is necessary to investigate the generation and absorption of CSF in ALS patients, as well as the extent of BBB disruption, for a comprehensive analysis of the role of the immune system in the occurrence and progression of ALS.

In the study, we found that CSF microprotein, IgG, albumin, and Q_{ALB} in male ALS patients were higher than those in female ALS patients, and the association between IgG_{index} and ALSFRS-R was found in male ALS patients, not in females. The male-to-female ratio of sporadic ALS is 1.3–1.5 (Logroscino et al., 2010). Hormones may play a protective role in the lower prevalence of ALS in females. The protective effect of female steroids may be due to their ability to prevent cell death and reduce the inflammatory component of the disease by acting directly on receptors expressed by motor neurons and muscle cells (Zhang et al., 2005). Therefore, sex differences should be paid attention to in the future.

Limitation

There are some limitations in the current study. First of all, although the research findings of this study were significant, the associations were relatively diverse, and this study only represents the situation of the local cohort; therefore, further validation is required through longitudinal multi-center studies. Secondly, it was not combined with other inflammatory and immune-related biomarkers in blood and CSF to analyze its correlation and its role in the disease progression and prognosis of ALS. Third, the study was observational only, and studies on the mechanism of changes of CSF IgG involved in the pathophysiology of ALS are needed in the future.

Conclusion

In the current study, we found that the higher CFS IgG was associated with increased mortality risk of ALS. Additionally, CSF

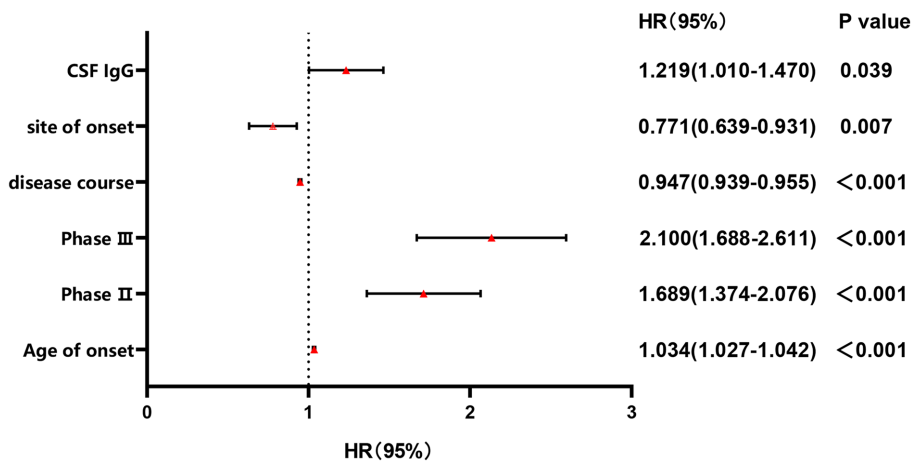

FIGURE 3
Forest plot of multivariable COX regression analysis for CSF IgG. Stage II: the odds ratio of mortality risk in Stage II compared to Stage I; Stage III: the odds ratio of mortality risk in Stage III compared to Stage I.

IgG_{index} may be associated with the severity of ALS, especially in male ALS.

Data availability statement

The original contributions presented in the study are included in the article/Supplementary material, further inquiries can be directed to the corresponding authors.

Ethics statement

The studies involving humans were approved by the ethical standards committee on human experimentation at West China Hospital. The studies were conducted in accordance with the local legislation and institutional requirements. The participants provided their written informed consent to participate in this study.

Author contributions

JF: Conceptualization, Data curation, Formal analysis, Investigation, Methodology, Software, Writing – original draft. XL: Conceptualization, Data curation, Formal analysis, Investigation, Software, Writing – original draft. QW: Conceptualization, Data curation, Investigation, Writing – original draft. XC: Conceptualization, Data curation, Investigation, Writing – original draft. HS: Conceptualization, Funding acquisition, Supervision, Writing – review & editing.

Funding

The author(s) declare that financial support was received for the research, authorship, and/or publication of this article. This study was supported by Sichuan Science and Technology Program (Grant No. 2022ZDZX0023) and the Clinical Research Incubation Project of West China Hospital of Sichuan University (Grant No. 20HXFH035), the grant from the Cadres Health Care Project in Sichuan Province (Grant No. 2023-111), the grant from the Beijing E-town Coorperation & Development Foundation (Grant No. YCXJ-JZ-2022-007), and grant from the Science and Technology Bureau Fund of Sichuan Province of China (No. 2023YFQ0098).

Acknowledgments

The authors gratefully acknowledge the participants in this study.

Conflict of interest

The authors declare that the research was conducted in the absence of any commercial or financial relationships that could be construed as a potential conflict of interest.

Publisher's note

Supplementary material

The Supplementary material for this article can be found online at: https://www.frontiersin.org/articles/10.3389/fnins.2024.1375892/full#supplementary-material

References

Akçimen, F., Lopez, E. R., Landers, J. E., Nath, A., Chiò, A., Chia, R., et al. (2023). Amyotrophic lateral sclerosis: translating genetic discoveries into therapies [published online ahead of print, 2023 Apr 6]. *Nat. Rev. Genet.* 24, 642–658. doi: 10.1038/s41576-023-00592-y

Alarcan, H., Vourc'h, P., Berton, L., Benz-de Bretagne, I., Piver, E., Andres, C. R., et al. (2023). Implication of central nervous system barrier impairment in amyotrophic lateral sclerosis: gender-related difference in patients. *Int. J. Mol. Sci.* 24:11196. doi: 10.3390/ijms241311196

Aragón-González, A., Shaw, P. J., and Ferraiuolo, L. (2022). Blood-brain barrier disruption and its involvement in neurodevelopmental and neurodegenerative disorders. *Int. J. Mol. Sci.* 23:15271. doi: 10.3390/ijms232315271

Assialioui, A., Domínguez, R., Ferrer, I., Andrés-Benito, P., and Povedano, M. (2022). Elevated cerebrospinal fluid proteins and albumin determine a poor prognosis for spinal amyotrophic lateral sclerosis. *Int. J. Mol. Sci.* 23:11063. doi: 10.3390/ijms231911063

Beaman, C., Kozii, K., Hilal, S., Liu, M., Spagnolo-Allende, A. J., Polanco-Serra, G., et al. (2022). Cerebral microbleeds, cerebral amyloid Angiopathy, and their relationships to quantitative markers of neurodegeneration. *Neurology* 98, e1605–e1616. doi: 10.1212/WNL.0000000000200142

Chen, L., Xu, L., Tang, L., Xia, K., Tian, D., Zhang, G., et al. (2021). Trends in the clinical features of amyotrophic lateral sclerosis: a 14-year Chinese cohort study. *Eur. J. Neurol.* 28, 2893–2900. doi: 10.1111/ene.14943

Edri-Brami, M., Rosental, B., Hayoun, D., Welt, M., Rosen, H., Wirguin, I., et al. (2012). Glycans in sera of amyotrophic lateral sclerosis patients and their role in killing neuronal cells. *PLoS One* 7:e35772. doi: 10.1371/journal.pone.0035772

Edri-Brami, M., Sharoni, H., Hayoun, D., Skutelsky, L., Nemirovsky, A., Porgador, A., et al. (2015). Development of stage-dependent glycans on the fc domains of IgG antibodies of ALS animals. *Exp. Neurol.* 267, 95–106. doi: 10.1016/j.expneurol.2015.02.023

Gårde, A., and Kjellin, K. G. (1971). Diagnostic significance of cereborspinal-fluid examinations in myelopathy. *Acta Neurol. Scand.* 47, 555–568. doi: 10.1111/j.1600-0404.1971.tb07508.x

Guiloff, J. F., McGregor, B., Thompson, E., Blackwood, W., and Paul, E. (1979). Age and cerebrospinal-fluid protein in motor-neuron disease. *N. Engl. J. Med.* 300, 437–438. doi: 10.1056/nejm197902223000820

Guiloff, R. J., McGregor, B., Thompson, E., Blackwood, W., and Paul, E. (1980). Motor neurone disease with elevated cerebrospinal fluid protein. *J. Neurol. Neurosurg. Psychiatry* 43, 390–396. doi: 10.1136/jnnp.43.5.390

Klose, V., Jesse, S., Lewerenz, J., Kassubek, J., Dorst, J., Tumani, H., et al. (2023). CSF oligoclonal IgG bands are not associated with ALS progression and prognosis. *Front. Neurol.* 14:1170360. Published 2023 May 5. doi: 10.3389/fneur.2023.1170360

La Bella, V., Goodman, J. C., and Appel, S. H. (1997). Increased CSF glutamate following injection of ALS immunoglobulins. *Neurology* 48, 1270–1272. doi: 10.1212/wnl.48.5.1270

Leonardi, A., Abbruzzese, G., Arata, L., Cocito, L., and Vische, M. (1984). Cerebrospinal fluid (CSF) findings in amyotrophic lateral sclerosis. *J. Neurol.* 231, 75–78. doi: 10.1007/BF00313720

Li, J. Y., Cai, Z. Y., Sun, X. H., Shen, D. C., Yang, X. Z., Liu, M. S., et al. (2022). Blood-brain barrier dysfunction and myelin basic protein in survival of amyotrophic lateral sclerosis with or without frontotemporal dementia. *Neurol. Sci.* 43, 3201–3210. doi: 10.1007/s10072-021-05731-z

Li, C., Liu, J., Lin, J., and Shang, H. (2022). COVID-19 and risk of neurodegenerative disorders: a Mendelian randomization study. *Transl. Psychiatry* 12:283. doi: 10.1038/s41398-022-02052-3

Logroscino, G., Traynor, B. J., Hardiman, O., Chio, A., Mitchell, D., Swingler, R. J., et al. (2010). Incidence of amyotrophic lateral sclerosis in Europe. *J. Neurol. Neurosurg. Psychiatry* 81, 385–390. doi: 10.1136/jnnp.2009.183525

Milošević, M., Milićević, K., Božić, I., Lavrnja, I., Stevanović, I., Bijelić, D., et al. (2017). Immunoglobulins G from sera of amyotrophic lateral sclerosis patients induce oxidative stress and upregulation of Antioxidative system in BV-2 microglial cell line. *Front. Immunol.* 8:1619. Published 2017 Nov 23. doi: 10.3389/fimmu.2017.01619

Norris, F. H., Burns, W., U, K. S., Mukai, E., and Norris, H. (1993). Spinal fluid cells and protein in amyotrophic lateral sclerosis. *Arch. Neurol.* 50, 489–491. doi: 10.1001/archneur.1993.00540050041012

Reiber, H., and Peter, J. B. (2001). Cerebrospinal fluid analysis: disease-related data patterns and evaluation programs. *J. Neurol. Sci.* 184, 101–122. doi: 10.1016/s0022-510x(00)00501-3

Rosenbohm, A., Liu, M., Nagel, G., Peter, R. S., Cui, B., Li, X., et al. (2018). Phenotypic differences of amyotrophic lateral sclerosis (ALS) in China and Germany. *J. Neurol.* 265, 774–782. doi: 10.1007/s00415-018-8735-9

Stenovec, M., Milošević, M., Petrušić, V., Potokar, M., Stević, Z., Prebil, M., et al. (2011). Amyotrophic lateral sclerosis immunoglobulins G enhance the mobility of Lysotracker-labelled vesicles in cultured rat astrocytes. *Acta Physiol (Oxf.)* 203, 457–471. doi: 10.1111/j.1748-1716.2011.02337.x

Sweeney, M. D., Sagare, A. P., and Zlokovic, B. V. (2018). Blood-brain barrier breakdown in Alzheimer disease and other neurodegenerative disorders. *Nat. Rev. Neurol.* 14, 133–150. doi: 10.1038/nrneurol.2017.188

Tarasiuk, J., Kułakowska, A., Drozdowski, W., Kornhuber, J., and Lewczuk, P. (2012). CSF markers in amyotrophic lateral sclerosis. *J. Neural Transm. (Vienna)* 119, 747–757. doi: 10.1007/s00702-012-0806-y

Wei, Q. Q., Hou, Y. B., Zhang, L. Y., Ou, R. W., Cao, B., Chen, Y. P., et al. (2022). Neutrophil-to-lymphocyte ratio in sporadic amyotrophic lateral sclerosis. *Neural Regen. Res.* 17, 875–880. doi: 10.4103/1673-5374.322476

Wu, Y., Yang, X., Li, X., Wang, H., and Wang, T. (2020). Elevated cerebrospinal fluid homocysteine is associated with blood-brain barrier disruption in amyotrophic lateral sclerosis patients. *Neurol. Sci.* 41, 1865–1872. doi: 10.1007/s10072-020-04292-x

Yang, T., Wei, Q., Li, C., Cao, B., Ou, R., Hou, Y., et al. (2022). Spatial-temporal pattern of propagation in amyotrophic lateral sclerosis and effect on survival: a cohort study. *Eur. J. Neurol.* 29, 3177–3186. doi: 10.1111/ene.15527

Yang, T., Xiao, Y., Cheng, Y., Huang, J., Wei, Q., Li, C., et al. (2023). Epigenetic clocks in neurodegenerative diseases: a systematic review. *J. Neurol. Neurosurg. Psychiatry* 94, 1064–1070. doi: 10.1136/jnnp-2022-330931

Zhang, R., Gascon, R., Miller, R. G., Gelinas, D. F., Mass, J., Hadlock, K., et al. (2005). Evidence for systemic immune system alterations in sporadic amyotrophic lateral sclerosis (sALS). *J. Neuroimmunol.* 159, 215–224. doi: 10.1016/j.jneuroim.2004.10.009

Zhao, X., Yang, F., Wang, H., Cui, F., Li, M., Sun, B., et al. (2020). The increase in CSF total protein and immunoglobulins in Chinese patients with sporadic amyotrophic lateral sclerosis: a retrospective study. *J. Neurol. Sci.* 414:116840. doi: 10.1016/j.jns.2020.116840

frontiers | Frontiers in Aging Neuroscience

TYPE Original Research
PUBLISHED 16 May 2024
DOI 10.3389/fnagi.2024.1357070

OPEN ACCESS

EDITED BY
Agnes Lumi Nishimura,
Queen Mary University of London,
United Kingdom

REVIEWED BY
Vinicius M. Borges,
Marshall University, United States
Patricia García-Sanz,
Andalusian Public Foundation Progress and Health-FPS, Spain

*CORRESPONDENCE
Xusheng Huang
✉ lewish301@sina.com

RECEIVED 17 December 2023
ACCEPTED 24 April 2024
PUBLISHED 16 May 2024

CITATION
Du R, Zhu Y, Chen P, Li M, Zhang Y and Huang X (2024) Causal association between obstructive sleep apnea and amyotrophic lateral sclerosis: a Mendelian randomization study.
Front. Aging Neurosci. 16:1357070.
doi: 10.3389/fnagi.2024.1357070

Causal association between obstructive sleep apnea and amyotrophic lateral sclerosis: a Mendelian randomization study

Rongrong Du[1,2], Yahui Zhu[1,3], Peng Chen[3,4], Mao Li[1], Ying Zhang[3,5] and Xusheng Huang[1,2,3]*

[1]Department of Neurology, The First Medical Center, Chinese PLA General Hospital, Beijing, China, [2]School of Medicine, Nankai University, Tianjin, China, [3]Medical School of Chinese PLA, Beijing, China, [4]Department of General Surgery and Institute of General Surgery, The First Medical Center of Chinese PLA General Hospital, Beijing, China, [5]The Fourth of the Health Department, The Second Medical Center, Chinese PLA General Hospital, Beijing, China

Background: Obstructive sleep apnea (OSA) had a high prevalence in the population. Whether OSA increases the risk of amyotrophic lateral sclerosis (ALS) is unknown. Our aim was to clarify this issue using two-sample Mendelian randomization (MR) analysis in a large cohort.

Methods: Two-sample MR was used to evaluate the potential causality between OSA and ALS by selecting single-nucleotide polymorphisms (SNPs) as instrumental variables (IVs) from genome-wide association studies (GWAS). The inverse-variance weighted (IVW) method was chosen as the primary method to estimate causal association. Weighted median, weighted mode and simple mode methods were used as sensitivity analyses to ensure the robustness of the results.

Results: In MR analysis, IVW mode showed genetic liability to OSA was found to be significantly associated with a higher ALS risk (OR, 1.220; 95% confidence interval, 1.031–1.443; $p = 0.021$). No evidence of heterogeneity and horizontal pleiotropy were suggested.

Conclusion: We found potential evidence for a causal effect of OSA on an increased risk of ALS.

KEYWORDS

obstructive sleep apnea, amyotrophic lateral sclerosis, causality, genetic association, Mendelian randomization

1 Introduction

Obstructive sleep apnea (OSA) is a common sleep disorder that results in decreased hemoglobin oxygen saturation and disrupted sleep due to repeated apnea. Loud snoring, insomnia and daytime sleepiness are the main clinical manifestations. The overall prevalence of OSA in the general population is estimated to be 9–38% (Senaratna et al., 2017), varying with BMI, sex, age, and apnea-hypopnea index definitions used for diagnosis. OSA is about twofold to threefold more prevalent among men (5.3–49.7%) than women (1.2–23.4%) (Heinzer et al., 2015).

However, it is important to highlight that despite increasing public awareness and more cases being diagnosed, 80% of individuals with moderate or severe OSA remain undiagnosed, including a large proportion of ethnic and other minorities, older adults, and women (Billings et al., 2021). Failure to promptly address this condition may lead to various mechanisms inherent to OSA, such as intermittent hypoxia, sleep structure disruption, and heightened oxidative stress, thereby elevating the likelihood of severe comorbidities (Giampa et al., 2023). For example, a meta-analysis of cross-sectional and longitudinal studies has demonstrated that untreated OSA was associated with an increased risk of hypertension in the general population (Hou et al., 2018). In addition, previous research has demonstrated that OSA potentially amplifies the risk of stroke (Redline et al., 2010), mild cognitive impairment, and Alzheimer's disease (AD) (Andrade et al., 2018; Ou et al., 2024), while also correlating with heightened Parkinson's disease (PD) severity (Elfil et al., 2021; Tang et al., 2024).

Amyotrophic lateral sclerosis (ALS) is a fatal neurodegenerative disease of the central nervous system, mainly caused by degeneration and loss of upper and lower motor neurons. The common clinical manifestations were progressive muscle weakness, muscular atrophy and dyspnea. At present, the exact pathogenesis is not clear, and there is no effective treatment. The prognosis of ALS patients is poor, and the median survival in ALS is only 2 to 4 years (Feldman et al., 2022). Previous studies have found that the mean survival in ALS patients with an obstructive apnea/hypopnea index (AHIo) $\geq$5 was significantly shorter than in ALS without OSA ($p = 0.0237$), suggesting that OSA may contribute to disease progression in ALS (Quaranta et al., 2017). OSA appears to be more common in ALS patients (Boentert et al., 2018; Boentert, 2019). A meta-analysis revealed significant reductions in sleep efficiency, total sleep time, and increases in oxygen desaturation index, and apnea hypopnea index in ALS patients compared with controls (Zhang et al., 2023). Previous studies have suggested a high prevalence of OSA in ALS patients, and OSA could predict a shorter survival of ALS. These studies might suggest a bidirectional effect between OSA and ALS, but whether OSA can increase the risk of ALS is unclear.

Although previous epidemiological studies have linked OSA to central nervous system (CNS) disorders, such as, OSA may be an important risk factor for stroke, ALS patients with an OSA phenotype were characterized by a worse prognosis, and OSA might potentiate neuropathological and clinical progression of AD (Yaggi et al., 2005; Quaranta et al., 2017; Andrade et al., 2018), it is not entirely clear whether OSA is associated with CNS disease or whether OSA increases the risk of CNS disease.

Mendelian randomization (MR) studies are causal studies that use genetic variants to assess the association between risk factors and outcomes (Davies et al., 2018). Because genetic variants are randomly assigned at birth, unconfounded investigations can be conducted and reverse causality in observational studies can be avoided. Given that the association between OSA and ALS risk is unclear, the aim of this study was to use MR study to assess the effect of OSA on ALS risk.

2 Materials and methods

Ethical review and approval were waived for this study, due to this study used summary data from GWAS and did not involve individual data. All studies that contributed data to this analysis were approved by the relevant institutional review board. Patient consent was waived due to this study used summary data from GWAS and did not involve individual data.

2.1 Data source

This MR study utilized pooled data from the OSA genome-wide association study (GWAS), with study participants from the FinnGen study (Strausz et al., 2021). The GWAS comprised 16,761 OSA patients and 201,194 controls. National health registries were employed for the identification of OSA cases, using ICD codes (ICD-9: 3472A, obstructive sleep apnea; ICD-10: G47.3, sleep apnea), as provided by the Finnish National Hospital Discharge Registry and the Cause of Death Registry, OSA was identified.

For ALS GWAS Iacoangeli et al. (2020) meta-analyzed the aggregated statistics of two ALS GWAS: an ALS study that included more than 80,000 individuals of European descent (Nicolas et al., 2018) and a Chinese ALS study with more than 4,000 individuals (Benyamin et al., 2017). The meta-analysis included a total of 84,694 individuals, including 22,040 cases and 62,654 controls, and a total of 5,356,204 SNPs.

2.2 The selection of instrumental variable

By employing genetic variants that exhibit a robust association with exposure as instrumental variables (IVs), MR subsequently examined the causal relationship between genetic predisposition to exposure and the desired outcomes. The MR analysis should adhere to three hypotheses: (1) Genetic variants must display a significant correlation with the exposure factors; (2) Genetic variants should not be linked to potential confounding variables; (3) Genetic variants should solely influence the outcome through the pathway of exposure (Figure 1). We used OSA GWAS from FinnGen Study. This GWAS identified 5 distinct genetic loci associated with OSA ($p < 5.0 \times 10^{-8}$). All these 5 SNPs were in different genomic regions and not in linkage disequilibrium ($r^2 < 0.20$). And all these 5 SNPs had a high imputation quality (INFO >0.9) (Strausz et al., 2021). Thus, five genetic variants associated with OSA were identified. After that, we obtained the corresponding SNPs from the outcome (ALS) GWAS summary data and made the data harmonization.

2.3 Statistical analysis

To evaluate the impact of genetically-predicted OSA on ALS for each SNP, we employed the Wald ratio (Hemani et al., 2018). The inverse variance weighted (IVW) model was used as the primary MR analysis to evaluate the aggregate effect of multiple SNPs (Bowden et al., 2019). The IVW method essentially assumes a zero intercept and performs a weighted regression of the SNP-exposure effects with the SNP-outcome effects.

In the context of MR study, it is imperative that three assumptions are fulfilled to ensure the validity of the MR method. Firstly, it is crucial that genetic variants exhibit a significant association with the risk factors (exposure). Consequently, to minimize any possible weak IV bias, the strength of the IV was assessed using the F-statistic, denoted

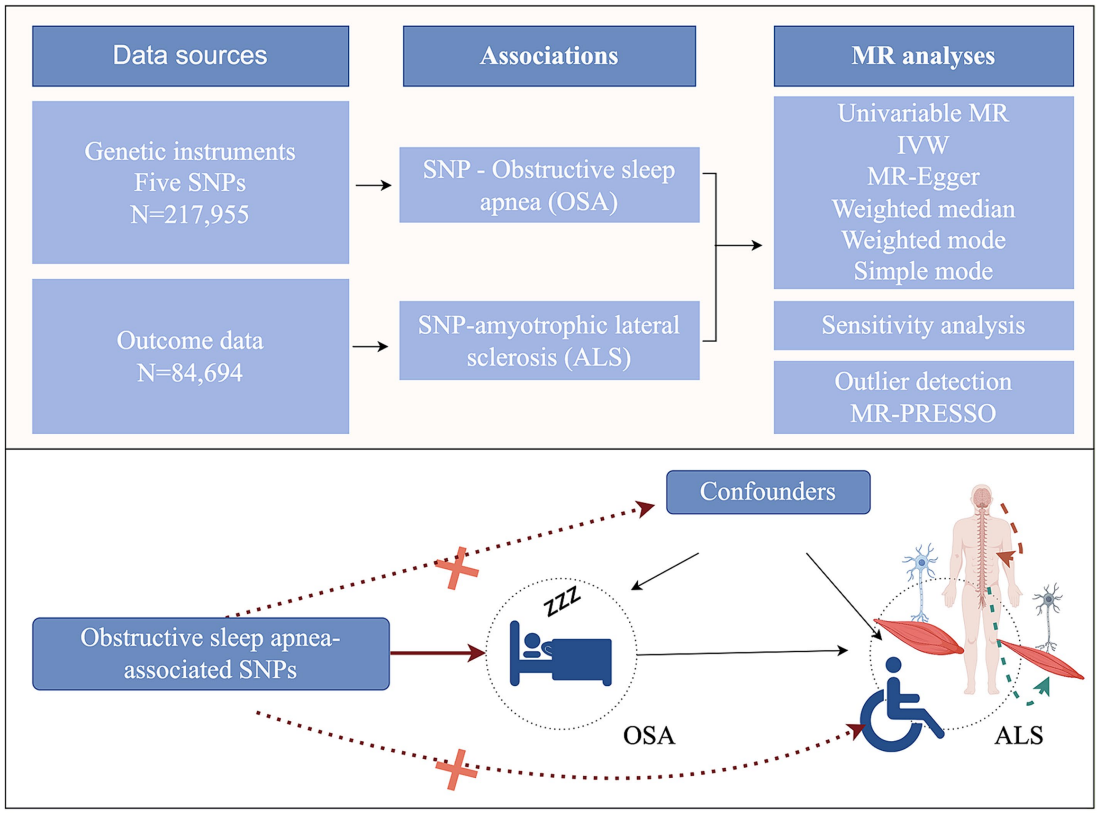

FIGURE 1
Study design of the two-sample Mendelian randomization for the effect of genetically predicted obstructive sleep apnea on amyotrophic lateral sclerosis (by Figdraw). MR, Mendelian randomization; IVW, inverse-variance weighted; SNPs, single-nucleotide polymorphisms.

as $F = \beta^2/se^2$ (where β represents the effect size of the SNP on the exposure and Se represents its corresponding standard error). A higher F-statistic corresponded to a smaller bias. And if F-statistic > 10, it indicates that the study had sufficient strength (Burgess et al., 2011). The second assumption is deemed valid only if the genetic variants do not exhibit any association with confounding factors influencing the relationship between OSA and ALS. That is, there is no horizontal pleiotropy. The MR-Egger intercept (Burgess and Thompson, 2017) was used to study the influence of potential horizontal pleiotropy. MR-Egger method tests and accounts for the presence of unbalanced pleiotropy by introducing a parameter for this bias and incorporating outline information estimates of causative effects from multiple individual variants. The MR-PRESSO method mainly detects horizontal pleoitropy by using residual sum (Verbanck et al., 2018). In MR-PRESSO method, it attempts to reduce pleoitropy in the estimate of the causal effect by removing outliers that contribute to the pleoitropy disproportionately more than expected. Heterogeneity was assessed using Cochrane's Q values, and if heterogeneity was present, the multiplicative random effects model was preferred.

We then performed sensitivity analyses, in which we assessed the consistency of MR results by using different methods established under different hypotheses to determine the robustness of our study. Weighted median, weighted mode and simple mode methods are used initially. The IVW approach requires that the pleiotropic effect of the genetic variants should be independent of exposure. Therefore, if the genetic variants do not conform to the hypothesis, the results of the weighted median method can offer a reliable effect estimation, despite up to 50% of the genetic variantions not aligning with the corresponding presumption. Furthermore, by assuming that the most common value of the bias in the estimation of Wald rations is zero, a weighted model-based approach can potentially yield coherent results without relying on measurement error assumptions that are not applicable. In addition, scatter plots were employed to illustrate effect estimates derived from different MR approaches.

In this study, we used R (version 4.1.2) and the "TwoSampleMR" and "MRPRESSO" packages (version 0.5.6) for analyses. In all of the above analyses, $p < 0.05$ indicates statistical significance.

3 Results

As part of this study, we evaluated the causal relationship between OSA and ALS. Table 1 shows the statistical data of the five SNPs selected as valid instrumental variables. The F statistic of each SNP was above the empirical threshold of 10.

Using the IVW method, our results suggested that genetically predicted OSA increased the risk of ALS [OR = 1.220 (1.031–1.443)] (Figure 2). Moreover, weighted median, weighted mode and simple mode also showed the same trend (Figure 2). Figure 3 showed the scatter plots of effect estimates derived from different MR methods.

No indications of heterogeneity were found in the causal effect estimates derived from the MR Egger and IVW analyses (all *p*-values

TABLE 1 Extracted SNPs for the exposure OSA based on a genome-wide significance threshold of 5E-08.

SNP	A1	A2	EAF	BETA	SE	P	F statistic
rs9937053	G	A	0.43	0.102	0.013	4.32E-16	61.6
rs10507084	C	T	0.179	0.109	0.016	2.80E-11	46.4
rs4837016	G	A	0.466	−0.071	0.013	1.53E-08	29.8
rs185932673	C	T	0.003	0.624	0.112	2.44E-08	31.0
rs10928560	C	T	0.195	−0.088	0.016	2.80E-08	30.3

OSA, obstructive sleep apnea; SNP, single-nucleotide polymorphism; A1, effect allele; A2, non-effect allele; EAF, Effect allele frequency; BETA, beta estimate for the association of SNP with exposure; SE, standard error of the Beta; *P*, two-sided *P*-value from the meta-analysis for exposure.

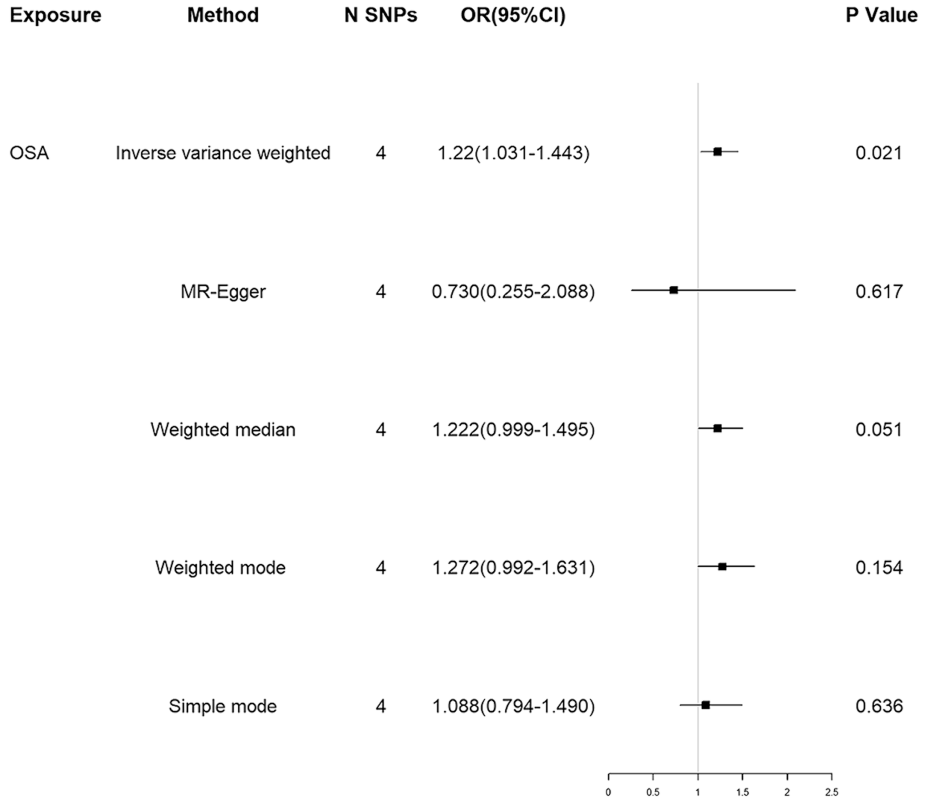

FIGURE 2
MR associations between genetically determined OSA and the risk of ALS. MR, Mendelian randomization; SNP, single nucleotide polymorphism; OR, odds ratio; CI, confidence interval; OSA, obstructive sleep apnea; ALS, amyotrophic lateral sclerosis.

<0.05, Table 2). The MR-PRESSO global test ($p = 0.522$) and MR Egger intercept (intercept = 0.047, $p = 0.434$, Table 2) suggested no horizontal pleiotropy for instrumental variables. The absence of heterogeneity and horizontal pleiotropy in this study suggested the robustness of the findings.

4 Discussion

Using MR method, our results suggested that genetically predicted OSA increased the risk of ALS, suggesting the need for timely OSA intervention to reduce the risk of ALS in individuals at high risk of ALS.

In observational studies, previous studies have shown that ALS patients with OSA have shorter survival, suggesting that OSA might promote disease progression in ALS (Quaranta et al., 2017). In addition, a meta-analysis of 11 studies revealed that OSA could hasten the severity of cognitive decline and exacerbate motor symptoms in individuals with PD (Elfil et al., 2021). Another study also indicated an increased risk of developing PD in those with OSA (Chen et al., 2015). Our findings, utilizing the MR method, suggest that OSA is associated with an augmented risk of developing ALS.

OSA could potentially increase the risk of developing ALS, as suggested by previous studies. Xie et al. (2013) found that natural sleep or anesthesia in live mice led to a 60% increase in interstitial space, which could result in a significant increase in convective exchange of cerebrospinal fluid with interstitial fluid, potentially contributing to ALS pathology. The increased flow of interstitial fluid during sleep, in turn, improves the clearancee of β-amyloid. Consequently, sleep is a fundamental part of the processes involved in the removal of brain

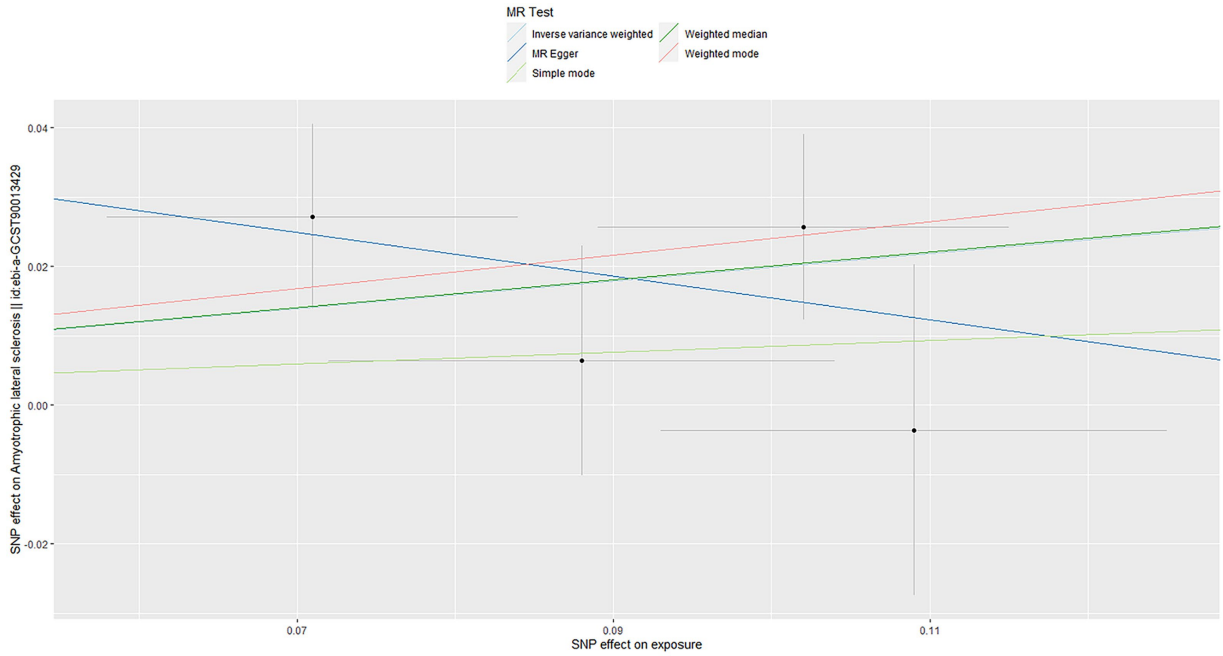

FIGURE 3
Scatter plots of genetic associations of OSA with ALS risk. The slopes of each line represent the causal association for each method. OSA, obstructive sleep apnea; ALS, amyotrophic lateral sclerosis.

TABLE 2 Heterogeneity and pleiotropy tests of instrument effects.

Exposure	N SNPs	Heterogeneity analysis				Pleiotropy analysis			
		Method	Q	Degree of freedom	*P*	Method	Egger intercept	SE	*P*
OSA	4	MR Egger	1.76	2	0.416	MR Egger intercept	0.047	0.048	0.434
		IVW	2.70	3	0.441	MR-PRESSO Global test			0.522

SNP, single nucleotide polymorphism; MR, Mendelian randomization; IVW, inverse variance weighted; OSA, obstructive sleep apnea; SE, standard error.

toxic metabolites (Xie et al., 2013). However, since OSA can cause sleep awakening and sleep fragmentation, affecting overall sleep quality, it is possible to increase the accumulation of toxic proteins in the brain of OSA patients, which may increase the risk of ALS.

Secondly, intermittent hypoxia (IH) is the main characteristic of OSA. It is well known that the brain is more sensitive to hypoxia than other organs, requiring more energy and oxygen consumption. The results of clinical and animal studies suggest that IH induced by OSA can lead to structural neuronal injury and dysfunction in the CNS, and oxidative stress and inflammatory damage are the pathophysiological basis (Liu et al., 2020). Accumulating evidence supports the idea that IH may induce ROS production, oxidative stress overactivation, and inflammatory damage in the CNS, leading to neuronal apoptosis and/or necrosis (Almendros et al., 2011). Similarly, in the mouse model of ALS, chronic intermittent hypoxia increases motor neuron death, neuromuscular weakness, and possibly cognitive dysfunction in mice (Kim et al., 2013). The generation of oxidative stress and the activation of inflammatory pathways may be related to it (Kim et al., 2013). In addition, previous studies have suggested that oxidative stress and inflammation are involved in the development of ALS (Teleanu et al., 2022). Therefore, we thought that intermittent hypoxia (due to OSA) promotes oxidative stress and inflammation of neurons (also characteristic of ALS), thereby further increasing ALS risk.

Thirdly, the respiratory force of respiratory collapse during OSA is associated with increased intrathoracic and intracranial pressures, and hemodynamic disturbance (Konecny et al., 2014; Wszedybyl-Winklewska et al., 2017). These studies hypothesized that this pressure impedes the flow of brain metabolites from interstitial fluid (ISF) to cerebrospinal fluid (CSF) via the glymphatic system (Ju et al., 2016), resulting in an increased accumulation of abnormal proteins in ISF and a significant decrease in neuro-derived proteins in CSF. Ju et al. (2016) elucidated the mechanism of neuro-derived proteins reduction in CSF and abnormal accumulation in ISF in patients with severe OSA. This suggests that the glymphatic clearing process is impaired in OSA patients. The decrease of abnormal SOD1 protein and TDP-43 protein clearance is considered to be one of the pathogenesis, which might also be another way for OSA to increase the risk of ALS.

Our study empolyed MR to assess the causal relationship between genetically predicted OSA and ALS risk. The study's main advantage is its inclusion of a large number of participants in ALS GWAS. Furthermore, the MR design prevents reverse causality bias and balances potential confounders, since genetic variants are not associated with other common comorbidities, such as obesity, stroke,

and high blood pressure, which can affect the results in observational studies. However, some limitations need to be noted in future studies: First, because OSA is a binary exposure, possible selection bias due to underdiagnosis cannot be well assessed. Second, because individual-level data were not available, potential bias due to medication status in ALS patients was not considered. Third, genetically predicted exposures frequently encompass enduring impacts, potentially intensified in magnitude, thereby rendering MR estimates distinct from clinical trial outcomes. Moreover, interventions targeting pertinent factors may not necessarily yield analogous clinical advantages as observed in MR studies. Fourth, the unavailability of stratified GWAS data for OSA severity hindered further exploration of the association between OSA severity and clinical characteristics. Fifth, the limited number of SNPs tested might affect the robustness of the results, and we will conduct further analysis in the future if larger OSA GWAS data and more SNPs are available. Sixth, we used the MR-Egger intercept and the MR-PRESSO method to evaluate the pleiotropy in this study. Although the results suggested that no horizontal pleiotropy for instrumental variables in this study, it cannot be completely ruled out whether the SNPs associated with exposure can have an impact on ALS risk through other ways. This is one of the limitations of this study. Finally, because this study focused primarily on participants of European descent, the results may not be extrapolated to populations of other ethnicities and will need to be further validated in other populations in the future.

While our study has limitations, it is the first to use MR method to examine the relationship between OSA and ALS. This study undertook a genetic perspective to evaluate the causal relationship between the two variables, suggesting that direct intervention with OSA may be beneficial in reducing the risk of ALS. It remains unclear how OSA raises ALS risk, and further studies are needed to discover how OSA affects neurodegenerative diseases in the brain.

5 Conclusion

Based on the results of the MR analysis, genetically predicted OSA leads to an increased risk of ALS. However, the mechanism by which OSA might increase the risk of ALS is currently unclear, and further study is needed to clarify it in the future.

Data availability statement

OSA GWAS summary data are publicly available and can be downloaded from GWAS catalog (https://www.ebi.ac.uk/gwas/) and ALS GWAS summary data are publicly available and can be downloaded from https://gwas.mrcieu.ac.uk/.

Ethics statement

Ethical approval was not required for the study involving humans in accordance with the local legislation and institutional requirements. Written informed consent to participate in this study was not required from the participants or the participants' legal guardians/next of kin in accordance with the national legislation and the institutional requirements.

Author contributions

RD: Conceptualization, Data curation, Writing – original draft. YaZ: Data curation, Formal analysis, Methodology, Writing – review & editing. PC: Data curation, Formal analysis, Writing – review & editing. ML: Data curation, Formal analysis, Writing – review & editing. YiZ: Investigation, Validation, Writing – review & editing. XH: Conceptualization, Project administration, Supervision, Validation, Writing – review & editing.

Funding

The author(s) declare that no financial support was received for the research, authorship, and/or publication of this article.

Acknowledgments

We would like to thank all investigators who make GWAS summary statistics publicly available.

Conflict of interest

The authors declare that the research was conducted in the absence of any commercial or financial relationships that could be construed as a potential conflict of interest.

Publisher's note

References

Almendros, I., Farré, R., Planas, A. M., Torres, M., Bonsignore, M. R., Navajas, D., et al. (2011). Tissue oxygenation in brain, muscle, and fat in a rat model of sleep apnea: differential effect of obstructive apneas and intermittent hypoxia. *Sleep* 34, 1127–1133. doi: 10.5665/sleep.1176

Andrade, A. G., Bubu, O. M., Varga, A. W., and Osorio, R. S. (2018). The relationship between obstructive sleep apnea and Alzheimer's disease. *J. Alzheimers Dis.* 64, S255–s270. doi: 10.3233/jad-179936

Benyamin, B., He, J., Zhao, Q., Gratten, J., Garton, F., Leo, P. J., et al. (2017). Cross-ethnic meta-analysis identifies association of the GPX3-TNIP1 locus with amyotrophic lateral sclerosis. *Nat. Commun.* 8:611. doi: 10.1038/s41467-017-00471-1

Billings, M. E., Cohen, R. T., Baldwin, C. M., Johnson, D. A., Palen, B. N., Parthasarathy, S., et al. (2021). Disparities in sleep health and potential intervention models: a focused review. *Chest* 159, 1232–1240. doi: 10.1016/j.chest.2020.09.249

Boentert, M. (2019). Sleep disturbances in patients with amyotrophic lateral sclerosis: current perspectives. *Nat Sci Sleep* 11, 97–111. doi: 10.2147/nss.S183504

Boentert, M., Glatz, C., Helmle, C., Okegwo, A., and Young, P. (2018). Prevalence of sleep apnoea and capnographic detection of nocturnal hypoventilation in amyotrophic lateral sclerosis. *J. Neurol. Neurosurg. Psychiatry* 89, 418–424. doi: 10.1136/jnnp-2017-316515

Bowden, J., Del Greco, M. F., Minelli, C., Zhao, Q., Lawlor, D. A., Sheehan, N. A., et al. (2019). Improving the accuracy of two-sample summary-data Mendelian randomization: moving beyond the NOME assumption. *Int. J. Epidemiol.* 48, 728–742. doi: 10.1093/ije/dyy258

Burgess, S., and Thompson, S. G. (2017). Interpreting findings from Mendelian randomization using the MR-egger method. *Eur. J. Epidemiol.* 32, 377–389. doi: 10.1007/s10654-017-0255-x

Burgess, S., Thompson, S. G., and Collaboration, C. C. G. (2011). Avoiding bias from weak instruments in Mendelian randomization studies. *Int J Epidemiol* 40, 755–764. doi: 10.1093/ije/dyr036

Chen, J. C., Tsai, T. Y., Li, C. Y., and Hwang, J. H. (2015). Obstructive sleep apnea and risk of Parkinson's disease: a population-based cohort study. *J. Sleep Res.* 24, 432–437. doi: 10.1111/jsr.12289

Davies, N. M., Holmes, M. V., and Davey Smith, G. (2018). Reading Mendelian randomisation studies: a guide, glossary, and checklist for clinicians. *BMJ* 362:k601. doi: 10.1136/bmj.k601

Elfil, M., Bahbah, E. I., Attia, M. M., Eldokmak, M., and Koo, B. B. (2021). Impact of obstructive sleep apnea on cognitive and motor functions in Parkinson's disease. *Mov. Disord.* 36, 570–580. doi: 10.1002/mds.28412

Feldman, E. L., Goutman, S. A., Petri, S., Mazzini, L., Savelieff, M. G., Shaw, P. J., et al. (2022). Amyotrophic lateral sclerosis. *Lancet* 400, 1363–1380. doi: 10.1016/S0140-6736(22)01272-7

Giampa, S. Q. C., Lorenzi-Filho, G., and Drager, L. F. (2023). Obstructive sleep apnea and metabolic syndrome. *Obesity (Silver Spring)* 31, 900–911. doi: 10.1002/oby.23679

Heinzer, R., Vat, S., Marques-Vidal, P., Marti-Soler, H., Andries, D., Tobback, N., et al. (2015). Prevalence of sleep-disordered breathing in the general population: the HypnoLaus study. *Lancet Respir. Med.* 3, 310–318. doi: 10.1016/s2213-2600(15)00043-0

Hemani, G., Bowden, J., and Davey Smith, G. (2018). Evaluating the potential role of pleiotropy in Mendelian randomization studies. *Hum. Mol. Genet.* 27, R195–r208. doi: 10.1093/hmg/ddy163

Hou, H., Zhao, Y., Yu, W., Dong, H., Xue, X., Ding, J., et al. (2018). Association of obstructive sleep apnea with hypertension: a systematic review and meta-analysis. *J. Glob. Health* 8:010405. doi: 10.7189/jogh.08.010405

Iacoangeli, A., Lin, T., Al Khleifat, A., Jones, A. R., Opie-Martin, S., Coleman, J. R. I., et al. (2020). Genome-wide Meta-analysis finds the ACSL5-ZDHHC6 locus is associated with ALS and links weight loss to the disease genetics. *Cell Rep.* 33:108323. doi: 10.1016/j.celrep.2020.108323

Ju, Y. E., Finn, M. B., Sutphen, C. L., Herries, E. M., Jerome, G. M., Ladenson, J. H., et al. (2016). Obstructive sleep apnea decreases central nervous system-derived proteins in the cerebrospinal fluid. *Ann. Neurol.* 80, 154–159. doi: 10.1002/ana.24672

Kim, S. M., Kim, H., Lee, J. S., Park, K. S., Jeon, G. S., Shon, J., et al. (2013). Intermittent hypoxia can aggravate motor neuronal loss and cognitive dysfunction in ALS mice. *PLoS One* 8:e81808. doi: 10.1371/journal.pone.0081808

Konecny, T., Khanna, A. D., Novak, J., Jama, A. A., Zawadowski, G. M., Orban, M., et al. (2014). Interatrial pressure gradients during simulated obstructive sleep apnea: a catheter-based study. *Catheter. Cardiovasc. Interv.* 84, 1138–1145. doi: 10.1002/ccd.25433

Liu, X., Ma, Y., Ouyang, R., Zeng, Z., Zhan, Z., Lu, H., et al. (2020). The relationship between inflammation and neurocognitive dysfunction in obstructive sleep apnea syndrome. *J. Neuroinflammation* 17:229. doi: 10.1186/s12974-020-01905-2

Nicolas, A., Kenna, K. P., Renton, A. E., Ticozzi, N., Faghri, F., Chia, R., et al. (2018). Genome-wide analyses identify KIF5A as a novel ALS gene. *Neuron* 97, 1267–1288. doi: 10.1016/j.neuron.2018.02.027

Ou, Y., Shen, C., Chen, Z., Liu, T., Peng, Y., Zong, D., et al. (2024). TDP43/HDAC6/Prdx1 signaling pathway participated in the cognitive impairment of obstructive sleep apnea via regulating inflammation and oxidative stress. *Int. Immunopharmacol.* 127:111350. doi: 10.1016/j.intimp.2023.111350

Quaranta, V. N., Carratù, P., Damiani, M. F., Dragonieri, S., Capozzolo, A., Cassano, A., et al. (2017). The prognostic role of obstructive sleep apnea at the onset of amyotrophic lateral sclerosis. *Neurodegener Dis* 17, 14–21. doi: 10.1159/000447560

Redline, S., Yenokyan, G., Gottlieb, D. J., Shahar, E., O'Connor, G. T., Resnick, H. E., et al. (2010). Obstructive sleep apnea-hypopnea and incident stroke: the sleep heart health study. *Am. J. Respir. Crit. Care Med.* 182, 269–277. doi: 10.1164/rccm.200911-1746OC

Senaratna, C. V., Perret, J. L., Lodge, C. J., Lowe, A. J., Campbell, B. E., Matheson, M. C., et al. (2017). Prevalence of obstructive sleep apnea in the general population: a systematic review. *Sleep Med. Rev.* 34, 70–81. doi: 10.1016/j.smrv.2016.07.002

Strausz, S., Ruotsalainen, S., Ollila, H. M., Karjalainen, J., Kiiskinen, T., Reeve, M., et al. (2021). Genetic analysis of obstructive sleep apnoea discovers a strong association with cardiometabolic health. *Eur. Respir. J.* 57:2003091. doi: 10.1183/13993003.03091-2020

Tang, H., Zhang, K., Zhang, C., Zheng, K., Gui, L., and Yan, B. (2024). Bioinformatics-based identification of key candidate genes and signaling pathways in patients with Parkinson's disease and obstructive sleep apnea. *Sleep Breath.* 1:3003. doi: 10.1007/s11325-024-03003-6

Teleanu, D. M., Niculescu, A. G., Lungu, I. I., Radu, C. I., Vladâcenco, O., Roza, E., et al. (2022). An overview of oxidative stress, Neuroinflammation, and neurodegenerative diseases. *Int. J. Mol. Sci.* 23:5938. doi: 10.3390/ijms23115938

Verbanck, M., Chen, C. Y., Neale, B., and Do, R.. (2018). Detection of widespread horizontal pleiotropy in causal relationships inferred from Mendelian randomization between complex traits and diseases. *Nat Genet*, 50:693–698. doi: 10.1038/s41588-018-0099-7

Wszedybyl-Winklewska, M., Wolf, J., Swierblewska, E., Kunicka, K., Mazur, K., Gruszecki, M., et al. (2017). Increased inspiratory resistance affects the dynamic relationship between blood pressure changes and subarachnoid space width oscillations. *PLoS One* 12:e0179503. doi: 10.1371/journal.pone.0179503

Xie, L., Kang, H., Xu, Q., Chen, M. J., Liao, Y., Thiyagarajan, M., et al. (2013). Sleep drives metabolite clearance from the adult brain. *Science* 342, 373–377. doi: 10.1126/science.1241224

Yaggi, H. K., Concato, J., Kernan, W. N., Lichtman, J. H., Brass, L. M., and Mohsenin, V. (2005). Obstructive sleep apnea as a risk factor for stroke and death. *N. Engl. J. Med.* 353, 2034–2041. doi: 10.1056/NEJMoa043104

Zhang, Y., Ren, R., Yang, L., Nie, Y., Zhang, H., Shi, Y., et al. (2023). Sleep in amyotrophic lateral sclerosis: a systematic review and meta-analysis of polysomnographic findings. *Sleep Med.* 107, 116–125. doi: 10.1016/j.sleep.2023.04.014

frontiers | Frontiers in Aging Neuroscience

TYPE Original Research
PUBLISHED 15 July 2024
DOI 10.3389/fnagi.2024.1421841

OPEN ACCESS

EDITED BY
Agnes Lumi Nishimura,
Queen Mary University of London,
United Kingdom

REVIEWED BY
Silvia Corrochano,
Health Research Institute of the Hospital Clínico San Carlos (IdISSC), Spain
Devesh Pant,
Emory University, United States

*CORRESPONDENCE
Xiaoxuan Liu
✉ lucyan_liu@bjmu.edu.cn
Dongsheng Fan
✉ dsfan2010@aliyun.com

RECEIVED 23 April 2024
ACCEPTED 02 July 2024
PUBLISHED 15 July 2024

CITATION
Zheng W, He J, Chen L, Yu W, Zhang N, Liu X and Fan D (2024) Genetic link between *KIF1A* mutations and amyotrophic lateral sclerosis: evidence from whole-exome sequencing.
Front. Aging Neurosci. 16:1421841.
doi: 10.3389/fnagi.2024.1421841

Genetic link between *KIF1A* mutations and amyotrophic lateral sclerosis: evidence from whole-exome sequencing

Wei Zheng[1,2,3], Ji He[1,2,3,4], Lu Chen[1,2,3], Weiyi Yu[1,2,3], Nan Zhang[1,2,3], Xiaoxuan Liu[1,2,3]* and Dongsheng Fan[1,2,3]*

[1]Department of Neurology, Peking University Third Hospital, Beijing, China, [2]Beijing Key Laboratory of Biomarker and Translational Research in Neurodegenerative Diseases, Beijing, China, [3]Key Laboratory for Neuroscience, National Health Commission/Ministry of Education, Peking University, Beijing, China, [4]Biomedical Pioneering Innovation Center (BIOPIC), Peking University, Beijing, China

Objectives: Genetics have been shown to have a substantial impact on amyotrophic lateral sclerosis (ALS). The ALS process involves defects in axonal transport and cytoskeletal dynamics. It has been identified that *KIF1A*, responsible for encoding a kinesin-3 motor protein that carries synaptic vesicles, is considered a genetic predisposing factor for ALS.

Methods: The analysis of whole-exome sequencing data from 1,068 patients was conducted to examine the genetic link between ALS and *KIF1A*. For patients with *KIF1A* gene mutations and a family history, we extended the analysis to their families and reanalyzed them using Sanger sequencing for cosegregation analysis.

Results: In our cohort, the *KIF1A* mutation frequency was 1.31% (14/1,068). Thirteen nonsynonymous variants were detected in 14 ALS patients. Consistent with the connection between *KIF1A* and ALS, the missense mutation p.A1083T (c.3247G>A) was shown to cosegregate with disease. The mutations related to ALS in our study were primarily located in the cargo-binding region at the C-terminal, as opposed to the mutations of motor domain at the N-terminal of *KIF1A* which were linked to hereditary peripheral neuropathy and spastic paraplegia. We observed high clinical heterogeneity in ALS patients with missense mutations in the *KIF1A* gene. *KIF5A* is a more frequent determinant of ALS in the European population, while *KIF1A* accounts for a similar proportion of ALS in both the European and Chinese populations.

Conclusion: Our investigation revealed that mutations in the C-terminus of *KIF1A* could increase the risk of ALS, support the pathogenic role of *KIF1A* in ALS and expand the phenotypic and genetic spectrum of *KIF1A*-related ALS.

KEYWORDS

amyotrophic lateral sclerosis, *KIF1A*, axonal transport, *KIF5A*, cosegregation analysis

Introduction

Amyotrophic lateral sclerosis (ALS) is a debilitating neurodegenerative disorder with an average life expectancy of merely 2–5 years following diagnosis (Brown and Al-Chalabi, 2017; Feldman et al., 2022). This disease presents itself as a degeneration of the limbs in spinal-onset ALS or challenges with speaking and/or swallowing in bulbar-onset ALS; gradual muscle weakness emerges, leading to death from respiratory failure in the end (Goutman et al., 2022b). The intricate pathophysiology of ALS remains incompletely understood. Genetics play a pivotal role in this phenomenon, and ALS can be hereditary, with familial ALS accounting for 15% of cases and the other 85% being classified as sporadic ALS (sALS) (Goutman et al., 2022a). At least 40 genes have been associated with ALS, providing significant insights into its pathophysiology (Chia et al., 2018; Brenner and Freischmidt, 2022). Nevertheless, the exact way in which ALS genes play a role in the development of ALS is yet to be determined.

Intracellular transport plays a vital role in maintaining the function, morphogenesis, and homeostasis of neurons. This is because neurons produce the majority of proteins necessary for axon and nerve terminal activities in the cell body, which then need to be transported to precise locations (Hirokawa et al., 2009). Numerous genetic, pathological, and neurobiological findings have established that axonal transport deficits act a significant role in the progression of ALS (Bilsland et al., 2010; Castellanos-Montiel et al., 2020). For example, numerous genes associated with ALS, including *DCTN1*, *KIF5A*, *ALS2*, *NEFH*, *PFN1*, and *SPAST*, participate in controlling cytoskeletal dynamics and function and regulate intracellular transport events (Liu et al., 2017; Nicolas et al., 2018; Castellanos-Montiel et al., 2020). In the process of ALS, the beginning phases entail the deterioration of extended axons in motor nerve cells, beginning at the farthest locations and advancing in a pattern known as "dying back" (Baldwin et al., 2016; Guo et al., 2017). Additionally, axonal transport deficits precede ALS symptoms; therefore, axonal transport could be an indicator of motor neuron degeneration (Fischer et al., 2004; Bilsland et al., 2010).

Kinesin superfamily proteins (KIFs) are a group of main molecular motors that responsible for transporting cargoes, including proteins, membranous organelles, and mRNAs, toward axon terminals along microtubules (Hirokawa et al., 2009). *KIF1A* encodes a molecular motor of the kinesin-3 variety, which is responsible for transporting synaptic vesicles, dense core vesicles, precursors of synaptic vesicles, and precursors of the active zone (Edwards et al., 2015; Guedes-Dias et al., 2019). Dense core vesicles mainly contain neurotransmitters and neuropeptides, while synaptic vesicle precursors and synaptic vesicles mainly transport VAMP2, RAB3A, and synaptophysin (Stucchi et al., 2018). *KIF1A* deficiency leads to remarkable impairments in motor and sensory functions, reduced density of synaptic vesicles at nerve terminals, and the buildup of transparent vesicles in neuronal cell bodies (Tanaka et al., 2016; Anazawa et al., 2022). To date, three *KIF1A*-associated disorders have been included in the OMIM classification: spastic paraplegia type 30 (SPG30, #610357), with recessive inheritance; and NESCAV syndrome (#614255), with dominant inheritance, and hereditary peripheral neuropathy, refer to hereditary sensory and autonomic neuropathy type 2 (HSAN2, #614213) (Nicita et al., 2021). Recently, *KIF1A* was recognized as a novel causative gene for ALS in the southern Chinese population (Liao et al., 2022). However, there is a lack of evidence indicating that *KIF1A* is a genetic risk factor for ALS. Therefore, we detected rare *KIF1A* variants in 1,068 ALS patients, comprising 988 sporadic and 80 familial cases, using whole-exome sequencing (WES), and analyzed the genotype–phenotype relationship in patients with *KIF1A* variants, deepening our understanding of how *KIF1A* deficiency affects ALS pathogenesis.

Materials and methods

Participants and data collection

A total of 1,068 Chinese ALS patients, 988 with sporadic ALS and 80 unrelated individuals with familial ALS, were enrolled at Peking University Third Hospital (PUTH) from 2007 to 2023. This cohort of ALS patients included 677 individuals, who underwent DNA extraction and exome sequencing in a previous study by our team (Liu et al., 2021). Patients diagnosed with probable or definite ALS based on the Airlie House diagnostic criteria were included in the study (Brooks et al., 2000). A total of 1,812 healthy controls, who had no previous neurological impairment, were also enrolled in the study. The exclusion criteria for both patients and controls was the unavailability of DNA sample. All patients and controls were of Han ethnicity. Baseline clinical data and demographic information, including age, sex, family history, smoking and drinking history, age at onset, location of initial symptoms, diagnostic delay, King's college staging system, and revised ALS functional rating scale scores, were collected during each patient's first visit to PUTH. The Edinburgh Cognitive and Behavioral Assessment Screen was used to assess patient cognition. Patients were followed up with by neurologists through in-person visits or by telephone every 3 months. The Institutional Ethics Committee of PUTH approved this study (IRB00006761), and all individuals involved gave their written informed consent.

DNA extraction

Samples of blood were collected from both patients and healthy volunteers. DNA was isolated from periphery venous blood. DNA extraction was performed using QIAmp DNA blood Mini Kit (QIAGEN, Hilden, Germany).

WES analysis

WES was used to screen all subjects, including both patients and healthy controls. Genomic DNA (1 μg) was fragmented into 200–300 base pair lengths using a Covaris Acoustic System. These DNA fragments underwent a series of processes including end repair, A-tailing, and adaptor ligation. Subsequently, a 4-cycle precapture polymerase chain reaction (PCR) amplification and a targeted sequence capture were performed. Postcapture, the DNA fragments were eluted and amplified through 15 cycles of PCR. The final sequencing products were read in 150 bp paired-end mode on the Illumina HiSeq X platform in accordance with the standard protocol. Using BWA 0.5.9,[1] pair-ended reads were mapped to the hg19/

1 http://bio-bwa.sourceforge.net/

TABLE 1 Demographic and clinical characteristics of ALS patients.

Variables	ALS	Control
Number of patients	1,068	1,812
Sex ratio (male/female)	1.6 (657/411)	1.0 (901/911)
Age at onset (years)	51.3 ± 11.2	–
Sporadic/familial	998/80	–

ALS, amyotrophic lateral sclerosis.

GRCh37 version of the human genome reference. To identify single nucleotide variants and small insertions and deletions (INDELs), Genome Analysis Toolkit (GATK) was employed[2] (McKenna et al., 2010). All suspected variants were validated by Sanger sequencing. Additional classical pathogenic ALS-related genes, including *SOD1*, *SETX*, *FUS*, *ALS2*, *OPTN*, *TARDBP*, *DCTN1*, *VAPB*, *Fig 4*, *TBK1*, *CHCHD10*, *ANXA11*, *NEK1*, and *SQSTM1* were examined by WES analysis. The length of *C9orf72* repeat alleles was evaluated using a two-step PCR method involving fluorescent fragment-length analysis followed by repeat-primed PCR, as described in previous studies (Tang et al., 2022).

Quality control (QC)

We conducted the QC procedures to filter out genetic variants through the following criteria: (1) genotype call rate under 99%; (2) Hardy–Weinberg equilibrium deviation in control groups ($p < 10E-6$); (3) significant missingness discrepancies between cases and controls ($p < 10E-6$); and (4) presence of three or more alleles. Variants that did not meet the quality control criteria were discarded.

Filtering of damaging mutations

KIF1A variants that met the following criteria were selected for further analysis: nonsynonymous, indel or putative splice site mutations; minor allele frequency (MAF) ≤ 0.1% for heterozygous variants; and MAF less than 1% in the Exome Aggregation Consortium (ExAC) and Genome Aggregation Database (gnomAD) databases. The pathogenicity of the identified variants was evaluated following American College of Medical Genetics and Genomics (ACMG) guidelines. To evaluate the potential functional outcomes of each variant, we employed eight bioinformatic tools designed to predict the potential effects of a substitution in the amino acid on the structure and established function of a human protein: MutationTaster,[3] SIFT,[4] PolyPhen-2,[5] MetaLR, MetaSVM, ClinPred,[6] M_CAP,[7] and CADD.[8]

Sanger sequencing

PCR was conducted in a total volume of 25 μL, comprised of genomic DNA, primers, and 2 × Taq PCR Master Mix (Tsingke Biotechnology Co., Ltd., Beijing, China). The PCR reaction parameters were the following: pre-heating at 94°C for 5 min, denaturing at 94°C for 30 s, annealing at 55°C for 30 s, extending at 72°C for 30 s, with a total of 35 cycles, ending with a final extension at 72°C for 5 min, followed by cooling to 4°C. Subsequently, the PCR samples underwent sequencing utilizing the Sanger Chain Termination technique.

Cosegregation analysis for families

Genomic DNA extracted from blood samples from patient families underwent genomic analysis. PCR was employed to screen all individuals for *KIF1A* sequences, encompassing the same region examined in the proband. To facilitate the amplification process, forward (CAGGGCCTCACTTGAACTGG) and reverse primers (AAGAGCTTCGCATCGTGGAG) were used. Using the CodonCode Aligner software, the DNA sequences obtained from the samples were compared and matched with the UCSC hg19 reference human genome.

Statistical analysis

Descriptive statistics (means ± SDs) were calculated for continuous variables. Statistical analysis was conducted using GraphPad Prism version 8.4.0.

Results

Mutation analysis of the *KIF1A* gene

We analyzed the *KIF1A* sequence in a group of 1,068 ALS patients. The demographic and clinical features of the ALS patients are presented in Table 1. Thirteen nonsynonymous variants were detected in 14 ALS patients, all of which were heterozygous. In our cohort, the *KIF1A* mutation frequency was 1.31% (14/1,068). Among the 13 variants, 12 had missense variations, while one had a delete-insert mutation. Except for the variant p.A918deinsGA (c.2753_2754insGGA, P2), the other 12 variants had a <0.1% allele frequency in the gnomAD and ExAC databases (Table 2). Additionally, p.P424 L (c.1271C>T, P1) and p.P1178S (c.3533 T>C, P6) were not reported in any of the databases. The functional predictions revealed that 11 missense variants were predicted pathogenic at least one silico tool based on eight silico tools totally (Table 2). Four variants [p.E979K (c.2935G>A, P3), p.V1255M (c.3763G>A, P8), p.D1711N (c.5131G>A, P13), and p.R1717L (c.5150G>T, P14)] were predicted pathogenic through 5–6 silico tools. Four variants were identified as likely pathogenic (LP) according to the ACMG standards and guidelines (Table 2): p.V1255M (c.3763G>A, P8), p.P1593L (c.4778C>T, P10), p.D1643N (c.4927G>A, P11), and p.R1717L (c.5150G>T, P14). The ACMG evidence for the pathogenicity of these variants was strong, and they were predicted to be damaging by bioinformatic tools. Among them, p.D1643N (c.4927G>A, P11) and p.R1717L (c.5150G>T, P14) were reported previously in Human Gene Mutation Database (HGMD) (Table 2).

2 http://www.broadinstitute.org/gatk
3 http://www.mutationtaster.org
4 http://sift.jcvi.org/
5 http://genetics.bwh.harvard.edu/pph2/
6 https://sites.google.com/site/clinpred/
7 http://bejerano.stanford.edu/mcap/
8 https://cadd.gs.washington.edu

TABLE 2 Overview of variants in the *KIF1A* gene identified in ALS patients.

ID	Position (hg19)	Refseq ID	cDNA change	Protein change	dbSNP	Minor allele frequencies		Functional predictions									ACMG	
						gnomAD_genome_ALL	gnomAD_exome_ALL	SIFT	Polyphen2	Mutation Taster	MetaSVM	MetaLR	ClinPred	M_CAP	CADD	Pathogenic (total)	Evidence	Classification
P1	chr2:241710533	NM_001330290	c.1271C>T	p.Pro424Leu	rs1254343314	–	–	–	–	–	–	–	–	–	–	–	PM2	VUS
P2	chr2:241696840	NM_001244008	c.2753_2754insGGA	p.Asp918delinsGluAsp	rs758125020	1.68E-02	1.74E-02	–	–	–	–	–	–	–	–	–	PM2, PM4	VUS
P3	chr2:241689888	NM_001244008	c.2935G>A	p.Glu979Lys	rs764324827	–	4.00E-06	T	P	D	T	D	D	D	35	6 (8)	PM2, BP4	VUS
P4	chr2:241685282	NM_001244008	c.3247G>A	p.Ala1083Thr	rs201793635	4.00E-04	3E-06	T	B	P	T	T	T	D	5.97	1 (8)	BP4	VUS
P5	chr2:241685282	NM_001244008	c.3247G>A	p.Ala1083Thr	rs201793635	4.00E-04	3.00E-04	T	B	P	T	T	T	D	5.97	1 (8)	BP4	VUS
P6	chr2:241683410	NM_001244008	c.3533 T>C	p.Phe1178Ser	-	–	–	D	D	D	–	–	–	–	25.6	3 (3)	PM2, PM1, PP3	VUS
P7	chr2:241680755	NM_001244008	c.3680C>T	p.Pro1227Leu	rs374244985	2.00E-04	2.00E-04	T	B	D	T	T	T	D	21.2	3 (8)	PM1, BP4	VUS
P8	chr2:241679768	NM_001244008	c.3763G>A	p.Val1255Met	rs752703226	–	1.20E-05	D	D	D	T	T	D	D	24.2	6 (8)	PM2, PM1, PP2, PP3	LP
P9	chr2:241661285	NM_001244008	c.4682C>T	p.Thr1561Met	rs769101887	–	4.00E-06	T	B	D	T	T	T	D	19.77	3 (8)	PM2, PM1, BP4	VUS
P10	chr2:241660421	NM_001244008	c.4778C>T	p.Pro1593Leu	rs200902828	3.00E-04	5.00E-04	D	B	D	T	T	T	D	23.6	4 (8)	PM2, PM1, PP2, PP3	LP
P11	chr2:241659285	NM_001244008	c.4927G>A	p.Asp1643Asn	rs200141437	1.00E-04	3.00E-04	T	B	D	T	T	T	T	18.6	2 (8)	PM2, PS4, PM1, PP2, BP4	LP
P12	chr2:241659257	NM_001244008	c.4955G>A	p.Arg1652Gln	rs376658420	9.70E-05	2.00E-04	T	B	P	T	T	T’	T	6.526	0 (8)	PM2, PM1, BP4	VUS
P13	chr2:241658506	NM_001244008	c.5131G>A	p.Asp1711Asn	rs199574770	3.20E-05	5.70E-05	D	D	D	T	T	T	D	34	5 (8)	PM1, PP3	VUS
P14	chr2:241658487	NM_001244008	c.5150G>T	p.Arg1717Leu	rs760970824	5.00E-05	2.40E-05	D	D	D	T	T	D	D	35	6 (8)	PM2, PM1, PP2, PP3	LP

ALS, amyotrophic lateral sclerosis; SNP, Single-nucleotide polymorphism; ACMG, American College of Medical Genetics and Genomics; VUS, uncertain significance; LP, likely pathogenic; HGMD, Human Gene Mutation Database; SIFT, sorting intolerant from tolerant; PolyPhen2, polymorphism phenotyping version 2; SVM, support vector machine; CADD, combined annotation dependent depletion; M_CAP, Mendelian clinically applicable pathogenicity; SIFT (D: Damaging; T: Tolerable); Polyphen2 (D: Probably_Damaging; P: Possibly_Damaging; B:Benign); Mutation Taster (D: Disease_causing; P: Polymorphism); MetaSVM (T: Tolerable); MetaLR (D: Damaging; T: Tolerable); ClinPred (D: Deleterious; T: Tolerable); M_CAP (D: Damaging; T: Tolerable); CADD: (D: Damaging; T: Tolerable).

10.3389/fnagi.2024.1421841

Additionally, other nine variants were uncertain significance (VUS) according to the ACMG standards. In total, 11 variants were recognized novel variants in ALS patients. The detailed variant information is listed in Table 2.

In addition, 14 ALS patients with *KIF1A* mutation did not cover other ALS-related genes, including *SOD1*, *SETX*, *FUS*, *ALS2*, *OPTN*, *TARDBP*, *DCTN1*, *VAPB*, *Fig 4*, *TBK1*, *CHCHD10*, *ANXA11*, *NEK1*, *SQSTM1*, and *C9orf72*, which were classical pathogenic genes in ALS, by WES analysis. And no additional potential candidates were identified among these 14 ALS patients. In total, different nonsynonymous variants that fulfilled the same screening criteria were detected in 10 healthy controls. Ten variants (1798: p.I119T, c.356 T>C; 443: p.R355H, c.1064G>A; 1,410: p.R422C, c.1264C>T; 1,380: p.T810M, c.2429G>A; 1,158: p.D918delinsED, c.2753_2754insGGA; 568: p.E1025K, c.3073G>A; 277: p.A1083T, c.3247G>A; 1,677: p.P1227L, c.3680C>T; 1,082: p.R1296C, c.3886C>T and 1,612: p.P1688L, c.5063C>T) were detected in 1,812 healthy controls. Among them, three variants (P2: p.A918delinsED, c.2753_2754insGGA; P4, P5: p.A1083T, c.3247G>A and P7: p.P1227L, c.3680C>T), detected in ALS patients, were also found in controls. The details of these variants in *KIF1A* gene detected in controls are listed in Supplementary Table 2. In our healthy controls, the frequency of *KIF1A* variants was 0.55%. Besides, we screened the other two databases to figure out the actual frequency in Chinese population. We found the frequency was 0.49% in "gnomAD v2" database (East Asian) and 0.61% in "HUA BIAO" database, which were similar to the result in our control cohort (Supplementary Table 3).

Regions of variants associated with ALS in the *KIF1A* gene

KIF1A has been recognized as a causal gene in HSAN2, SPG30, and NESCAV syndrome. Given the overlap of clinical symptoms between these three diseases and ALS, we conducted a thorough examination of ALS patients with variations in *KIF1A* to ensure that they were not misdiagnosed. Unreported variations were detected in our patient cohort with SPG30, HSAN2, and NESCAV syndrome. To explore the correlation between *KIF1A* gene mutation and their manifestations, we examined the rare ALS-related mutations found in our research and compared them to ClinVar pathogenic variants linked to other conditions (SPG30, HSAN2, and NESCAV syndrome) (Figure 1). Specifically, mutations linked to SPG and HSAN2 were mainly found at motor domain of N-terminal of *KIF1A*, whereas those associated with ALS in our investigation and a previous investigation were primarily situated in the cargo-binding region at the C-terminal (Liao et al., 2022). Interestingly, five variants [three in our cohort and two in another ALS cohort (Liao et al., 2022)] were located in the phosphatidylinositol-binding pleckstrin homology (PH) domain.

Genotype–phenotype correlation in patients with *KIF1A* variants

Of the 14 ALS patients with *KIF1A* mutations, two had a familial background of ALS, other 12 were sALS. The mean age of onset was 47.7 ± 12.9 years, with an age range of 23–64 years. The male-to-female ratio was 9:5. Among 14 patients, 11 were spinal-onset, while three were bulbar-onset. The mean delay in diagnosis was 35.8 ± 35.9 months. Interestingly, two patients had FTD symptoms (P3, p.E979K, c.2935G>A; and P6, p.F1178S, c.3533 T>C). Additionally, patient P6, a female, presented with repeated falls, slurred speech, and behavioral and personality changes. A neurological examination revealed that she had a masked face and a positive pull-back test result, demonstrating extrapyramidal manifestations. Interestingly, patient P10 (p.P1593L, c.4778C>T) presented with right lower limb tremor, abnormal walking gait, and progressive limb weakness. P12 walked unsteadily, had unclear articulation, and had limb weakness. Physical examination revealed increased involuntary limb movements and abnormal gait and posture. These three patients all presented extrapyramidal manifestations. Table 3 outlines the specific clinical characteristics of individuals with ALS who possess mutations in the *KIF1A* gene.

Cosegregation analysis of families

Next, we further corroborated the connection between missense mutations in the *KIF1A* gene and ALS through segregation analysis. Two patients (P2 and P5) had a family history. We extended the analysis to their families and reanalyzed them using Sanger sequencing (Figure 2). P2 presented with lower-limb onset and late disease onset. As shown in Supplementary Table 4, in the P2 family, the patient's father (I:1) and older brother (II:4) presented with lower-limb onset, and upper and lower limbs muscle atrophy and weakness, similar to P2's symptoms, and were diagnosed with ALS. Both his father and older brother had an earlier onset age, and more longer survival time than him, showing a slower progression. Detailed clinical features of ALS patients in families of P2 were shown in Supplementary Table 4. Unfortunately, the father, brother, and sisters of the proband had all passed away prior to the study, resulting in a lack of available DNA samples for cosegregation analysis.

Patient 2 also had two older sisters (II:1 and II:2; Figure 2A) who did not exhibit any ALS symptoms during their lifetime. However, unfortunately, his father, brother, and sisters had all died before the time of the study; thus, no DNA samples were available for cosegregation. The other patient (P5 and III:4; Figure 2B) with a family history had an early disease onset (46 years) and a long diagnostic delay (77 months). Four of P5's relatives were diagnosed with ALS or self-reported symptoms consistent with ALS (father (II:1), grandfather (I:1), uncle (II:4), and older sister (III:2); Figure 2B). P5's father and older sister had symptoms similar to hers. Her grandfather and uncle had muscle atrophy and weakness before they died. The *KIF1A* variant identified from P5 was assessed in her older sister, younger brother, and husband. Interestingly, her older sister carried the same *KIF1A* variant, while her younger brother did not. It could not be determined whether her father carried the loss-of-function mutation. Besides ALS, we did not find "other related" disorders running in the families of 14 ALS patients carried *KIF1A* mutation, such as frontotemporal dementia, cervical spondylosis, syringomyelia, peripheral neuropathy, Parkinson's disease, and Alzheimer's disease.

Discussion

Thirteen variants of the *KIF1A* gene were detected in 14 of 1,068 ALS patients, resulting in a frequency of 1.31% (14/1,068) in

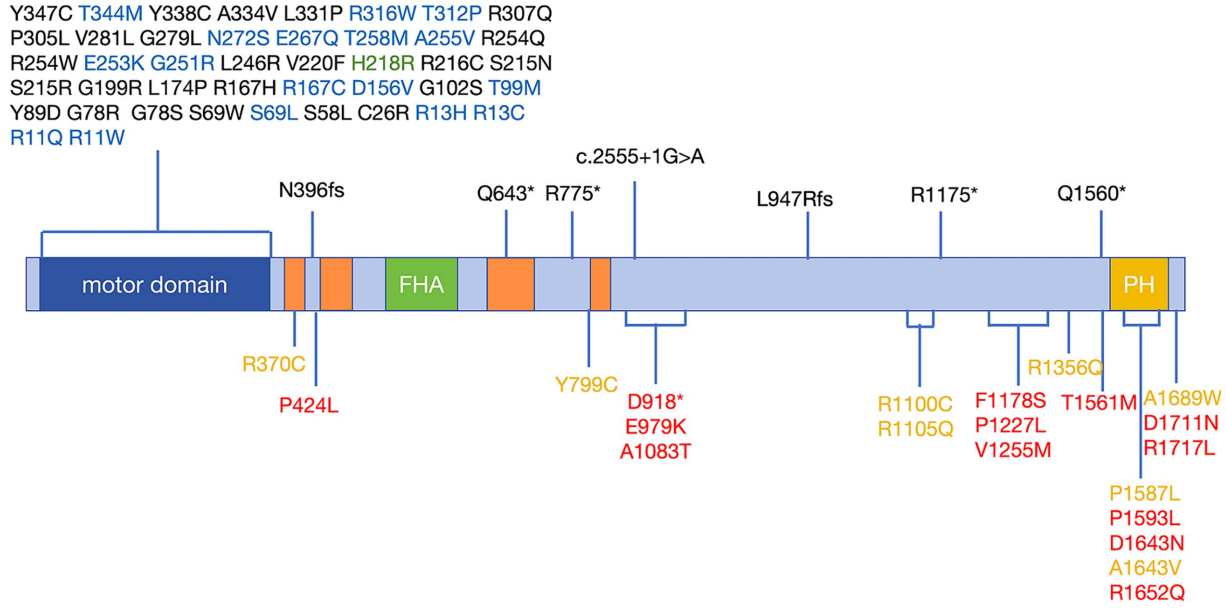

FIGURE 1
Schematic distribution of mutations in the *KIF1A* gene in KANDs. Previously reported variants associated with SPG30 and HSAN2 are listed above the schematic and are associated with SPG30 (including cases described as NESCAV syndrome) (black), HSAN2 (green), and multiple phenotypes (SPG30 and HSAN2) (blue). Variants associated with ALS are listed below the schematic and were identified in our cohort (red) and another ALS cohort (yellow). Motor domain (amino acids 5–354); CC: coiled-coil domain, CC1 (amino acids 366–383); CC2 (amino acids 429–462); CC3 (amino acids 622–681); CC4 (amino acids 801–822); FHA: Forkhead-associated domain, amino acids 516–572; and PH: pleckstrin homology domain, amino acids 1,575–1,673. Protein domains were determined according to UniProt (https://www.uniprot.org). Variants were annotated with reference to the canonical transcript NM_001244008 (p.P424L was identified in only the NM_001330290 transcript). ALS, amyotrophic lateral sclerosis; KANDs, *KIF1A*-associated neurological disorders; HSAN2, hereditary sensory and autonomic neuropathy type 2; SPG30, spastic paraplegia type 30.

KIF1A. This frequency aligns with the mutation frequency observed in a research conducted in southern China (Liao et al., 2022), which revealed a frequency of 1.06% (10/941). Our study represents the largest cohort of ALS patients with mutations in the *KIF1A* gene to date. Our research revealed 11 novel mutation variants in the *KIF1A* gene linked to ALS. Four different mutations [p.E979K (c.2935G>A, P3), p.V1255M (c.3763G>A, P8), p.D1711N (c.5131G>A, P13), and p.R1717L (c.5150G>T, P14)] were identified as potentially harmful by a combination of 5–6 computational tools. Additionally, four of 14 mutations [p.V1255M (c.3763G>A, P8), p.P1593L (c.4778C>T, P10), p.D1643N (c.4927G>A, P11), and p.R1717L (c.5150G>T, P14)] were identified to be pathogenic according to the ACMG recommendations and software prediction results, highlighting the significance of the *KIF1A* gene as a potential genetic determinant of ALS. Additionally, we did not find 10 controls who were detected *KIF1A* mutations have any obvious neurological impairment. In Chinese population, the frequencies was 0.49–0.61% based on our healthy controls (1,812 controls) and other database (11,708 controls). Consistent with the connection between *KIF1A* and ALS, the missense mutation p.A1083T (c.3247G>A) was shown to cosegregate with the disease. Although lack of available DNA samples for cosegregation analysis, we found three patients in families of P2 all presented with lower-limb onset and late disease onset, via reviewing their medical records to gather additional clinical history and neurological examination data.

This study revealed high clinical heterogeneity among ALS individuals harboring *KIF1A* gene missense mutations. Disease onset age spanned from 23 to 64 years, while the diagnostic delay varied from 5 to 99 months. The research demonstrated significant clinical diversity. Interestingly, several genotype–phenotype correlations were noted. Among the 13 ALS patients harboring the *KIF1A* gene, three had onset in the bulbar region, eight had onset in the upper limbs, and only two had onset in the lower limbs. Additionally, extrapyramidal symptoms were observed in three of these ALS patients, suggesting that upper limb onset and extrapyramidal manifestations may be characteristic of the ALS phenotype caused by the *KIF1A* gene; however, additional evidence is required. Unlike the patient cohort in a prior study conducted in China (Liao et al., 2022), our cohort of ALS patients harboring *KIF1A* missense mutations did not exhibit obvious sensory impairment, highlighting the high clinical heterogeneity of ALS patients harboring *KIF1A* variants.

KIF1A and *KIF5A* are KIFs that function as molecular motors, utilizing chemical energy from ATPs to transport cargo along microtubules. Studies have indicated that the mutation frequency of *KIF5A* in the Chinese sALS population ranges from 0.16% (1/645) (Zhang et al., 2019) to 0.41% (2/581) (Gu et al., 2019; He et al., 2020). In the Western population, the mutation frequency of *KIF5A* is reported to be 0.47–0.53% (Brenner et al., 2018; Nicolas et al., 2018), which is greater than that in the Chinese population. Another study of the Norwegian population revealed that *KIF1A* risk variants were present in 1.08% (3/279) of ALS patients, consistent with the findings in the Chinese population (Olsen et al., 2024). These results demonstrate that *KIF1A* is a more prevalent ALS-associated gene than *KIF5A* in the Chinese population. *KIF5A* is a more frequent determinant of ALS in the European population, while *KIF1A* accounts for a similar proportion of ALS patients in European and Chinese populations.

TABLE 3 Clinical features of ALS patients with mutations in *KIF1A* gene.

ID	Sex	Age at onset (years)	Site of onset	Weakness	Atrophy	Dysarthria	Dysphagia	Sensory	Reflexes	FTD symptoms	Diagnosis of delay (months)	KCSS	Survival time (months)	Family history
P1	Male	34	LL	LL	UL, LL	–	–	–	Hyper	–	12	Stage 1	135	–
P2	Male	64	LL	UL, LL	UL, LL	–	–	–	Hyper	–	9	Stage 2	85	+
P3	Male	39	G	G, UL, LL	UL	+	+	–	Hyper	+	12	Stage 3	35	–
P4	Male	23	LL	UL, LL	LL	+	–	–	Hyper	–	7	Stage 2	141	–
P5	Female	46	LL	LL	No	–	–	–	Hyper	–	77	Stage 2	>96	+
P6	Female	60	LL	LL	LL	–	–	–	Hyper	+	77	Stage 2	92	–
P7	Female	55	LL	LL	LL	–	–	–	Hyper	–	24	Stage 3	72	–
P8	Female	50	LL	UL, LL	UL, LL	–	–	–	Hypo	–	71	Stage 3	190	–
P9	Male	67	LL	UL, LL	LL	–	–	–	Hyper	–	5	Stage 1	9	–
P10	Female	51	UL	UL, LL	UL	–	–	–	Hypo	–	82	Stage 2	175	–
P11	Male	28	UL	UL, LL	UL	–	–	–	Hyper	–	12	Stage 2	32	–
P12	Male	48	G	G, UL, LL	UL, LL	+	+	–	Hypo	–	7	Stage 1	43	–
P13	Male	50	LL	LL	LL	–	–	–	Hyper	–	99	Stage 1	65	–
P14	Male	53	G	G	G	+	+	–	Hyper	–	7	Stage 1	81	–

ALS, amyotrophic lateral sclerosis; LL, lower limbs; UL, upper limbs; G, global; Hyper, hyperreflexia; Hypo, hyporeflexia; FTD, frontotemporal dementia; KCSS, King's college staging system; "+", affected; "–", normal.

10.3389/fnagi.2024.1421841

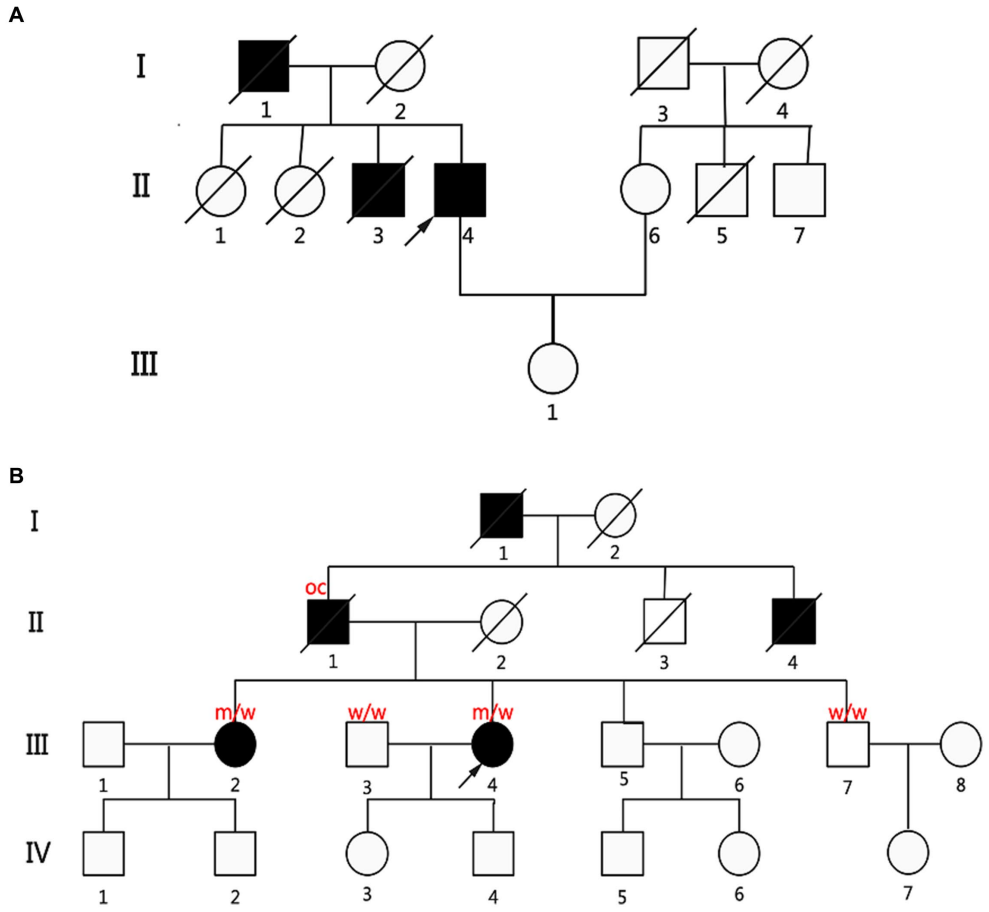

FIGURE 2
Pedigrees of two fALS patients carried the *KIF1A* missense variants. **(A)** Pedigree diagram of P2, p.A918delinsGA (c.2753_2754insGGA). **(B)** Genealogy diagram of P5, p.A1083T (c.3247G>A). Genetic analysis showing cosegregation of the *KIF1A* missense variants. Obligate carriers of the respective variant are abbreviated as "oc." m = mutant allele; w = wild-type allele; arrow: proband; filled symbol: affected; empty symbol: unaffected; slashed symbol, decreased; square: man; circle: woman.

There is genetic overlap among SPG, HSAN2, and ALS. For example, SPG11 and *KIF5A* have been found to be pathogenic in both ALS and SPG (Stevanin et al., 2007; Orlacchio et al., 2010; Nicolas et al., 2018), and *SPTLC1* has been recognized as a novel risk gene factor in ALS and HSAN2 (Lone et al., 2022). Our latest discoveries and prior investigations indicate that *KIF1A* might potentially serve as a shared causative gene linked to SPG, HSAN2, and ALS. Based on this, we posit that SPG, HSAN2, and ALS may represent a range of characteristics linked to variations in the *KIF1A* gene. Similar to findings associated with *KIF5A*, we have identified varying mutation distributions in *KIF1A* across different diseases. Specifically, in HSP/Charcot-Marie-Tooth 2 patients, the majority of *KIF5A* mutations are situated in the motor domain, whereas ALS patients tend to have mutations in the C-terminal cargo-binding domain. Mutations in *KIF1A* linked to SPG and HSAN2 mainly occurred in the motor domain at the N-terminal, while alterations associated with ALS, as indicated by our study and corroborated by prior research, were mainly found in the cargo-binding region at the C-terminal (Liao et al., 2022). It could be speculated that *KIF1A* and *KIF5A* mutations tend to lead to the ALS phenotype when the C-terminal cargo-binding region is influenced and hereditary peripheral neuropathy and the HSP phenotype when the N-terminal motor domain is influenced. The clinical manifestations of *KIF1A*-related neuropathy disorders vary widely, with *KIF1A* being the common cause. As a result, these conditions are classified as "*KIF1A*-associated neurological disorders (KAND)" (Boyle et al., 2021). Differences in gene function may cause the diversity of clinical phenotypes.

Conclusion

In conclusion, we demonstrated that pathogenic *KIF1A* variants were associated with ALS and analyzed the genotype–phenotype correlation of patients with *KIF1A* variants. Our finding widened the genotypic spectrum of *KIF1A* and supplement prior findings of *KIF1A*-related ALS.

Data availability statement

The datasets presented in this study can be found in the article/Supplementary material.

Ethics statement

The studies involving humans were approved by the Institutional Ethics Committee of PUTH, IRB00006761. The studies were conducted in accordance with the local legislation and institutional requirements. The participants provided their written informed consent to participate in this study.

Author contributions

WZ: Conceptualization, Methodology, Writing – original draft. JH: Writing – review & editing. LC: Investigation, Writing – review & editing. WY: Resources, Writing – review & editing. NZ: Validation, Writing – review & editing. XL: Funding acquisition, Project administration, Supervision, Writing – review & editing. DF: Funding acquisition, Project administration, Supervision, Writing – review & editing.

Funding

The author(s) declare that financial support was received for the research, authorship, and/or publication of this article. WZ was funded by Beijing Natural Science Foundation (7244428), Peking University Medicine Sailing Program for Young Scholars' Scientific and Technological Innovation (BMU2023YFJHPY034). DF was funded by the National Natural Science Foundation of China (81873784 and 82071426), Clinical Cohort Construction Program of Peking University Third Hospital (BYSYDL2019002). XL was supported by Beijing Natural Science Foundation (7242170), Clinical Cohort Construction Program of Peking University Third Hospital (BYSYDL2021007, BYSYZD2022009).

Acknowledgments

We wish to thank all the participants and authors for their contribution to this research.

Conflict of interest

The authors declare that the research was conducted in the absence of any commercial or financial relationships that could be construed as a potential conflict of interest.

Publisher's note

All claims expressed in this article are solely those of the authors and do not necessarily represent those of their affiliated organizations, or those of the publisher, the editors and the reviewers. Any product that may be evaluated in this article, or claim that may be made by its manufacturer, is not guaranteed or endorsed by the publisher.

Supplementary material

The Supplementary material for this article can be found online at: https://www.frontiersin.org/articles/10.3389/fnagi.2024.1421841/full#supplementary-material

References

Anazawa, Y., Kita, T., Iguchi, R., Hayashi, K., and Niwa, S. (2022). De novo mutations in KIF1A-associated neuronal disorder (KAND) dominant-negatively inhibit motor activity and axonal transport of synaptic vesicle precursors. *Proc. Natl. Acad. Sci. U. S. A.* 119:e2113795119. doi: 10.1073/pnas.2113795119

Baldwin, K. R., Godena, V. K., Hewitt, V. L., and Whitworth, A. J. (2016). Axonal transport defects are a common phenotype in Drosophila models of ALS. *Hum. Mol. Genet.* 25, 2378–2392. doi: 10.1093/hmg/ddw105

Bilsland, L. G., Sahai, E., Kelly, G., Golding, M., Greensmith, L., and Schiavo, G. (2010). Deficits in axonal transport precede ALS symptoms in vivo. *Proc. Natl. Acad. Sci. U. S. A.* 107, 20523–20528. doi: 10.1073/pnas.1006869107

Boyle, L., Rao, L., Kaur, S., Fan, X., Mebane, C., Hamm, L., et al. (2021). Genotype and defects in microtubule-based motility correlate with clinical severity in KIF1A-associated neurological disorder. *HGG Adv.* 2:100026. doi: 10.1016/j.xhgg.2021.100026

Brenner, D., and Freischmidt, A. (2022). Update on genetics of amyotrophic lateral sclerosis. *Curr. Opin. Neurol.* 35, 672–677. doi: 10.1097/WCO.0000000000001093

Brenner, D., Yilmaz, R., Muller, K., Grehl, T., Petri, S., Meyer, T., et al. (2018). Hot-spot KIF5A mutations cause familial ALS. *Brain* 141, 688–697. doi: 10.1093/brain/awx370

Brooks, B. R., Miller, R. G., Swash, M., and Munsat, T. L.World Federation of Neurology Research Group on Motor Neuron Diseases (2000). El Escorial revisited: revised criteria for the diagnosis of amyotrophic lateral sclerosis. *Amyotroph. Lateral Scler. Other Motor Neuron Disord.* 1, 293–299. doi: 10.1080/146608200300079536

Brown, R. H., and Al-Chalabi, A. (2017). Amyotrophic lateral sclerosis. *N. Engl. J. Med.* 377, 162–172. doi: 10.1056/NEJMra1603471

Castellanos-Montiel, M. J., Chaineau, M., and Durcan, T. M. (2020). The neglected genes of ALS: cytoskeletal dynamics impact synaptic degeneration in ALS. *Front. Cell. Neurosci.* 14:594975. doi: 10.3389/fncel.2020.594975

Chia, R., Chio, A., and Traynor, B. J. (2018). Novel genes associated with amyotrophic lateral sclerosis: diagnostic and clinical implications. *Lancet Neurol.* 17, 94–102. doi: 10.1016/S1474-4422(17)30401-5

Edwards, S. L., Yorks, R. M., Morrison, L. M., Hoover, C. M., and Miller, K. G. (2015). Synapse-assembly proteins maintain synaptic vesicle cluster stability and regulate synaptic vesicle transport in *Caenorhabditis elegans*. *Genetics* 201, 91–116. doi: 10.1534/genetics.115.177337

Feldman, E. L., Goutman, S. A., Petri, S., Mazzini, L., Savelieff, M. G., Shaw, P. J., et al. (2022). Amyotrophic lateral sclerosis. *Lancet* 400, 1363–1380. doi: 10.1016/S0140-6736(22)01272-7

Fischer, L. R., Culver, D. G., Tennant, P., Davis, A. A., Wang, M., Castellano-Sanchez, A., et al. (2004). Amyotrophic lateral sclerosis is a distal axonopathy: evidence in mice and man. *Exp. Neurol.* 185, 232–240. doi: 10.1016/j.expneurol.2003.10.004

Goutman, S. A., Hardiman, O., Al-Chalabi, A., Chio, A., Savelieff, M. G., Kiernan, M. C., et al. (2022a). Emerging insights into the complex genetics and pathophysiology of amyotrophic lateral sclerosis. *Lancet Neurol.* 21, 465–479. doi: 10.1016/S1474-4422(21)00414-2

Goutman, S. A., Hardiman, O., Al-Chalabi, A., Chio, A., Savelieff, M. G., Kiernan, M. C., et al. (2022b). Recent advances in the diagnosis and prognosis of amyotrophic lateral sclerosis. *Lancet Neurol.* 21, 480–493. doi: 10.1016/S1474-4422(21)00465-8

Gu, X., Li, C., Chen, Y., Wei, Q., Cao, B., Ou, R., et al. (2019). Mutation screening of the KIF5A gene in Chinese patients with amyotrophic lateral sclerosis. *J. Neurol. Neurosurg. Psychiatry* 90, 245–246. doi: 10.1136/jnnp-2018-318395

Guedes-Dias, P., Nirschl, J. J., Abreu, N., Tokito, M. K., Janke, C., Magiera, M. M., et al. (2019). Kinesin-3 responds to local microtubule dynamics to target synaptic cargo delivery to the presynapse. *Curr. Biol.* 29:e268, 268–282.e8. doi: 10.1016/j.cub.2018.11.065

Guo, W., Naujock, M., Fumagalli, L., Vandoorne, T., Baatsen, P., Boon, R., et al. (2017). HDAC6 inhibition reverses axonal transport defects in motor neurons derived from FUS-ALS patients. *Nat. Commun.* 8:861. doi: 10.1038/s41467-017-00911-y

He, J., Liu, X., Tang, L., Zhao, C., He, J., and Fan, D. (2020). Whole-exome sequencing identified novel KIF5A mutations in Chinese patients with amyotrophic lateral sclerosis

and Charcot-Marie-Tooth type 2. *J. Neurol. Neurosurg. Psychiatry* 91, 326–328. doi: 10.1136/jnnp-2019-320483

Hirokawa, N., Noda, Y., Tanaka, Y., and Niwa, S. (2009). Kinesin superfamily motor proteins and intracellular transport. *Nat. Rev. Mol. Cell Biol.* 10, 682–696. doi: 10.1038/nrm2774

Liao, P., Yuan, Y., Liu, Z., Hou, X., Li, W., Wen, J., et al. (2022). Association of variants in the KIF1A gene with amyotrophic lateral sclerosis. *Transl. Neurodegener.* 11:46. doi: 10.1186/s40035-022-00320-2

Liu, X., He, J., Chen, L., Zhang, N., Tang, L., Liu, X., et al. (2021). TBK1 variants in Chinese patients with amyotrophic lateral sclerosis. *Neurobiol. Aging* 97, 149.e9–149.e15. doi: 10.1016/j.neurobiolaging.2020.07.028

Liu, X., Yang, L., Tang, L., Chen, L., Liu, X., and Fan, D. (2017). DCTN1 gene analysis in Chinese patients with sporadic amyotrophic lateral sclerosis. *PLoS One* 12:e0182572. doi: 10.1371/journal.pone.0182572

Lone, M. A., Aaltonen, M. J., Zidell, A., Pedro, H. F., Morales Saute, J. A., Mathew, S., et al. (2022). SPTLC1 variants associated with ALS produce distinct sphingolipid signatures through impaired interaction with ORMDL proteins. *J. Clin. Invest.* 132:e161908. doi: 10.1172/JCI161908

Mckenna, A., Hanna, M., Banks, E., Sivachenko, A., Cibulskis, K., Kernytsky, A., et al. (2010). The genome analysis toolkit: a MapReduce framework for analyzing next-generation DNA sequencing data. *Genome Res.* 20, 1297–1303. doi: 10.1101/gr.107524.110

Nicita, F., Ginevrino, M., Travaglini, L., D'arrigo, S., Zorzi, G., Borgatti, R., et al. (2021). Heterozygous KIF1A variants underlie a wide spectrum of neurodevelopmental and neurodegenerative disorders. *J. Med. Genet.* 58, 475–483. doi: 10.1136/jmedgenet-2020-107007

Nicolas, A., Kenna, K. P., Renton, A. E., Ticozzi, N., Faghri, F., Chia, R., et al. (2018). Genome-wide analyses identify KIF5A as a novel ALS gene. *Neuron* 97:e1266. doi: 10.1016/j.neuron.2018.02.027

Olsen, C. G., Busk, O. L., Holla, O. L., Tveten, K., Holmoy, T., Tysnes, O. B., et al. (2024). Genetic overlap between ALS and other neurodegenerative or neuromuscular disorders. *Amyotroph. Lateral Scler. Frontotemporal. Degener.* 25, 177–187. doi: 10.1080/21678421.2023.2270705

Orlacchio, A., Babalini, C., Borreca, A., Patrono, C., Massa, R., Basaran, S., et al. (2010). SPATACSIN mutations cause autosomal recessive juvenile amyotrophic lateral sclerosis. *Brain* 133, 591–598. doi: 10.1093/brain/awp325

Stevanin, G., Santorelli, F. M., Azzedine, H., Coutinho, P., Chomilier, J., Denora, P. S., et al. (2007). Mutations in SPG11, encoding spatacsin, are a major cause of spastic paraplegia with thin corpus callosum. *Nat. Genet.* 39, 366–372. doi: 10.1038/ng1980

Stucchi, R., Plucińska, G., Hummel, J. J. A., Zahavi, E. E., Guerra San Juan, I., Klykov, O., et al. (2018). Regulation of KIF1A-driven dense core vesicle transport: ca(2+)/CaM controls DCV binding and Liprin-alpha/TANC2 recruits DCVs to postsynaptic sites. *Cell Rep.* 24, 685–700. doi: 10.1016/j.celrep.2018.06.071

Tanaka, Y., Niwa, S., Dong, M., Farkhondeh, A., Wang, L., Zhou, R., et al. (2016). The molecular motor KIF1A transports the TrkA neurotrophin receptor and is essential for sensory neuron survival and function. *Neuron* 90, 1215–1229. doi: 10.1016/j.neuron.2016.05.002

Tang, L., Chen, L., Liu, X., He, J., Ma, Y., Zhang, N., et al. (2022). The repeat length of C9orf72 is associated with the survival of amyotrophic lateral sclerosis patients without C9orf72 pathological expansions. *Front. Neurol.* 13:939775. doi: 10.3389/fneur.2022.939775

Zhang, K., Liu, Q., Shen, D., Tai, H., Liu, S., Wang, Z., et al. (2019). Mutation analysis of KIF5A in Chinese amyotrophic lateral sclerosis patients. *Neurobiol. Aging* 73, 229.e1–229.e4. doi: 10.1016/j.neurobiolaging.2018.08.006

Frontiers in
Cellular Neuroscience

Leading research in cellular mechanisms underlying brain function and development

Part of the world's most cited neuroscience journal series that advances our understanding of the cellular mechanisms underlying cell function in the nervous system across all species.

Discover the latest Research Topics

See more →

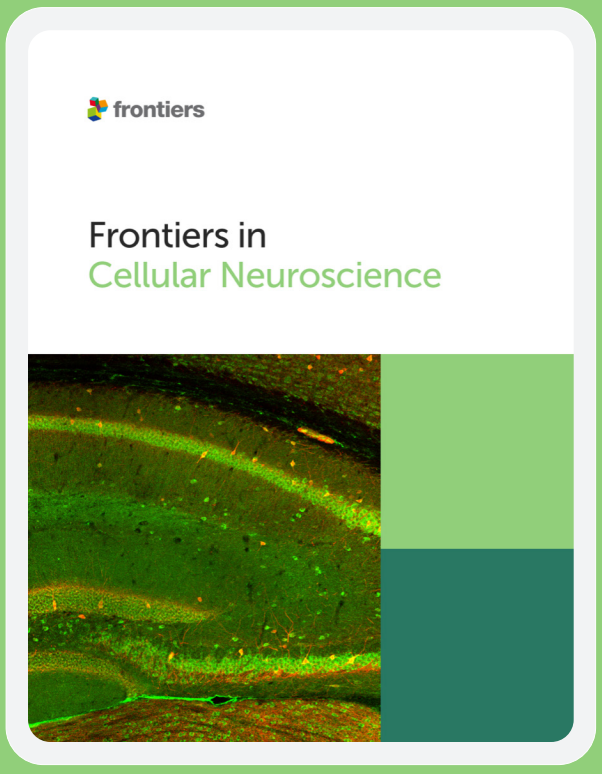

Frontiers

Avenue du Tribunal-Fédéral 34
1005 Lausanne, Switzerland
frontiersin.org

Contact us

+41 (0)21 510 17 00
frontiersin.org/about/contact